BEST AVAILABLE IMAGES

Defective images within this document are accurate representations of the original documents submitted by the applicant.

Defects in the images may include (but are not limited to):

- BLACK BORDERS
- TEXT CUT OFF AT TOP, BOTTOM OR SIDES
- FADED TEXT
- ILLEGIBLE TEXT
- SKEWED/SLANTED IMAGES
- COLORED PHOTOS
- BLACK OR VERY BLACK AND WHITE DARK PHOTOS
- GRAY SCALE DOCUMENTS

IMAGES ARE BEST AVAILABLE COPY.

As rescanning documents *will not* correct images, please do not report the images to the Image Problem Mailbox.

d his

(FILE 'HOME' ENTERED AT 16:33:17 ON 12 FEB 2003)

FILE 'MEDLINE, EMBASE, SCISEARCH, BIOSIS, USPATFULL' ENTERED AT 16:34:58 ON 12 FEB 2003

L1 9452 S (INTRACEL?) (P) (NMR OR (NUCLEAR MAGNETIC RESONANCE))
L2 0 S (1H, 15N, 13C, 19F, 31P) (P) (NMR OR (NUCLEAR MAGNETIC RESONA

FILE 'MEDLINE, EMBASE, SCISEARCH, BIOSIS, USPATFULL, CAPLUS' ENTERED AT 16:37:16 ON 12 FEB 2003

L3 12128 S (INTRACEL?) (P) (NMR OR (NUCLEAR MAGNETIC RESONANCE))
L4 0 S (1H, 15N, 13C, 19F, 31P) (P) (NMR OR (NUCLEAR MAGNETIC RESONA
L5 1 S (H, N, C, F, P) (P) (NMR OR (NUCLEAR MAGNETIC RESONANCE))
L6 268026 S (1H OR 15N OR 13C OR 19F OR 31P) (P) (NMR OR (NUCLEAR MAGNETI
L7 6369 S L3 (6P) L6
L8 26 S L7 AND HSQC
L9 2 S L7 AND (TRIPLE RESONANCE NMR)
L10 4 S L7 AND TROSY
L11 1 S L7 AND HNCA
L12 13 S L7 AND HMQC
L13 11 DUP REM L8 (15 DUPLICATES REMOVED)
L14 2 DUP REM L9 (0 DUPLICATES REMOVED)
L15 2 DUP REM L10 (2 DUPLICATES REMOVED)
L16 5 DUP REM L12 (8 DUPLICATES REMOVED)
L17 11620 S L6 AND DEUTER?
L18 95 S L17 (6P) L3
L19 6936 S L6 (6P) DEUTER?
L20 43 S L19 (6P) L3
L21 19 DUP REM L20 (24 DUPLICATES REMOVED)

L13 ANSWER 5 OF 11 USPATFULL
ACCESSION NUMBER: 2001:139272 USPATFULL
TITLE: LINKING GENE SEQUENCE TO GENE FUNCTION BY THREE DIMESIONAL (3D) PROTEIN STRUCTURE DETERMINATION
INVENTOR(S): ANDERSON, STEPHEN, PRINCETON, NJ, United States
MONTELIONE, GAETANO, HIGHLAND PARK, NJ, United States

	NUMBER	KIND	DATE	
PATENT INFORMATION:	US 2001016314	A1	20010823	
APPLICATION INFO.:	US 1998-181601	A1	19981029	(9)

DOCUMENT TYPE: Utility
FILE SEGMENT: APPLICATION
LEGAL REPRESENTATIVE: JANE MASSEY LICATA, ESQ., LAW OFFICES OF JANE MASSEY LICATA, 66 E. MAIN STREET, MARLTON, NJ, 08053
NUMBER OF CLAIMS: 17
EXEMPLARY CLAIM: 1
NUMBER OF DRAWINGS: 6 Drawing Page(s)
LINE COUNT: 1595
CAS INDEXING IS AVAILABLE FOR THIS PATENT.

AB The present invention provides a structure-functional analysis engine for the high-throughput determination of the biochemical function of proteins or protein domains of unknown function. The present invention uses bioinformatics, molecular biology and nuclear magnetic resonance tools for the rapid and automated determination of the three-dimensional structures of proteins and protein domains.

DRWD [0053] FIG. 6 provides the results of the NMR .sup.15N-.sup.1H heteronuclear single quantum coherence (**HSQC**) spectral analysis of the NTD2-3 domain collected on a Varian Unity 500 spectrometer.

DRWD [0054] FIG. 7 provides the 2D .sup.15N-.sup.1H.sup.N **HSQC** spectrum of CspA at pH 6.0 and 30.degree. C.

DETD [0075] It is preferable to further characterize the isolated domain by .sup.**1H**-**NMR** spectroscopy. Preferably, the isolated domain is in a moderately concentrated solution (.about.100 .mu.M). A high dispersion pattern of the proton. . .

DETD [0080] Uniform biosynthetic enrichment with .sup.**15N**, .sup.**13C** and .sup.2H isotopes has been reported to be a prerequisite for the analysis of macromolecular structures by **NMR** spectroscopy. Some **NMR** strategies have also been reported to benefit from random enrichment with .sup.2H isotopes. The principal obstacle for isotope-enriched protein production in most recombinant production systems is the high cost of the enriched media components (e.g. .sup.**13C**-glucose @$330/g), and the limiting possibilities for scale-up to controlled multi-liter fermenters. The less well-controlled conditions of shaker flask cultivations often result in lower protein production levels. The production of .sup.**15N**-,.sup.**13C**-, and/or .sup.2H-enriched proteins thus requires an efficient system cable of providing high level production of the desired protein in small-scale. . .

DETD [0081] Under one preferred embodiment, the present invention employs a bacterial production system for .sup.**15N**, .sup.**13C** -enriched recombinant proteins. Preferably, the bacterial production system is based on **intracellular** production of recombinant proteins in E. coli as fusions to an IgG-binding domain analogue, Z, derived from staphylococcal Protein A. . . In this system, transcription is initiated from the efficient promoter of the E. coli trp operon. This allows for efficient **intracellular** production of fusion proteins. These fusion proteins can then be purified by IgG affinity chromatography. Using this approach it is. . . mg/L) production in defined minimal media of a number of isotope-enriched proteins (see, for example, Jansson et al., J. Biomol. **NMR** 7:131-141 (1996)).

DETD [0083] Under another preferred embodiment, .sup.**15N**, .sup.**13C**, .sup.2H-enriched recombinant proteins can be produced by acclimating a bacterial production system to grow in 95% .sup.2H.sub.2O. Recombinant bacterial production. . . protein production levels of acclimated bacteria grown in 95% .sup.2H.sub.2O are identical to those obtained in H.sub.2O. Using protiated [uniformly .sup.**13C**-enriched]-glucose as the carbon source, .sup.2H-enrichment levels of 70 - 80% can be achieved; high incorporation of .sup.2H from the .sup.2H.sub.2O. . . amino acid biosynthesis. While the resulting proteins are not 100% perdeuterated, they are sufficiently enriched for the purpose of slowing .sup.**13C** transverse relaxation rates and enhancing the sensitivity for certain types of triple-resonance **NMR** experiments. 100% perdeuterated samples can also be produced using .sup.2H.sub.2O solvent and [uniformly 21H, .sup.**13C**-enriched]-glucose as the carbon source.

DETD . . . (<.about.30 kD), isotopically enriched samples are scored in terms of their suitability for structure determination by NMR using standard 2D **HSQC**, 2D NOESY, and/or 2D CBCANH triple-resonance spectra. The protein samples that provide good quality data for these NMR experiments are. . .

DETD [0107] Input to AUTOASSIGN includes a peak-picked 2D (H-N)-**HSQC** spectrum and the following seven peak-picked 3D spectra: HNCO, CANH, CA(CO)NH, CBCANH, CBCA(CO)NH, H(CA)NH, and H(CA)(CO)NH. This family of triple-resonance. . .

DETD [0158] NMR .sup.15N-**HSQC** spectra is collected on a Varian Unity 500 spectrometer. The .sup.15N-**HSQC** spectral analysis is shown in FIG. 6. The good dispersion in both the .sup.15N and .sup.1H dimensions demonstrate that this. . .

DETD . . . frequency synthesizer for carbonyl decoupling as described by Feng et al., Biochemistry 37:10881-10896 (1998). FIG. 7 provides the 2D .sup.15N-.sup.1H.sup.N **HSQC** spectrum of CSPA at pH 6.0 and 30.degree. C.

DETD [0160] The collected spin resonances are analyzed using AUTOASSIGN. The input for AUTOASSIGN includes peaks from 2D .sup.15N-.sup.1H.sup.N **HSQC** and 3D HNCO spectra along with peak lists from three intraresidue (CANH, CBCANH and HCANH) and three interresidue (CA(CO)NH, CBCA(CO)NH. . .

DETD . . . by reference in its entirety. Interatomic distance constraints are derived from three NOESY data sets 2D NOESY and 3D .sup.15N-edited NOESY-**HSQC** spectra recorded with a mixing time of t.sub.m of 60 ms of a CspA sample dissolved in 90% H.sub.2O/10% .sup.2H.sub.2O. . . recorded with a mixing time t.sub.m of 50 ms of a sample dissolved in 100% .sup.2H.sub.2O. The intensity of the NOESY-**HSQC** spectrum is corrected for .sup.15N relaxation effects, and the cross-peak intensities are converted into interproton distance constraints.

TABLE 1

Summary of. . .

CLM What is claimed is:

. . . or more spectra selected from the group consisting of nuclear Overhauser effect spectroscopy (NOESY), pulsed-field gradient .sup.15N-heteronuclear single-quantum coherence spectroscopy (PFG-**HSQC**), pulsed-field gradient triple-resonance HCCNH .sup.13C-.sup.13C total correlation spectroscopy (PFG-HCCNH-TOCSY), pulsed-field gradient HCC(CO)NH .sup.13C-.sup.13C TOCSY (PFG-HCC(CO)NH-TOCSY), HCCH COSY, HCCNH-TOCSY, HNCO, CANH,. . .

L13 ANSWER 7 OF 11 MEDLINE DUPLICATE 3
ACCESSION NUMBER: 1999313450 MEDLINE
DOCUMENT NUMBER: 99313450 PubMed ID: 10386878
TITLE: Real-time NMR studies on a transient folding intermediate of barstar.
AUTHOR: Killick T R; Freund S M; Fersht A R
CORPORATE SOURCE: Cambridge Centre for Protein Engineering, Department of Chemistry, University of Cambridge, United Kingdom.
SOURCE: PROTEIN SCIENCE, (1999 Jun) 8 (6) 1286-91.
Journal code: 9211750. ISSN: 0961-8368.
PUB. COUNTRY: United States
DOCUMENT TYPE: Journal; Article; (JOURNAL ARTICLE)
LANGUAGE: English
FILE SEGMENT: Priority Journals
ENTRY MONTH: 199907
ENTRY DATE: Entered STN: 19990727
Last Updated on STN: 20000303
Entered Medline: 19990715

AB The refolding of barstar, the **intracellular** inhibitor of barnase, is dominated by the slow formation of a cis peptidyl prolyl bond in the native protein. The triple mutant C40/82A P27A in which two cysteine residues and one trans proline were replaced by alanine was used as model system to investigate the kinetics and structural consequences of the trans/cis interconversion of Pro48. One- and two-dimensional real-time **NMR** spectroscopy was used to follow the trans/cis interconversion after folding was initiated by rapid dilution of the urea denatured protein. Series of **1H**, **15N HSQC** spectra acquired with and without the addition of peptidyl prolyl isomerase unambiguously revealed the accumulation of a transient trans-Pro48 intermediate within the dead time of the experiment. Subtle chemical shift differences between the native state and the intermediate spectra indicate that the intermediate is predominantly native-like with a local rearrangement in the Pro48 loop and in the beta-sheet region including residues Tyr47, Ala82, Thr85, and Val50.

AB The refolding of barstar, the **intracellular** inhibitor of barnase, is dominated by the slow formation of a cis peptidyl prolyl bond in the native protein. The. . . as model system to investigate the kinetics and structural consequences of the trans/cis interconversion of Pro48. One- and two-dimensional real-time **NMR** spectroscopy was used to follow the trans/cis interconversion after folding was initiated by rapid dilution of the urea denatured protein. Series of **1H**, **15N HSQC** spectra acquired with and without the addition of peptidyl prolyl isomerase unambiguously revealed the accumulation of a transient trans-Pro48 intermediate. . .

L13 ANSWER 8 OF 11 EMBASE COPYRIGHT 2003 ELSEVIER SCI. B.V.DUPLICATE 4
ACCESSION NUMBER: 1999256949 EMBASE
TITLE: Identification and quantitation of phosphorus metabolites in yeast neutral pH extracts by nuclear magnetic resonance spectroscopy.
AUTHOR: Teleman A.; Richard P.; Toivari M.; Penttila M.
CORPORATE SOURCE: A. Teleman, Swedish Pulp/Paper Res. Institute, STFI, PO Box 5604, S-114 86 Stockholm, Sweden. Anita.Teleman@stfi.se
SOURCE: Analytical Biochemistry, (15 Jul 1999) 272/1 (71-79).
Refs: 15
ISSN: 0003-2697 CODEN: ANBCA2
COUNTRY: United States
DOCUMENT TYPE: Journal; Article
FILE SEGMENT: 023 Nuclear Medicine
029 Clinical Biochemistry
LANGUAGE: English
SUMMARY LANGUAGE: English
AB **31P NMR** spectroscopy offers a possibility to obtain a survey of all low-molecular-weight phosphorylated compounds in yeast. The yeast cells have been extracted using chloroform into a neutral aqueous phase. The use of high fields and the neutral pH extracts, which are suitable for **NMR** analysis, results in well-resolved **31P NMR** spectra. Two-dimensional **NMR** experiments, such as proton-detected heteronuclear single quantum (**1H-31P HSQC**) and **31P** correlation spectroscopy (**31P** COSY), have been used to assign the resonances. In the phosphomonoester region many of the signals could be assigned to known metabolites in the glycolytic and pentose phosphate pathways, although some signals remain unidentified. Accumulation of ribulose 5-phosphate, xylulose 5-phosphate, and ribose 5-phosphate was observed in a strain lacking transketolase activity when grown in synthetic complete medium. No such accumulation occurred when the cells were grown in yeast- peptone-dextrose medium. Trimetaphosphate (**intracellular** concentration about 0.2 mM) was detected in both cold methanol-chloroform and perchloric acid extracts.
AB **31P NMR** spectroscopy offers a possibility to obtain a survey of all low-molecular-weight phosphorylated compounds in yeast. The yeast cells have been. . . chloroform into a neutral aqueous phase. The use of high fields and the neutral pH extracts, which are suitable for **NMR** analysis, results in well-resolved **31P NMR** spectra. Two-dimensional **NMR** experiments, such as proton-detected heteronuclear single quantum (**1H-31P HSQC**) and **31P** correlation spectroscopy (**31P** COSY), have been used to assign the resonances. In the phosphomonoester region many of the signals could be assigned to. . . when grown in synthetic complete medium. No such accumulation occurred when the cells were grown in yeast- peptone-dextrose medium. Trimetaphosphate (**intracellular** concentration about 0.2 mM) was detected in both cold methanol-chloroform and perchloric acid extracts.

L13 ANSWER 9 OF 11 MEDLINE DUPLICATE 5
ACCESSION NUMBER: 1998434375 MEDLINE
DOCUMENT NUMBER: 98434375 PubMed ID: 9760238
TITLE: Identification of the binding surface on Cdc42Hs for p21-activated kinase.
AUTHOR: Guo W; Sutcliffe M J; Cerione R A; Oswald R E
CORPORATE SOURCE: Department of Molecular Medicine, Cornell University, Ithaca, New York 14853, and Department of Chemistry, Leicester University, Leicester, LE1 7RK, UK.
CONTRACT NUMBER: R01 GM56233 (NIGMS)
T32GM08210 (NIGMS)
SOURCE: BIOCHEMISTRY, (1998 Oct 6) 37 (40) 14030-7.
Journal code: 0370623. ISSN: 0006-2960.
PUB. COUNTRY: United States
DOCUMENT TYPE: Journal; Article; (JOURNAL ARTICLE)

LANGUAGE: English
FILE SEGMENT: Priority Journals
ENTRY MONTH: 199811
ENTRY DATE: Entered STN: 19990106
Last Updated on STN: 20020420
Entered Medline: 19981104

AB The Ras superfamily of GTP-binding proteins is involved in a number of cellular signaling events including, but not limited to, tumorigenesis, **intracellular** trafficking, and cytoskeletal organization. The Rho subfamily, of which Cdc42Hs is a member, is involved in cell morphogenesis through a GTPase cascade which regulates cytoskeletal changes. Cdc42Hs has been shown to stimulate DNA synthesis as well as to initiate a protein kinase cascade that begins with the activation of the p21-activated serine/threonine kinases (PAKs). We have determined previously the solution structure of Cdc42Hs [Feltham et al. (1997) Biochemistry 36, 8755-8766] using **NMR** spectroscopy. A minimal-binding domain of 46 amino acids of PAK was identified (PBD46), which binds Cdc42Hs with a KD of approximately 20 nM and inhibits GTP hydrolysis. The binding interface was mapped by producing a fully deuterated sample of **15N** -Cdc42Hs bound to PBD46. A **1H,15N**-NOESY-**HSQC** spectrum demonstrated that the binding surface on Cdc42Hs consists of the second beta-strand (beta2) and a portion of the loop between the first alpha-helix (alpha1) and beta2 (switch I). A complex of PBD46 bound to **15N**-Cdc42Hs.GMPPCP exhibited extensive chemical shift changes in the **1H,15N-HSQC** spectrum. Thus, PBD46 likely produces structural changes in Cdc42Hs which are not limited to the binding interface, consistent with its effects on GTP hydrolysis. These results suggest that the kinase-binding domain on Cdc42Hs is similar to, but more extensive than, the c-Raf-binding domain on the Ras antagonist, Rap1 [Nassar et al. (1995) Nature 375, 554-560)].

AB . . . Ras superfamily of GTP-binding proteins is involved in a number of cellular signaling events including, but not limited to, tumorigenesis, **intracellular** trafficking, and cytoskeletal organization. The Rho subfamily, of which Cdc42Hs is a member, is involved in cell morphogenesis through a. . . serine/threonine kinases (PAKs). We have determined previously the solution structure of Cdc42Hs [Feltham et al. (1997) Biochemistry 36, 8755-8766] using **NMR** spectroscopy. A minimal-binding domain of 46 amino acids of PAK was identified (PBD46), which binds Cdc42Hs with a KD of approximately 20 nM and inhibits GTP hydrolysis. The binding interface was mapped by producing a fully deuterated sample of **15N**-Cdc42Hs bound to PBD46. A **1H**, **15N**-NOESY-**HSQC** spectrum demonstrated that the binding surface on Cdc42Hs consists of the second beta-strand (beta2) and a portion of the loop between the first alpha-helix (alpha1) and beta2 (switch I). A complex of PBD46 bound to **15N**-Cdc42Hs.GMPPCP exhibited extensive chemical shift changes in the **1H,15N** -**HSQC** spectrum. Thus, PBD46 likely produces structural changes in Cdc42Hs which are not limited to the binding interface, consistent with its. . .

3 ANSWER 11 OF 11 MEDLINE DUPLICATE 7
ACCESSION NUMBER: 95392182 MEDLINE
DOCUMENT NUMBER: 95392182 PubMed ID: 7663142
TITLE: Secondary structure determination by NMR spectroscopy of an immunoglobulin-like domain from the giant muscle protein titin.
AUTHOR: Pfuhl M; Gautel M; Politou A S; Joseph C; Pastore A
CORPORATE SOURCE: European Molecular Biology Laboratory, Heidelberg, Germany.
SOURCE: JOURNAL OF BIOMOLECULAR NMR, (1995 Jul) 6 (1) 48-58.
Journal code: 9110829. ISSN: 0925-2738.
PUB. COUNTRY: Netherlands
DOCUMENT TYPE: Journal; Article; (JOURNAL ARTICLE)
LANGUAGE: English
FILE SEGMENT: Priority Journals
ENTRY MONTH: 199510
ENTRY DATE: Entered STN: 19951020
Last Updated on STN: 19951020
Entered Medline: 19951010

AB We present the complete **15N** and **1H NMR** assignment and the secondary structure of an immunoglobulin-like domain from the giant muscle protein titin. The assignment was obtained using homonuclear and **15N** heteronuclear 2D and 3D experiments. The complementarity of 3D TOCSY-NOESY and 3D **15N** NOESY-**HSQC** experiments, using WATERGATE for water suppression, allowed an efficient assignment of otherwise ambiguous cross peaks and was helpful in overcoming poor TOCSY transfer for some amino acids. The secondary structure is derived from specific NOEs between backbone alpha- and amide protons, secondary chemical shifts of alpha-protons and chemical exchange for the backbone amide protons. It consists of eight beta-strands, forming two beta-sheets with four strands each, similar to the classical beta-sandwich of the immunoglobulin superfamily, as previously predicted by sequence analysis. Two of the beta-strands are connected by type II beta-turns; the first beta-strand forms a beta-bulge. The whole topology is very similar to the only **intracellular** immunoglobulin-like domain for which a structure has been determined so far, i.e., telokin.
AB We present the complete **15N** and **1H NMR** assignment and the secondary structure of an immunoglobulin-like domain from the giant muscle protein titin. The assignment was obtained using homonuclear and **15N** heteronuclear 2D and 3D experiments. The complementarity of 3D TOCSY-NOESY and 3D **15N** NOESY-**HSQC** experiments, using WATERGATE for water suppression, allowed an efficient assignment of otherwise ambiguous cross peaks and was helpful in overcoming. . . connected by type II beta-turns; the first beta-strand forms a beta-bulge. The whole topology is very similar to the only **intracellular** immunoglobulin-like domain for which a structure has been determined so far, i.e., telokin.

L16 ANSWER 2 OF 5 BIOSIS COPYRIGHT 2003 BIOLOGICAL ABSTRACTS INC.DUPLICATE 1
ACCESSION NUMBER: 2002:134321 BIOSIS
DOCUMENT NUMBER: PREV200200134321
TITLE: Chemosensitization of a multidrug-resistant Leishmania tropica line by new sesquiterpenes from Maytenus magellanica and Maytenus chubutensis.
AUTHOR(S): Kennedy, Maria L.; Cortes-Selva, Fernando; Perez-Victoria, Jose M.; Jimenez, Ignacio A.; Gonzalez, Antonio G.; Munoz, Orlando M.; Gamarro, Francisco; Castanys, Santiago; Ravelo, Angel G. (1)
CORPORATE SOURCE: (1) Instituto Universitario de Bio-Organica "Antonio Gonzalez", Universidad de La Laguna, Avenida Astrofisico Francisco Sanchez, 2, 38206, La Laguna, Tenerife: castanys@ipb.csic.es, agravelo@ull.es Spain
SOURCE: Journal of Medicinal Chemistry, (December 20, 2001) Vol. 44, No. 26, pp. 4668-4676. print.
ISSN: 0022-2623.
DOCUMENT TYPE: Article
LANGUAGE: English

AB Parasite resistance to drugs has emerged as a major problem in current medicine, and therefore, there is great clinical interest in developing compounds that overcome these resistances. In an intensive study of South American medicinal plants, herein we report the isolation, structure elucidation, and biological activity of dihydro-beta-agarofuran sesquiterpenes from the roots of Maytenus magellanica (1-14) and M. chubutensis (14-17). This type of natural products may be considered as privileged structures. The structures of 10 new compounds, 1, 3, 6-9, and 12-15, were determined by means of **1H** and **13C** **NMR** spectroscopic studies, including homonuclear (COSY and ROESY) and heteronuclear correlation experiments (**HMQC** and HMBC). The absolute configurations of eight hetero- and homochromophoric compounds, 1, 3, 6-9, 12, and 13, were determined by means of CD studies. Fourteen compounds, 1-3 and 6-16, have been tested on a multidrug-resistant Leishmania tropica line overexpressing a P-glycoprotein-like transporter to determine their ability to revert the resistance phenotype and to modulate **intracellular** drug accumulation. From this series, 1, 2, 3, 14, and 15 showed potent activity, 1 being the most active compound. The structure-activity relationships of the different compounds are discussed.

AB. . . considered as privileged structures. The structures of 10 new compounds, 1, 3, 6-9, and 12-15, were determined by means of **1H** and **13C** **NMR** spectroscopic studies, including homonuclear (COSY and ROESY) and heteronuclear correlation experiments (**HMQC** and HMBC). The absolute configurations of eight hetero- and homochromophoric compounds, 1, 3, 6-9, 12, and 13, were determined by. . . multidrug-resistant Leishmania tropica line overexpressing a P-glycoprotein-like transporter to determine their ability to revert the resistance phenotype and to modulate **intracellular** drug accumulation. From this series, 1, 2, 3, 14, and 15 showed potent activity, 1 being the most active compound.. . .

IT . . . & Equipment
CD study [circular dichroism study]: analytical method; COSY [correlation spectroscopy]: analytical method; HMBC [heteronuclear multiple-bond correlation]: analytical method; **HMQC** [heteronuclear multiple quantum correlation spectroscopy]: analytical method; NMR spectroscopy: analytical method; ROESY [rotating frame nuclear Overhauser effect spectroscopy]: analytical method

L16 ANSWER 3 OF 5 SCISEARCH COPYRIGHT 2003 ISI (R) DUPLICATE 2
ACCESSION NUMBER: 2001:701677 SCISEARCH
THE GENUINE ARTICLE: 467LR
TITLE: TCA cycle kinetics in the rat heart by analysis of C-13 isotopomers using indirect H-1[C-13] detection
AUTHOR: Carvalho R A; Zhao P; Wiegers C B; Jeffrey F M H; Malloy C R; Sherry A D (Reprint)
CORPORATE SOURCE: Univ Texas, SW Med Ctr, Mary Nell & Ralph B Rogers Magnet Resonance Ctr, Dept Radiol, 5801 Forest Pk Rd, Dallas, TX 75390 USA (Reprint); Univ Texas, SW Med Ctr, Mary Nell & Ralph B Rogers Magnet Resonance Ctr, Dept Radiol, Dallas, TX 75390 USA; Univ Texas, SW Med Ctr, Dept Internal Med, Dallas, TX 75216 USA; Dept Vet Affairs Med Ctr, Dallas, TX 75216 USA; Univ Texas, Dept Chem, Richardson, TX 75083 USA
COUNTRY OF AUTHOR: USA
SOURCE: AMERICAN JOURNAL OF PHYSIOLOGY-HEART AND CIRCULATORY PHYSIOLOGY, (SEP 2001) Vol. 281, No. 3, pp. H1413-H1421. Publisher: AMER PHYSIOLOGICAL SOC, 9650 ROCKVILLE PIKE, BETHESDA, MD 20814 USA.
ISSN: 0363-6135.
DOCUMENT TYPE: Article; Journal
LANGUAGE: English
REFERENCE COUNT: 32

ABSTRACT IS AVAILABLE IN THE ALL AND IALL FORMATS

AB This study was designed to test the hypothesis that indirect H-1 [C-13] detection of tricarboxylic acid (TCA) cycle intermediates using heteronuclear multiple quantum correlation-total correlation spectroscopy (**HMQC**-TOCSY) **nuclear magnetic resonance** (**NMR**) spectroscopy provides additional C-13 isotopomer information that better describes the kinetic exchanges that occur between **intracellular** compartments than direct C-13 **NMR** detection. **NMR** data were collected on extracts of rat hearts perfused at various times with combinations of [2-C-13]acetate, propionate, the transaminase inhibitor aminooxyacetate, and **13C** multiplet areas derived from spectra of tissue glutamate were fit to a standard kinetic model of the TCA cycle. Although the two **NMR** methods detect different populations of **13C** isotopomers, similar values were found for TCA cycle and exchange fluxes by analyzing the two data sets. Perfusion of hearts with unlabeled propionate in addition to [2-C-13]acetate resulted in an increase in the pool size of all four-carbon TCA cycle intermediates. This allowed the addition of isotopomer data from aspartate and malate in addition to the more abundant glutamate. This study illustrates that metabolic inhibitors can provide new insights into metabolic transport processes in intact tissues.

AB . . . the hypothesis that indirect H-1 [C-13] detection of tricarboxylic acid (TCA) cycle intermediates using heteronuclear multiple quantum correlation-total correlation spectroscopy (**HMQC**-TOCSY) **nuclear magnetic resonance** (**NMR**) spectroscopy provides additional C-13 isotopomer information that better describes the kinetic exchanges that occur between **intracellular** compartments than direct C-13 **NMR** detection. **NMR** data were collected on extracts of rat hearts perfused at various times with combinations of [2-C-13]acetate, propionate, the transaminase inhibitor aminooxyacetate, and **13C** multiplet areas derived from spectra of tissue glutamate were fit to a standard kinetic model of the TCA cycle. Although the two **NMR** methods detect different populations of **13C** isotopomers, similar values were found for TCA cycle and exchange fluxes by analyzing the two data sets. Perfusion of hearts. . .

L16 ANSWER 5 OF 5 MEDLINE DUPLICATE 4
ACCESSION NUMBER: 1998399491 MEDLINE
DOCUMENT NUMBER: 98399491 PubMed ID: 9729792
TITLE: Conformational analysis of a Chlamydia-specific disaccharide alpha-Kdo-(2-->8)-alpha-Kdo-(2-->O)-allyl in aqueous solution and bound to a monoclonal antibody: observation of intermolecular transfer NOEs.
AUTHOR: Sokolowski T; Haselhorst T; Scheffler K; Weisemann R; Kosma P; Brade H; Brade L; Peters T
CORPORATE SOURCE: Institut fur Chemie, Medizinische Universitat Lubeck, Germany.
SOURCE: JOURNAL OF BIOMOLECULAR NMR, (1998 Jul) 12 (1) 123-33. Journal code: 9110829. ISSN: 0925-2738.
PUB. COUNTRY: Netherlands
DOCUMENT TYPE: Journal; Article; (JOURNAL ARTICLE)
LANGUAGE: English
FILE SEGMENT: Priority Journals
ENTRY MONTH: 199810
ENTRY DATE: Entered STN: 19981020
Last Updated on STN: 19981020
Entered Medline: 19981007

AB The disaccharide alpha-Kdo-(2-->8)-alpha-Kdo (Kdo: 3-deoxy-D-manno-oct-2-ulosonic acid) represents a genus-specific epitope of the lipopolysaccharide of the obligate **intracellular** human pathogen Chlamydia. The conformation of the synthetically derived disaccharide alpha-Kdo-(2-->8)-alpha-Kdo-(2-->O)-allyl was studied in aqueous solution, and complexed to a monoclonal antibody S25-2. Various **NMR** experiments based on the detection of NOEs (or transfer NOEs) and ROEs (or transfer ROEs) were performed. A major problem was the extensive overlap of almost all **1H NMR** signals of alpha-Kdo-(2-->8)-alpha-Kdo-(2-->O)-allyl. To overcome this difficulty, **HMQC**-NOESY and **HMQC**-trNOESY experiments were employed. Spin diffusion effects were identified using trROESY experiments, QUIET-trNOESY experiments and MINSY experiments. It was found that protein protons contribute to the observed spin diffusion effects. At 800 MHz, intermolecular trNOEs were observed between ligand protons and aromatic protons in the antibody binding site. From **NMR** experiments and Metropolis Monte Carlo simulations, it was concluded that alpha-Kdo-(2-->8)-alpha-Kdo-(2-->O)-allyl in aqueous solution exists as a complex conformational mixture. Upon binding to the monoclonal antibody S25-2, only a limited range of conformations is available to alpha-Kdo-(2-->8)-alpha-Kdo-(2-->O)-allyl. These possible bound conformations were derived from a distance geometry analysis using transfer NOEs as experimental constraints. It is clear that a conformation is selected which lies within a part of the conformational space that is highly populated in solution. This conformational space also includes the conformation found in the crystal structure. Our results provide a basis for modeling studies of the antibody-disaccharide complex.

AB The disaccharide alpha-Kdo-(2-->8)-alpha-Kdo (Kdo: 3-deoxy-D-manno-oct-2-ulosonic acid) represents a genus-specific epitope of the lipopolysaccharide of the obligate **intracellular** human pathogen Chlamydia. The conformation of the synthetically derived disaccharide alpha-Kdo-(2-->8)-alpha-Kdo-(2-->O)-allyl was studied in aqueous solution, and complexed to a monoclonal antibody S25-2. Various **NMR** experiments based on the detection of NOEs (or transfer NOEs) and ROEs (or transfer ROEs) were performed. A major problem was the extensive overlap of almost all **1H NMR** signals of alpha-Kdo-(2-->8)-alpha-Kdo-(2-->O)-allyl. To overcome this difficulty, **HMQC**-NOESY and **HMQC**-trNOESY experiments were employed. Spin diffusion effects were identified using trROESY experiments, QUIET-trNOESY experiments and MINSY experiments. It was found that. . . effects. At 800 MHz, intermolecular trNOEs were observed between ligand protons and aromatic protons in the antibody binding site. From **NMR**

experiments and Metropolis Monte Carlo simulations, it was concluded that alpha-Kdo-(2-->8)-alpha-Kdo-(2-->O)-allyl in aqueous solution exists as a complex conformational mixture.. . .

=>

L21 ANSWER 12 OF 19 MEDLINE DUPLICATE 6
ACCESSION NUMBER: 97027906 MEDLINE
DOCUMENT NUMBER: 97027906 PubMed ID: 8873993
TITLE: Locations of local anesthetic dibucaine in model membranes and the interaction between dibucaine and a Na+ channel inactivation gate peptide as studied by 2H- and 1H-NMR spectroscopies.
AUTHOR: Kuroda Y; Ogawa M; Nasu H; Terashima M; Kasahara M; Kiyama Y; Wakita M; Fujiwara Y; Fujii N; Nakagawa T
CORPORATE SOURCE: Faculty of Pharmaceutical Sciences, Kyoto University, Japan.
SOURCE: BIOPHYSICAL JOURNAL, (1996 Sep) 71 (3) 1191-207.
Journal code: 0370626. ISSN: 0006-3495.
PUB. COUNTRY: United States
DOCUMENT TYPE: Journal; Article; (JOURNAL ARTICLE)
LANGUAGE: English
FILE SEGMENT: Priority Journals
ENTRY MONTH: 199703
ENTRY DATE: Entered STN: 19970321
Last Updated on STN: 19970321
Entered Medline: 19970311

AB To study the molecular mechanisms of local anesthesia, locations of local anesthetic dibucaine in model membranes and the interactions of dibucaine with a Na+ channel inactivation gate peptide have been studied by 2H- and **1H-NMR** spectroscopies. The 2H-**NMR** spectra of dibucaine-d9 and dibucaine-d1, which are **deuterated** at the butoxy group and at the 3 position in its quinoline ring, respectively, have been observed in multilamellar dispersions of the lipid mixture composed of phosphatidylcholine, phosphatidylserine, and phosphatidylethanolamine. 2H-**NMR** spectra of **deuterated** palmitic acids incorporated, as a probe, into the lipid mixture containing cholesterol have also been observed. An order parameter, SCD, for each carbon segment was calculated from the observed quadrupole splittings. Combining these results, we concluded that first, the butoxy group of dibucaine is penetrating between the acyl chains of lipids in the model membranes, and second, the quinoline ring of dibucaine is located at the polar region of lipids but not at the hydrophobic acyl chain moiety. These results mean that dibucaine is situated in a favorable position that permits it to interact with a cluster of hydrophobic amino acids (Ile-Phe-Met) within the **intracellular** linker between domains III and IV of Na+ channel protein, which functions as an inactivation gate. To confirm whether the dibucaine molecule at the surface region of lipids can really interact with the hydrophobic amino acids, we synthesized a model peptide that includes the hydrophobic amino acids (Ac-GGQDIFMTEEQK-OH, MP-1), the amino acid sequence of which corresponds to the linker part of rat brain type IIA Na+ channel, and the one in which Phe has been substituted by Gln (MP-2), and measured **1H-NMR** spectra in both phosphate buffer and phosphatidylserine liposomes. It was found that the quinoline ring of dibucaine can interact with the aromatic ring of Phe by stacking of the rings; moreover, the interaction can be reinforced by the presence of lipids. In conclusion, we wish to propose that local anesthesia originates from the pi-stacking interaction between aromatic rings of an anesthetic molecule located at the polar headgroup region of the so-called boundary lipids and of the Phe in the **intracellular** linker between domains III and IV of the Na+ channel protein, prolonging the inactivated state and consequently making it impossible to proceed to the resting state.

AB . . . model membranes and the interactions of dibucaine with a Na+ channel inactivation gate peptide have been studied by 2H- and **1H-NMR** spectroscopies. The 2H-**NMR** spectra of dibucaine-d9 and dibucaine-d1, which are **deuterated** at the butoxy group and at the 3 position in its quinoline ring, respectively, have been observed in multilamellar dispersions of the lipid mixture

composed of phosphatidylcholine, phosphatidylserine, and phosphatidylethanolamine. 2H-**NMR** spectra of **deuterated** palmitic acids incorporated, as a probe, into the lipid mixture containing cholesterol have also been observed. An order parameter, SCD,. . . situated in a favorable position that permits it to interact with a cluster of hydrophobic amino acids (Ile-Phe-Met) within the **intracellular** linker between domains III and IV of Na+ channel protein, which functions as an inactivation gate. To confirm whether the. . . rat brain type IIA Na+ channel, and the one in which Phe has been substituted by Gln (MP-2), and measured **1H-NMR** spectra in both phosphate buffer and phosphatidylserine liposomes. It was found that the quinoline ring of dibucaine can interact with. . . an anesthetic molecule located at the polar headgroup region of the so-called boundary lipids and of the Phe in the **intracellular** linker between domains III and IV of the Na+ channel protein, prolonging the inactivated state and consequently making it impossible. . .

L21 ANSWER 15 OF 19 MEDLINE DUPLICATE 9
ACCESSION NUMBER: 89123371 MEDLINE
DOCUMENT NUMBER: 89123371 PubMed ID: 2644271
TITLE: Contribution of a conserved arginine near the active site of Escherichia coli D-serine dehydratase to cofactor affinity and catalytic activity.
AUTHOR: Marceau M; Lewis S D; Kojiro C L; Shafer J A
CORPORATE SOURCE: Department of Biological Chemistry, University of Michigan, Ann Arbor 48109.
CONTRACT NUMBER: HL32006 (NHLBI)
SOURCE: JOURNAL OF BIOLOGICAL CHEMISTRY, (1989 Feb 15) 264 (5) 2753-7.
Journal code: 2985121R. ISSN: 0021-9258.
PUB. COUNTRY: United States
DOCUMENT TYPE: Journal; Article; (JOURNAL ARTICLE)
LANGUAGE: English
FILE SEGMENT: Priority Journals
ENTRY MONTH: 198903
ENTRY DATE: Entered STN: 19900308
Last Updated on STN: 19980206
Entered Medline: 19890321

AB We have employed site-directed mutagenesis to investigate the contribution of a conserved arginyl residue to the catalytic activity and cofactor affinity of D-serine dehydratase, a model pyridoxal 5'-phosphate (vitamin B6) enzyme. Replacement of R-120 in the active site peptide of D-serine dehydratase by L decreased the affinity of the enzyme for pyridoxal 5'-phosphate by 20-fold and reduced turnover by 5-8-fold. kappa cat displayed modified substrate alpha-**deuterium** isotope effects and altered dependence on both temperature and pH. Analysis of the pH rate profiles of DSD and the R-120----L variant indicated that R-120 interacts electrostatically with catalytically essential ionizable groups at the active site of wild type D-serine dehydratase. The decrease in cofactor affinity observed for DSD(R120L) was not accompanied by significant perturbations in the UV, CD, or **31P NMR** spectrum of the holoenzyme, suggesting that the contribution of R-120 to pyridoxal phosphate affinity may be indirect or else involve an interaction with a cofactor functional group other than the 5'-phosphoryl moiety. The properties of two other site-directed variants of D-serine dehydratase indicated that the pyridoxal 5'-phosphate:K-118 Schiff base was indifferent to a small change in the shape of the side chain at position 117 (I-117----L), whereas replacement of K-118 by H resulted in undetectable levels of enzyme. A poor ability to bind cofactor may have rendered DSD(K118H) susceptible to **intracellular** proteolysis.

AB . . . the affinity of the enzyme for pyridoxal 5'-phosphate by 20-fold and reduced turnover by 5-8-fold. kappa cat displayed modified substrate alpha-**deuterium** isotope effects and altered dependence on both temperature and pH. Analysis of the pH rate profiles of DSD and the. . . dehydratase. The decrease in cofactor affinity observed for DSD(R120L) was not accompanied by significant perturbations in the UV, CD, or **31P NMR** spectrum of the holoenzyme, suggesting that the contribution of R-120 to pyridoxal phosphate affinity may be indirect or else involve. . . by H resulted in undetectable levels of enzyme. A poor ability to bind cofactor may have rendered DSD(K118H) susceptible to **intracellular** proteolysis.

QP501.J7
mm
NPL

STIC-ILL

From: Gabel, Gailene
Sent: Wednesday, February 12, 2003 5:14 PM
To: STIC-ILL
Subject: 09/905,439

Please provide a copy of the following literature ASAP:

1) Killick, Real-time NMR studies on a transient folding intermediate of barstar. PROTEIN SCIENCE, (1999 Jun) 8 (6) 1286-91.

2) Guo et al., Identification of the binding surface on Cdc42Hs for p21-activated kinase. BIOCHEMISTRY, (1998 Oct 6) 37 (40) 14030-7.

3) Pfuhl et al., Secondary structure determination by NMR spectroscopy of an immunoglobulin-like domain from the giant muscle protein titin. JOURNAL OF BIOMOLECULAR NMR, (1995 Jul) 6 (1) 48-58.

4) Kennedy et al., Chemosensitization of a multidrug-resistant Leishmania tropica line by new sesquiterpenes from Maytenus magellanica and Maytenus chubutensis, Journal of Medicinal Chemistry, (December 20, 2001) Vol. 44, No. 26, pp. 4668-4676.

5) Carvalho et al., TCA cycle kinetics in the rat heart by analysis of C-13 isotopomers using indirect H-1[C-13] detection, AMERICAN JOURNAL OF PHYSIOLOGY-HEART AND CIRCULATORY PHYSIOLOGY, (SEP 2001) Vol. 281, No. 3, pp. H1413-H1421.

6) Sokolowski et al., Conformational analysis of a Chlamydia-specific disaccharide alpha-Kdo-(2-->8)-alpha-Kdo-(2-->O)-allyl in aqueous solution and bound to a monoclonal antibody: observation of intermolecular transfer NOEs. JOURNAL OF BIOMOLECULAR NMR, (1998 Jul) 12 (1) 123-33.

7) Kuroda et al., Locations of local anesthetic dibucaine in model membranes and the interaction between dibucaine and a Na+ channel inactivation gate peptide as studied by 2H- and 1H-NMR spectroscopies. BIOPHYSICAL JOURNAL, (1996 Sep) 71 (3) 1191-207.

8) Marceau et al., Contribution of a conserved arginine near the active site of Escherichia coli D-serine dehydratase to cofactor affinity and catalytic activity. JOURNAL OF BIOLOGICAL CHEMISTRY, (1989 Feb 15) 264 (5) 2753-7.

Thanks a bunch,
Gail R. Gabe
7B15
CM1
305-0807

THE JOURNAL OF BIOLOGICAL CHEMISTRY
Vol. 264, No. 5, Issue of February 15, pp. 2753-2757, 1989
Printed in U.S.A.

Contribution of a Conserved Arginine Near the Active Site of *Escherichia coli* D-Serine Dehydratase to Cofactor Affinity and Catalytic Activity*

(Received for publication, June 23, 1988)

Michelle Marceau, Sidney D. Lewis, Christopher L. Kojiro, and Jules A. Shafer‡

From the Department of Biological Chemistry, University of Michigan, Ann Arbor, Michigan 48109

We have employed site-directed mutagenesis to investigate the contribution of a conserved arginyl residue to the catalytic activity and cofactor affinity of D-serine dehydratase, a model pyridoxal 5′-phosphate (vitamin B_6) enzyme. Replacement of R-120 in the active site peptide of D-serine dehydratase by L decreased the affinity of the enzyme for pyridoxal 5′-phosphate by 20-fold and reduced turnover by 5–8-fold. k_{cat} displayed modified substrate α-deuterium isotope effects and altered dependence on both temperature and pH. Analysis of the pH rate profiles of DSD and the R-120→L variant indicated that R-120 interacts electrostatically with catalytically essential ionizable groups at the active site of wild type D-serine dehydratase. The decrease in cofactor affinity observed for DSD(R120L) was not accompanied by significant perturbations in the UV, CD, or ^{31}P NMR spectrum of the holoenzyme, suggesting that the contribution of R-120 to pyridoxal phosphate affinity may be indirect or else involve an interaction with a cofactor functional group other than the 5′-phosphoryl moiety.

The properties of two other site-directed variants of D-serine dehydratase indicated that the pyridoxal 5′-phosphate:K-118 Schiff base was indifferent to a small change in the shape of the side chain at position 117 (I-117→L), whereas replacement of K-118 by H resulted in undetectable levels of enzyme. A poor ability to bind cofactor may have rendered DSD(K118H) susceptible to intracellular proteolysis.

The model pyridoxal 5′-phosphate (PLP)[1] enzyme D-serine dehydratase removes a potent growth inhibitor of *Escherichia coli* by converting D-serine to pyruvate and ammonia (1, 2). The sequence of the monomeric protein (M_r = 47,920) has been determined by both amino acid and DNA sequence analysis (3, 4), and the substrate and cofactor specificities of DSD as well as the individual steps of the catalytic pathway have been examined in detail (1, 5–14). The only active site residues to have been identified, however, are the PLP-binding lysyl residue at position 118 (3) and 2 conserved glycyl residues (G-279 and G281) that lie in a glycine-rich region required for the structural integrity of the cofactor binding site (4).

Chemical modification studies and x-ray diffraction analysis have shown that several PLP requiring enzymes use arginyl side chains to bind either the 5′-phosphoryl group of the cofactor (γ-aminobutyrate aminotransferase (15), glutamate decarboxylase (16), and glycogen phosphorylase (17, 18) or a carboxylate group of the substrate (aspartate aminotransferase (19), tryptophanase (20, 21), and tryptophan synthetase β-subunit (22). Several lines of evidence suggest that one or more arginyl residues contribute to the PLP binding site of DSD. Chemical modification studies by Kazarinoff and Snell (23) showed that apoDSD is inactivated by the arginine selective reagents, phenylglyoxal and butanedione, but the presence of PLP in DSD holoenzyme affords protection against inactivation. ^{31}P NMR studies of DSD led Schnackerz *et al.* (24, 25) to propose that an arginyl residue interacts with the phosphate group of the cofactor during catalysis, analogous to the situation in aspartate aminotransferase (19).

DSD contains 18 arginyl residues, 15 of which lie in a portion of DSD (residues 61–431) that shares homology with three different threonine dehydratases; biosynthetic and biodegradative L-threonine dehydratase from *E. coli* and yeast biosynthetic L-threonine dehydratase (3, 4, 26–28). Overall sequence homology between these four proteins ranges from 22–28%, whereas specific subregions display up to 83% homology. Among these subregions are the sequence surrounding the PLP-binding lysine and a glycine-rich region about 120 residues downstream of the PLP binding site (4, 26). Arginine is conserved at only one position in the four enzymes; however, at a site 2 residues to the carboxyl side of the PLP-binding lysyl residue (K-118 of DSD). The conservation of R-120 during evolution, its strategic placement near the active site lysine, the general implications of the ^{31}P NMR and DSD chemical modification studies (23–25), and the observation that an arginyl residue (R-266) near active site K-258 of aspartate aminotransferase forms an important ion pair with the PLP phosphoryl group (19), together suggested that R-120 of DSD might play a role in cofactor binding and/or catalysis.

Site-directed mutagenesis offered a particularly attractive approach to investigate the role of R-120. DSD is one of the few monomeric PLP enzymes. Thus, structure/activity relationships can be evaluated without the complication of subunit-subunit interactions or the presence of multiple, heterogeneous PLP binding sites (1, 2). In this report, we describe

* This work was supported by Grant HL32006 from the National Institutes of Health. Part of this work is taken from a Ph.D. thesis to be submitted by M. M. to the Graduate School of The University of Michigan. The costs of publication of this article were defrayed in part by the payment of page charges. This article must therefore be hereby marked "*advertisement*" in accordance with 18 U.S.C. Section 1734 solely to indicate this fact.

‡ To whom correspondence and reprint requests should be addressed.

[1] The abbreviations used are: PLP, pyridoxal 5′-phosphate; DSD, D-serine dehydratase; DTT, dithiothreitol; EA, 2-hydroxyethylamine; MOPS, 3-(*N*-morpholino)propanesulfonic acid; GLY, glycine; DSD:PLP and PLP:GLY denote the Schiff base formed between PLP and K-118 of DSD and GLY, respectively. The single letter abbreviations for amino acid residues appear in **bold type**.

the replacement of **R**-120 by **L** and the effect of the substitution on the cofactor affinity, spectral properties, and catalytic activity of DSD. DSD(**R**120**L**) shows a 5–8-fold decrease in k_{cat} and an altered dependence of k_{cat} on both temperature and pH. Comparison of the pH rate profiles of the wild type enzyme and the **R**→**L** variant suggests that electrostatic interactions exist between **R**-120 and catalytically essential ionizable groups at the active site of wild type DSD. Additionally, **R**-120 enhances the affinity of the active site for PLP about 20-fold and appears to do so without direct electrostatic interaction with the 5′-phosphoryl group of the cofactor.

MATERIALS AND METHODS

Chemicals and Enzymes—DTT and PLP were ordered from Calbiochem or Boehringer Mannheim. EA and β-mercaptoethanol were purchased from Aldrich. D-Serine, L-serine, D-threonine, L-threonine, isoserine, MOPS, EDTA, ampicillin, and glycine were ordered from Sigma. Syntheses of D- and L-[2-^{2}H]serine, D-*allo*-threonine, D-[2-^{2}H]threonine, and D-[2-^{2}H]*allo*-threonine have been described (13). ^2H_2O were obtained from ICN Biochemicals, Inc. Tryptone and yeast extract for culture media were purchased from Difco. Restriction enzymes, T_4 DNA ligase, polynucleotide kinase, and DNA polymerase I Klenow fragment were obtained from New England Biolabs, and [α-^{35}S]thio-dATP (>1000 mCi/mmol) and [γ-^{32}P]ATP (>1000 mCi/mmol) were purchased from Amersham. All other reagents were analytical grade.

Bacterial Strains, Plasmids, and Bacteriophages—Expression plasmid pTC-21 (ampR *dsdA*+) used as the template for mutagenesis contains the structural gene for wild type DSD (*dsdA*) fused to the *tac* promoter of plasmid ptac12 (4). Derivatives of pTC-21 created by mutagenesis were designated pTC-R120L, pTC-K118H, and pTC-I117L to denote the DSD amino acid replacement. Bacteriophage M13mp19 used for subcloning and sequencing of mutagenized *dsdA* was purchased from Bethesda Research Laboratories, and *E. coli* JM101 (*supE thi lac- proAB F′ traD36 lacIqZ M15*) used as the host strain for both plasmids and M13 phage derivatives was the generous gift of Dr. Dale Oxender (University of Michigan). Cultures were grown in LB medium (29) or LB supplemented with 45 μg/ml ampicillin.

Recombinant DNA Procedures—The *in vitro* recombinant DNA techniques outlined by Maniatis *et al.* (29) were used for routine DNA manipulations. Dideoxy sequencing was performed with Sequenase (United States Biochemical Corp.), using the protocol supplied with the enzyme. The mutagenic oligonucleotides shown in Fig. 1 were synthesized on an Applied Biosystems Model 380A DNA synthesizer, purified by preparative gel electrophoresis and 5′-phosphorylated with polynucleotide kinase prior to use.

Site-directed mutagenesis was performed by the plasmid heteroduplex method described by Inouye and Inouye (30). Plasmid pTC-21 was linearized with *Pst*I or treated with *Eco*RI and *Ava*I and purified by gel electrophoresis to remove a 0.7-kilobase pair target region prior to heat denaturation and annealing of the mutagenic oligonucleotide. JM101 transformants were screened for the presence of the mutation by colony hybridization to the appropriate ^{32}P-labeled oligonucleotide mutagen (30). Plasmid DNA was purified from clones that gave a positive hybridization signal, and the 0.7-kilobase pair *Eco*RI/*Ava*I target fragment was isolated and sequenced in both directions. After verifying that only the desired nucleotide change was present, the fragment was subcloned back into pTC-21 from which the corresponding wild type 0.7-kilobase pair *Eco*RI/*Ava*I fragment had previously been removed. The resulting expression plasmids, pTC-R120L, pTC-K118H, and pTC-I117L, were used to produce the DSD protein variants in JM101.

Enzyme Purification and Steady State Kinetics—Enzymes were purified in the presence of 80 μM PLP and assayed for activity with D-serine as previously described (4). k_{cat} and K_m for D-serine, D-threonine, D-*allo*-threonine, L-serine, and their deuterated counterparts were determined from the dependence of the initial velocity on substrate concentration at 25 °C in 0.1 M potassium phosphate, 4 μM PLP, pH 7.8, as described by Federiuk *et al.* (13) and by Wilkinson (31). The dependence of k_{cat} on temperature (at pH 7.8) and pH (at 25 °C) was measured in buffered solutions (0.1 M potassium phosphate, pH 6–7.8, 0.03 M potassium pyrophosphate, pH 7.8–9.4, containing sufficient potassium chloride to maintain an ionic strength of 0.30) containing 17–18 nM DSD or DSD(R120L) and 40 μM PLP. At each pH or temperature, k_{cat} was determined with two concentrations of D-serine (11.9 mM and 23.8 mM) to confirm saturating levels of substrate. At pH values 6.0 and 9.4 and temperatures of 35 °C and 45 °C, k_{cat} was also measured at two concentrations of PLP (20 μM and 40 μM) to determine whether a decrease in reaction velocity might be attributed to cofactor dissociation from the enzyme. All kinetic measurements were recorded on a GCA McPherson spectrophotometer equipped with a water-circulated cell holder and temperature probe.

Determination of K_P and K_{PG}, the Equilibrium Constants for Dissociation of PLP and PLP:GLY from DSD—K_P and K_{PG} were determined in 0.1 M potassium phosphate, 10 mM EDTA, 5 mM DTT, pH 7.8, as previously described (32). Incubation mixtures for K_P determinations contained 100 μl of ~150 μM DSD(R120L) and 11 μl of 1–2 M EA. Incubation mixtures for K_{PG} determinations consisted of 100 μl of enzyme, 0.2–0.5 M glycine, and 0.1 M EA (total volume 110–115 μl). Free and enzyme-bound PLP were separated by the spun column method following a 2–3-h incubation at room temperature (4, 33).

Spectral Measurements—UV and CD spectra were recorded under the conditions previously described for analysis of DSD variants DSD(G279D) and DSD(G281D) (32). Enzyme samples for ^{31}P NMR spectroscopy (175–200 μM in a total volume of ~1.0 ml) were equilibrated in 50 mM MOPS, 2 mM EDTA, 1 mM DTT adjusted to pH 6.6 or pH 7.8 (±) 0.02 with 1 M HCl or 1 M NaOH. Buffers for NMR spectroscopy were treated with Chelex 100 (100–200 mesh, Bio-Rad) prior to use, and 1% ^2H_2O was added as a deuterium lock signal. The pH of the sample was checked before and after obtaining each NMR spectrum. UV spectra and assays of enzyme activity confirmed that both enzymes were catalytically competent in each of the buffers employed for the NMR experiments.

^{31}P NMR spectra were recorded at 25 °C on a General Electric GN500 NB spectrometer using the ^{31}P chemical shift of 85% H_3PO_4 as an external reference. Samples were placed in 10-mm flat bottom NMR tubes fitted with a Teflon plug and observed at 202 MHz using a 10-mm broad band probe. Pulse widths were less than or equal to 60°, and the recycle time was about 1 s. 30,000 to 80,000 acquisition scans (8,192 data points) were recorded over a spectral width of 8,000 Hz. Data were processed with an added exponential line broadening of 13 Hz, assuming a Lorentzian line shape for the purpose of curve and line width analyses and the deconvolution program (General Electric GENCAP program). GENCAP was run on a Nicolet 1280 computer.

RESULTS AND DISCUSSION

The sequences of the oligonucleotide mutagens used to produce the DSD variants DSD(**R**120**L**), DSD(**I**117**L**), and DSD(**K**118**H**) are shown in Fig. 1. Expression vector ptac12 was used for mutagenesis of a 1.5-kilobase pair *dsdA* insert by the heat denaturation/reannealing technique (30) and for subsequent expression of the variant DSD proteins in *E. coli* JM101. The desired mutations were identified by colony

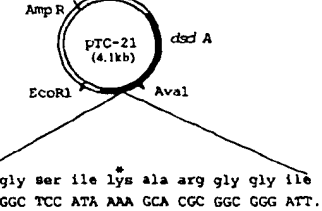


```
Wild type sequence        ser gly ser ile lys ala arg gly gly ile
      (DSD 114-123) 5'.. TCC GGC TCC ATA AAA GCA CGC GGC GGG ATT...3'
Replacement:
       ile117-->leu       3'...G AGG AAT TTT CGT GCG C...5'
       lys118-->his       3'...G AGG TAT GTA CGT GCG C...5'
       arg120-->leu             3'...TTT CGT GAG CCG CCC T...5'
```

FIG. 1. **Oligonucleotide-directed mutagenesis of *dsdA*.** Expression plasmid pTC-21 (4) is a derivative of ptac12 containing a 1.5-kilobase pair *Rsa*I/*Hin*cII fragment encoding wild type DSD. DSD is expressed upon induction of the *tac* promoter (indicated by the *arrow*) with isopropyl-1-thio-β-D-galactopyranoside. Variants of pTC-21 were created as described under "Materials and Methods" using the oligonucleotides shown above. The PLP-binding lysine in the wild type amino acid sequence is marked with an *asterisk*, and the nucleotide substitution(s) introduced by mutagenesis are *underlined*.

hybridization of JM101 transformants to the appropriate ^{32}P-labeled oligonucleotide mutagen and confirmed by DNA sequencing. DSD(**R120L**) and DSD(**I117L**) were expressed at levels comparable to the wild type enzyme (~7–8% of the soluble protein (4)) and were purified to >95% homogeneity as judged by 9% reducing sodium dodecyl sulfate-polyacrylamide gel electrophoresis. Both co-migrated with wild type DSD at an M_r of ~48,000. DSD(**K118H**) protein was not detected. Since wild type apoDSD is known to be susceptible to proteolysis (1, 5), it is possible that apoDSD(**K118H**) was unable or only poorly able to bind PLP and was thus rendered susceptible to intracellular degradation.[2] The cofactor affinity, spectral properties, and catalytic activity of purified DSD(**I117L**) were identical with those of wild type DSD. Since PLP binding and catalytic activity are extremely sensitive to subtle perturbations in *cofactor* structure (5, 6, 14), the indifference of PLP:**K**-118 to the shape of the adjacent side chain suggests that **K**-118 exists in an extended conformation similar to that determined for aspartate aminotransferase (19) and glycogen phosphorylase (18), wherein the lysyl-linked cofactor lies outside of van der Waals contact with **I**-117.

R-120 contributes both to cofactor affinity and to DSD catalysis, although it does not appear to be an essential residue. Replacement of **R**-120 by **L** yielded a partially active enzyme that displayed a 20-fold decrease in affinity for PLP. The equilibrium constant (K_P) for the dissociation of PLP from DSD(**R120L**) was 2.4 (± 0.4) μM *versus* 0.12 (± 0.01) μM for wild type DSD. This finding strongly suggests that **R**-120 contributes to PLP binding, either through direct interaction with the cofactor or by stabilizing a protein conformation that enhances the affinity of the active site for PLP. The spectral properties of the variant did not distinguish between these possibilities, however. The UV and CD spectra of DSD (**R120L**) were similar to those of wild type DSD, suggesting that the variant binds PLP via the normal Schiff base linkage and retains those noncovalent interactions responsible for constraining the imine-linked cofactor asymmetrically. Direct electrostatic interaction between **R**-120 and the 5′-phosphoryl group of PLP appears unlikely. The ^{31}P NMR spectra of the variant and wild type holoenzymes were virtually indistinguishable at both pH 6.6 and pH 7.8, suggesting that the pK of the phosphate (~6.2 (24)) was unperturbed by the **R**→**L** replacement.

It was possible that **R**-120 contributed importantly to PLP binding only during catalysis, when the covalent linkage between cofactor and protein is broken. Schnackerz *et al.* (24, 25) have proposed that transimination, the initial catalytic step wherein the PLP:**K**-118 Schiff base is transferred to the α-amino group of an incoming substrate amino acid, induces formation of a salt linkage between the phosphate group of PLP and an arginyl residue. This noncovalent linkage then anchors the cofactor:amino acid Schiff base to the active site during catalysis (24). We were thus particularly interested in determining how the **R**→**L** replacement affected several parameters associated with the transimination process.

Previous studies have shown that wild type DSD displays a 10-fold increase in fluorescence upon transimination by several α-amino acids (36). This characteristic fluorescence enhancement has been attributed to the conformational change required to expel the active site lysyl residue and lock the newly formed PLP:amino acid Schiff base into the active site for catalysis (13, 36). In addition, the equilibrium constant (K_{PXi}) for dissociation of the PLP:amino acid Schiff base from the active site quantifies the strength of the noncovalent interactions that bind the transimination complex to the active site (32, 36, 37). If **R**-120 formed an important interaction with the PLP phosphoryl group or the substrate carboxyl group upon transimination, then loss of this anchoring interaction in the **R**→**L** variant should be reflected in an increased value of K_{PXi} (relative to K_P) and a decrease in substrate-induced fluorescence. In the presence of the amino acid glycine, however, the degree of fluorescence enhancement was similar to that observed for wild type DSD and the ability of DSD(**R120L**) to bind the PLP:glycine Schiff base via noncovalent interactions was not selectively impaired.[3] The ratio of the equilibrium constant (K_{PG}) for dissociation of PLP:GLY and the equilibrium constant (K_P) for dissociation of *un*complexed PLP was ~2.8 for wild type DSD (K_{PG}:K_P = 0.34 μM/0.12 μM) and ~1.5 for the variant (3.7 μM/2.4 μM).[4] Thus, the **R**→**L** replacement did not impair the ability of the active site to retain PLP:GLY by noncovalent interactions to a greater extent than the replacement impaired the binding of uncomplexed PLP (via both covalent and noncovalent interactions). If an arginyl residue does serve to anchor the PLP phosphate group or the carboxyl group of a substrate amino acid upon transimination, the fluorescence properties of DSD(**R120L**) and the K_{PG}:K_P ratio suggest that it is not the single arginine conserved between the threonine dehydratases and DSD.

The turnover number of DSD(**R120L**) is about 5-fold lower than that of wild type DSD with the substrates D-serine, L-serine, and D-threonine and about 8-fold lower with D-*allo*-threonine (Table I). The decrease in k_{cat} may reflect perturbation of one or more of the rate and equilibrium constants that define a catalytic pathway involving at least 10 discrete steps and 9 enzyme-bound intermediates. The magnitude of a substrate α-deuterium isotope effect on k_{cat} yields an estimate of the degree to which one of these steps, removal of the substrate proton at C-2, limits turnover (13). Previous studies have shown that this isotope effect, as well as the rate-determining step(s) in catalysis, vary with the substrate (13). For example, the isotope effect of 1.1 for D-serine and D-threonine (Table I) indicates that removal of the C-2 proton from these substrates is considerably faster than the step(s) limiting their rate of conversion to products. The corresponding values of 1.3 and 1.4 observed for DSD(**R120L**) suggest that a step or steps other than removal of the C-2 proton must account for the 5-fold decrease in k_{cat} observed for D-serine and D-threonine. Replacement of **R**-120 by **L** did significantly alter the α-deuterium isotope effect on k_{cat} for the DSD substrates D-*allo*-threonine and L-serine, however (Table I). The isotope effect on k_{cat} for L-serine decreased from a near maximum value of 8.7 to 5.2, indicating that

[2] It is interesting to note that an active site variant of *E. coli* aspartate aminotransferase in which the active site lysine was changed to alanine yielded a stable protein that retained the ability to bind PLP via noncoalent interactions (34, 35). Replacement of **K**-118 by a residue that minimally perturbed the structure of the DSD active site might similarly permit retention of PLP by noncovalent interactions. An active site variant of this type would be useful for quantifying the contribution of the Schiff base linkage to the overall affinity of the active site for PLP and the contribution of **K**-118 to catalysis.

[3] Unlike the PLP:D-serine Schiff base, the enzyme-bound PLP:glycine transimination complex is not further processed by DSD (36). This feature permits both fluorescence spectra and determination of the equilibrium constant (K_{PG}) for dissociation of PLP:GLY from the active site (32, 36).

[4] The small reduction in the affinity of both proteins for the PLP:amino acid complex relative to their affinity for PLP suggests that loss of the covalent linkage upon transimination is not fully compensated for by an increase in noncovalent interactions between DSD and the PLP:amino acid Schiff base (32, 37).

TABLE I

Steady state kinetic parameters and C-2 deuterium isotope effects for DSD and DSD(R120L)-catalyzed reactions

Substrate C-2 deuterium isotope effects for k_{cat} and K_m are given in parentheses as the quotient of k_{cat} or K_m for substrate with a hydrogen at C-2 and the corresponding value for substrate with a deuterium atom at C-2. All measurements were performed in 0.1 M potassium phosphate, 4 μM PLP, pH 7.8, 25 °C, as described under "Materials and Methods."

Substrate	k_{cat}		K_m		$10^3 \times k_{cat}/K_m$		k_{cat}/K_m[a]	
	Wild type	R120L	Wild type	R120L	Wild type	R120L	Wild type	R120L
	s^{-1}		mM		$M^{-1}\,s^{-1}$			
D-Serine	105 (1.1)	23 (1.3)	0.38 (0.9)	0.17 (1.3)	280	135	1.0	1.0
D-Threonine	14 (1.1)	2.5 (1.4)	0.77 (0.7)	0.87 (0.8)	18	2.8	0.065	0.021
D-*allo*-Threonine[b]	0.85 (3.7)	0.10 (7.2)	1.3 (0.5)	1.0 (0.5)	0.66	0.10	2.3×10^{-3}	7.4×10^{-4}
L-Serine	0.10 (8.7)	0.021 (5.2)	3.5 (1.1)	4.5 (0.7)	0.031	5.0×10^{-3}	1.1×10^{-4}	3.7×10^{-5}

[a] Relative to D-serine.

[b] The k_{cat} and K_m for wild type DSD are 2-fold less than those previously reported for this substrate (13). The reason for the discrepancy is not clear.

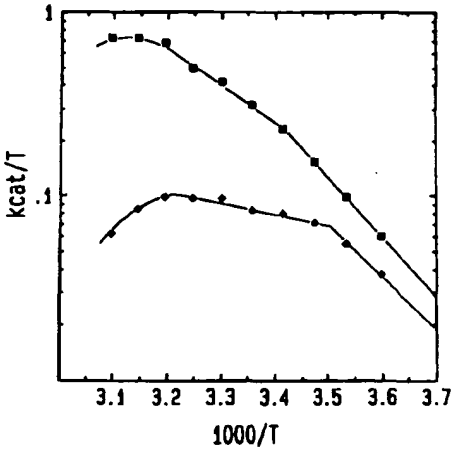

FIG. 2. **Temperature dependence of k_{cat} for DSD and DSD(R120L).** Initial velocity was measured in 0.1 M K_2HPO_4, 40 μM PLP, pH 7.8, as described under "Materials and Methods." The values of k_{cat} were not affected by halving the PLP concentration or the D-serine concentration. □, DSD; ◇, DSD(R120L)).

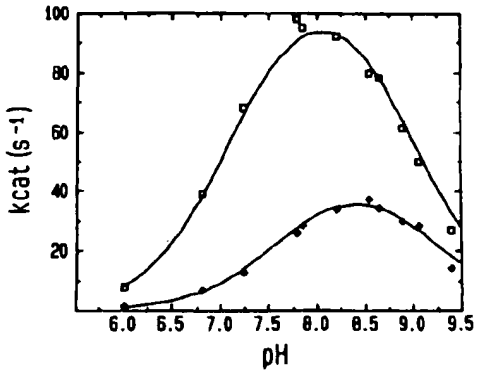

FIG. 3. **pH dependence of k_{cat} for DSD and DSD(R120L).** k_{cat} for each pH value was determined by measuring initial velocity at 25 °C immediately after diluting a stable (pH 7.8) stock solution of enzyme into the assay buffer, as described under "Materials and Methods." The values of k_{cat} were not affected by doubling the PLP concentration or the D-serine concentration. The data were fitted to a model for ionization (Equation 1) assuming that (i) the reactivity of DSD and DSD(R120L) are controlled by the protonation state of two ionizable groups, and (ii) enzymic activity requires protonation of one group and deprotonation of the second. The *solid lines* were determined by Equation 1 with k_{cat}, pK_1, and pK_2 set to 115, 7.1, and 9.0 for DSD and 47, 7.6, and 9.2 for DSD(R120L). □, DSD; ◇, DSD(R120L).

removal of the α-proton, normally the slowest step in the conversion of L-serine to pyruvate and ammonia, is considerably faster (relative to the other steps) in catalysis of this substrate by DSD(R120L). In contrast, the R→L replacement significantly reduced the relative efficiency of proton removal from D-*allo*-threonine, as shown by the doubling of the isotope effect on k_{cat} (3.7→7.2). These findings suggest that the 5–8-fold decrease in turnover number observed for DSD(R120L) reflects *differential* perturbation of one or more rate-controlling steps of catalysis rather than a uniform decrease in the efficiency of all the steps, as might be expected if there existed a larger proportion of enzyme in a catalytically inactive conformation. If the latter were true, the active fraction of DSD(R120L) should proceed through the catalytic cycle in a normal fashion and display isotope effects identical with those of wild type enzyme.

The temperature dependence of k_{cat} can be described by the linear relationship

$$\ln k_{cat}/T = -\Delta H\dagger/RT + \Delta S\dagger/R - \ln kT/h$$

for the simple case in which the rate-controlling step does not change with temperature (where k, h, $\Delta H\dagger$, and $\Delta S\dagger$ represent Boltzmann's constant, Planck's constant, and the standard enthalpy and entropy of activation, respectively). The nonlinear Eyring plots for the temperature dependence of k_{cat} for DSD and DSD(R120L) shown in Fig. 2 suggest that both enzymes undergo a change in the rate-determining step with temperature. The break in the curve occurs around 19 °C for the wild type enzyme and 13 °C for the variant. In the physiological temperature range (~19–40 °C), the rate-determining step for the conversion of D-serine to pyruvate and ammonia is normally the decomposition of the enamine intermediate α-aminoacrylate (10). Interestingly, the lower slope of the curve for DSD(R120L) in this temperature range indicates that the R→L replacement favorably affected the activation enthalpy for this step (Fig. 2). Alternately, the rate-determining step itself may have changed to one with a lower activation enthalpy. Among the simplest explanations for the favorable effect of the amino acid replacement on activation enthalpy is the loss of a hydrogen bond or other interaction in DSD(R120L) that must be broken in the wild type enzyme (or *E*:S complex) before catalysis can occur. Since the replacement has a favorable effect on activation enthalpy, but an overall negative effect on the turnover number, the increase in activation *energy* ($\Delta G\dagger$) must reflect a less favorable entropy of activation for DSD(R120L). Although hydration volume and other factors can significantly influence $\Delta S\dagger$ (38),

the unfavorable change in activation entropy might reflect loss of an interaction that contributes to proper orientation of enzyme and substrate for reaction.

In contrast to the altered activation enthalpy observed for DSD(**R120L**) in the physiological temperature range, the parallel curves observed in the range from 0–13 °C suggest that the **R→L** replacement did not alter the activation enthalpy for catalysis at low temperature (Fig. 2). The displacement of the *y*-intercept for DSD(**R120L**) again indicates a less favorable activation entropy for reaction, however. The thermal stability of DSD was not significantly perturbed by the **R→L** replacement, with denaturation occurring ~40 °C in each case (Fig. 2).[5]

Comparison of the pH rate profiles of DSD and DSD(**R120L**) suggests that a major contribution of **R**-120 to the catalytic efficiency of DSD is the influence of its positive charge on the pK values of catalytically essential residues (Fig. 3). The pH optimum for catalysis of D-serine shifted from 8.0 for wild type DSD to 8.5 for DSD(**R120L**). To quantify the effect of the **R→L** replacement on the ionization state of catalytically important groups, the data in Fig. 3 were fitted to Equation 1, which assumes that (i) the reactivity of the enzyme:substrate complex is controlled by the protonation state of two ionizable groups, and (ii) in the active form of the enzyme:substrate complex, one of the groups must be protonated and one deprotonated:

$$k_{cat} = k^{\circ}_{cat}/(1 + [H]/K_1 + K_2/[H]) \quad (1)$$

where k°_{cat} is the value of k_{cat} when the ionizable groups affecting activity are in their catalytically active prototropic states and K_1 and K_2 are the acid dissociation constants of the two groups.[6] The fit of Equation 1 to the observed pH dependence of k_{cat} indicates that the **R**-120→**L** replacement increased pK_1 from 7.1 to 7.6 and pK_2 from 9.0 to 9.2. The simplest explanation for these pK perturbations is close proximity of the side chain at position 120 to the catalytically important groups, a structural arrangement that would allow electrostatic interaction between **R**-120 and these ionizable groups at the active site of wild type DSD.

In summary, our results indicate that the single arginyl residue that is conserved between DSD and the threonine dehydratases contributes both to DSD catalysis and to cofactor affinity, but is not an essential residue. **R**-120 enhances the affinity of the active site for PLP about 20-fold, but does not appear to interact with the 5′-phosphate group of PLP or the carboxyl group of a PLP:amino acid substrate complex. DSD(**R120L**) displayed a 5–8 fold reduction in turnover, altered substrate α-deuterium isotope effects, and altered dependencies of k_{cat} on temperature and pH. The specific perturbations indicate that the **R→L** replacement (i) differentially rather than uniformly perturbed the efficiency of rate-controlling steps, (ii) lowered the activation enthalpy for catalysis, either by decreasing $\Delta H\dagger$ for the step that normally controls turnover or else by changing the rate-determining step, and (iii) increased the pK values of at least two catalytically essential ionizable groups. Further studies are underway to establish the identify and function of these ionizable groups.

[5] Consistent with this interpretation, the initial velocity of product formation rapidly decreased with time when the enzymes were incubated above 40 °C.

[6] Equation 1 is an oversimplification of the pH dependence of k_{cat}, since it neglects the possibility that changes in the rate-determining step with pH could perturb the values of K_1 and K_2 (39).

REFERENCES

1. Dowhan, W., Jr., and Snell, E. E. (1970) *J. Biol. Chem.* **245**, 4618–4628
2. Maas, W. K., and Davis, B. D. (1950) *J. Bacteriol.* **60**, 733–745
3. Schiltz, E., and Schmitt, W. (1981) *FEBS Lett.* **134**, 57–62
4. Marceau, M., McFall, E., Lewis, S. D., and Shafer, J. A. (1988) *J. Biol. Chem.* **263**, 16926–16933
5. Dowhan, W., Jr., and Snell, E. E. (1970) *J. Biol. Chem.* **245**, 4629–4635
6. Groman, E., Huang, Y. Z., Watanabe, T., and Snell, E. E. (1972) *Proc. Natl. Acad. Sci. U. S. A.* **69**, 3297–3300
7. Schonbeck, N. D., Skalski, M., and Shafer, J. A. (1975) *J. Biol. Chem.* **250**, 5352–5358
8. Reed, T. A., and Schnackerz, K. D. (1979) *Eur. J. Biochem.* **94**, 207–214
9. Ehrlich, J. H., and Schnackerz, K. D. (1973) *Hoppe-Seyler's Z. Physiol. Chem.* **354**, 1183–1184
10. Schnackerz, K. D., Ehrlich, J. H., Griesemann, W., and Reed, T. A. (1979) *Biochemistry* **18**, 3557–3563
11. Yang, I. Y., Huang, Y. A., and Snell, E. E. (1975) *Fed. Proc.* **34**, 496
12. Cheung, Y.-F., and Walsh, C. (1976) *J. Am. Chem. Soc.* **98**, 3397–3398
13. Federiuk, C. S., Bayer, R., and Shafer, J. A. (1983) *J. Biol. Chem.* **258**, 5379–5385
14. Morino, Y., and Snell, E. E. (1967) *Proc. Natl. Acad. Sci. U. S. A.* **57**, 1692–1699
15. Tunnicliff, G. (1980) *Biochem. Biophys. Res. Commun.* **97**, 160–165
16. Cheung, S. T., and Fonda, M. (1979) *Arch. Biochem. Biophys.* **198**, 541–547
17. Oikonomakos, N. G., Johnson, L. N., Acharya, K. R., Stuart, D. I., Barford, D., Hajdu, J., Varvill, K. M., Melpidou, A. E., Papageorgiou, T., Graves, D. J., and Palm, D. (1987) *Biochemistry* **26**, 8381–8389
18. Madsen, N. B., and Withers, S. G. (1986) in *Vitamin B_6: Pyridoxal Phosphate* (Dolphin, D., Poulson, R., and Avramovic, O., eds) pp. 356–389, John Wiley & Sons, New York
19. Torchinsky, U. M. (1986) in *Vitamin B_6: Pyridoxal Phosphate* (Dolphin, D., Poulson, R., and Avramovic, O., eds) pp. 170–221, John Wiley & Sons, New York
20. Schnackerz, K. D., and Snell, E. E. (1983) *J. Biol. Chem.* **258**, 4839–4841
21. Kazarinoff, M. N., and Snell, E. E. (1977) *J. Biol. Chem.* **252**, 7598–7602
22. Tanizawa, K., and Miles, E. W. (1983) *Biochemistry* **22**, 3594–3603
23. Kazarinoff, M. N., and Snell, E. E. (1976) *J. Biol. Chem.* **251**, 6179–6182
24. Schnackerz, K. D., Feldmann, K., and Hull, W. E. (1979) *Biochemistry* **18**, 1536–1539
25. Schnackerz, K. D., and Feldmann, K. (1980) *Biochem. Biophys. Res. Commun.* **95**, 1832–1838
26. Datta, P., Goss, T. J., Omnaas, J. R., and Patil, R. V. (1987) *Proc. Natl. Acad. Sci. U. S. A.* **84**, 393–397
27. Kielland-Brandt, M. C., Holmberg, S., Petersen, J. G. L., and Nilsson-Tillgren, T. (1984) *Carlsberg Res. Commun.* **49**, 567–575
28. Lawther, R. P., Wek, R. C., Lopes, J. M., Pereira, R., Taillon, B. E., and Hatfield, G. W. (1987) *Nucleic Acids Res.* **15**, 2137–2154
29. Maniatis, T., Fritsch, E. F., and Sambrook, J. (eds) (1982) *Molecular Cloning: A Laboratory Manual*, Cold Spring Harbor Laboratory, Cold Spring Harbor, NY
30. Inouye, S., and Inouye, M. (1987) in *Synthesis and Applications of DNA and RNA* (Narang, S., ed.) pp. 181–206, Academic Press, Orlando, FL
31. Wilkinson, G. N. (1961) *Biochem. J.* **80**, 324–332
32. Marceau, M., Lewis, S. D., and Shafer, J. A. (1988) *J. Biol. Chem.* **263**, 16934–16941
33. Penefsky, H. S. (1979) *Methods Enzymol.* **56**, 527–530
34. Kochhar, S., Finlayson, W. L., Kirsch, J. F., and Christen, P. (1987) *J. Biol. Chem.* **262**, 11446–11448
35. Malcolm, B. A., and Kirsch, J. F. (1985) *Biochem. Biophys. Res. Commun.* **132**, 915–921
36. Federiuk, C. S., and Shafer, J. A. (1983) *J. Biol. Chem.* **258**, 5372–5378
37. Schonbeck, N. D., Skalski, M., and Shafer, J. A. (1975) *J. Biol. Chem.* **250**, 5359–5363
38. Jencks, W. P. (1969) *Catalysis in Chemistry and Enzymology*, McGraw-Hill Book Co., New York
39. Schmidt, D. E., Jr., and Westheimer, F. H. (1971) *Biochemistry* **10**, 1249–1253

STIC-ILL

From: Gabel, Gailene
Sent: Wednesday, February 12, 2003 4:14 PM
To: STIC-ILL
Subject: 09/905,439

Please provide a copy of the following references ASAP:

1) Gillies et al., NMR in Physiology and Biomedicine, Academic Press: San Diego (1994).

2) Yamazaki et al., J. Am. Chem. Soc. 120: 5591-5592 (1998).

3) Severinov et al., J. Biol. Chem. 273: 16205-16209 (1998).

4) Muir et al. (Proc. Natl. Acad. Sci USA, 95: 6705-6710 (1998).

5) Xu et al. Proc. Natl. Acad. Sci., 96: 388-393 (1999).

6) Lippens et al., In NMR in Supramolecular Chemistry, Pons M. Ed., Kluwer Academic Publishers, 191-226 (1999).

Thanks a bunch,
Gail R. Gabel
7B15
CM1
305-0807

THE JOURNAL OF BIOLOGICAL CHEMISTRY
Vol. 273, No. 26, Issue of June 26, pp. 16205–16209, 1998
Printed in U.S.A.

Expressed Protein Ligation, a Novel Method for Studying Protein-Protein Interactions in Transcription*

(Received for publication, February 2, 1998, and in revised form, April 4, 1998)

Konstantin Severinov‡§ and Tom W. Muir¶‖

From the ‡Department of Genetics and Waksman Institute, the State University of New Jersey, Rutgers, Piscataway, New Jersey 08854 and the ¶Laboratory of Synthetic Protein Chemistry, The Rockefeller University, New York, New York 10021

Expressed protein ligation is a novel protein semi-synthesis method that permits the *in vitro* ligation of a chemically synthesized C-terminal segment of a protein to a recombinant N-terminal segment fused through its C terminus to an intein protein splicing element. In principle, the practical convenience of this method, combined with the expanded opportunities in protein engineering that it provides, makes it well suited for probing the molecular basis of complex processes such as transcription. Here we describe the successful application of expressed protein ligation to the ~600 amino acid σ^{70} subunit of *Escherichia coli* RNA polymerase. The resulting semi-synthetic σ^{70} constructs are shown to be fully functional and have been used to map the binding region of the bacteriophage T4 anti-sigma protein, AsiA, to within amino acids 567–600 of σ^{70}. The success of these semi-synthesis studies sets the stage for the future generation of semi-synthetic σ^{70} molecules in which unnatural amino acids and biophysical probes are site-specifically incorporated in the RNA polymerase complex.

It is becoming increasingly clear that regulation of transcription involves protein-protein contacts between RNA polymerase and transcription factors (1). Characterization of these interactions, at the molecular level, is a prerequisite to fully understanding transcription mechanism and regulation. The ability to site-specifically incorporate unnatural amino acids (containing biophysical or biochemical probes) into the protein components of the transcription apparatus would greatly aid the study of these complex macromolecular machines.

Recent years have seen the development of a number of methods designed to allow the incorporation of unnatural amino acids into proteins (2–6). These approaches include *in vitro* protein expression (3), site-specific protein modification (4, 5), and protein total synthesis (6). Although powerful, each of these techniques has associated with it certain practical or synthetic limitations which have to some extent restricted their widespread application. Total chemical synthesis, which provides unparalleled freedom to manipulate protein structure, has been dominated in recent years by the use of chemical ligation techniques (7–13). Among these, the "native chemical ligation" approach by Kent *et al.* (14) has proven a particularly useful route to synthetic proteins. In this process, an N-terminal cysteine-containing peptide is chemically ligated to a peptide possessing a C-terminal thioester group with the resultant formation of a normal peptide bond at the ligation site. Despite the generality of the ligation chemistry, the strategy has been constrained by the need to generate the peptide building blocks using stepwise solid phase peptide synthesis (SPPS).[1] The size limitations imposed by this requirement have restricted the application of native chemical ligation to the study of small proteins and protein domains (6).

Protein semi-synthesis, in which synthetic peptides and protein cleavage fragments are linked together, offers an attractive route to the generation of large protein analogs containing unnatural amino acids (15). The utility of existing semi-synthesis strategies is, however, tempered by the need to have unique chemical or enzymatic cleavage sites at the appropriate position within the protein of interest. The recently introduced expressed protein ligation technique directly addresses these limitations by providing a general way of chemically attaching synthetic peptides (via a putative native chemical ligation step) to the C terminus of recombinant proteins without the need to perform any intervening fragmentation steps (2). Here we report the results of model studies designed to explore further the chemical mechanism of expressed protein ligation. Insights gained from this preliminary work were then successfully applied to the generation of a functional semi-synthetic version of the 613 residue σ^{70} subunit of *Escherichia coli* RNA polymerase.

EXPERIMENTAL PROCEDURES

Cloning, Expression, and Purification of Proteins—The plasmid pCYB2_$\sigma_{500-566}$, which expresses a 66-amino acid fragment of σ fused to intein-CBD from an isopropyl-1-thio-β-D-galactopyranoside-inducible *trc* promoter, was constructed by polymerase chain reaction amplification of the corresponding fragment of *rpoD* and recloning it in *Nde*I-*Sma*I-treated plasmid pCYB2 (New England Biolabs). A linker of two non-natural amino acids (Ala-Gly) was inserted between the last amino acid of σ (Ile^{566}) and Cys^1 of the intein. pCYB2_σ_{1-566} was constructed similarly. The natural *Nde*I site at codon 452 of *rpoD* was removed by site-directed mutagenesis to facilitate the cloning. The protein sequence remained the same due to degeneracy of the genetic code. The plasmids were transformed into the *E. coli* XL1-blue; cells were grown to mid-log phase in 2 liters of LB medium plus 200 μg of ampicillin/ml and induced with 1 mM isopropyl-1-thio-β-D-galactopyranoside overnight. The expression level was low (~1 mg/liter), and we could barely detect the band of the overexpressed proteins on SDS gels.

After recovery by centrifugation, cells were resuspended in 40 ml of

* This work was supported by Burroughs Wellcome Fund Career award in the Biomedical Sciences, and the start up funds from the Waksman Institute (to K. S.), National Institutes of Health Grant GM55843-01 (to T. W. M), and by a Pew Scholarship in the Biomedical Sciences (to T. W. M). The costs of publication of this article were defrayed in part by the payment of page charges. This article must therefore be hereby marked "*advertisement*" in accordance with 18 U.S.C. Section 1734 solely to indicate this fact.

§ To whom correspondence may be addressed: Waksman Institute, Rutgers, the State University of New Jersey, 190 Frelinghuysen Rd., Piscataway, NJ 08854.

‖ To whom correspondence may be addressed: Rockefeller University, 1230 York Ave., New York NY 10021.

[1] The abbreviations used are: SPPS, solid phase peptide synthesis; His_6-tag, hexahistidine-tag; PAGE, polyacrylamide gel electrophoresis; NTA, nitrilotriacetic acid; HPLC, high pressure liquid chromatography; Fmoc, *N*-(9-fluorenyl)methoxycarbonyl.

50 mM Tris-HCl, 500 mM NaCl, 10 mM EDTA, pH 7.9, and lysed by passage through a French press, and the lysate was cleared by low speed centrifugation. The overexpressed proteins were recovered from the cytosolic fraction by affinity chromatography on a 2-ml chitin column equilibrated in the same buffer as suggested by the manufacturer. The column was washed with 50 ml of buffer, and 25 ml of 0.2 M phosphate buffer, pH 7.3, 0.2 M NaCl and drained, and the beads were stored as a 50% suspension in the same buffer at 4 °C until further use.

AsiA was purified as described by Severinova *et al.* (16). Plasmid expressing AsiA genetically fused to a C-terminal promoter was provided by D. Hinton. The protein was overexpressed in BL21(DE3) cells and purified to homogeneity by IMAC. AsiA proteins were concentrated using a Centricon 3 centrifugal filter (Amicon) and stored at −20 °C in a buffer containing 50% glycerol.

Synthesis of Peptides—All peptides were chemically synthesized according to optimized *t*-butyloxycarbonyl SPPS (17) and purified by preparative reverse-phase HPLC using a Vydac C-18 column. In all cases, peptide composition and purity were confirmed by electrospray mass spectrometry and analytical HPLC. Fluorescein was attached to the ϵ-amino group of the lysine residue in the peptide NH_2-CEDNEYTARE-aminocaproate-K-CO_2H prior to the the final cleavage/deprotection step using a *t*-butyloxycarbonyl-Lys-ϵ-(NH-Fmoc) orthogonal protection strategy. The construct His_6-Cys-[SCH_2]-aminocaproate-$\sigma_{568-600}$ was prepared by chemically ligating the purified, unprotected peptides NH_2-His_6-Cys-CO_2H and bromo-acetyl (BrAc)aminocaproate-$\sigma_{568-600}$ using the previously described thioether-based chemical ligation strategy (11).

Protein Ligation—100–500 μl of 50% chitin bead suspension was combined with various cofactors in the presence or in the absence of 1 mM synthetic peptide. Cofactors were used at 100 mM concentration (dithiothreitol, mercaptoacetic acid, *N*-acetylcysteine, and cysteine) and 1.5% v/v (thiophenol). Reactions were performed in 0.2 M phosphate buffer, pH 7.3, 200 mM NaCl (dithiothreitol, thiophenol, and cysteine), or 0.5 M phosphate buffer, pH 7.3 (*N*-acetylcysteine and mercaptoacetic acid). All reactions were incubated overnight with gentle agitation and then diluted 10-fold with transcription buffer (20 mM Tris-HCl, pH 7.9, 100 mM KCl, 10 mM $MgCl_2$). Model experiments involving $\sigma_{500-566}$ were carried out at room temperature. Experiments involving σ_{1-566} were carried out in the cold room, and all buffers were supplemented with 1 mM phenylmethylsulfonyl fluoride to minimize proteolytic degradation. The beads were allowed to settle, and the supernatant was dialyzed against two 1-liter changes of transcription buffer. The protein was then concentrated on a C-30 concentrator (Amicon) to ~1 mg/ml, diluted 2-fold with glycerol, and stored at −20 °C.

Ni-NTA Binding—100-μl reactions contained 15 μl of Ni^{2+}-NTA-agarose (Quigen), 50–100 pmol of σ^{70} or σ^{70} derivative, 200 pmol of $AsiA_{His}$, 20 mM Tris-HCl, pH 7.9, 100 mM KCl, 10 mM $MgCl_2$. Reactions were preincubated for 15 min at room temperature, after which the beads were pelleted by brief centrifugation, and the supernatant containing the unbound material was removed. The beads were then washed three times with the same buffer containing 10 mM imidazole, pH 8.0, resuspended in 50 μl of the buffer containing 100 mM imidazole, and incubated for an additional 15 min at room temperature. The supernatant containing the bound material was then withdrawn. Aliquots of the reactions were then analyzed on 8–25% Phast gels (Amersham Pharmacia Biotech) and silver-stained. For transcription reactions, washed Ni^{2+}-NTA-agarose beads containing σ^{70} or the ligation product immobilized through $AsiA_{His}$ were treated with an equal volume of 7 M guanidine HCl (15 min at room temperature with agitation). 10 μl of the supernatants was removed, diluted to 100 μl with transcription buffer, and used for transcription reactions.

In Vitro Transcription—Abortive initiation reactions were performed in 20 μl of transcription buffer containing 20 nM of either the 123-base pair T7 A2 promoter containing DNA fragment (18) or the 150-base pair *gal* P1 fragment (19), 40 nM RNAP core enzyme (β′, β, α_{235}-dimer), 0.5 mM CpG (T7 A2) or ApU (*gal* P1), and 50 μM α-[^{32}P]CTP (30 Ci/mmol), 40 mM Tris-HCl, pH 7.9, 40 mM KCl, and 10 mM $MgCl_2$. Reactions were supplemented with 5 μl (~10 pmol) of σ^{70} or ligation product prepared as described above. The amount of cleavage product added to the reaction was equal to that of σ^{70} or ligation product based on visual inspection of stained SDS gels. Reactions proceeded for 15 min at 37 °C and were terminated by addition of an equal volume of loading buffer containing 6 M urea. Transcription products were analyzed by urea-polyacrylamide gel electrophoresis (7 M urea, 20% polyacrylamide), followed by autoradiography.

TABLE I
Identification of the expressed protein cleavage and ligation products

Cofactor	Observed mass	Calculated mass[a]
	Da	
N-Acetylcysteine	ND[b]	
Cysteine	7314	7315
Mercaptoacetic acid	7286	7288
DTT[c]	7211	7214
Thiophenol	7303	7306
Thiophenol + NaOH[d]	7211	7214
Synthetic peptide + thiophenol	9023	9024

[a] Average isotope composition. Note, calculation takes into account removal of N-terminal methionine from the σ^{70} fragment, as well as the observed oxidation of an internal methionine in the sequence to Met(O).
[b] ND, not detected.
[c] Reaction with dithiothreitol (DTT) gives the peptide carboxylate as the final product.
[d] Hydrolysis of the phenyl ᵃthioester derivative of the peptide to the free acid with 1 N NaOH at 0 °C for 1 min.

RESULTS

Rationale—The long term objective of our studies is to explore transcription mechanism through the generation of semi-synthetic versions of the various subunits of *E. coli* RNA polymerase. In the current work, we are interested in systematically chemically modifying the C-terminal region of the σ^{70} subunit. Our approach is based around the chemical ligation of a synthetic peptide (corresponding to the C-terminal region of σ^{70}) to a recombinant protein constituting the remainder of the σ^{70} sequence. Our previous studies have shown that the commercially available pCYB expression plasmids (New England Biolabs) offer a way of generating recombinant proteins that are able to participate in ligation reactions with synthetic peptides possessing cysteine residues at their N terminus (2). Since pCYB expression vectors make use of a genetically manipulated protein splicing system (20), a process which has been shown to involve the intermediacy of a thioester (21), it is presumed that the reaction of the synthetic peptide with the recombinant protein goes via native chemical ligation (14).

Before attempting the generation of a full size semi-synthetic σ^{70} subunit, a series of model studies were carried out using a smaller recombinant fragment of the protein more amenable to accurate mass spectrometric analysis. The purpose of these studies were 2-fold: (i) to study the chemical mechanism of expressed protein ligation, and (ii) to explore the feasibility of applying the semi-synthesis approach to the σ^{70} system.

Preliminary Studies—As a model system, a short recombinant fragment corresponding to amino acids 500–566 of the 613-amino acid long *E. coli* RNA polymerase σ^{70} subunit was cloned into the pCYB vector. Subsequent overexpression in *E. coli* resulted in the generation of a protein chimera in which the desired σ^{70} fragment was C-terminally fused to an intein protein splicing element itself linked to a chitin binding domain (CBD), included to allow rapid purification by affinity chromatography on chitin beads (20).

Our initial investigations focused on the release of the desired σ^{70} fragment from the immobilized chimera through the treatment with various thiol-containing molecules. As can be seen from Table I, *N*-acetylcysteine was the only agent tried that failed to support detectable cleavage of the polypeptide from the support. In contrast, dithiothreitol, cysteine, mercaptoacetic acid, and thiophenol all caused efficient cleavage of the chimeric protein. Analysis of cleavage supernatants by reverse-phase HPLC revealed, in all cases, the presence of two main peaks. Electrospray mass spectrometry indicated that the first HPLC peak (~75% of the total product) corresponded to σ amino acids 501–566 plus the two C-terminal linker amino

acids Ala-Gly (see "Experimental Procedures") and thus had the first methionine residue removed. The second, minor peak contained the unprocessed product with the first methionine in place. The molecular weights of the major processed products of the different cleavage reactions are shown in Table I. The products of the cysteine, mercaptoacetic acid, and thiophenol cleavages had masses consistent with C-terminally derivatized polypeptides, whereas the major product of the dithiothreitol-mediated cleavage had a free C-terminal carboxyl group.

Of particular relevance to the mechanism of expressed protein ligation is the exact chemical nature of the C-terminal group present on the cleavage product following treatment with a thiol agent. To investigate this, the major product from the thiophenol cleavage reaction was isolated and subsequently exposed to elevated pH. This resulted in its clean conversion into an earlier eluting form (by HPLC) with a mass exactly 92 Da less than before. Such a mass change is indicative of the hydrolysis of the phenyl α-thioester derivative of the sigma polypeptide back to the free acid. Note, the product of the cysteine cleavage reaction was stable to high pH, evidence that the initial thioester product had, as expected, rearranged to a stable amide.

Next we evaluated whether the immobilized σ^{70} fragment could be chemically ligated to a short synthetic peptide (NH_2-Cys-Glu-Asp-Asn-Glu-Tyr-Thr-Ala-Arg-Glu-aminocaproate-Lys-ϵ-[fluorescein]-CO_2H) containing an N-terminal cysteine to facilitate ligation and a C-terminal fluorescein reporter group. Initial studies in which the beads were simply treated with a solution containing 1 mM peptide at pH 7.3 were unsuccessful, and neither ligation nor protein cleavage was detected, even after prolonged incubations. The presence of thiol cofactors can appreciably accelerate native chemical ligation reactions both in solution (22) and on solid phase (23). Consequently, we investigated the effect of thiol co-factors on our model ligation reaction (Table I). Consistent with our previous findings (2), thiophenol was the only cofactor that supported efficient ligation of the synthetic peptide to the recombinant σ^{70} fragment. Inclusion of 1.5% v/v of thiophenol in the ligation mixture at pH 7.3 containing the synthetic peptide (1 mM) resulted in extremely efficient ligation (>90% after overnight incubation) as indicated by HPLC and electrospray mass spectrometry analysis. The ligation product had a mass of 9023 Da and thus corresponded to the desired semi-synthetic polypeptide (expected mass = 9024 Da since the masses of σ fragment and synthetic peptide were 7215 and 1827 Da, respectively). The stability of the ligation product to the high concentration of thiophenol present in the ligation buffer confirms the presence of an amide linkage (and not a labile-thioester bond) at the ligation junction (14, 22). Note that no ligation was detected using a control peptide that did not contain an N-terminal cysteine residue.

The absolute requirement of thiophenol as a cofactor taken together with the results of our initial cleavage studies, indicates that the phenyl α-thioester derivative of the σ polypeptide is being generated *in situ* during the reaction and is then reacting with the synthetic peptide via a native chemical ligation reaction. Interestingly, both thiophenol-mediated cleavage and ligation reactions were found to follow similar kinetics (each taking several hours to go to completion) and are appreciably slower than is typically observed when using synthetic fragments (22, 23). The slow kinetics of the thiophenol-mediated cleavage/ligation probably reflects the position of the equilibrium in the initial A → S acyl transfer within the chimera. Based on the data from these model studies we propose the ligation mechanism shown in Fig. 1 in which the highly reactive phenyl α-thioester derivative of the recombinant polypeptide is produced *in situ* during the ligation process. Once generated this derivative will quickly and irreversibly react with the synthetic peptide to give the final product, thus generating a reaction sink.

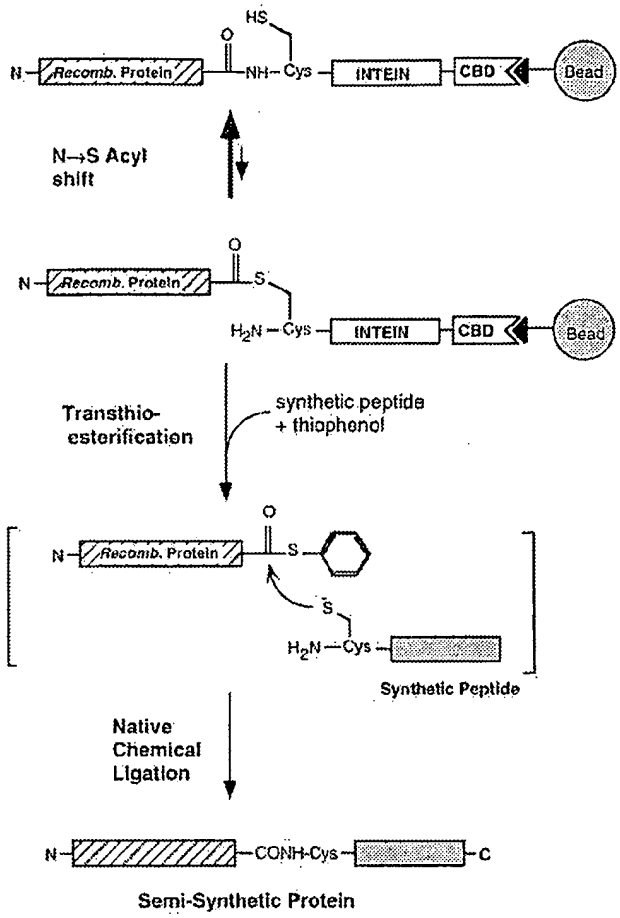

FIG. 1. **Mechanism of expressed protein ligation.** The protein or protein fragment of interest is expressed as an intein-CBD fusion using the pCYB cloning vector. Following affinity purification, exposure of the immobilized fusion protein to a combination of thiophenol and synthetic peptide results in native chemical ligation of the peptide to the protein. Thiophenol is key to this process since it generates the reactive phenyl α-thioester derivative of the protein *in situ*.

Preparation of a Semi-synthetic σ^{70} Derivative—We next investigated whether a functional semi-synthetic σ^{70} could be obtained by expressed protein ligation. Genetic and biochemical data indicate that in the context of bacterial RNA polymerase holoenzyme, protein-DNA contacts between the evolutionary conserved C-terminal region 4.2 of σ^{70} and the −35 promoter element are crucial for promoter recognition (24–26). In addition, protein-protein contacts between σ region 4.2 and transcription factors are crucial for transcription activation (27, 28). Thus, we decided to focus our efforts on the semi-synthesis of a σ^{70} analog containing a chemically synthesized region 4.2. A recombinant protein containing the first 566 amino acids of σ^{70} fused to intein-CBD was used in the ligation reaction. This fragment was chosen because the region of σ^{70} defined by residues 560–570 is evolutionarily variable in length and sequence (29) and is likely to tolerate a non-natural cysteine introduced as a result of ligation. Sequence comparisons also indicate that region 4.2 does not extend past σ^{70} His^{600} on the C-terminal side (29). Based on these data, a 34-residue peptide was synthesized that corresponded to amino acids 568–600 of σ^{70} with an additional cysteine residue at the

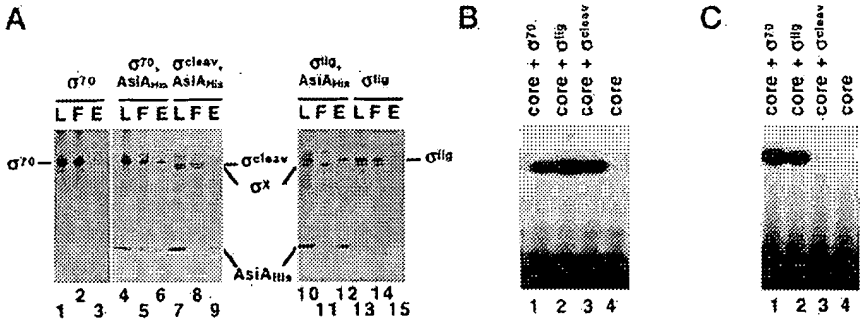

FIG. 2. *A*, binding of full-length σ^{70} and the ligation product (σ^{lig}), but not the cleavage product (σ^{cleav}), to immobilized $AsiA_{His}$ by the Ni^{2+} co-immobilization assay. The indicated proteins were loaded onto Ni^{2+}-NTA-agarose beads (*L*), and the unbound protein was removed (*F*). The beads were extensively washed, and the bound protein was eluted with buffer containing 100 mM imidazole (*E*). The protein fractions were analyzed by SDS-PAGE on an 8–25% Phast-Gel (Amersham Pharmacia Biotech). A contaminating band (σ^X) in the cleavage and ligation products lanes results from an uncharacterized proteolytic event during ligation/cleavage reactions and does not associate with $AsiA_{His}$ (*lanes 11* and *12*). *B*, full-length σ^{70}, σ^{lig}, and σ^{cleav} support promoter-dependent transcription by *E. coli* RNA polymerase core on an extended −10 type promoter. RNA polymerase holoenzyme was reconstituted from RNA polymerase core and the indicated σ proteins, and abortive initiation reaction was performed on the *gal* P1 promoter in the presence of 0.5 mM ApU and 50 μM α-[^{32}P]CTP (30 Ci/mmol). Reaction proceeded for 15 min at 37 °C, and reaction products were resolved by PAGE. An autoradiogram of a 20% urea gel is presented. *C*, full-length σ^{70} and σ^{lig}, but not σ^{cleav} support promoter-dependent transcription by *E. coli* RNA polymerase core on a −10/−35 type promoter. RNA polymerase holoenzyme was reconstituted as in *B*, and abortive initiation reaction was performed on the T7 A2 promoter in the presence of 0.5 mM CpG and 50 μM α-[^{32}P]CTP (30 Ci/mmol). Reaction products were resolved and analyzed as in *B*.

N terminus to promote ligation. Chemical ligation of the synthetic 34-mer to the 568-residue recombinant protein (residues 1–566 of σ^{70} + Ala-Gly) was carried out using the general conditions described above. As a control, a second reaction was performed in the absence of the synthetic peptide and thus should have contained the cleavage product only. Analysis of the crude reaction mixtures by SDS-PAGE showed the presence of the expected ~70- and ~65-kDa bands in the ligation and control reactions, respectively (Fig. 2*A*). As in the model studies, the crude ligation reaction was essentially free of unligated material, although the mixture did contain a contaminant band at around 55 kDa (labeled σ^X on Fig. 2*A*, see below).

Semi-synthetic σ^{70} Is Functional—The bacteriophage T4 anti-sigma protein, AsiA, engineered with a C-terminal hexahistidine tag was used in a Ni^{2+}-NTA-agarose co-immobilization assay to investigate the binding of the ligation product, the cleavage product, and the full-length recombinant σ^{70} to AsiA (Fig. 2*A*). A mixture of $AsiA_{His}$ and recombinant σ^{70} was loaded onto Ni^{2+}-NTA-agarose beads (*lane 4*), and the unbound material was removed (*lane 5*). The beads were subsequently washed with 10 mM imidazole buffer and then eluted with 100 mM imidazole buffer. Both σ^{70} and $AsiA_{His}$ were found in eluted fractions (*lane 6*). Since recombinant σ^{70} in the absence of $AsiA_{His}$ did not interact with the beads (*lane 3*), we conclude that σ^{70} was retained on the beads through direct protein-protein interaction with $AsiA_{His}$, as expected (16). When a mixture of $AsiA_{His}$ and the cleavage product, containing the first 566 amino acids of σ^{70}, was loaded onto Ni^{2+}-NTA-agarose beads (*lane 7*), all of the σ^{70} fragment appeared in the unbound fraction (*lane 8*), whereas an analogous experiment with the ligation product indicated interaction of the semi-synthetic 602-amino acid long σ^{70} derivative with $AsiA_{His}$ (*lane 12*). In the absence of $AsiA_{His}$, semi-synthetic σ^{70} did not interact with the Ni^{2+}-NTA-agarose beads (*lane 15*).

The crude cleavage and ligation reactions each contain an additional protein (labeled σ^X on Fig. 2*A*) that migrates faster than either the expected cleavage or ligation products. The appearance of this band is dependent on the addition of σ-intein overproducing lysates to the chitin beads, and we conclude that this band is probably a product of σ proteolysis. As this σ

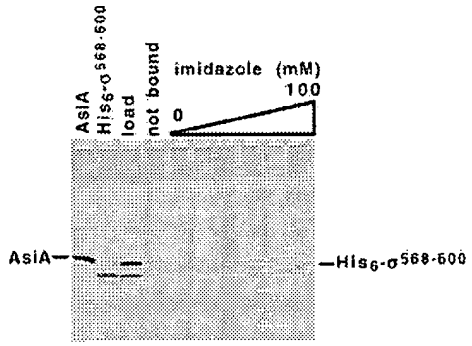

FIG. 3. **Binding AsiA to immobilized $(His)_6$-Cys-$[SCH_2]$-aminocaproate-σ-(568–600).** $(His)_6$-Cys-$[SCH_2]$-amino-caproate-σ-(568–600) and a molar excess of AsiA (load) were incubated with Ni^{2+}-NTA-agarose beads in a buffer containing no imidazole. The beads were then washed with a buffer containing no imidazole (not bound) and washed subsequently with buffer containing increasing concentrations of imidazole as indicated.

fragment may interfere with the function of the desired ligation product, we removed it using the AsiA immobilization method described above (see "Experimental Procedures"). When the purified ligation product and the corresponding amount of the cleavage product were combined with *E. coli* RNA polymerase core, the resulting holoenzymes were active on the *gal*P1 promoter as was the holoenzyme reconstituted with full-length recombinant σ^{70} (Fig. 2*B*). The *gal*P1 promoter belongs to the "extended −10" promoter class and is active even in the absence of sigma region 4.2 (30). From this experiment we conclude that both the cleavage and the ligation products retained their biological activity during the overnight incubation with thiophenol.

A similar experiment was repeated on the T7 A2 promoter. T7 A2 is a strong promoter of the "−10/−35 class" and requires interaction between σ region 4.2 and the −35 box for its activity. As can be seen from the autoradiogram shown on Fig. 2*C* the holoenzyme reconstituted with the ligation product was almost as active as the holoenzyme reconstituted with the full-length recombinant σ^{70}. In contrast, the holoenzyme reconstituted with the cleavage product was completely unable to

support transcription by the core enzyme on T7 A2 (*lane 3*). We conclude that the semi-synthetic, 602-amino acid long σ^{70} derivative is functional in promoter-dependent transcription. The results also establish, as expected, that the non-natural cysteine introduced at the ligation site does not interfere with σ^{70} function and, in agreement with the data of Kumar *et al.* (30), that the last 13 amino acids of σ^{70} are not necessary for unregulated transcription.

σ^{70} Amino Acids 568–600 Are Sufficient for Interaction with AsiA—The results presented in Fig. 2*A* demonstrate that σ^{70} amino acids 568–600 are necessary for AsiA binding. In order to show that σ^{70} amino acids 558–600 are also sufficient for interaction with AsiA, we performed a Ni^{2+}-NTA-agarose co-immobilization experiment with the synthetic σ 33-mer. Two different experiments were performed, and the same result was obtained. The first experiment was essentially a repetition of the experiment shown in Fig. 2*A* and demonstrated that the synthetic 33-mer can be immobilized on Ni^{2+}-NTA-agarose through $AsiA_{His}$ (data not shown). The complementary experiment was done using wild type, untagged AsiA. Instead, a synthetic hexahistidine tag was chemically ligated to the N terminus of $\sigma_{568-600}$ as described under "Experimental Procedures." AsiA and His-tagged σ fragment were loaded on Ni^{2+}-NTA beads; the beads were washed and eluted with increasing concentrations of imidazole in the buffer. As can be seen, AsiA was found in the fractions containing elevated concentrations of imidazole, and the elution profiles of AsiA and His-tagged $\sigma_{568-600}$ from Ni^{2+}-NTA-agarose beads were identical, indicating strong interaction (Fig. 3). A control experiment showed that AsiA did not interact with Ni^{2+}-NTA-agarose (Ref. 16 and data not shown). We conclude that σ^{70} amino acids 568–600 are sufficient for interaction with AsiA.

DISCUSSION

Expressed protein ligation is a novel approach that allows synthetic peptides to be chemically ligated to the C terminus of recombinant proteins fused to an intein protein splicing element (2). Based on the requirement for an N-terminal cysteine within the synthetic peptide, as well as the known involvement of thioesters in protein splicing (21), it is assumed that the process involves a native chemical ligation (14) step. This has been confirmed in the present study through a series of model studies which, moreover, indicate a phenyl α-thioester derivative of the recombinant protein to be the key reactive species in the process. This thioester derivative is also believed to be generated quite slowly during the process, meaning that the ligation reaction is probably pseudo-first order with the synthetic peptide being present in huge excess at any given time (Fig. 1).

We also describe the preparation, using this new approach, of a 602-amino acid long semi-synthetic σ^{70} protein with an intact biological function. This molecule was used to map the determinants of AsiA binding within amino acids 568–600 of σ^{70}. Our result is in excellent agreement with that of Colland *et al.* (31), who used hydroxyl radical protein-protein footprinting to demonstrate that the only region of σ^{70} that is protected from radical cleavage by AsiA is located between residues 572 and 588. σ^{70} amino acids 568–600 comprise the evolutionarily conserved region 4.2 of the σ family of proteins. This region is thought to assume a helix-turn-helix conformation and to interact directly with the −35 box of the promoter. The present results, taken together with our finding that the binding of region 4.2 to the −35 box or AsiA is mutually exclusive,[2] suggests that AsiA may inhibit transcription directly, by occluding the DNA binding surface region 4.2.

The results presented here illustrate the enormous potential of the expressed protein ligation technique for exploring the mechanism and regulation of complex biomolecular machines. In the case of *E. coli* RNA polymerase, we have demonstrated that the ligation conditions do not destroy protein function and that semi-synthetic σ^{70} subunits can be reconstituted with the RNA polymerase core enzyme to give a fully functional holoenzyme. The stage is thus set for future studies in which biochemical and biophysical probes are site-specifically introduced into the σ^{70} subunit. For example, we are currently site-specifically introducing cross-linkable probes into semi-synthetic σ^{70}. Promoter complexes formed by RNA polymerase holoenzymes reconstituted with derivatized, cross-linkable sigmas will allow us to study protein-protein and protein-nucleic acids contacts that govern transcription activation and promoter recognition. Finally, it is worth noting that other semi-synthetic subunits of the *E. coli* RNA polymerase complex can be reconstituted *in vitro*,[3] suggesting expressed protein ligation will have widespread utility in this multiprotein system.

Acknowledgments—K. S. is grateful to Seth Darst for support and encouragement during the early stages of this work. We are grateful to Deborah Hinton for pet21AsiA$_{His}$ plasmid and to Annie Kolb for communicating data prior to publication.

REFERENCES

1. Ptashne, M., and Gann, A. (1997) *Nature* **386,** 569–577
2. Muir, T. W., Sondhi, D., and Cole, P. A. (1998) *Proc. Natl. Acad. Sci. U. S. A.*, in press
3. Cornish, V. W., Mendel, D., and Schultz, P. G. (1995) *Angew. Chem. Int. Ed. Engl.* **34,** 621–633
4. Chen, Y., Ebright, Y. W., and Ebright, R. H. (1994) *Science* **265,** 90–92
5. Hubbell, W. L., Mchaourab, H. S., Altenbach, C., and Lietzow, M. A. (1996) *Structure* **4,** 779–783
6. Muir, T. W. (1995) *Structure* **3,** 649–652
7. Kemp, D. S., and Carey, R. I. (1993) *J. Org. Chem.* **58,** 2216–2222
8. Liu, C.-F., and Tam, J. P. (1994) *J. Am. Chem. Soc.* **116,** 4149–4153
9. Schnölzer, M., and Kent, S. B. H. (1992) *Science* **1992, 256,** 221–225
10. Gaertner, H. F., Rose, K., Cotton, R., Timms, D., Camble, R., and Offord, R. E. (1992) *Bioconjugate Chem.* **3,** 262–268
11. Muir, T. W., Williams, M. J., Ginsberg, M. H., and Kent, S. B. H. (1994) *Biochemistry* **33,** 7701–7708
12. Rose, K. (1994) *J. Am. Chem. Soc.* **116,** 30–33
13. Nefzi, A., Sun, X., and Mutter, M. (1995) *Tetrahedron Lett.* **36,** 229–230
14. Dawson, P. E., Muir, T. W., Clark-Lewis, I., and Kent, S. B. H. (1994) *Science* **266,** 776–779
15. Wallace, C. J. A. (1995) *Curr. Opin. Biotechnol.* **6,** 403–410
16. Severinova, E., Severinov, K., Fenyö, D., Marr, M., Brody, E. N., Roberts, J. W., Chait, B. T., and Darst, S. A. (1996) *J. Mol. Biol.* **263,** 637–647
17. Schnölzer, M., Alewood, P., Jones, A., Alewood, D., and Kent, S. B. H. (1992) *Int. J. Pept. Protein Res.* **40,** 180–193
18. Severinov, K., and Darst, S. A. (1997) *Proc. Natl. Acad. Sci. U. S. A.* **94,** 13481–13486
19. Minchin, S., and Busby S. (1993) *Biochem. J.* **289,** 771–775
20. Chong, S., Mersha, F. B., Comb, D. G., Scott, M. E., Landry, D., Vence, L. M., Perler, F. B., Benner, J., Kucera, R. B., Hirnonen, C. A., Pelletier, J. J., Paulus, H., and Xu, M.-Q. (1997) *Gene (Amst.)* **192,** 271–28120
21. Xu, M.-Q., and Perler, F. B. (1996) *EMBO J.* **15,** 5146–5153
22. Dawson, P. E., Churchill, M. J., Ghadiri, M. R., and Kent, S. B. H. (1997) *J. Am. Chem. Soc.* **119,** 4325–4329
23. Camarero, J. A., Cotton, G. C., Adeva, A., and Muir, T. W. (1998) *J. Pept. Sci.* **51,** 303–316
24. Burton, Z., Burgess, R. R., Lin, J., Moore, D., Holder, S., and Gross, C. A. (1981) *Nucleic Acids Res.* **9,** 2889–2903
25. Gardella, T., Moyle, T., and Susskind, M. M. (1989) *J. Mol. Biol.* **206,** 579–590
26. Siegele, D. A., Hu, J. C., Walter, W. A., and Gross, C. A. (1989) *J. Mol. Biol.* **206,** 591–603
27. Kumar, A., Grimes, B., Fujita, N., Makino, K., Malloch, R. A., Hayward, R. S., and Ishihama, A. (1994) *J. Mol. Biol.* **235,** 405–413
28. Li, M., Muyle, H., and Susskind, M. M. (1994) *Science* **263,** 75–77
29. Lonetto, M., Gribskov, M., and Gross, C. A. (1992) *J. Bacteriol.* **174,** 3843–3849
30. Kumar, A., Malloch, R. A., Fujita, N., Smillie, D. A., Ishihama, A., and Hayward, R. S. (1993) *J. Mol. Biol.* **232,** 406–418
31. Colland, F., Orsini, G., Brody, E. N., Buc, H., and Kolb, A. (1998) *Mol. Microbiol.* **27,** 819–829

[2] E. Severinova, K. Severinov, and S. A. Darst, submitted for publication.

[3] K. Severinov, unpublished observations.

STIC-ILL

From: Gabel, Gailene
Sent: Wednesday, February 12, 2003 4:14 PM
To: STIC-ILL
Subject: 09/905,439

Please provide a copy of the following references ASAP:

1) Gillies et al., NMR in Physiology and Biomedicine, Academic Press: San Diego (1994).

2) Yamazaki et al., J. Am. Chem. Soc. 120: 5591-5592 (1998).

3) Severinov et al., J. Biol. Chem. 273: 16205-16209 (1998).

4) Muir et al. (Proc. Natl. Acad. Sci USA, 95: 6705-6710 (1998).

5) Xu et al. Proc. Natl. Acad. Sci., 96: 388-393 (1999).

6) Lippens et al., In NMR in Supramolecular Chemistry, Pons M. Ed., Kluwer Academic Publishers, 191-226 (1999).

Thanks a bunch,
Gail R. Gabel
7B15
CM1
305-0807

Proc. Natl. Acad. Sci. USA
Vol. 95, pp. 6705–6710, June 1998
Biochemistry

Expressed protein ligation: A general method for protein engineering

TOM W. MUIR*†‡, DOLAN SONDHI†§, AND PHILIP A. COLE†‡§

Laboratories of *Synthetic Protein Chemistry and §Bioorganic Chemistry, Rockefeller University, 1230 York Avenue, New York, NY 10021

Communicated by Samuel J. Danishefsky, Memorial Sloan–Kettering Cancer Center, New York, NY, April 1, 1998 (received for review January 27, 1998)

ABSTRACT **A protein semisynthesis method—expressed protein ligation—is described that involves the chemoselective addition of a peptide to a recombinant protein. This method was used to ligate a phosphotyrosine peptide to the C terminus of the protein tyrosine kinase C-terminal Src kinase (Csk). By intercepting a thioester generated in the recombinant protein with an N-terminal cysteine containing synthetic peptide, near quantitative chemical ligation of the peptide to the protein was achieved. The semisynthetic tail-phosphorylated Csk showed evidence of an intramolecular phosphotyrosine-Src homology 2 interaction and an unexpected increase in catalytic phosphoryl transfer efficiency toward a physiologically relevant substrate compared with the non-tail-phosphorylated control. This work illustrates that expressed protein ligation is a simple and powerful new method in protein engineering to introduce sequences of unnatural amino acids, posttranslational modifications, and biophysical probes into proteins of any size.**

The ability to alter protein structure and function by introducing unnatural amino acids has great potential to enhance our understanding of proteins, generate new tools for biomedical research, and create novel therapeutic agents (1–6). For example, site-specific incorporation of posttranslational modifications such as phosphoamino acids could lead to molecules having altered structural and functional properties that would be useful tools in understanding complex processes such as signal transduction. Equally, the introduction of small molecules like fluorescent tags, spin resonance probes, or cross-linking agents into proteins at well-defined positions could lead to new biochemical insights in countless biological systems. Although powerful, each of the currently existing techniques to introduce unnatural molecules into proteins has associated with it certain synthetic or practical limitations that have limited their widespread application (1–6).

In so-called "native chemical ligation" an N-terminal cysteine-containing peptide is chemically ligated to a second peptide possessing an $^{\alpha}$thioester group with the resultant formation of a native peptide bond at the ligation junction (5). Until now, peptide $^{\alpha}$thioesters for use in native chemical ligation have been generated solely through chemical synthesis, a technically demanding process that imposes certain size constraints on the technique. Thus, native chemical ligation has proven very useful for the total synthesis of small proteins and protein domains, but has not been extended to the synthesis of proteins beyond ≈15 kDa. One way to overcome this size limitation would be to chemically ligate small synthetic sequences to much larger recombinant protein fragments. Although methods for the generation of recombinant proteins possessing N-terminal cysteine residues have been reported (7), there is currently no way of producing recombinant protein $^{\alpha}$thioesters for use in native chemical ligation. Thus, native chemical ligation has not been completely interfaced with recombinant protein semisynthesis. The current challenge was therefore to devise a way of generating the necessary protein $^{\alpha}$thioesters by using a straightforward and widely available recombinant expression method.

Protein splicing, the process in which a protein undergoes an intramolecular rearrangement resulting in the extrusion of an internal sequence (intein) and the joining of the lateral sequences (exteins), has been shown to involve the intermediacy of a thioester (8, 9). A mutant version of the splicing protein has been demonstrated to be defective in completion of the splicing reaction but still capable of thioester intermediate formation (8, 9). The commercially available pCYB vectors for *Escherichia coli* protein expression result in the generation of $^{\alpha}$thioesters where a protein of interest can be expressed in frame fused with an intein-chitin binding domain (CBD) sequence (9). In the standard experiment, the protein of interest is cleaved from the intein-CBD with DTT or 2-mercaptoethanol by a transthioesterification reaction while the chimera is bound to a chitin column. We suspected that it might be possible to intercept the $^{\alpha}$thioester with a synthetic peptide rather than DTT, thereby generating a semisynthetic protein containing a chemoselectively ligated synthetic peptide sequence.

To investigate the feasibility of this ligation process we decided to undertake the synthesis of a pair of semisynthetic C-terminal Src kinase (Csk) proteins. This target system was chosen in part because it satisfied two principal objectives of this initial study, which were: (*i*) to demonstrate that intein-fusion constructs could be used as a source of large recombinant protein $^{\alpha}$thioesters for use in native chemical ligation, and (*ii*) to synthesize challenging molecules that could not have been generated any other way.

Csk is a 50-kDa protein that catalyzes the phosphorylation of a highly conserved tyrosine within the C-terminal tail of Src family members (10–17). This modification results in an intramolecular interaction between the Src homology 2 (SH2) domain and the C-terminal phosphotyrosine within Src, an association that leads to a significant conformational change and catalytic repression *in vivo* (Fig. 1*A*) (10–15). Csk is similar in architectural layout to Src family members and is 40–50% identical in amino acid sequence to this protein family (16, 17), however, it lacks a C-terminal tyrosine-containing tail and is not known to be regulated through phosphorylation (Fig. 1) (10, 11). We were therefore interested in the possibility of adding a phosphotyrosine tail to Csk and determining the

Abbreviations: Csk, C-terminal Src kinase; Csk^{PEP}, Csk-[CONH]-peptide (the ligation production of Csk and unphosphorylated peptide); Csk^{pPEP}, Csk-[CONH]-phosphopeptide (the ligation product of Csk and phosphopeptide); CBD, chitin binding domain; SH2, Src homology 2.

†T.W.M., D.S., and P.A.C. contributed equally to this work.
‡To whom reprint requests should be addressed. e-mail: cole@rockvax.rockefeller.edu and muirt@rockvax.rockefeller.edu.

The publication costs of this article were defrayed in part by page charge payment. This article must therefore be hereby marked "*advertisement*" in accordance with 18 U.S.C. §1734 solely to indicate this fact.

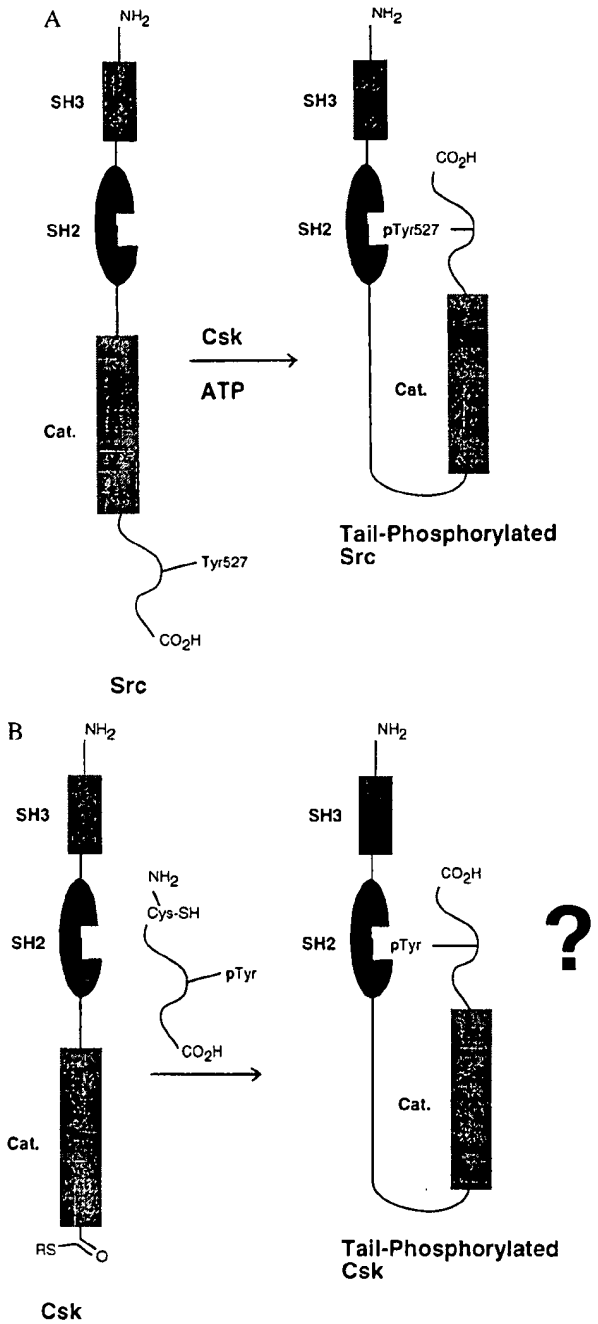

FIG. 1. Phosphotyrosine tails in Src and Csk. (*A*) Phosphorylation of the Src tail on tyrosine-527 is catalyzed by Csk. This phosphorylation results in a conformational change involving an intramolecular interaction between the Src tail and the SH2 domain. (*B*) Csk is highly homologous to Src but lacks a C-terminal tyrosine-containing tail. Proposed ligation of a phosphotyrosine tail might lead to a conformational change like that found in Src. Csk is not a Src family member and in addition to its lack of a C-terminal tail, Csk also lacks two key Src features: an activating tyrosine-containing loop, as well as an N-terminal myristoylation site (16, 17).

potential effects of this modification on conformation (Fig. 1*B*) and catalytic behavior.

Although extending the Csk C terminus could in principle be carried out using recombinant methods (18), there would be no way of directing specific phosphorylation of a single engineered tyrosine (wild-type Csk has 20 tyrosine residues) by chemical or enzymatic methods. Bacterial recombinant protein expression of wild-type human Csk is complex because it requires chaperonins for significant soluble expression (18). In fact, attempts at simply adding a 9-aa tyrosine-containing tail to wild-type Csk led to very poor protein expression using these established methods (P.A.C., unpublished data). Furthermore, none of the existing protein engineering techniques appeared to be suitable for the generation of this large and complex protein. For example, the current size limit of total chemical synthesis by native chemical ligation is 100 ± 50 aa, putting the 450-aa Csk well beyond the range of this approach. Similarly, the presence of 10 cysteine residues in wild-type Csk prohibits a site-selective cysteine-modification strategy. Thus, producing the desired semisynthetic Csk protein(s) in sufficient quantities for enzymatic and biochemical studies was a significant chemical challenge.

MATERIALS AND METHODS

Peptide Synthesis. Phosphorylated and unphosphorylated peptides were manually synthesized by fluorenylmethoxycarbonyl and *tert*-butoxycarbonyl solid phase peptide synthesis, respectively. Phosphotyrosine was introduced during fluorenylmethoxycarbonyl chain assembly in the phosphate unprotected form. Orthogonal protection of the ε-NH_2 group of the C-terminal Lys residue with either fluorenylmethoxycarbonyl (*tert*-butoxycarbonyl strategy) or dimethyldioxocyclohexylidene (fluorenylmethoxycarbonyl strategy) allowed direct attachment of fluorescein (activated as an *N*-hydroxysuccinimide ester) before the final cleavage step. After cleavage, peptides were purified to homogeneity by HPLC and characterized by electrospray MS.

Expressed Protein Ligation. See Fig. 2 for the overall strategy. Primers containing an *Nde*I site (upstream) and a *Sma*I site (downstream) were used to PCR amplify full-length wild-type human *csk* DNA for in frame insertion upstream of the intein/CBD encoding sequence in the vector pCYB2 (New England Biolabs). The resultant plasmid pCYB2-CSK, which was free of mutations in the Csk coding region based on DNA sequencing, was then cotransformed into *E. coli* DH5α with the GroES and GroEL expression plasmid pREP4-groESL using dual selection with ampicillin and kanamycin and cells grown and lysed as described (19). Chitin resin (1 ml) in a disposable plastic column was washed with 20 ml of equilibration buffer (25 mM Na·Hepes, pH 7.0/250 mM NaCl/1 mM Na·EDTA/0.1% Triton X-100). Cell lysate (10 ml, made 0.1% in Triton X-100) was passed through the column at a flow rate of 0.5 ml/min and the flow-through was reapplied at a similar rate. The column was then washed with 30 ml of equilibration buffer and treated with 2 ml 2% vol/vol thiophenol in equilibration buffer (minus Triton X-100) at 1 ml/min followed immediately by 1 ml of 2 mM peptide + 2% thiophenol + equilibration buffer (minus Triton X-100). After 24 h standing at 25°C, the column was eluted with equilibration buffer and the desired product appeared in the initial 2.5 ml; it was dialyzed (Dispodialyzer, 25 kDa cutoff, Fisher) against 25 mM Na·Hepes (pH 7.7), 2 mM DTT, 500 mM NaCl at 4°C for 4–5 days to remove unligated peptide. Protein was estimated to be ≈20% pure by SDS/PAGE with the principal contaminants shown to be GroEL (60%) and DnaK (20%) (see Fig. 3). Quantification of the semisynthetic Csk proteins was based on the intensity of Coomassie blue stained bands on SDS/PAGE compared with known amounts of wild-type Csk and relative amounts of Csk semisynthetic proteins further confirmed by quantitative fluorescence imaging (Storm, Molecular Dynamics). Expressed protein ligation reactions were carried out at least three times and gave reproducible yields. Purification of the proteins by phosphotyrosine affinity chromatography (see below) allowed chaperonin removal (Fig. 3) and showed that chaperonins did not effect kinase activity of either Csk-

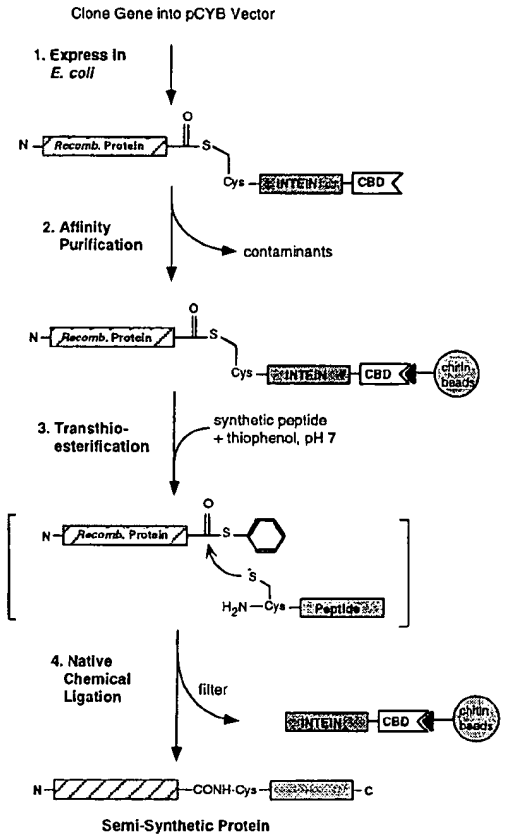

FIG. 2. The principle of expressed protein ligation. In the first step, the gene or gene fragment is cloned into the commercially available PCYB2-IMPACT vector (New England Biolabs) by using the *Nde*I and *Sma*I restriction sites. This cloning strategy results in the addition of a Pro-Gly appended to the native C terminus of the protein of interest. The presence of a C-terminal glycine has been shown to accelerate native chemical ligation (24) and thus reduces the chance of side reactions. After expression and affinity purification of the fusion protein by binding to the chitin resin, the chemical ligation step is initiated by incubating the resin-bound protein with thiophenol and synthetic peptide in buffer. This results in the *in situ* generation of a highly reactive phenyl $^{\alpha}$thioester derivative of the protein that then rapidly ligates with the synthetic peptide to afford the desired semisynthetic protein.

[CONH]-peptide (Csk^{PEP}) or Csk-[CONH]-phosphopeptide (Csk^{pPEP}). Complete characterization of the proteins by MS was carried out after reverse-phase HPLC purification (Fig. 3*C*).

Kinase Assays with Poly(Glu,Tyr). These were performed as described (20) where transfer of ^{32}P from [γ-^{32}P]ATP to poly(Glu,Tyr) was monitored. Autophosphorylation of the semisynthetic Csk ligation proteins was shown to be insignificant. Kinetic parameters were as follows: Csk^{PEP}, K_m of ATP = 31 ± 2 μM, K_m of poly(Glu,Tyr) = 19 ± 3 μg/ml, k_{cat} = 17 ± 1 min^{-1}; Csk^{pPEP}, K_m of ATP = 34 ± 11 μM, K_m of poly(Glu,Tyr) = 30 ± 3 μg/ml, k_{cat} = 19 ± 1 min^{-1}; wild-type Csk (20), K_m of ATP = 12 ± 1 μM, K_m of poly(Glu,Tyr) = 48 ± 2 μg/ml, k_{cat} = 40 ± 5 min^{-1}.

Phosphotyrosine Affinity Chromatography. This was performed in a manner analogous to procedures described (19, 21). A preequilibrated 8 × 8 mm column of *O*-phospho-L-tyrosine-agarose resin was eluted over 5 min with 1 ml of a semisynthetic protein solution (≈1 μM) and eluted at 0.5 ml/min with eight column volumes of low salt buffer (25 mM Hepes, pH 7.7/2 mM DTT) followed by eight column volumes of high salt buffer (25 mM Hepes, pH 7.7/2 mM DTT/500 mM NaCl). The material eluted under high salt conditions was quantitated by fluorescence imaging on SDS/PAGE. The amount bound in the case of Csk^{PEP} was 50 ± 10% and that for Csk^{pPEP} was 10 ± 4%. Binding studies gave similar results on two separate occasions.

Gel Filtration. Gel filtration of semisynthetic proteins was carried out on a Superdex-75 column (Pharmacia) in 20 mM Tris·acetate (pH 8.0) at 0.5 ml/min at room temperature using the proteins ribonuclease A (13,700 Da), carbonic anhydrase (29 kDa), ovalbumin (43 kDa), and BSA (66 kDa) to generate a standard curve. Detection of the standards and wild-type Csk was done by monitoring UV absorbance at 280 nm and for the semisynthetic Csk proteins was done by monitoring fluorescence emission at 520 nm. The concentration of the semisynthetic Csk proteins during column loading was ≈1 μM. The calculated molecular masses were: wild-type Csk (50 kDa), Csk^{PEP} (54 kDa), and Csk^{pPEP} (54 kDa) with an estimated SE ± 10%.

RESULTS AND DISCUSSION

An intein-CBD expression plasmid containing full-length wild-type human Csk DNA was generated and coexpressed in *E. coli* along with GroES and GroEL. The soluble fraction was passed over chitin resin and the resin was washed and then treated with 50 mM DTT containing buffer overnight. This led to generation of full-length Csk protein. Kinase assay of the Csk generated in this manner showed that it was fully active. Treatment of the resin bound Csk-intein-chitin fusion with mercaptoacetic acid and cysteine also afforded comparable quantities of Csk (whereas treatment with *N*-acetylcysteine, for reasons that are unclear, gave no detectable yield of Csk).

Given these results, we designed and synthesized the tyrosine phosphorylated and unphosphorylated forms of the peptide NH_2-Cys-Glu-Asp-Asn-Glu-Tyr-Thr-Ala-Arg-Glu-aminocaproate-Lys-ε-[fluorescein]-CO_2H. Although not homologous to the Src tail, the sequence is derived from the highly conserved activating autophosphorylation site of Src family kinases (10, 11) and is of a similar length to the Src tail. In its tyrosine phosphorylated form, this sequence has been shown to bind specifically to the SH2 domain of Csk (21–23). In the projected semisynthetic protein, the number of amino acids between the highly conserved phosphotyrosine-interacting FLVRES motif of the Csk SH2 domain and the engineered phosphotyrosine in the tail is identical to the analogous spacing in the Src family member Lck. The N-terminal cysteine residue was included in the peptide to facilitate native chemical ligation. Incorporation of a C-terminal fluorescent tag via a flexible linker was envisaged to serve as a sensitive marker of successful ligation and as a probe for further biochemical studies.

Initial efforts to react the unphosphorylated peptide with the resin-bound Csk-intein-CBD fusion protein without added thiol cofactors were unsuccessful, and coaddition of mercaptoacetic acid led to cleavage of Csk from the fusion protein, without any detectable ligation. However, inclusion of 2% thiophenol in the reaction buffer led to extremely efficient (>90%) ligation of the synthetic peptide to the recombinant protein as evidenced by the production of a highly fluorescent 52-kDa protein band on SDS/PAGE (Figs. 2–4). As illustrated in Fig. 2, we hypothesize a two-step, one-pot process involving an initial transthioesterification event followed by immediate native chemical ligation. The initial transthioesterification step is critical as it alleviates any steric hindrance present around the fusion protein thioester, and creates a reaction sink involving the formation of a highly reactive phenyl $^{\alpha}$thioester derivative of the recombinant Csk protein (24). The corresponding mercaptoacetic acid thioester would be expected to be much less reactive than the phenyl thioester thus accounting for the results in our preliminary studies.

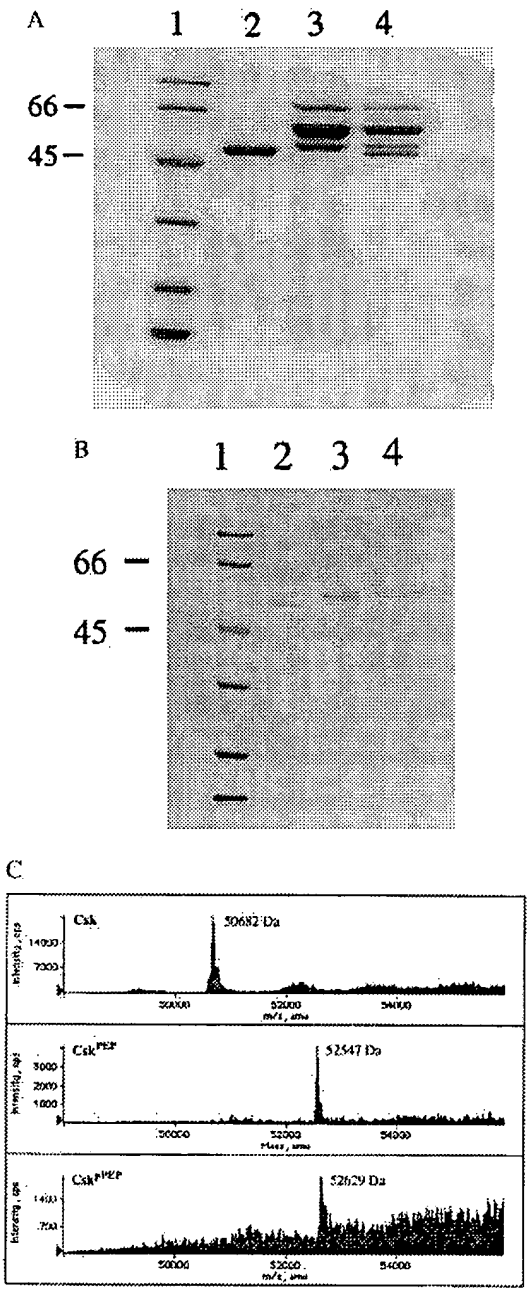

FIG. 3. Characterization of semisynthetic proteins. (*A*) A Coomassie-stained 10% SDS/PAGE gel of Csk^{PEP} crude reaction product mixture. Lane 1: molecular mass markers from the top: 97, 66, 45, 31, and 21.5 kDa. Lane 2: Wild-type Csk. Lane 3: Csk^{PEP} crude ligation product mixture; a combination of N-terminal sequencing and electrospray MS indicated that the bands at 56 kDa and 69 kDa were GroEL and DnaK, respectively. Lane 4: Comixture of wild-type Csk and Csk^{PEP} crude ligation product mixture. (*B*) A Coomassie-stained 10% SDS/PAGE gel of the purified semisynthetic Csk proteins. Lane 1: Molecular mass markers as listed in *A*. Lane 2: Wild-type Csk. Lane 3: Csk^{pPEP} purified by reverse-phase HPLC. Lane 4: Csk^{PEP} purified by phosphotyrosine affinity chromatography. (*C*) Characterization of semisynthetic proteins by electrospray MS. (*Top*) Full-length wild-type Csk, expected mass = 50,705 Da (average isotope). (*Middle*) Csk^{PEP}, expected mass = 52,540 Da (average isotope). (*Bottom*) Csk^{pPEP}, expected mass = 52,619 Da (average isotope). Each sample was isolated by reverse-phase HPLC and mass analyzed by using a Perkin–Elmer-Sciex (Thornhill, ON, Canada) API-100 mass spectrometer. Predicted masses were calculated by using the program MACBIOMASS (S. Vemuri and T. Lee, City of Hope, Duarte, CA). Note, the ligated Csk products were engineered to have the sequence Pro-Gly added to their C termini, and Edman sequencing indicated that the N-terminal methionine had been removed from the Csk expressed in the pCYB2 vector. That the ligation products contained only one N terminus (i.e., from Csk) combined with the MS data provides unambiguous characterization of the semisynthetic proteins.

In each of the two ligation reactions, the crude product mixtures were nearly free of unligated material as exemplified by lanes 3 and 4 of Fig. 3*A*, but both preparations were contaminated with GroEL and DnaK. Although yields were not optimized, an estimated 0.5 mg of ligation product per 2.5 l bacterial cell culture was produced. Ligation conditions were not disruptive to Csk protein folding because both semisynthetic constructs were catalytically active (see *Materials and Methods*). Further characterization of Csk^{PEP} and Csk^{pPEP} after chromatographic purification to remove the chaperonins demonstrates the slightly higher apparent molecular weights of the ligation products compared with wild-type Csk on SDS/PAGE (see Fig. 3*B*). The enzymologic activity of the purified material was identical to the chaperone-containing mixture. Electrospray MS of the purified semisynthetic proteins gave molecular masses in good agreement with the predicted values (Fig. 3*C*). Interestingly, Edman sequencing revealed that the N-terminal methionine residue in the protein produced as an intein-CBD fusion was completely removed (no such cleavage is observed when Csk is expressed in the standard form).

The Csk ligation products were subjected to extensive dialysis to remove unreacted peptide. After dialysis, affinity purification over a phosphotyrosine column (19, 21) was attempted for both Csk^{PEP} and Csk^{pPEP} to assess potential conformational differences. While about 50% of Csk^{PEP} bound to the phosphotyrosine resin under low salt conditions, comparable to wild-type Csk, only ≈10% Csk^{pPEP} bound to the phosphotyrosine resin under similar conditions. It is presumed that the SH2 domain of Csk^{pPEP} is less available for affinity column interaction because it is prebound to the phosphotyrosine sequence of Csk^{pPEP}. Similar behavior has been reported with Src family members (10, 21, 25).

In the case of Src family members, the interaction between the phosphotyrosine tail and the SH2 domain has been shown to be intramolecular (12, 13, 15). Nondenaturing PAGE (6%) with fluorescence imaging showed that Csk^{pPEP} had a slightly faster migration time compared with Csk^{PEP}, consistent with Csk^{pPEP} being monomeric with an increased electrostatic effect (data not shown). A nondenaturing PAGE of the Src family member Lck in its tail-phosphorylated and unphosphorylated form showed very similar behavior (25). Gel filtration further suggested that both the semisynthetic Csk proteins were monomeric (see *Materials and Methods*), evidence that the proposed interaction between the phosphotyrosine tail and SH2 domain in Csk^{pPEP} is intramolecular.

Limited proteolysis studies with subtilisin further suggested a conformational difference between Csk^{PEP} and Csk^{pPEP}, with Csk^{pPEP} showing a reproducibly slower proteolytic degradation rate as demonstrated by the persistent fluorescent bands on SDS/PAGE in Fig. 4. Varying the time and protease concentration failed to reveal the build-up of a fluorescent intermediate with molecular mass of >14 kDa for proteolysis of Csk^{PEP} suggesting that the fluorescent peptide tail was cleaved rapidly in this semisynthetic protein. The ≈38 kDa fragment produced in the proteolysis of Csk^{pPEP} clearly contains an intact C terminus because of its fluorescence, and is ≈7 kDa larger than the primary site of wild-type Csk cleavage under similar conditions, with the cleavage site in the latter at the SH2 domain-catalytic domain junction (data not shown). The position of cleavage in Csk^{pPEP} is nearer to the N-terminal edge of the SH2 domain. Interestingly, tail-phosphorylated and unphosphorylated forms of Src show distinct proteolytic

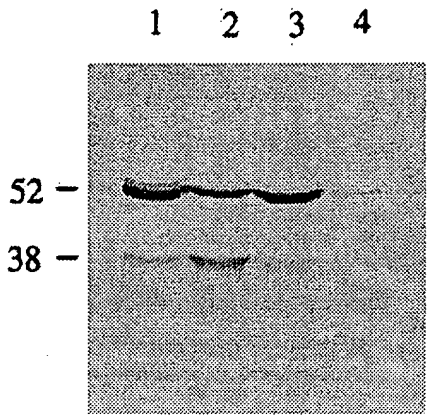

FIG. 4. Fluorescence imaging of an SDS/PAGE showing the results of proteolytic digestions of Csk^{PEP} and Csk^{pPEP} with subtilisin. Lane 1: Csk^{pPEP} – subtilisin; lane 2: Csk^{pPEP} + subtilisin; lane 3: Csk^{PEP} – subtilisin; lane 4: Csk^{PEP} + subtilisin. Reactions conditions: Csk^{PEP} and Csk^{pPEP} (1 μg) in 20 μl buffer (20 mM Tris·acetate, pH 8.0/10% glycerol/2 mM DTT) treated with subtilisin Carlsberg (12.5 ng) for 30 min at 4°C. Fluorescence imaging was done on a Storm instrument (Molecular Dynamics). Proteolysis reactions were performed in parallel under identical conditions with different protein preparations on four different occasions and all gave comparable results to those shown here.

degradation patterns, comparable to those of the semisynthetic Csk proteins (10, 26). In the case of Src, the overall proteolysis rate is reduced for the tail-phosphorylated form and the C-terminal tail region is particularly resistant to proteolysis when phosphorylated compared with the unphosphorylated form (26). It is important to emphasize that the fluorescein probe greatly simplified the analysis of this proteolysis data and that, in general, the ability to label the C terminus of proteins with fluorescent markers using expressed protein ligation should be of significant value in protein mapping and footprinting experiments.

In sum, the phosphotyrosine affinity, nondenaturing PAGE, gel filtration, and proteolysis results support the proposition that appending a phosphotyrosine tail to Csk results in a new conformation involving an intramolecular interaction between the SH2 domain and the tail phosphotyrosine. Such a conformational switch could lead to new biological activities in cell signal transduction. As a first stage toward investigating this possibility, the catalytic behavior of the semisynthetic Csk proteins was investigated using both peptide and protein substrates.

The chemical mechanism of peptide and protein substrate phosphorylation by Csk appears to be similar but the basis for selectivity is different for the two substrate classes (25). Specifically, the interaction of Csk with its physiologic substrates appears to require multidomain structural interactions, so that it could be expected that a perturbed Csk conformation might well lead to altered catalytic effects with a Src family substrate. This is indeed observed to be the case, but in contrast to expectations based on the Src model, Csk^{pPEP} is significantly more active than Csk^{PEP} in phosphorylating the physiologically relevant substrate Lck (Fig. 5 *A* and *B*). Both phosphorylation reactions showed linear activity as a function of time and enzyme concentration (Fig. 5 *A* and *B*). At low Lck substrate concentration, the rate of phosphorylation by the Csk^{pPEP} is ≈5-fold *higher* compared with Csk^{PEP}. This is likely to be primarily a specific Lck-binding difference to the two semisynthetic Csk proteins because the difference in the rates becomes less at higher Lck concentration (see Fig. 5*C*) and because the kinetics with the peptide substrate poly(Glu,Tyr) were so similar for Csk^{PEP} and Csk^{pPEP} (see *Materials and Methods*).

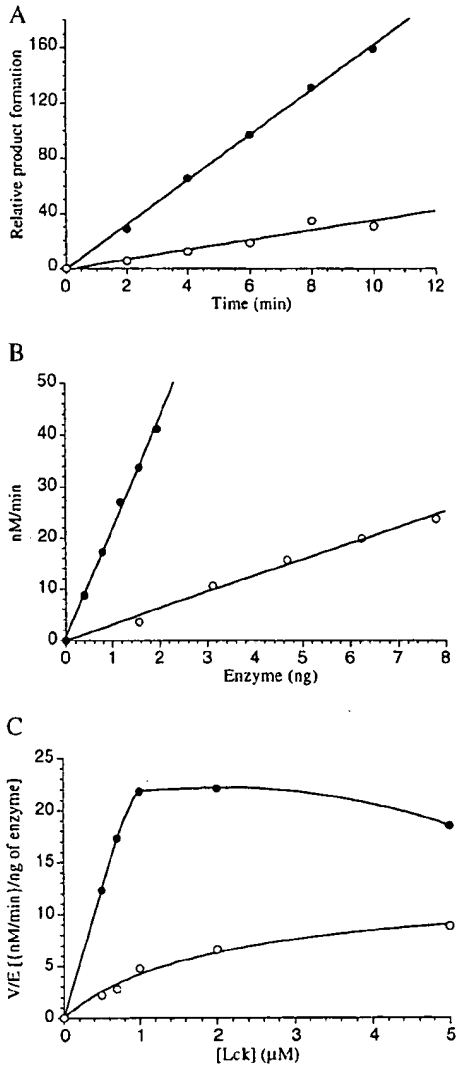

FIG. 5. Phosphorylation of Lck catalyzed by semisynthetic Csk proteins. (*A*) Time course of Csk^{PEP} and Csk^{pPEP}-catalyzed phosphorylation of Lck. ●, Csk^{pPEP}; ○, Csk^{PEP}. Relative product formation is corrected for the amount of Csk^{PEP} and Csk^{pPEP} utilized. [Lck] = 1 μM. (*B*) Kinase activity vs. Csk^{PEP} and Csk^{pPEP} concentration with the substrate Lck. ●, Csk^{pPEP}; ○, Csk^{PEP}. [Lck] = 1 μM. Reaction time = 2 min. (*C*) Rate of phosphorylation of Lck catalyzed by Csk^{PEP} and Csk^{pPEP} vs. Lck concentration. ●, Csk^{pPEP}; ○, Csk^{PEP}. The data for Csk^{pPEP} could not be strictly fit to standard Michaelis-Menten kinetics because of apparent substrate inhibition. For Csk^{pPEP} the K_m (apparent) (Lck) estimated as the substrate concentration necessary for 50% maximal velocity is 0.4 ± 0.1 μM. The data for Csk^{PEP} was fit to the Michaelis-Menten equation and gave K_m (apparent) (Lck) = 2 ± 0.5 μM. The Lck K_m with wild-type Csk enzyme under these conditions is 3–5 μM (25). All assays were performed as described (25) on a 15 μl scale at 30°C by using catalytically impaired Lck (N-terminal 63 aa deleted, containing a K273R mutation) at fixed and near-saturating ATP concentration [10 μM, ≈3 × K_m (apparent)] and optimal $MnCl_2$ concentration (5 mM) under initial conditions (<10% turnover of the limiting substrate). All assays were carried out at least two times and duplicate points generally agreed within 10%. Kinase activity was shown to be identical for the phosphotyrosine-affinity purified and unpurified semisynthetic proteins by using Lck as substrate. Kinase specificity for the 505-tyrosine of Lck was confirmed by demonstrating that 505-phosphorylated Lck was not detectably phosphorylated by either semisynthetic protein using conditions described (25).

It should also be noted that the repression of Src kinase activity in its tail phosphorylated form involves a complex

network of intramolecular interactions within the Src protein (13, 15, 27), and Csk appears to lack the ability to recapitulate this inhibited state.‖ Although the structural basis for increased kinase activity of tail-phosphorylated Csk on a physiologic substrate is not yet understood,** these results allow the prediction that conformational engineering using expressed protein ligation should give rise to interesting effects in signal transduction.

In this paper, we have introduced a method in protein engineering. Our approach "expressed protein ligation" is very simple, involving a single chemical step, and effectively unites the fields of synthetic peptide chemistry and recombinant protein biotechnology. In doing so, it allows proteins to be subjected to the same level of systematic chemical investigation previously restricted to the study of small bioactive peptides. In addition to the work described in this report, we have now successfully applied expressed protein ligation to two other polypeptide systems, including the entire sigma subunit of bacterial RNA polymerase (28). Furthermore, N-terminal methionine deletion that has been observed in the several cases using the intein expression vector creates the possibility for ligation of peptides or proteins to an N-terminal cysteine (placed at the second codon of the recombinant protein). This may further expand the utility of expressed protein ligation as a means of inserting unnatural or isotopically labeled amino acids in the middle as well as at the ends of recombinant proteins.

‖Repression of Src largely requires an unphosphorylated activating loop in addition to tail phosphorylation. A major feature of Src repression appears to be that tail phosphorylation results in a conformational change that prevents autophosphorylation of the activating loop (14, 27). Because Csk does not have an activating loop it would have been impossible to predict the results on Csk's catalytic activity resulting from the conformational change due to tail phosphorylation. However, these results implicitly argue that one or more structural features that lead to catalytic repression in tail-phosphorylated Src is/are absent in tail-phosphorylated Csk.

**The simple model where the increased catalytic efficiency results from an interaction of the Lck-SH2 domain with the phosphotyrosine tail of Csk^{pEEP} appears unlikely because the addition of the peptide NH_2-Cys-Glu-Asp-Asn-Glu-phosTyr-Thr-Ala-Arg-Glu-aminocaproate-Lys-ε-[fluorescein]-CO_2H (250 μM) had minimal effect on either Csk^{pEEP} or Csk^{pEP} catalyzed Lck phosphorylation.

We are grateful to G. Cotton, I. Moarefi, K. Severinov, J. Kuriyan, W. Xu, M. Eck, S. Burley, D. Cowburn, R. Alani, M.-Q. Xu, and F. Perler for advice and assistance, and to the Damon Runyon Scholars Award Program (P.A.C), the Irving A. Hansen Memorial Foundation (P.A.C.), the National Institutes of Health (T.W.M. and P.A.C.), and the Pew Scholars Program in the Biomedical Sciences (T.W.M.) for financial support.

1. Noren, C. J., Anthony-Cahill, S. J., Griffith, M. C. & Schultz, P. G. (1989) *Science* **244,** 182–188.
2. Wallace, C. J. A. (1995) *Curr. Opin. Biotechnol.* **6,** 403–410.
3. Witte, K., Sears, P., Martin, R. & Wong, C.-H. (1997) *J. Am. Chem. Soc.* **119,** 2114–2118.
4. Jackson, D. Y., Burnier, J., Quan, C., Stanley, M., Tom, J. & Wells, J. A. (1994) *Science* **266,** 243–247.
5. Dawson, P. E., Muir, T. W., Clark-Lewis, I. & Kent, S. B. H. (1994) *Science* **266,** 776–779.
6. Muir, T. W., Dawson, P. E. & Kent, S. B. H. (1997) *Methods Enzymol.* **289,** 266–298.
7. Erlanson, D. A., Chytil, M. & Verdine, G. L. (1996) *Chem. Biol.* **3,** 981–991.
8. Xu, M.-Q. & Perler, F. B. (1996) *EMBO J.* **15,** 5146–5153.
9. Chong, S., Mersha, F. B., Comb, D. G., Scott, M. E., Landry, D., Vence, L. M., Perler, F. B., Benner, J., Kucera, R. B., Hirvonen, C. A., *et al.* (1997) *Gene* **192,** 271–281.
10. Brown, M. T. & Cooper, J. A. (1996) *Biochim. Biophys. Acta* **1287,** 121–149.
11. Superti-Furga, G. & Courtneidge, S. A. (1995) *BioEssays* **17,** 321–330.
12. Boerner, R. J., Kassel, D. B., Barker, S. C., Ellis, B., DeLacy, P. & Knight, W. B. (1996) *Biochemistry* **35,** 9519–9525.
13. Sicheri, F., Moarefi, I. & Kuriyan, J. (1997) *Nature (London)* **385,** 602–609.
14. Moarefi, I., LaFevre-Bernt, M., Sicheri, F., Huse, M., Lee, C.-H., Kuriyan, J. & Miller, W. T. (1997) *Nature (London)* **385,** 650–653.
15. Xu, W., Harrison, S. C. & Eck, M. J. (1997) *Nature (London)* **385,** 595–602.
16. Nada, S., Okada, M., MacAuley, A., Cooper, J. A. & Nakagawa, H. (1991) *Nature (London)* **351,** 69–72.
17. Partanen, J., Armstrong, E., Bergman, M., Makela, T. P., Hirvonen, H., Huebner, K. & Alitalo, K. (1991) *Oncogene* **6,** 2013–2018.
18. Cole, P. A. (1996) *Structure (London)* **4,** 239–242.
19. Grace, M. R., Walsh, C. T. & Cole, P. A. (1997) *Biochemistry* **36,** 1874–1881.
20. Cole, P. A., Burn, P., Takacs, B. & Walsh, C. T. (1994) *J. Biol. Chem.* **269,** 30880–30887.
21. Koegel, M., Kypta, R. M., Bergman, M., Alitalo, K. & Courtneidge, S. A. (1994) *Biochem. J.* **302,** 737–744.
22. Songyang, Z., Shoelson, S. E., McGlade, J., Olivier, P., Pawson, T., Bustelo, X. R., Barbacid, M., Sabe, H., Hanafusa, H., Yi, T., *et al.* (1994) *Mol. Cell. Biol.* **14,** 2777–2785.
23. Bougeret, C., Delaunay, T., Romero, F., Jullien, P., Sabe, H., Hanafusa, H., Benarous, R. & Fischer, S. (1996) *J. Biol. Chem.* **271,** 7465–7472.
24. Dawson, P. E., Churchill, M. J., Ghadiri, M. R. & Kent, S. B. H. (1997) *J. Am. Chem. Soc.* **119,** 4325–4329.
25. Sondhi, D., Xu, W., Songyang, Z., Eck, M. J. & Cole, P. A. (1998) *Biochemistry* **37,** 165–172.
26. MacAuley, A. & Cooper, J. A. (1989) *Mol. Cell. Biol.* **9,** 2648–2656.
27. Hardwick, J. S. & Sefton, B. M. (1997) *J. Biol. Chem.* **272,** 25429–25432.
28. Severinov, K. & Muir, T. W. (1998) *J. Biol. Chem.* **273,** in press.

STIC-ILL

Q 1.A.5

From: Gabel, Gailene
Sent: Wednesday, February 12, 2003 5:14 PM
To: STIC-ILL
Subject: 09/905,439

Please provide a copy of the following literature ASAP:

1) Killick, Real-time NMR studies on a transient folding intermediate of barstar. PROTEIN SCIENCE, (1999 Jun) 8 (6) 1286-91.

2) Guo et al., Identification of the binding surface on Cdc42Hs for p21-activated kinase. BIOCHEMISTRY, (1998 Oct 6) 37 (40) 14030-7.

3) Pfuhl et al., Secondary structure determination by NMR spectroscopy of an immunoglobulin-like domain from the giant muscle protein titin. JOURNAL OF BIOMOLECULAR NMR, (1995 Jul) 6 (1) 48-58.

4) Kennedy et al., Chemosensitization of a multidrug-resistant Leishmania tropica line by new sesquiterpenes from Maytenus magellanica and Maytenus chubutensis, Journal of Medicinal Chemistry, (December 20, 2001) Vol. 44, No. 26, pp. 4668-4676.

5) Carvalho et al., TCA cycle kinetics in the rat heart by analysis of C-13 isotopomers using indirect H-1[C-13] detection, AMERICAN JOURNAL OF PHYSIOLOGY-HEART AND CIRCULATORY PHYSIOLOGY, (SEP 2001) Vol. 281, No. 3, pp. H1413-H1421.

6) Sokolowski et al., Conformational analysis of a Chlamydia-specific disaccharide alpha-Kdo-(2-->8)-alpha-Kdo-(2-->O)-allyl in aqueous solution and bound to a monoclonal antibody: observation of intermolecular transfer NOEs. JOURNAL OF BIOMOLECULAR NMR, (1998 Jul) 12 (1) 123-33.

7) Kuroda et al., Locations of local anesthetic dibucaine in model membranes and the interaction between dibucaine and a Na+ channel inactivation gate peptide as studied by 2H- and 1H-NMR spectroscopies. BIOPHYSICAL JOURNAL, (1996 Sep) 71 (3) 1191-207.

8) Marceau et al., Contribution of a conserved arginine near the active site of Escherichia coli D-serine dehydratase to cofactor affinity and catalytic activity. JOURNAL OF BIOLOGICAL CHEMISTRY, (1989 Feb 15) 264 (5) 2753-7.

Thanks a bunch,
Gail R. Gabe
7B15
CM1
305-0807

Am J Physiol Heart Circ Physiol
281: H1413–H1421, 2001.

TCA cycle kinetics in the rat heart by analysis of ^{13}C isotopomers using indirect $^{1}H[^{13}C]$ detection

R. A. CARVALHO,[1] P. ZHAO,[1] C. B. WIEGERS,[3] F. M. H. JEFFREY,[1]
C. R. MALLOY,[1,2] AND A. D. SHERRY[1,3]
[1]*Mary Nell and Ralph B. Rogers Magnetic Resonance Center, Department of Radiology, University of Texas Southwestern Medical Center, Dallas 75390-9085;* [2]*Department of Internal Medicine, University of Texas Southwestern Medical Center and Department of Veterans Affairs Medical Center, Dallas 75216; and* [3]*Department of Chemistry, University of Texas at Dallas, Richardson, Texas 75083-0688*

Received 20 March 2001; accepted in final form 13 May 2001

Carvalho, R. A., P. Zhao, C. B. Wiegers, F. M. H. Jeffrey, C. R. Malloy, and A. D. Sherry. TCA cycle kinetics in the rat heart by analysis of ^{13}C isotopomers using indirect $^{1}H[^{13}C]$ detection. *Am J Physiol Heart Circ Physiol* 281: H1413–H1421, 2001.—This study was designed to test the hypothesis that indirect $^{1}H[^{13}C]$ detection of tricarboxylic acid (TCA) cycle intermediates using heteronuclear multiple quantum correlation-total correlation spectroscopy (HMQC-TOCSY) nuclear magnetic resonance (NMR) spectroscopy provides additional ^{13}C isotopomer information that better describes the kinetic exchanges that occur between intracellular compartments than direct ^{13}C NMR detection. NMR data were collected on extracts of rat hearts perfused at various times with combinations of [2-^{13}C]acetate, propionate, the transaminase inhibitor aminooxyacetate, and ^{13}C multiplet areas derived from spectra of tissue glutamate were fit to a standard kinetic model of the TCA cycle. Although the two NMR methods detect different populations of ^{13}C isotopomers, similar values were found for TCA cycle and exchange fluxes by analyzing the two data sets. Perfusion of hearts with unlabeled propionate in addition to [2-^{13}C]acetate resulted in an increase in the pool size of all four-carbon TCA cycle intermediates. This allowed the addition of isotopomer data from aspartate and malate in addition to the more abundant glutamate. This study illustrates that metabolic inhibitors can provide new insights into metabolic transport processes in intact tissues.

^{13}C isotopomers; aminooxyacetate; metabolism; NMR; glutamate

STUDIES OF INTERMEDIARY metabolism (7, 22) in intact tissues by ^{13}C nuclear magnetic resonance (NMR) isotopomer analysis of glutamate are most often made with the assumption that exchange between α-ketoglutarate and glutamate is rapid compared with tricarboxylic acid (TCA) cycle flux. Recent NMR kinetic studies (25, 29, 30, 33) of perfused hearts have shown that the rate of the ^{13}C appearance in glutamate in heart tissue is influenced by an exchange process (F_1 and V_X have both been used as a symbol of this flux) likely related to transport across the inner mitochondrial membrane. We recently reported the effects of aminooxyacetate (AOA), a widely used transaminase inhibitor (11, 28, 29), on the rate of ^{13}C incorporation into glutamate C4 and C3 from [2-^{13}C]acetate in isolated perfused rat hearts and showed that inhibition of transaminases results in a decreased rate of ^{13}C enrichment at both glutamate C4 and C3, with similar rates of ^{13}C incorporation at these two carbons (25). These observations were consistent with a two compartment model where a small glutamate pool exchanges more rapidly with a metabolically active pool of α-ketoglutarate (presumably mitochondrial), followed by slower exchange of this ^{13}C enriched glutamate with a larger pool of unenriched glutamate (presumably cytosolic). Results from a subsequent study (9) suggested that there may be an advantage to using ^{13}C multiplets appearing in the glutamate spectrum over ^{13}C enrichment data for determining TCA cycle kinetics.

In this study, we applied two-dimensional (2D) heteronuclear multiple quantum correlation-total correlation spectroscopy (HMQC-TOCSY) (15), to further examine the influence of AOA on the kinetics of ^{13}C appearance in glutamate in rat hearts perfused with [2-^{13}C]acetate. This method indirectly detects ^{13}C enrichment via attached ^{1}H but differs from direct ^{13}C detection in that it reports different groups of ^{13}C isotopomers (3). The 2D technique thereby offers the possibility of providing new insights into the distribution of ^{13}C in various metabolites during isotopic enrichment of cycle intermediates. The method was validated by comparing TCA cycle kinetic constants derived from HMQC-TOCSY data with constants derived from ^{13}C NMR isotopomer data collected on the same tissue extracts. Kinetic data from hearts perfused with 2 mM [2-^{13}C]acetate plus 1.5 mM propionate were also evaluated. As propionate increases the level of all four-carbon TCA cycle intermediates (18, 24), ^{13}C isotopomer data from glutamate, aspartate, and malate could then be included in the kinetic analysis.

Address for reprint requests and other correspondence: A. D. Sherry, Mary Nell and Ralph B. Rogers Magnetic Resonance Center, 5801 Forest Park Rd., Dallas, TX 75390-9085 (E-mail: dean.sherry@utsouthwestern.edu).

The costs of publication of this article were defrayed in part by the payment of page charges. The article must therefore be hereby marked "*advertisement*" in accordance with 18 U.S.C. Section 1734 solely to indicate this fact.

METHODS

Materials

[2-^{13}C]acetate sodium salt (99%) was purchased from Cambridge Isotope Laboratories (Andover, MA). AOA (hemihydrochloride), sodium propionate, Dowex 50W resin (100–200 mesh, hydrogen form), and Dowex 1-X8 resin (100–200 mesh, chloride form) were purchased from Sigma (St. Louis, MO). All other reagents from commercially available sources were of the highest quality. Male Sprague-Dawley rats, 250–300 g, were purchased from Sasco (Houston, TX).

Heart Perfusions

After general anesthesia was performed, rat hearts were rapidly excised and placed in an ice-cold perfusion medium. The aorta was immediately cannulated, and hearts were perfused using standard Langendorff methods at a column height of 70 cmH_2O. A modified Krebs-Hensleit (KH) buffer containing (in mM) 119.2 NaCl, 4.7 KCl, 1.25 $CaCl_2$, 1.2 $MgSO_4$, and 25 $NaHCO_3$ was bubbled with 95% O_2-5% CO_2. The entire all-glass perfusion system was jacketed and maintained at 37°C. Before sodium [2-^{13}C]acetate (2 mM) or a mixture of sodium [2-^{13}C]acetate (2 mM) plus sodium propionate (1.5 mM) was added, hearts were perfused for 30 min with 300 ml of recirculating unenriched (either 2 mM acetate or a mixture of 2 mM acetate plus 1.5 mM propionate) KH buffer (control group) or unenriched KH buffer containing 0.5 mM AOA. This period ensured equilibration of the inhibitor into all cellular compartments (13). Hearts were then perfused with sodium [2-^{13}C]acetate ± sodium propionate for variable periods of time (3, 6, 9, 12, 15, and 45 min) before being freeze-clamped in liquid N_2. Frozen tissues were extracted in 3.6% perchloric acid (PCA), neutralized with KOH, freeze-dried, and dissolved in 0.6 ml of deuterated water (^2H_2O) for NMR analysis.

^{13}C NMR

Proton-decoupled ^{13}C NMR spectra of tissue extracts at pH 7.2 were acquired at 125.7 MHz on a Varian INOVA spectrometer by using a 5-mm broad-band probe. The acquisition parameters consisted of a 45° pulse and a repetition time of 3 s. Broad-band proton decoupling was achieved by using Waltz decoupling at two power levels, and the temperature was maintained at 25°C. The relative areas of the multiplet components in each glutamate resonance were determined by deconvolution using the NUTS NMR program (Acorn; Fremont, CA).

HMQC-TOCSY

2D HMQC-TOCSY spectra were acquired on the same tissue extracts after adjustment of the pH to 2.75 (3) using either the 500- or 600-MHz Varian INOVA spectrometer and 5-mm internal diameter probes. The positional ^{13}C isotopomer information was obtained from the ^1H-^{13}C off-diagonal cross peaks, as reported previously (3). Integration of the cross-peak volumes was achieved using standard peak-picking Varian NMR software (ll2d subroutine).

Isolation of Glutamate

After NMR spectra were collected, glutamate was purified from carboxylic acids and neutral amino acids using sequential ion-exchange columns. A column containing 6 ml of Dowex 50W in a 10-ml disposable syringe was washed with 50 ml of 2 N HCl, followed by washing with distilled water. A tissue extract (pH 2.75) was applied to the cation column, washed with 25 ml of distilled water to remove carboxylic acids, and then washed with 30 ml of 2 M NH_4OH to recover all amino acids. A second column, prepared from 2.5 ml of Dowex 1-X8 in a 0.6-cm diameter glass Pasteur pipette, was washed with 50 ml of 2 M sodium acetate, followed by distilled water. The amino acid fraction from the first column was freeze-dried and redissolved in 2 ml of distilled water, and the pH was adjusted to 8, using KOH as necessary. This sample was applied to the second column and washed with 50 ml of distilled water to remove neutral amino acids and glycerol. Glutamate and aspartate were eluted from the column using 10 ml of 0.5 M acetic acid. This acetic acid fraction was subsequently freeze-dried and dissolved in 600 μl ^2H_2O for ^1H NMR analysis. The pH was adjusted to 2.5–3.0 to simplify the ^1H spectrum of the prochiral glutamate H3 protons (3).

^{13}C Fractional Enrichments

^1H NMR spectra of purified glutamate were run on a Varian INOVA 600 MHz spectrometer using a 5-mm internal diameter probe. Relative fractional enrichments were measured by deconvolution of the glutamate ^1H resonances using the NUTS software.

HPLC

Krebs cycle intermediates (citrate, malate, succinate, fumarate, and α-ketoglutarate) were determined by HPLC using a Dionex DX500 chromatography system (Dionex; Sunnyvale, CA) containing an IonPac AS_{11} analytical column, an anion self-regenerating suppressor in autosuppression external water mode, and a CD20 conductivity detector (29). With the use of a computer, the column eluent was generated by the mixture of appropriate volumes of aqueous NaOH (200 mM) and 16% methanol. The initial eluant was composed of 2% NaOH-98% methanol. After an initial 5-min equilibration period, NaOH was increased linearly from 2 to 35% over 25 min (flow rate of 2.0 ml/min.). This provided the best separation of TCA cycle dicarboxylic and TCA. This method did not, however, resolve aspartate and glutamate, so these were assayed independently with the use of a fluorometric assay (17). Chromatographic peak areas were measured using the PeakNet software provided by Dionex and converted to quantitative values by calibration with known standards.

Modeling

Metabolite pool sizes, ^{13}C fractional enrichments, and HMQC-TOCSY and ^{13}C NMR multiplet data were used in a kinetic model (tcaFLUX) to evaluate TCA cycle flux (V_{TCA}), the exchange flux (V_X), anaplerosis (y), and the fractional contribution of [2-^{13}C]acetate to acetyl-CoA (F_{C2}). The program tcaFLUX (9) is an extension of a kinetic model based on the study by Chance et al. (4).

RESULTS

Hearts Perfused with [2-^{13}C]acetate ± AOA

Tissue levels of TCA cycle intermediates. Table 1 summarizes analytic data for a few TCA cycle intermediates plus glutamate and aspartate. Only aspartate and citrate were significantly higher in hearts perfused with AOA versus controls.

^{13}C NMR spectra. [2-^{13}C]acetate is efficiently oxidized by heart tissue and this is reflected in isotopic scrambling of the ^{13}C tracer into all possible positions

Table 1. *Total tissue metabolite content in hearts perfused with 2 mM [2-^{13}C]acetate*

Metabolite	Amount, μmol/g dry wt	
	Control (n = 31)	With AOA (n = 37)
Glutamate	32.0 ± 8.2	30.9 ± 6.5
Aspartate	2.21 ± 0.77	5.32 ± 1.75[a]
Fumarate	0.01 ± 0.01	0.03 ± 0.02
α-Ketoglutarate	0.07 ± 0.04	0.06 ± 0.05
Malate	0.10 ± 0.03	0.09 ± 0.02
Succinate	0.25 ± 0.07	0.20 ± 0.03
Citrate	0.32 ± 0.08	0.83 ± 0.22[a]

Values are means ± SD; n, no. of rats. AOA, aminooxyacetate. Glutamate and aspartate data were obtained by fluorometric assay; others by HPLC. [a]$P < 0.05$, significantly different from controls.

of TCA cycle intermediates and all other metabolites in exchange with those intermediates (i.e., aspartate and glutamate) (4). This ^{13}C isotopic scrambling is evident in the time-dependent evolution of glutamate multiplets (4, 9, 18). For example, the glutamate C3 resonance evolves as a singlet (C3S, reflecting isotopomers enriched at C3 but not at C2 or C4), a doublet (C3D, reflecting isotopomers enriched at C3 and either C2 or C4), and a triplet (C3T, reflecting isotopomers enriched at C2, C3, and C4). The C3 resonances shown in Fig. 1 collected at two early perfusion times illustrate the sensitivity of these multiplets to partial inhibition of transaminases by AOA. The graphs on the *right* illustrate the complete temporal evolution of the glutamate C3D and C3T over 45 min after exposure to [2-^{13}C]acetate ± AOA. For hearts with AOA, C3D was always lower than C3T, whereas in control hearts, C3D was greater than C3T at both 3 and 6 min. The glutamate C4 and C2 multiplets also evolve with time of perfusion and reach an apparent isotopic steady state at 45 min (data not shown).

HMQC-TOCSY spectra. Figure 2 illustrates HMQC-TOCSY spectra of extracts of hearts perfused for 6 min with 2 mM [2-^{13}C]acetate ± AOA. These 2D spectra show several ^{1}H-^{13}C cross peaks that can be attributed to groups of glutamate ^{13}C isotopomers that differ from those reported by the one-dimensional ^{13}C spectra (3). For example, the triad of cross peaks labeled C3H4 reflect two groups of glutamate ^{13}C isotopomers, those enriched in both C3 and C4 (given by the outer C3H4D cross peaks) and those enriched in C3 but not C4 (given by the central C3H4S cross peak). The graphs above each HMQC-TOCSY spectrum report the C3H4D and C3H2D cross-peak volumes as a function of perfusion time. As illustrated for only two HMQC-TOCSY multiplets, these spectra are also sensitive to the presence or absence of AOA. Similar graphs were obtained for all other HMQC-TOCSY cross-peak multiplet volumes.

^{1}H NMR spectra of isolated glutamate. Figure 3 shows expanded regions of the ^{1}H NMR spectra of glutamate isolated from hearts perfused with sodium [2-^{13}C]acetate ± AOA for 6 min. Clearly, hearts perfused without AOA achieve a much higher level of ^{13}C enrichment than do hearts perfused with the inhibitor at this early time point. The graphs above the two spectra in Fig. 3 show the ^{13}C-fractional enrichments of glutamate C3 and C4 as a function of perfusion time. Both C3 and C4 reach steady-state ^{13}C fractional enrichment at ~30 min in control hearts but these values appear to be only approaching steady state at 45 min in hearts perfused with AOA. Nevertheless, glutamate reaches the same level of ^{13}C enrichment at isotopic steady state in both experiments (±AOA) as evidenced by the identical F_{C_2} values (see Tables 2 and 3).

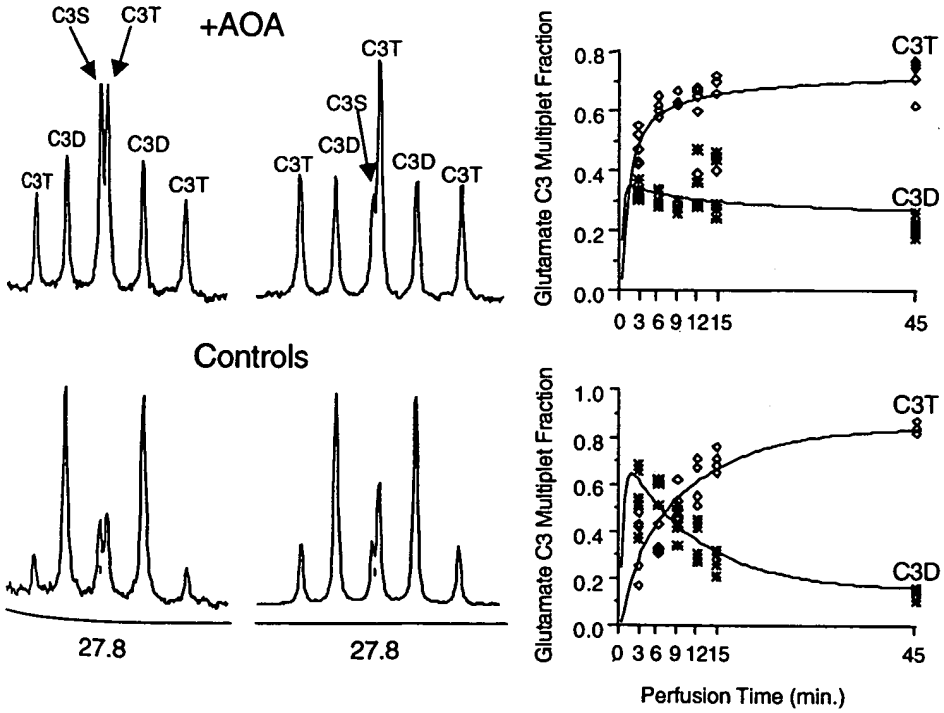

Fig. 1. Glutamate C3 expansions from 150.9-MHz ^{13}C nuclear magnetic resonance (NMR) spectra of extracts from rat hearts perfused for either 3 min or 6 min with 2 mM [2-^{13}C]acetate ± 0.5 mM aminooxyacetate (AOA). The ^{13}C multiplet component C3T is relatively more intense in the AOA-perfused than in control hearts both at 3 and 6 min. *Right*: temporal evolution of C3T and C3D multiplets (see text for details).

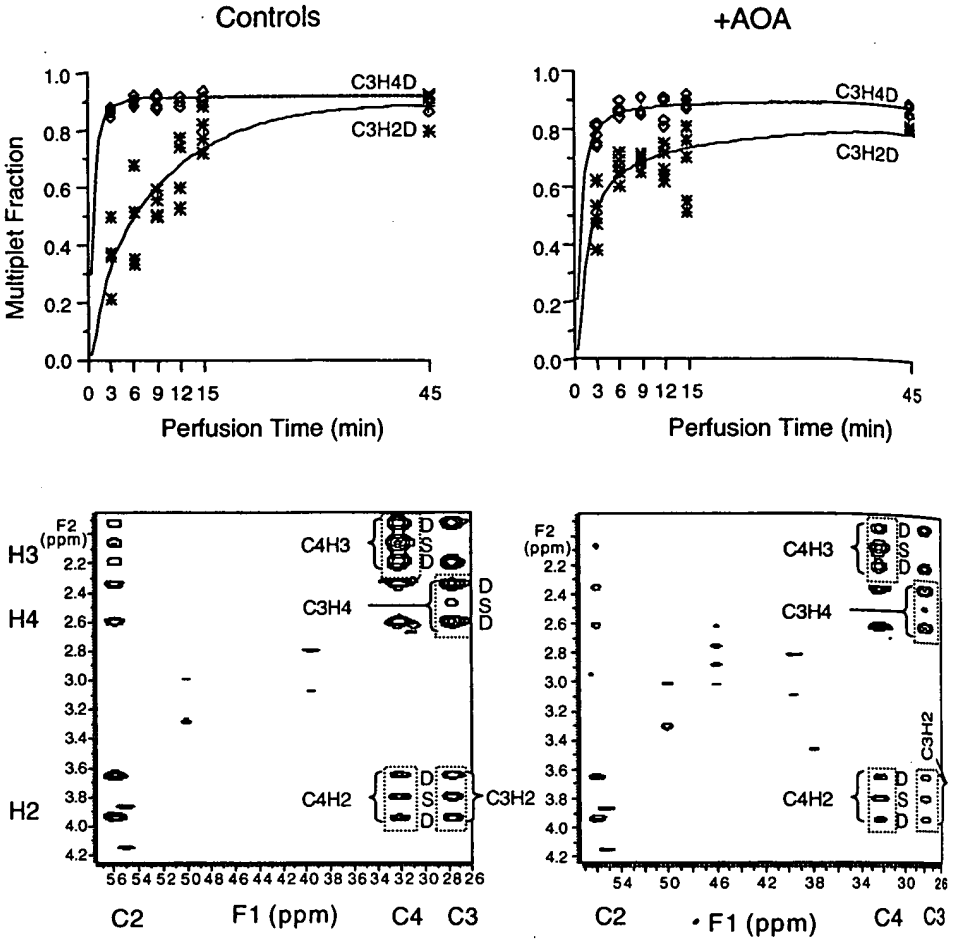

Fig. 2. Heteronuclear multiple quantum correlation-total correlation spectroscopy (HMQC-TOCSY) (600 MHz) spectra from the extracts of two rat hearts perfused for 6 min with 2 mM [2-^{13}C]acetate in the presence (*right*) and absence (*left*) of 0.5 mM AOA. The dashed-line boxes highlight some of the cross-peaks that can be used in a ^{13}C isotopomer analysis. *Top*: graphs showing temporal evolution of two HMQC-TOCSY multiplet components, C3H4D and C3H2D, for both control and AOA-perfused hearts. In the AOA-perfused hearts, the curves approach each other, reflecting similar kinetics of ^{13}C appearance in C4 and C2.

Kinetic modeling using tcaFLUX. Table 2 reports values for V_{TCA}, V_X, y, and the contribution [2-^{13}C]acetate to acetyl-CoA (F_{C2}) for control and AOA perfused hearts obtained by fitting the ^{13}C NMR multiplet data to tcaFLUX. Values in parentheses are 5–95% confidence limits determined for each parameter. V_{TCA} was significantly higher (~1.5–2-fold), whereas V_X was dramatically lower (~10-fold), in hearts perfused with AOA compared with controls. F_{C2} and y were essentially unaffected by the inhibitor. These values are consistent with previous reports (25, 29).

Table 3 summarizes flux values and other parameters determined by fitting the HMQC-TOCSY cross-peak multiplet data to the same kinetic model. There was excellent agreement between all parameters determined by the two NMR methods (none of the parameters of Table 3 differ significantly from the corresponding parameter of Table 2). Again, V_{TCA} tended to be higher (although the confidence intervals do overlap), whereas V_X was lower, in hearts perfused with AOA. This comparison shows that HMQC-TOCSY data, although reflecting different groups of isotopomers than ^{13}C NMR, is sensitive to TCA cycle and related pathway kinetics. The solid lines drawn through the data of Figs. 1–3 represent the best fit of all data, ^{13}C NMR multiplets, HMQC-TOCSY cross-peak volumes, and ^{13}C fractional enrichments to the kinetic model. In general, the agreement is quite good for all of the data shown; the largest deviation was found for the limiting fractional ^{13}C enrichments in control hearts as determined by ^{1}H NMR (Fig. 3).

Hearts Perfused With [2-^{13}C]acetate and Propionate

Tissue levels of TCA cycle intermediates. Table 4 summarizes analytic data for selected TCA cycle intermediates, glutamate, and aspartate for hearts perfused with a combination of acetate and propionate. Total tissue glutamate was lower by ~3-fold, aspartate was ~10-fold higher, while malate was ~120-fold higher, for hearts perfused with a combination of acetate plus propionate compared with acetate alone (24). The sum of all tissue metabolites shown was ~33% higher in hearts perfused with acetate plus propionate compared with acetate alone. These changes reflect an altered metabolic steady state resulting from influx of propionate into the TCA cycle pools via succinyl-CoA and matched by an equivalent disposal flux of a four-carbon intermediate, likely malate to pyruvate [flux of this pyruvate into acetyl-CoA and the TCA cycle, previously given the symbol y_{ox} (in Ref. 10), is therefore assumed equal to y].

HMQC-TOCSY spectra. Figure 4 shows selected regions of HMQC-TOCSY spectra of extracts of hearts

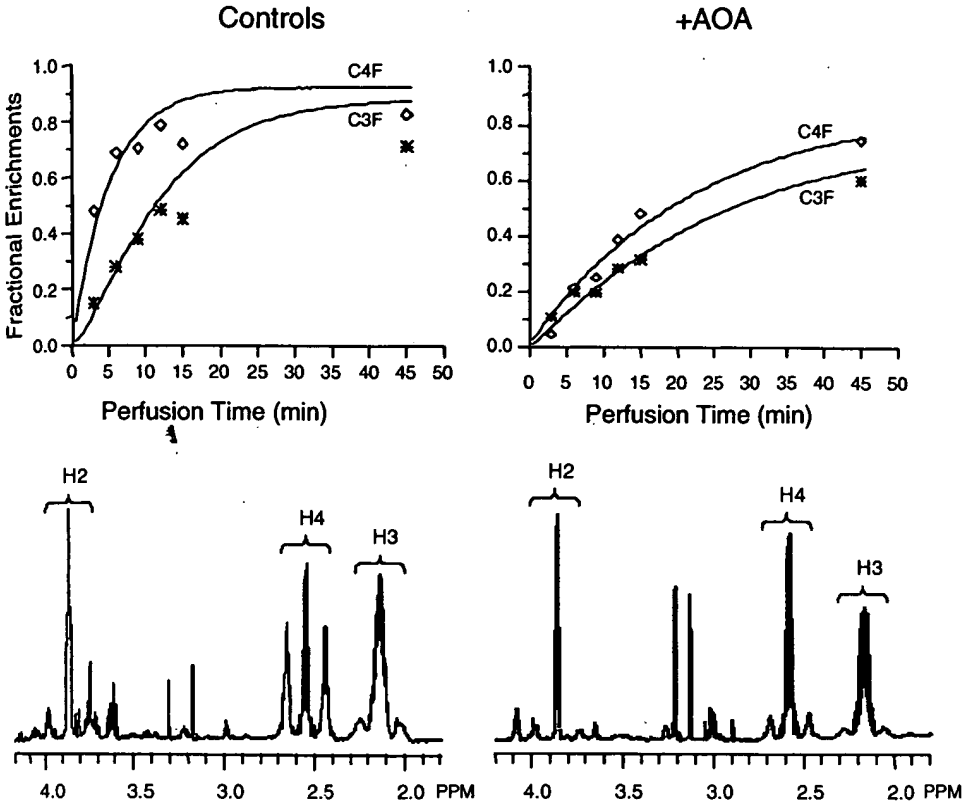

Fig. 3. Temporal evolution of ^{13}C fractional enrichments in glutamate carbons C3 and C4 for control (*left*) and AOA-perfused rat hearts (*right*). *Bottom*: spectra show the corresponding ^{1}H NMR spectra of glutamate purified from heart extracts after perfusion with [2-^{13}C]acetate for 6 min, without (*left*) and with (*right*) AOA. The ^{13}C fractional enrichment of all carbons is higher and there is a greater difference between the ^{13}C fractional enrichments of glutamate C4 and the two other carbons, C2 and C3, in the control heart. The ^{1}H spectrum of the AOA heart shows that much more unenriched glutamate is present at 6 min than in the control heart.

perfused for 6 min with 2.0 mM [2-^{13}C]acetate plus 1.5 mM propionate ± 0.5 mM AOA. These regions illustrate that isotopomer data can be derived for at least two four-carbon intermediates associated with the TCA cycle (malate and aspartate) in addition to glutamate. The triad cross peaks of aspartate C3H2 and malate C3H2 show that both four-carbon intermediates at the 6-min time-point are made up of isotopomers with ^{13}C enrichment at both C3 and C2 (the doublets) and isotopomers with ^{13}C enrichment at C3 but not C2 (the singlets). Clearly, the doublet component in each cross peak is higher in hearts perfused with AOA than without AOA. Also, the doublet components of aspartate C3H2 and malate C3H2 were equal in spectra collected at 6 min in control hearts, but the malate C3H2 doublet was higher than the aspartate C3H2 doublet at this same time-point in hearts with AOA. This illustrates that AOA has differential effects on ^{13}C enrichment of the four-carbon TCA cycle intermediate, malate, compared with the four-carbon intermediate that is in exchange with cycle intermediates, aspartate. The graphs illustrate how these and other HMQC-TOCSY cross-peak volumes change as a function of perfusion time.

Kinetic modeling. The HMQC-TOCSY data derived from hearts perfused with acetate plus propionate were fit to the same kinetic model as described above for hearts perfused with acetate alone. Because propionate is essentially completely oxidized via pyruvate and acetyl-CoA in heart tissue (10, 24), it was assumed that $y = y_{ox}$, i.e., flux of propionate through the TCA cycle and into acetyl-CoA. Table 5 summarizes the best-fit parameters and their 5–95% confidence limits. As anticipated, V_{TCA} was ~2-fold lower and y was ~10-fold higher in hearts perfused with acetate plus propionate compared with acetate alone (compare Tables 3 and 5). Furthermore, the contribution of acetate

Table 2. *Kinetic analysis of hearts perfused with [2-^{13}C]acetate using ^{13}C isotopomer data derived from ^{13}C NMR spectra*

Flux, μmol·min^{-1}·g dry wt^{-1}	Control (5–95%)	+AOA (5–95%)
V_{TCA}	10.9 (10.0–11.9)	19.4 (16.7–22.7)[a]
V_X	14.0 (11.0–17.9)	1.50 (1.31–1.71)[a]
y	0.02 (0.00–0.09)	0.05 (0.03–0.08)
F_{C2}	0.92 (0.90–0.95)	0.88 (0.86–0.89)

NMR, nuclear magnetic resonance; V_{TCA}, tricarboxylic acid (TCA) cycle flux; V_X, exchange flux; y, anaplerosis; F_{C2}, fractional contribution of [2-^{13}C]acetate to acetyl-CoA. [a]$P < 0.05$, significantly different from the control group.

Table 3. *Kinetic analysis of hearts perfused with [2-^{13}C]acetate using ^{13}C isotopomer data derived from 2D HMQC-TOCSY spectra*

Flux, μmol·min^{-1}·g dry wt^{-1}	Control (5–95%)	+AOA (5–95%)
V_{TCA}	12.5 (11.1–14.0)	16.3 (13.8–19.1)
V_X	17.3 (11.1–27.0)	1.97 (1.30–3.00)[a]
y	0.03 (0.01–0.08)	0.08 (0.06–0.11)
F_{C2}	0.92 (0.89–0.94)	0.90 (0.88–0.92)

2D, two-dimensional; HMQC-TOCSY, heteronuclear multiple quantum spectroscopy correlation. [a]$P < 0.05$, significantly different from the control group.

Table 4. *Total tissue metabolite content in hearts perfused with 2.0 mM [2-^{13}C]acetate plus 1.5 mM propionate*

Metablite	Amount, μmol/g dry wt	
	Control (n = 4)	+AOA (n = 4)
Glutamate	10.3 ± 1[a]	10.5 ± 1[c]
Aspartate	21.7 ± 5[a]	12.8 ± 2[c,e]
Fumarate	1.3 ± 0.2[b]	1.3 ± 0.2[c]
α-Ketoglutarate	0.03 ± 0.01[b]	0.03 ± 0.01[d]
Malate	9.7 ± 2[b]	7.3 ± 2[c,e]
Succinate	0.6 ± 0.4[b]	0.6 ± 0.4[d]
Citrate	0.6 ± 0.3[b]	0.6 ± 0.3[d]

Values are means ± SD; n, no. of rat hearts. [a]Determined by enzymatic assay and fluorometric detection of reduced nicotinamide adenine dinucleotide, [b]by HPLC, and [c]by ^{13}C NMR using an internal standard of [3-^{13}C]propionate. [d]These metabolites were not detected in ^{13}C NMR spectra so were assumed equal to that determined by HPLC in extracts of control hearts. [e]$P < 0.05$, significantly different from controls.

to acetyl-CoA was considerably reduced in the presence of propionate (from 92 to 57%). V_X was comparable to V_{TCA} in this group, although the uncertainty in V_X was noticeably higher. AOA had similar metabolic effects in hearts perfused with the acetate-propionate substrate combination compared with acetate alone; V_{TCA} increased in response to AOA (almost twofold), V_X was again lower (but less so that without propionate), anaplerosis was stimulated by AOA, whereas the contribution made by [2-^{13}C]acetate to acetyl-CoA (the F_{C2} parameter) was unaffected by AOA.

DISCUSSION

This study demonstrates that ^{13}C isotopomer data derived from multiplet areas in ^{13}C NMR spectra or from multiplet volumes in HMQC-TOSCY spectra of heart extracts exposed to ^{13}C-enriched substrates for variable time periods can be used as input to kinetic models of the TCA cycle. In hearts perfused with 2 mM [2-^{13}C]acetate alone, V_{TCA} was 11.7 μmol·min^{-1}·g dry wt^{-1} (average of 2 values), whereas V_X was 15.6 μmol·min^{-1}·g dry wt^{-1} (average of 2 values) as estimated using either NMR data set. The value of V_{TCA} determined here was similar to values reported previously for hearts perfused with acetate [7.5 (25); 10.1 (33); 10.67 (31)] but V_X determined here appears to be somewhat higher than the corresponding flux reported previously [7.5 (25); 9.3 (33); 10.18 (31)]. The transaminase inhibitor AOA had multiple complex effects on the kinetic data. First, the multiplets arising from multiply labeled isotopomers (see, for example, C3T in Fig. 1 and C3H2D in Fig. 2) appeared more rapidly with time in both NMR data sets. This is indicative of more rapid turnover of a smaller pool of tissue metabolites in the presence of AOA, consistent with rapid α−KG⇆Glu exchange within the mitochondrial matrix, followed by slower exchange of both metabolites with their larger cytosolic components (25). As anticipated, V_X was substantially lower in the presence of AOA, decreasing ~10-fold from 15.6 to 1.74 μmol·min^{-1}·g dry wt^{-1}. As discussed below, V_X determined in the presence of AOA likely reflects a rate-limiting transaminase flux and not a metabolite exchange flux. Again, both NMR data sets reported similar values for V_X. The decrease in V_X brought about by 0.5 mM AOA in these experiments (10-fold) was much larger than that found by Weiss et al. (29) using only 0.1 mM AOA (twofold).

One unanticipated result was an increase in V_{TCA} found for all hearts perfused with AOA. A fit of the ^{13}C NMR data set indicated that V_{TCA} increased from 10.9 to 19.4 μmol·min^{-1}·g dry wt^{-1}, whereas a fit of the 2D data set predicted an increase from 12.5 to 16.3 μmol·min^{-1}·g dry wt^{-1}. This 30–70% increase in V_{TCA} brought about by partial inhibition of transaminases likely reflects a redistribution of metabolites between the cytosol and mitochondrial. We have shown previously that tissue glutamate is not fully visible by NMR in isolated hearts exposed to AOA and ascribed this to a net shift in glutamate from the cytosol to the mitochondrial matrix (25). This could also occur with other components of the malate-aspartate shuttle and thereby give the cell less ability to transport reducing equivalents from the cytosol to the mitochondria. Thus the increase in V_{TCA} brought about by partial inhibition of transaminases indicates that the contribution of cytosolic reduced nicotinamide adenine dinucleotide to overall energy production is lower in hearts perfused with acetate plus AOA. We demonstrated previously that AOA does not alter O_2 consumption by heart tissue (25), so any decrease in contribution of cytosolic reducing equivalents would require a higher flux through the oxidative TCA cycle.

Hearts perfused with [2-^{13}C]acetate plus propionate showed substantial kinetic differences compared with those perfused with [2-^{13}C]acetate alone. We have shown in previous reports that propionate is efficiently oxidized in heart tissue via the TCA cycle, pyruvate, and subsequently acetyl-CoA (10, 24). Thus, given that additional $FADH_2$ is produced by propionate at the level of succinate dehydrogenase plus two additional reducing equivalents are formed at the level of the malic enzyme and pyruvate dehydrogenase (PDH), one would anticipate that V_{TCA} would be significantly reduced in hearts perfused with propionate. Clearly, V_{TCA} was significantly reduced when propionate was present, compared with acetate alone (5.3 vs. 11.7 μmol·min^{-1}·g dry wt^{-1}) because of the three extra reducing equivalents produced along this oxidative pathway (succinyl-CoA → malate → pyruvate → acetyl-CoA). It has been shown (S. C. Burgess, E. Babcock, A. D. Sherry, and C. R. Malloy, unpublished observations, 32, 33) that perfusion of hearts with any substrate that contributes non-TCA cycle-reducing equivalents (i.e., butyrate, lactate, or octanoate) results in a decrease in V_{TCA} relative to hearts perfused with acetate alone. Given that y was ~35% of V_{TCA} in hearts perfused with acetate plus propionate, one would predict that propionate (the only anaplerotic substrate present) would contribute one (0.35 × 3 = 1.05) extra reducing equivalent for each turn of the

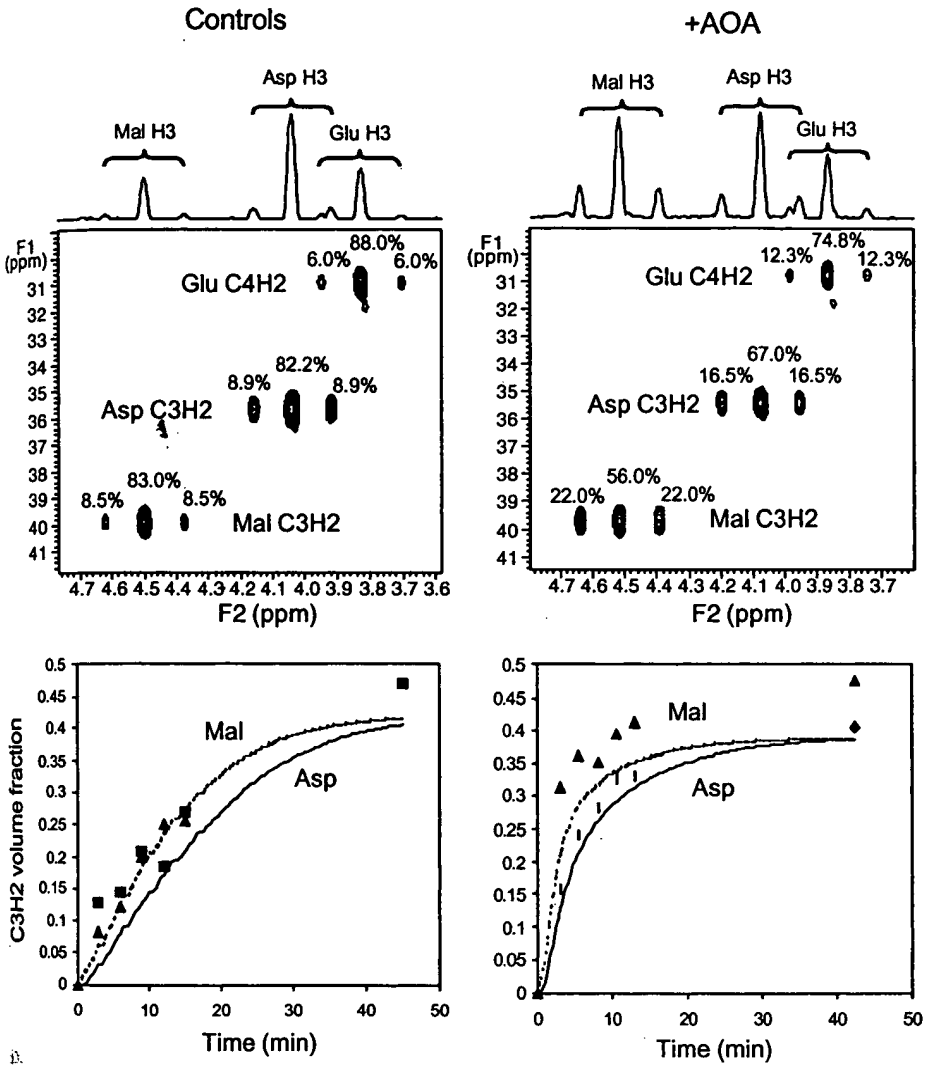

Fig. 4. HMQC-TOCSY (600 MHz) spectra of extracts of hearts perfused for 6 min with 2.0 mM [2-^{13}C]acetate plus 1.5 mM propionate in the presence (*right*) and absence (*left*) of 0.5 mM AOA. HMQC-TOCSY 2D plots illustrate the difference in ^{13}C labeling between malate (Mal), a tricarboxylic acid (TCA) cycle intermediate, and glutamate (Glu) and aspartate (Asp), two metabolic intermediates in exchange with TCA cycle intermediates. *Bottom*: complete temporal appearance of the malate and aspartate C3H2D cross-peak volumes.

TCA cycle (4 reducing equivalents). Given this stoichiometry and the assumption that O_2 consumption is not altered by propionate, V_{TCA} should be ~25% lower in the presence of propionate. The fact that we observed an ~50% decrease in V_{TCA} indicates that propionate has more complex effects on metabolism. Latipää et al. (14) have shown that propionate fully activates the pyruvate dehydrogenase complex via phosphorylation yet flux through PDH is reduced in the presence of propionate due to the combined effects of low-tissue CoA and partial inhibition of PDH by the high tissue levels of propionyl-CoA and methylmalonyl-CoA. This suggests that hearts may turn toward alternative, nonglycolytic sources of acetyl-CoA in the presence of propionate, consistent with a lowering of the contribution of [2-^{13}C]acetate to acetyl-CoA (the F_{C2} parameter) observed here. A lowering of free CoA by propionate could also directly alter V_{TCA} by lowering flux through α-ketoglutarate dehydrogenase, an enzyme that has a strict requirement for free CoA.

Table 5. *Kinetic analysis of hearts perfused with [2-^{13}C]acetate and propionate based on ^{13}C isotopomer data derived from 2D HMQC-TOCSY spectra.*

Flux, μmol·min^{-1}·g dry wt^{-1}	Control, 5%–95%	+AOA, 5%–95%
V_{TCA}	5.3 (4.7–6.0)	8.6 (7.5–9.8)[b]
V_X	6.3 (3.3–12.2)	2.3 (1.3–3.9)
y[a]	0.35 (0.27–0.44)	0.56 (0.49–0.64)[b]
F_{C2}	0.57 (0.55–0.59)	0.61 (0.59–0.63)

Data for glutamate, aspartate, and malate were included in the fitting procedure. [a]Here, anaplerotic flux of propionate (1.5 mM) into the TCA cycle (relative to V_{TCA}) must equal flux of a cycle intermediate into pyruvate, acetyl-CoA, and the oxidative branch of the TCA cycle (given as y_{ox} in Ref. 10). [b]$P < 0.05$, significantly different from the control group.

Interestingly, V_X was also substantially lower in the presence of propionate (6.3 vs. 15.7 μmol·min^{-1}·g dry wt^{-1} for acetate alone). Although one might anticipate that the "extra" reducing equivalents produced by oxidation of propionate would stimulate the malate-aspartate shuttle and hence increase V_X as suggested before for lactate (32), the exact opposite was observed. This indicates again that propionate has multiple contrasting effects on metabolism. Some of the enzymes required for complete oxidation of propionate are mitochondrial in origin (succinyl-CoA → malate) so pro-

pionate directly contributes mitochondrial-reducing equivalents without invoking the malate-aspartate shuttle. It is perhaps then not surprising that less shuttle activity is required for propionate oxidation and, hence, V_X decreases. The metabolic consequences of propionate are complex; it reduces the TCA cycle energy requirement by directly producing mitochondrial-reducing equivalents yet, at the same time, it reduces the level of free CoA available to mitochondrial enzymes. The net metabolic result is a reduction in both V_{TCA} and V_X. We have observed (unpublished observations) that hearts do not perform well when perfused with propionate as their sole substrate for an extended period of time (~2 h), consistent with limited energy production by mitochondrial reactions.

The addition of AOA to hearts perfused with acetate plus propionate had predictable effects on both V_{TCA} and V_X. V_X was further decreased in the presence of AOA and, interestingly, to nearly the same level as in hearts perfused with acetate alone (compare 1.5 vs. 2.3 $\mu mol \cdot min^{-1} \cdot g$ dry wt^{-1} for acetate vs. acetate plus propionate, respectively). This is consistent with V_X reflecting a different rate-limiting step in the presence of AOA than in its absence. The fact that V_X dropped to the same level on addition of AOA to acetate versus acetate plus propionate hearts is consistent with a rate limited by transaminase flux. Interestingly, AOA partially reverses the deleterious effect propionate has on V_{TCA}, exactly as expected for a metabolic system that may be limited by levels of mitochondrial α-KG. This again is consistent with a net shift in intermediates from the cytosol to the mitochondria in the presence of AOA, thereby stimulating V_{TCA} and energy production.

What additional kinetic information, if any, is provided by the malate and aspartate isotopomers detected in HMQC-TOCSY spectra (Fig. 4) of hearts perfused with acetate plus propionate compared with glutamate isotopomers alone? Table 6 compares the spread in 5–95% confidence limits for V_{TCA} and V_X that one finds by fitting glutamate isotopomer data alone, glutamate plus aspartate isotopomer data, glutamate plus malate isotopomer data, and isotopomer data from all three metabolites combined. The time-dependent appearance of aspartate isotopomers basically parallels that seen in glutamate because both molecules are enriched via transamination of TCA cycle intermediates. The data in Table 6 show that inclusion of both glutamate and aspartate data does little to improve the confidence limits for V_{TCA} but does improve slightly the confidence limits for V_X. A similar improvement in the confidence limits for V_{TCA} and V_X was observed by comparing the fits of glutamate data alone versus the glutamate plus malate data in control hearts. In AOA-perfused hearts, however, inclusion of the malate data makes a marked improvement on the confidence limits for V_X.

Table 6. *Comparison of confidence intervals for V_{TCA} and V_X obtained by fitting isotopomer data from glutamate alone, glutamate plus asparate, and glutamate plus malate vs. all 3 metabolites*

Isotopomers Included in Fit	Confidence Intervals (95%–5%) Control Hearts		Confidence Intervals (95%–5%) +AOA	
	V_{TCA}	V_X	V_{TCA}	V_X
Glu alone	1.5	18.8	2.2	7.9
Glu + Asp	1.4	11.1	2.2	4.9
Glu + Mal	1.4	12.0	2.6	2.7
Glu + Asp + Mal	1.3	9.0	2.3	2.6

Glu, glutamate; Mal, malate; Asp, asparate.

One would predict a priori that malate would become enriched somewhat faster in the presence of AOA because the size of the exchanging aspartate and glutamate pools would be effectively smaller during isotopic turnover. Plots of the temporal appearance of malate and aspartate C3H2D are compared in Fig. 4. The solid lines through the data reflect the isotopomer populations predicted by the kinetic model described in Table 5. Here, one sees that the malate and aspartate C3H2D volumes essentially track one another in control hearts although enrichment of aspartate requires an additional transaminase step. In the presence of AOA, both malate and aspartate become enriched more quickly, as predicted for smaller exchanging pool sizes, but the malate also clearly approaches steady-state enrichment more rapidly than aspartate. Here, the kinetic model reproduces the aspartate and glutamate data reasonably well but rather poorly predicts the isotopomer distribution in malate. This indicates that V_X reported by the kinetic analysis of these hearts reflects transaminase flux, whereas a fit of the malate data alone would give a different V_X value reflecting instead a transport step. All of our observations are consistent with the hypothesis offered by Yu et al. (33) that V_X in control hearts reflects a transport process involving exchange of a metabolite labeled in the TCA cycle with a larger counterpart in the cytosol. In hearts perfused with AOA, V_X is apparently limited by flux through the transaminases rather than a transport flux so a separate fit of malate isotopomer data may allow the determination of both the transaminase and transport fluxes.

This study has shown that equivalent kinetic data is derived from ^{13}C isotopomer data obtained by either direct ^{13}C observe or indirect HMQC-TOCSY NMR spectroscopy. Thus the possible advantages offered by the greater sensitivity of the 2D method were not realized in this study because the amount of tissue available for analysis was not limiting. However, the HMQC-TOCSY method could prove important when analyzing kinetic data in situations where tissue samples may be limiting (i.e., tissue biopsies or perfused mouse hearts) or if a high-field NMR spectrometer is not available. The reported ~5-fold increased sensitivity of the method (3) does offer the possibility of detecting more metabolites than direct ^{13}C observe spectroscopy and such data should provide added value in fitting ^{13}C isotopomer data to ever increasingly more complex kinetic models.

This work was supported in part by National Institutes of Health Grants HL-34557 and RR-02584. R. A. Carvalho was supported by

Portuguese Foundation for Science and Technology (PRAXIS XXI) Grant BD-3604/94.

Present address of R. A. Carvalho: Department of Biochemistry, University of Coimbra, 3000 Coimbra, Portugal.

REFERENCES

1. **Bhattacharya M, Fuhrman L, Ingram A, Nickerson KW, and Conway T.** Single-run separations and detection of multiple metabolic intermediates by anion-exchange high-performance liquid chromatography and application to cell pool extracts prepared from *Escherichia coli*. *Anal Biochem* 232: 98–106, 1995.
3. **Carvalho RA, Jeffrey FMH, Sherry AD, and Malloy CR.** ^{13}C isotopomer analysis of glutamate by heteronuclear multiple quantum coherence-total correlation spectroscopy (HMQC-TOCSY). *FEBS Lett* 440: 382–386, 1998.
4. **Chance EM, Seeholzer SH, Kobayashi K, and Williamson JR.** Mathematical analysis of isotope labeling in the citric acid cycle with applications to ^{13}C NMR studies in perfused rat hearts. *J Biol Chem* 258: 13785–13794, 1983.
5. **Chatham JC, Forder JR, Glickson JD, and Chance EM.** Calculation of absolute metabolic flux and the elucidation of the pathways of glutamate labeling in perfused rat heart by ^{13}C NMR spectroscopy and nonlinear least square analysis. *J Biol Chem* 270: 7999–8008, 1995.
6. **Chatham JC and Chance EM.** Biological magnetic resonance. In: *In Vivo Carbon-13 NMR*, edited by Berliner LJ and Robitaille P-M. New York: Kluwer-Plenum, ch. 3, vol. 15, p. 99–116, 1998.
7. **Fitzpatrick SM, Heterington HP, Behar KL, and Shulman RG.** The flux from glucose to glutamate in the rat brain in vivo as determined by ^{1}H-observed, ^{13}C-edited NMR spectroscopy. *J Cereb Blood Flow Metab* 10: 170–179, 1990.
8. **Gruetter R, Novotny EJ, Boulware SD, Mason GF, Rothman DL, Shulman GI, Prichard JW, and Shulman RG.** Localized ^{13}C NMR spectroscopy in the human brain of amino acid labeling from D-[1-^{13}C]glucose. *J Neurochem* 63: 1377–1385, 1994.
9. **Jeffrey FMH, Reshetov A, Storey CJ, Carvalho RA, Sherry AD, and Malloy CR.** Use of a single resonance of glutamate for measuring oxygen consumption in intact tissues. *Am J Physiol Endocrinol Metab* 277: E1103–E1110, 1999.
10. **Jeffrey FMH, Storey CJ, Sherry AD, and Malloy CR.** ^{13}C isotopomer model for estimation of anaplerotic substrate oxidation via acetyl-CoA. *Am J Physiol Endocrinol Metab* 271: E788–E799, 1996.
11. **Kauppinen RA, Sihra TS, and Nicholls DG.** Aminooxyacetic acid inhibits the malate-aspartate shuttle in isolated nerve terminals and prevents the mitochondria from utilizaing glycolytic substrates. *Biochim Biophys Acta* 930: 173–178, 1987.
12. **Kihara M and Kubo T.** Aspartate aminotransferase for synthesis of transmitter glutamate in the medulla oblongata: effect of aminooxyacetic acid and 2-oxoglutarate. *J Neurochem* 52: 1127–1134, 1989.
13. **LaNoue KF, Nicklas WJ, and Williamson JR.** Control of citric acid cycle activity in rat heart mitochondria. *J Biol Chem* 245: 102–111, 1970.
14. **Latipää PM, Peuhkurinen KJ, Hiltunen JK, and Hassinen IE.** Regulation of pyruvate dehydrogenase during infusion of fatty acids of varying chain lengths in the perfused rat heart. *J Mol Cell Cardiol* 17: 1161–1171, 1985.
15. **Lerner L and Bax A.** Sensitivity-enhanced two-dimensional heteronuclear relayed coherence transfer NMR spectroscopy. *J Magn Reson* 69: 375–380, 1986.
16. **Lewandowski ED.** Biological magnetic resonance. In: *In Vivo Carbon-13 NMR*, edited by Berliner LJ and Robitaille P-M. New York: Kluwer-Plenum, ch. 4, vol. 15, p. 117–159, 1998.
17. **Lowry OH and Passonneau JV.** Typical fluorometric procedures for metabolic assays. In: *Flexible System of Enzymatic Assays*. New York: Academic, 1972.
18. **Malloy CR, Sherry AD, and Jeffrey FMH.** Evaluation of carbon flux and substrate selection through alternate pathways involving the citric acid cycle of the heart by ^{13}C NMR spectroscopy. *J Biol Chem* 263: 6964–6971, 1988.
19. **Mason GF, Gruetter Rothman DL, Behar KL, Shulman RG, and Novotny EJ.** Simultaneous determination of the rates of the TCA cycle, glucose utilization, α-ketoglutarate/glutamate exchange, and glutamine synthesis in human brain by NMR. *J Cereb Blood Flow Metab* 15: 12–25, 1995.
20. **Mason GF, Rothman DL, Behar KL, and Shulman RG.** NMR determination of the TCA cycle rate and α-ketoglutarate/glutamate exchange in rat brain. *J Cereb Blood Flow Metab* 12: 434–447, 1992.
21. **O'Donnell JM, Doumen C, LaNoue KF, White LT, Yu X, Alpert NM, and Lewandowski ED.** Dehydrogenase regulation of metabolite oxidation and efflux from mitochondria in intact hearts. *Am J Physiol Heart Circ Physiol* 274: H467–H476, 1998.
22. **Robitaille PML, Rath DP, Skinner TE, Abduljalil AM, and Hamlin RL.** Transaminase reaction rates, transport activities and TCA cycle analysis by post-steady state ^{13}C NMR. *Magn Reson Med* 30: 262–266, 1993.
23. **Shen J, Petersen KF, Behar KL, Brown P, Nixon TW, Mason GF, Petroff OA, Shulman GI, Shulman RG, and Rothman DL.** Determination of the rate of the glutamate/glutamine cycle in the human brain by in vivo ^{13}C NMR. *Proc Natl Acad Sci USA* 96: 8235–8240, 1999.
24. **Sherry AD, Malloy CR, Roby RE, Rajagopal A, and Jeffrey FMH.** Propionate metabolism in the rat heart by ^{13}C NMR spectroscopy. *Biochem J* 254: 593–598, 1988.
25. **Sherry AD, Zhao P, Wiethoff AJ, Jeffrey FMH, and Malloy CR.** Effects of aminooxyacetate on glutamate compartmentation and TCA cycle kinetics in rat hearts. *Am J Physiol Heart Circ Physiol* 274: H591–H599, 1998.
26. **Sibson NR, Dhankhar A, Mason GF, Rothman DL, Behar KL, and Shulman RG.** Stoichiometric coupling of brain glucose metabolism and glutamatergic neuronal activity. *Proc Natl Acad Sci USA* 95: 316–321, 1998.
27. **Sibson NR, Dhankhar A, Mason GF, Behar KL, Rothman DL, and Shulman RG.** In vivo ^{13}C NMR measurements of cerebral glutamine synthesis as evidence for glutamate-glutamine cycling. *Proc Natl Acad Sci USA* 94: 2699–2704, 1997.
28. **Smith SB, Briggs S, Triebwasser KC, and Freedland RA.** Re-evaluation of amino-oxyacetate as an inhibitor. *Biochem J* 162: 453–455, 1977.
29. **Weiss RG, Stern MD, De Albuquerque CP, Vandegaer K, Chacko VP, and Gerstenblith G.** Consequences of altered aspartate aminotransferase activity on ^{13}C-glutamate labelling by the tricarboxylic acid cycle in intact rat hearts. *Biochim Biophys Acta* 1243: 543–548, 1995.
30. **White LT, O'Donnell M, Griffin J, and Lewandowski ED.** Cytosolic redox state mediates postischemic response to pyruvate dehydrogenase stimulation. *Am J Physiol Heart Circ Physiol* 277: H626–H634, 1999.
31. **Yu X, Alpert NM, and Lewandowski ED.** Modeling enrichment kinetics from dynamic ^{13}C NMR spectra: theoretical analysis and practical considerations. *Am J Physiol Cell Physiol* 272: C2037–C2048, 1997.
32. **Yu X, White LT, Alpert NM, and Lewandowski ED.** Subcellular metabolite transport and carbon isotope kinetics in the intramyocardial glutamate pool. *Biochemistry* 35: 6963–6968, 1996.
33. **Yu X, White LT, Doumen C, Damico LA, LaNoue KF, Alpert NM, and Lewandowski ED.** Kinetic analysis of dynamic ^{13}C NMR spectra: metabolic flux, regulation, and compartmentation in hearts. *Biophys J* 69: 2090–2102, 1995.

STIC-ILL

QH505.A1 B537

From: Gabel, Gailene
Sent: Wednesday, February 12, 2003 5:14 PM
To: STIC-ILL
Subject: 09/905,439

Please provide a copy of the following literature ASAP:

1) Killick, Real-time NMR studies on a transient folding intermediate of barstar. PROTEIN SCIENCE, (1999 Jun) 8 (6) 1286-91.

2) Guo et al., Identification of the binding surface on Cdc42Hs for p21-activated kinase. BIOCHEMISTRY, (1998 Oct 6) 37 (40) 14030-7.

3) Pfuhl et al., Secondary structure determination by NMR spectroscopy of an immunoglobulin-like domain from the giant muscle protein titin. JOURNAL OF BIOMOLECULAR NMR, (1995 Jul) 6 (1) 48-58.

4) Kennedy et al., Chemosensitization of a multidrug-resistant Leishmania tropica line by new sesquiterpenes from Maytenus magellanica and Maytenus chubutensis, Journal of Medicinal Chemistry, (December 20, 2001) Vol. 44, No. 26, pp. 4668-4676.

5) Carvalho et al., TCA cycle kinetics in the rat heart by analysis of C-13 isotopomers using indirect H-1[C-13] detection, AMERICAN JOURNAL OF PHYSIOLOGY-HEART AND CIRCULATORY PHYSIOLOGY, (SEP 2001) Vol. 281, No. 3, pp. H1413-H1421.

6) Sokolowski et al., Conformational analysis of a Chlamydia-specific disaccharide alpha-Kdo-(2-->8)-alpha-Kdo-(2-->O)-allyl in aqueous solution and bound to a monoclonal antibody: observation of intermolecular transfer NOEs. JOURNAL OF BIOMOLECULAR NMR, (1998 Jul) 12 (1) 123-33.

7) Kuroda et al., Locations of local anesthetic dibucaine in model membranes and the interaction between dibucaine and a Na+ channel inactivation gate peptide as studied by 2H- and 1H-NMR spectroscopies. BIOPHYSICAL JOURNAL, (1996 Sep) 71 (3) 1191-207.

8) Marceau et al., Contribution of a conserved arginine near the active site of Escherichia coli D-serine dehydratase to cofactor affinity and catalytic activity. JOURNAL OF BIOLOGICAL CHEMISTRY, (1989 Feb 15) 264 (5) 2753-7.

Thanks a bunch,
Gail R. Gabe
7B15
CM1
305-0807

Locations of Local Anesthetic Dibucaine in Model Membranes and the Interaction between Dibucaine and a Na^+ Channel Inactivation Gate Peptide as Studied by ^2H- and ^1H-NMR Spectroscopies

Yoshihiro Kuroda,* Masahiro Ogawa,* Hirosato Nasu,* Maiko Terashima,* Mikio Kasahara,* Yasunori Kiyama,# Misako Wakita,* Yasuhiro Fujiwara,§ Nobutaka Fujii,* and Terumichi Nakagawa*

*Faculty of Pharmaceutical Sciences, Kyoto University; #Nippon Shinyaku Co.; and §Kyoto Pharmaceutical University, Kyoto, Japan

ABSTRACT To study the molecular mechanisms of local anesthesia, locations of local anesthetic dibucaine in model membranes and the interactions of dibucaine with a Na^+ channel inactivation gate peptide have been studied by ^2H- and ^1H-NMR spectroscopies. The ^2H-NMR spectra of dibucaine-d_9 and dibucaine-d_1, which are deuterated at the butoxy group and at the 3 position in its quinoline ring, respectively, have been observed in multilamellar dispersions of the lipid mixture composed of phosphatidylcholine, phosphatidylserine, and phosphatidylethanolamine. ^2H-NMR spectra of deuterated palmitic acids incorporated, as a probe, into the lipid mixture containing cholesterol have also been observed. An order parameter, S_{CD}, for each carbon segment was calculated from the observed quadrupole splittings. Combining these results, we concluded that first, the butoxy group of dibucaine is penetrating between the acyl chains of lipids in the model membranes, and second, the quinoline ring of dibucaine is located at the polar region of lipids but not at the hydrophobic acyl chain moiety. These results mean that dibucaine is situated in a favorable position that permits it to interact with a cluster of hydrophobic amino acids (Ile-Phe-Met) within the intracellular linker between domains III and IV of Na^+ channel protein, which functions as an inactivation gate. To confirm whether the dibucaine molecule at the surface region of lipids can really interact with the hydrophobic amino acids, we synthesized a model peptide that includes the hydrophobic amino acids (Ac-GGQDIFMTEEQK-OH, MP-1), the amino acid sequence of which corresponds to the linker part of rat brain type IIA Na^+ channel, and the one in which Phe has been substituted by Gln (MP-2), and measured ^1H-NMR spectra in both phosphate buffer and phosphatidylserine liposomes. It was found that the quinoline ring of dibucaine can interact with the aromatic ring of Phe by stacking of the rings; moreover, the interaction can be reinforced by the presence of lipids. In conclusion, we wish to propose that local anesthesia originates from the π-stacking interaction between aromatic rings of an anesthetic molecule located at the polar headgroup region of the so-called boundary lipids and of the Phe in the intracellular linker between domains III and IV of the Na^+ channel protein, prolonging the inactivated state and consequently making it impossible to proceed to the resting state.

INTRODUCTION

Since the discovery by Sigmund Freud in Heidelberg of local anesthesia by cocaine, many chemicals have been proposed as local anesthetics (Ritchie and Greene, 1985; Covino, 1987). Their molecular structures have a similarity in that they have the following chemical arrangement: an aromatic ring, an intermediate chain including an amide or an ester linkage, and a tertiary amine nitrogen. Thus these chemicals are amphiphilic in nature, and owing to the presence of the tertiary amine nitrogen, they can exist as both cationic and uncharged molecular forms, depending on their pK_a and the pH of the fluid surrounding nerve membranes. The mechanism of action of the local anesthetics upon excitable membranes, which appears to be well established so far, is 1) diffusion of the uncharged form of the local anesthetic across the nerve sheath and nerve membrane; 2) reequilibration between the uncharged and cationic forms on the axoplasmic surface of the nerve membrane; and 3) penetration into and attachment to a receptor at a site within the sodium channel (Covino, 1987; Strichartz and Ritchie, 1987). However, the molecular nature of the local anesthetic site(s) of action remains unclear. Debate has focused on whether such sites are purely lipid in nature or whether protein targets may be involved. A good correlation between the potency of local anesthetics and their ability to penetrate artificial lipid membranes gives support for the former view (Trudell, 1977, 1980), whereas the use-dependent anesthetic block, the stereospecific effects of local anesthetics, and the higher affinity binding of anesthetic for the inactivated channels than for the activated ones support the latter (Strichartz and Ritchie, 1987; Courtney and Strichartz, 1987).

Recently two notable papers that urge us to study the molecular mechanisms of local anesthesia have been published. One is related to the Na^+ channel inactivation gate in rat brain type IIA Na^+ channel by Catterall et al. (Patton et al., 1992; West et al., 1992), and the other is related to the amine blockers of the cytoplasmic mouth of Na^+ channels by Zamponi and French (1994). Catterall et al. have reported that they successfully specified the amino acid residues required for fast Na^+ channel inactivation and have proposed a "hinged-lid" model of the Na^+ channel inacti-

Received for publication 26 December 1995 and in final form 3 June 1996.

Address reprint requests to Dr. Yoshihiro Kuroda, Faculty of Pharmaceutical Sciences, Kyoto University, Kyoto, 606-01, Japan. Tel.: +81-75-753-4530; Fax: +81-75-753-4578; E-mail: yokuroda@pharm.kyoto-u.ac.jp.

0006-3495/96/09/1191/17 $2.00

vation gate (Patton et al., 1992; West et al., 1992). In this model, a cluster of hydrophobic amino acids, Ile-1488, Phe-1489, and Met-1490 within the intracellular linker between domains III and IV of the channel protein (Fig. 1), occludes the intracelluar mouth of the activated Na^+ channel (Fig. 2) and stabilizes the inactivated state, making use of Gly-1484 (or Gly-1485, or both) and Pro-1509 residues on either side of the IFM domain as hinge points. On the other hand, Zamponi and French have reported that for a drug to function as an inactivation enhancer, it is necessary that the aromatic ring of the drug bind to a hydrophobic domain (Fig. 2) within the internal mouth of the channel (Zamponi and French, 1994).

By taking these two reports into consideration and by noting that there are negatively charged amino acids only on both sides of the IFM amino acid residues (Asp-1487, Glu-1492, and Glu-1493; see Figs. 1 and 2) in the linker, we hypothesized as follows: 1) local anesthetics locate within lipid membranes surrounding domains III and IV, allowing their hydrophobic moieties to interact simultaneously with both lipids and one or two of the three hydrophobic amino acids of Ile-1488, Phe-1489, or Met-1490; 2) the tertiary amine nitrogen, especially in its protonated quaternary ammonium form, interacts electrostatically with one of the three negatively charged amino acids that occur on both sides of the three hydrophobic amino acids. These assumptions can explain all of the reasoning involved in the two conflicting models of molecular mechanisms of local anesthesia. However, for these assumptions to be proved correct, as a first step we should confirm whether all local anesthetic

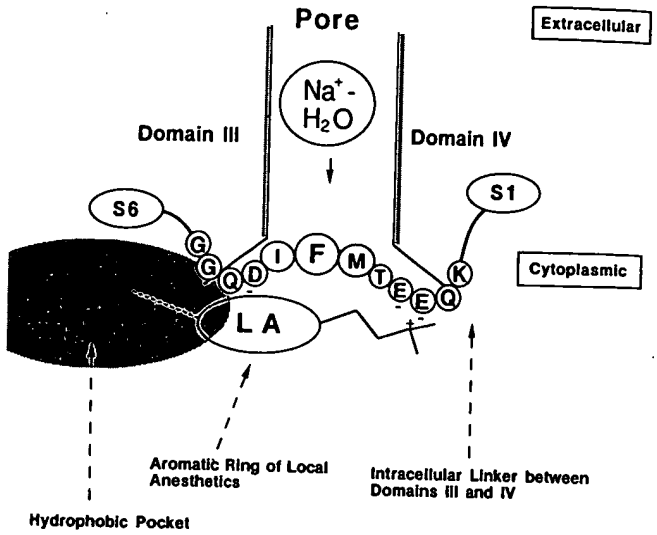

FIGURE 2 A hinged-lid model for Na^+ channel inactivation (Patton et al., 1992; West et al., 1992) and schematic representation of the interaction between a local anesthetic drug and the amino acid residues in the inactivation gate peptide.

molecules reside at the polar headgroup region of the membranes, rather than at the hydrophobic acyl chain region. This is because the "hinged lid" occupies a position within the aqueous channel pore (Fig. 2), and thus local anesthetics should also locate at a site within the hydrophilic regions of the channel. We assumed that such an interfacial site between the hydrophobic site suggested by Zamponi and

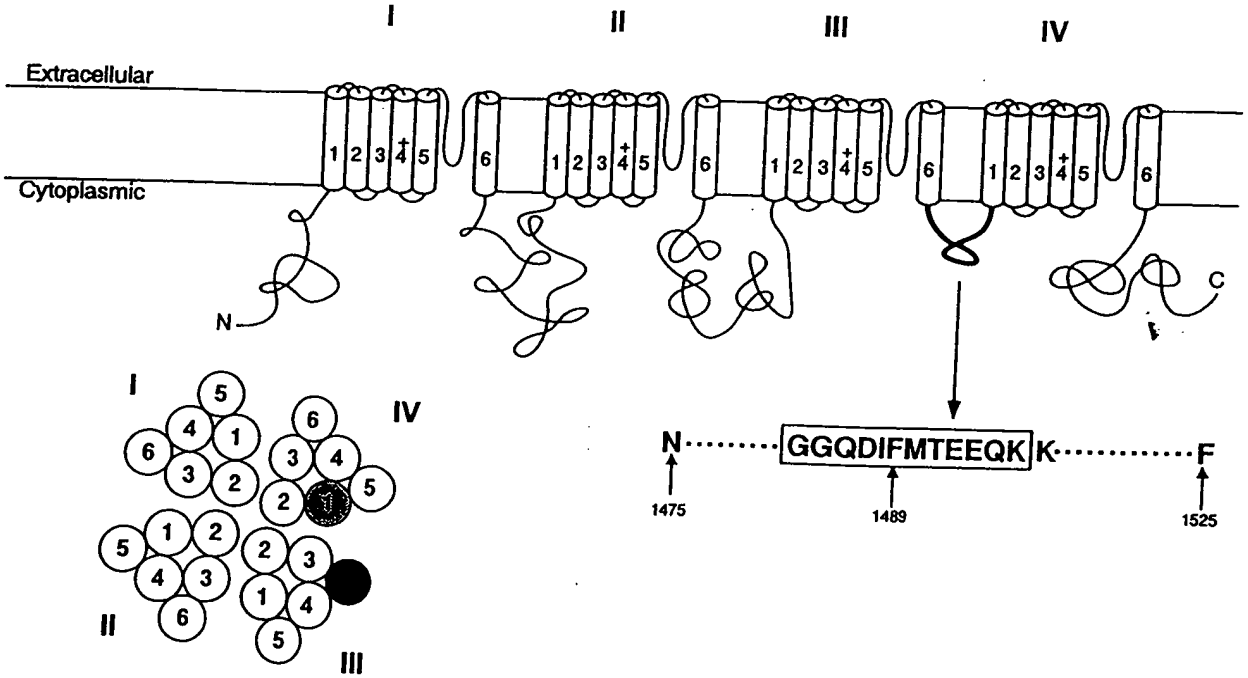

FIGURE 1 Schematic representation for the Na^+-channel α subunit. It is considered to be composed of four homologous domains (I–IV). Each domain has six α-helices (1–6). A space that is surrounded by the 24 α-helices is thought to be a pore through which the Na^+ ion passes (Noda et al., 1986). The numbering and the amino acid sequence at the intracelluar linker between domains III and IV is in the rat brain IIA Na^+ channel (Noda et al., 1986).

French and the hydrophilic region in which the hinged-lid exists is provided by the polar headgroup region of the so-called boundary lipids, and not by the channel protein.

The local anesthetic dibucaine (Fig. 3) was selected for use in the present experiments. The molecule consists of a big quinoline ring, which seems to be the most hydrophobic aromatic ring among the clinically used local anesthetics. Therefore, elucidating its location in lipid membranes can be a promising means of testing the above assumptions. ^{2}H-NMR spectroscopy has been employed to investigate the location of the dibucaine molecule (Seelig, 1977). The ^{2}H-NMR spectra of the deuterated dibucaine at the 3 position in its quinoline ring and at the butoxy group in multilamellar dispersions of phospholipids, composed of phosphatidylcholine (PC), phosphatidylserine (PS), and phosphatidylethanolamine (PE, PC:PS:PE = 1:1:2.5 molar ratio), which contain or do not contain cholesterol (phospholipids:cholesterol = 7:3 molar ratio), have been observed. The ratio of the amount of each lipid (PC:PS:PE = 1:1:2.5 molar ratio) is that reported for the phospholipids at the inside of human erythrocyte ghost (Op den Kamp, 1979), whereas the ratio of the amount of the total phospholipids to cholesterol (7:3 molar ratio) is approximately one-half that reported for the total phospholipids and cholesterol of the whole human ghost (Maraviglia et al., 1982), but approximately equal to that reported for the excitable membranes of the garfish olfactory nerve (Chacko et al., 1976). Moment analyses (Bloom et al., 1978; Davis et al., 1979; Nichol et al., 1980) have been applied to the observed ^{2}H-NMR spectra, because the observed spectra are made up by the superposition of spectra due to variously oriented dibucaine molecules.

Effects of dibucaine on the orientational order of methylene groups of the multilamellar dispersions of phospholipids have been studied by ^{2}H-NMR spectroscopy. Deuterated palmitic acid was incorporated into the lipid mixture as a probe of the lipid structure. An order parameter S_{CD} for each carbon segment was calculated from the quadrupole splitting in the ^{2}H-NMR spectra. By taking all of these ^{2}H-NMR spectroscopic data into account, we deduced the location of dibucaine in membranes and concluded that the quinoline ring of dibucaine is located at the polar headgroup region of lipids.

To ascertain whether the dibucaine molecule located at the polar headgroup region of lipids can actually interact with the hydrophobic amino acids, especially with Phe, we synthesized a model peptide that includes the IFM domain in the linker (Ac-GGQDIFMTEEQK-OH) named MP-1 and another in which Phe has been substituted by Gln (MP-2). ^{1}H-NMR spectra of dibucaine in the presence of MP-1 or MP-2 in both phosphate buffer and phosphatidylserine liposomes have been observed to obtain information on the interactions. Finally, we discuss all of the results in relation to the interaction between local anesthetics and the Na^+ channel inactivation gate to elucidate the molecular mechanisms of local anesthesia.

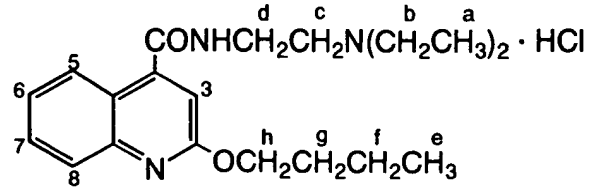

FIGURE 3 Chemical structure of dibucaine hydrochloride and the numbering scheme.

MATERIALS AND METHODS

Materials

Dibucaine hydrochloride deuterated at the 3 position in the quinoline ring (dibucaine-d_1) was synthesized from isatin according to the scheme shown in Fig. 4 (Miescher, 1932) (m.p. 91–96°C). The percentage of deuteration was checked by ^{1}H-NMR spectroscopy and was found to be 83%; this rather low percentage of deuteration was later found to be due to the use of C_4H_9OH instead of C_4H_9OD at the final stage of the reaction. The dibucaine hydrochloride deuterated at the butoxy group was synthesized by using C_4D_9OH instead of C_4H_9OH (Fig. 4). The percentage deuteration was greater than 99% (m.p. 91–96°C). Palmitic-d_2 acids deuterated at various positions (C4, C6, C9, or C10) were synthesized starting from relevant α-deuterated fatty acids and dicarboxylic acid monomethyl esters by the method of Kolbe electrolysis (Greaves et al., 1950); we followed the method described by Oldfield et al. (1978). The percentages of deuteration were checked by ^{1}H-NMR spectra and found to be greater than 85% for each palmitic-d_2 acid. Palmitic-d_{31} acid was obtained from MSD Isotopes (Montreal, Quebec, Canada). Palmitic-2,2-d_2 acid and palmitic-3,3-d_2 acid were obtained from C/D/N Isotope Inc. (Vaudreuil, Quebec, Canada). Peptides MP-1 (Ac-GGQDIFMTEEQK-OH) and MP-2 (Ac-GGQDIQMTEEQK-OH) were synthesized by the solid phase method using Fmoc chemistry; their N-termini were acetylated (denoted by Ac-), and their C-termini were free carboxylic acids (denoted by -OH). They were purified on a reverse-phase C_{18} high-performance liquid chromatography column using a gradient of 85% A, 15% B to 60% A, 40% B, where A is 0.1% trifluoroacetic acid (TFA) in water and B is 0.1% TFA in acetonitrile; the rate of decrease in A was 25%/50 min. They were characterized by determination of amino acid composition by ion spray mass spectrometry.

Egg yolk L-α-phosphatidylcholine (egg PC), bovine brain L-α-phosphatidylserine (PS), egg yolk L-α-phosphatidylethanolamine (PE), and cholesterol were obtained from Sigma and used without further purification.

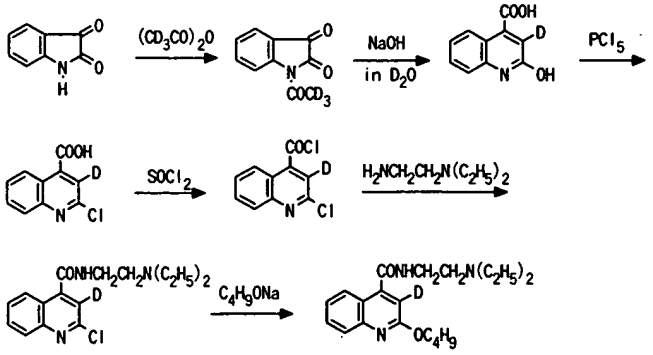

FIGURE 4 Reaction scheme to synthesize the dibucaine deuterated at the 3 position in the quinoline ring.

Deuterium-depleted water ($<5 \times 10^{-5}$ atom %D) was obtained from ISOTEC (Miamisburg, OH).

Determination of the gel-to-liquid crystalline phase transition temperature of multilamellar dispersions of the lipid mixture composed of PC, PS, and PE (PC:PS:PE = 1:1:2.5 molar ratio) was made by monitoring the lock signal provided from an isotonic (310 mOsm, 150 mM) phosphate buffer in ^2H_2O and was found to be 274 K.

The partition coefficients of dibucaine for the lipid mixture that contains cholesterol and palmitic acid and dispersed in the phosphate buffer (pH 7.2 and pH 5.2) were obtained by fluorometrically determining the concentrations of dibucaine not binding with the membranes. The measured solutions were obtained by ultrafiltration of the lipid mixture suspended in the phosphate buffer.

Preparation of sample solutions for ^{2}H-NMR measurements

Lipid mixture solutions

The thin films of the mixtures of PC, PS, and PE (PC:PS:PE = 1:1:2.5 molar ratio, 60–70 mM) that contain or do not contain cholesterol (phospholipids:cholesterol = 7:3 molar ratio) were prepared by concentrating their chloroform/methanol solution with a rotary evaporator and then pumping on a vacuum line overnight. Their multilamellar dispersions were prepared by vortexing vigorously the round-bottomed flask containing the thin films and an isotonic (310 mOsm, 150 mM, pH 7.4 or 5.6) phosphate buffer in deuterium-depleted water for 5 min. A weighed amount of dibucaine-d_1 (12 mM) or dibucaine-d_9 (3 mM) dissolved in the phosphate buffer was added before the vortexing. To equilibrate the state of anesthetics interacting with lipids completely, the multilamellar dispersions of model membranes were subjected to five freeze-thaw-vortex cycles (Westman et al., 1982). Finally, the pH of the sample solution was checked and adjusted to a desired value by adding a trace amount of Na_2HPO_4 or NaH_2PO_4.

Lipid mixture solutions with cholesterol and deuterated palmitic acid

The PC, PS, and PE in a chloroform/methanol solution (60 mM) were mixed with cholesterol (25 mM) and deuterated palmitic acid (20 mM), and then the solvent was evaporated by pumping with a vacuum line overnight. Thus obtained thin films were dispersed into the deuterium-depleted water (310 mOsm, pH 7.4 or 5.8) by vortexing. A weighed amount of dibucaine (3 mM) was dissolved in the suspension and then subjected to five freeze-thaw-vortex cycles.

Preparation of sample solutions for ^{1}H-NMR measurements

A weighed amount of dibucaine hydrochloride (3 mM) with or without peptide (3 mM) was dissolved in the phosphate buffer (10% ^2H_2O-90% H_2O, 310 mOsm, 150 mM), and the pH of the sample solution was adjusted to 7.4 by adding a trace amount of Na_2HPO_4 or NaH_2PO_4. Single bilayer vesicles (liposomes) of PS were prepared by ultrasonic irradiation of the phosphate buffer suspension (in ^2H_2O) of dried PS (15 mM) for 20 min, cooling in an ice/water bath, and bubbling with nitrogen gas. A weighed amount of dibucaine (3 mM) with or without peptide (3 mM) was added to the solution of preformed vesicles; the pH was adjusted to 7.4 by adding a trace amount of Na_2HPO_4 or NaH_2PO_4.

Measurements

^{2}H-NMR spectra were observed at 92 MHz on a Bruker AM-600 spectrometer equipped with a usual broadband probe for high-resolution NMR spectroscopy. The quadrupolar echo sequence was employed (Davis et al., 1976); $\pi/2 = 10$ μs, and its pulse spacing was 50 μs. A typical observing spectral width was 50,000 Hz for 16 K data points, and the recycle time was 0.26 s. The acquired number of transients was typically 300,000 (~22 h) for a sample solution containing dibucaine-d_1, 200,000 (~15 h) for a sample solution containing dibucaine-d_9, and 250,000 (~20 h) for a sample solution containing 20 mM deuterated palmitic acid. No symmetrization procedure was performed. An exponential weighting function with a line broadening factor of 50–100 Hz was applied to the free induction decay acquired with 16 K data points and zero-filled to 64 K. The quadrupole splittings reported in the following were read directly from the CRT display of an AM-600 spectrometer. ^{1}H-NMR spectra were observed on a Bruker AM-600 (600 MHz) spectrometer with a digital resolution of 0.18 Hz/point; the ambient probe temperature was 27°C. The chemical shifts were referenced to TSP (3-trimethylsilyl-propionic acid-d_4 sodium salt).

Moment analyses for ^{2}H-NMR spectra and calculations of order parameters, S_{CD}, for the segments of a flexible hydrocarbon chain

Moments of the ^{2}H-NMR spectra (Bloom et al., 1978; Davis et al., 1979; Nichol et al., 1980) were calculated according to

$$M_n = \int_0^\infty \omega^n f(\omega)\mathrm{d}\omega \Big/ \int_0^\infty f(\omega)\mathrm{d}\omega \qquad (1)$$

and by using IRIS Indigo for half the Fourier-transformed spectral data points (~16,000) written in the ASCII format according to the JCAMP-DX norm (McDonald and Wilks, 1988) in a Bruker X-32 computer. The half-spectra selected for calculations were from either the high- or the low-frequency sides, which do not include the resonance due to the solvent. Estimated errors in calculating the first (M_1) and the second (M_2) moments and the resulting mean order parameter (S_{CD}), which is defined by

$$S_{CD} = 2\sqrt{3}M_1/(e^2qQ/\hbar) \qquad (2)$$

and its dispersion (Δ_2), defined by

$$\Delta_2 = M_2/1.35M_1^2 - 1, \qquad (3)$$

where e^2qQ/h is the static quadrupole coupling constant, were within a few percent. The order parameter S_{CD} for each acyl chain carbon position (Stockton et al., 1976) was calculated by correlating the corresponding observed quadrupole splitting, $\Delta\nu q$ (in units of kilohertz), of specifically deuterated palmitic acids to the order parameter in the following way:

$$\Delta\nu q = 3/4(e^2qQ/h)S_{CD}. \qquad (4)$$

RESULTS

^{2}H-NMR spectra of dibucaine-d_1 in lipid mixtures

Fig. 5, *a* and *b*, shows ^{2}H-NMR spectra of dibucaine-d_1 (12 mM)-lipid mixture (70 mM) solutions at pH 7.4 and at 300 K in the absence and in the presence of cholesterol (phospholipids:cholesterol = 7:3 molar ratio), respectively. The dibucaine in the lipid mixture without cholesterol gave a trapezoid lineshape with an approximate maxium quadrupole splitting of 6.7 kHz. In contrast, this spectral feature drastically changed when the lipid mixture included cholesterol (spectrum b) and resulted in a narrow resonance with a half-height width of 0.6 kHz. The differences in these spectral features essentially disappeared, however, when the temperature was lowered to 279 K and resulted in closely similar spectra (spectra c and d); the

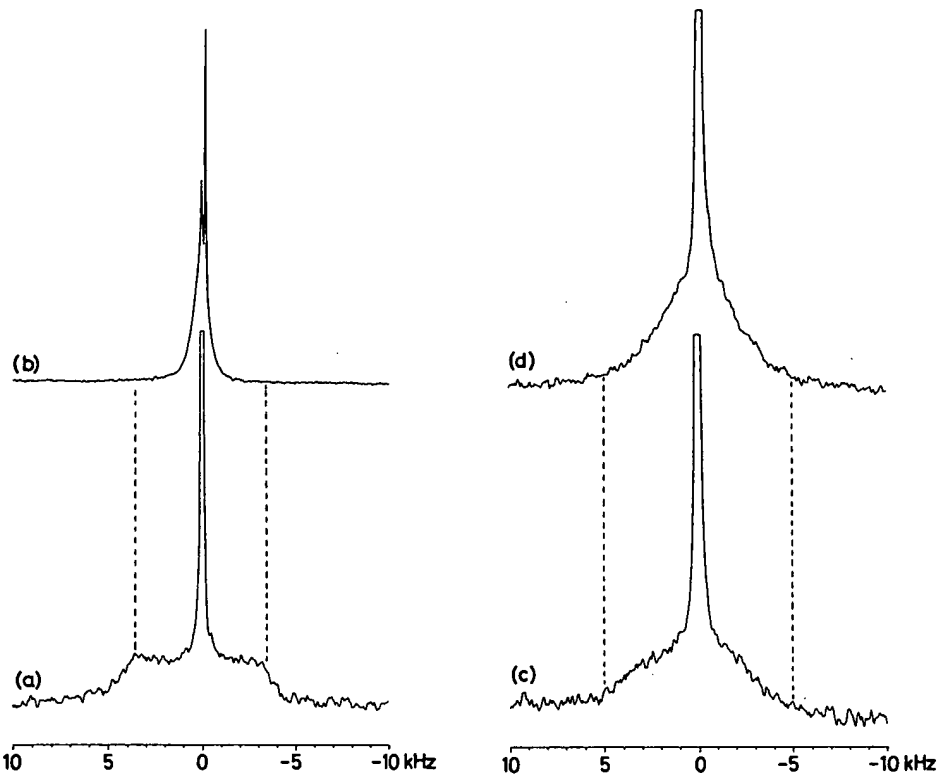

FIGURE 5 (*a*) ^{2}H-NMR spectrum of dibucaine-d_1 (12 mM) mixed lipid (PC:PS:PE = 1:1:2.5 molar ratio, 70 mM) solution at pH 7.4 and at 300 K. (*b*) As in *a*, but contains cholesterol (phospholipids:cholesterol = 7:3 molar ratio). (*c*) As in *a*, but at 279 K. (*d*) As in *b*, but at 279 K.

quadrupole splitting decreased in spectrum c, and the linewidth at half-height increased in spectrum d. Because the gel-to-liquid crystalline phase transition temperature of the lipid mixture with no cholesterol was 274 K, there is no doubt that the lipid mixture is in a liquid crystalline state. It is known that cholesterol increases the order of the acyl chains of lipid bilayers at temperatures above that of the gel-to-liquid crystalline phase transition (Stockton and Smith, 1976; Bloom and Mouritsen, 1988). Thus the spectral change from spectrum a to spectrum b can be considered to be due to changes in the location of dibucaine toward the polar region, which may result in decreased order of the quinoline rings of dibucaine molecules. On the other hand, the close resemblance between spectra c and d suggests that at a low temperature dibucaine molecules locate at a similar environment with a similar manner, irrespective of the presence or absence of cholesterol. The change in the lineshape from spectrum a to spectrum c implies that the quinoline ring of dibucaine was squeezed out of the original binding site to the more unordered binding site as a consequence of increased degree of order of the lipids owing to decreased temperature.

A similar observation was also noted at pH 5.8. The observed maximum quadrupole splitting was 4.6 kHz; this value was somewhat smaller than that of the neutral solution (6.7 kHz).

^{2}H-NMR spectra of dibucaine-d_9 in lipid mixtures

Fig. 6 shows ^{2}H-NMR spectra of dibucaine-d_9 (3 mM) in multilamellar dispersions of the lipid mixture in the absence (Fig. 6, *a* and *c*) and presence (Fig. 6, *b* and *d*) of cholesterol at pH 7.4; spectra a and b were observed at 300 K and spectra c and d at 279 K. As shown in spectrum a, each methylene group of dibucaine-d_9 showed clearly resolved quadrupolar splittings ranging from 12 to 4.5 kHz; however, the methyl group showed no resolved splitting. In contrast to the spectra for dibucaine-d_1, all of these splittings increased when the membrane contained cholesterol, and even the terminal methyl group showed a clear quadrupolar splitting of 1.8 kHz (spectrum b). When the temperature was lowered to 279 K, the quadrupolar splittings due to the methylene groups increased, ranging from 14.5 to 6.2 kHz (spectrum c); however, those lineshapes became rather featureless in appearance. This tendency became more prominent when the lipid mixture contained cholesterol (spectrum d). The quadrupolar splittings due to the three methylene groups coalesced to give a broad trapezoid lineshape with a width of about 14 kHz, and that due to the methyl group increased (3.0 kHz). These observations indicate that dibucaine molecules are binding with the lipid membrane in such a manner that its butoxy group is between the acyl chains of lipids.

Fig. 7 shows ^{2}H-NMR spectra observed at acidic conditions. The quadrupole splittings in spectrum a decreased by about 0.4 kHz in each methylene group as compared to the corresponding one in the neutral pH solution (Fig. 6 *a*). However, no appreciable difference was noted when the lipid mixture contained cholesterol (compare spectrum b with Fig. 6 *b*). The tendencies for the spectral changes with added cholesterol or a temperature lowered to 279 K were

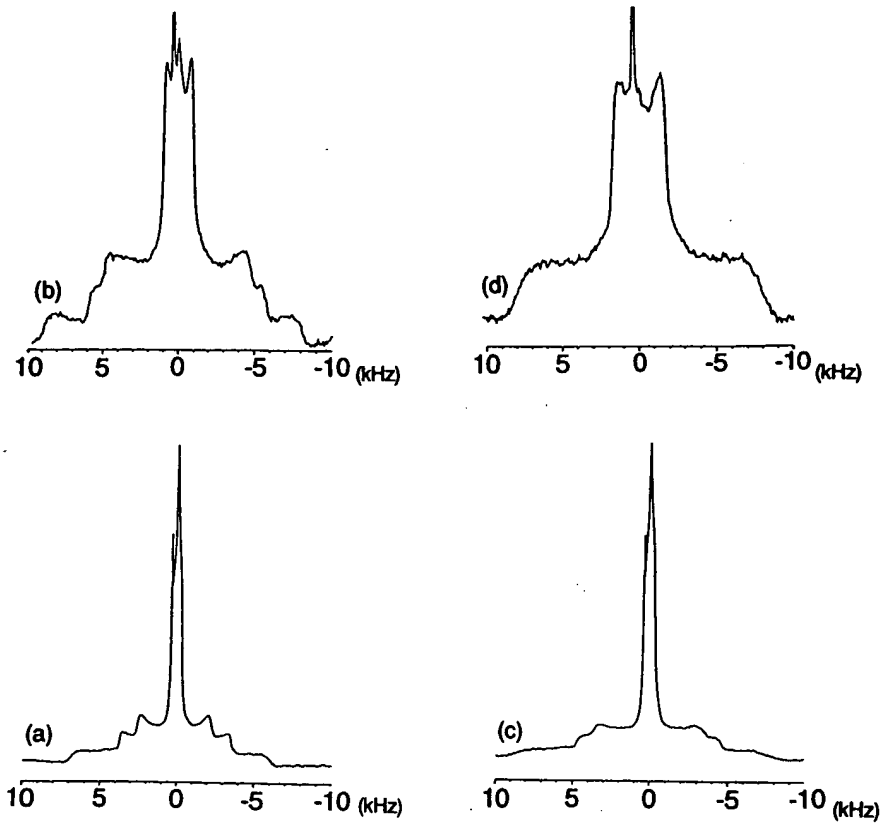

FIGURE 6 (*a*) ^{2}H-NMR spectrum of dibucaine-d_9 (3 mM) mixed lipid (PC:PS:PE = 1:1:2.5 molar ratio, 70 mM) solution at pH 7.4 and at 300 K. (*b*) As in *a*, but contains cholesterol (total lipids:cholesterol = 7:3 molar ratio). (*c*) As in *a*, but at 279 K. (*d*) As in *b*, but at 279 K.

the same as those noted for neutral pH solutions, except that spectrum c showed a more clear-cut quadrupole splitting for each methylene group; in fact, even the methyl group showd a small well-resolved quadrupole splitting (spectrum c).

Moment analyses for ^{2}H-NMR spectra of dibucaine-d_1 and dibucaine-d_9

Moment analyses (Bloom et al., 1978) have been applied to these ^{2}H-NMR spectra because the observed spectra are made up of a superposition of the spectra arising from variously oriented dibucaine molecules. Tables 1 and 2 show the first (M_1) and the second (M_2) moments, mean order parameter derived from the first moment (S_{CD}), and the mean square deviation of the order parameter (Δ_2) of dibucaine-d_1 and dibucaine-d_9, respectively. The static e^2qQ/h values assumed were 180 kHz (Burnett and Muller, 1971) in Table 1 and 167 kHz (Davis and Jeffrey, 1977) in Table 2; the former is a typical value for the C-^{2}H bond in an aromatic ring, and the latter is for the C-^{2}H bond in an aliphatic chain. All of the changes in spectral features described above were clearly reflected in these M_1, M_2, and S_{CD} values. Furthermore, we noticed that in dibucaine-d_1 the distribution of order parameters that is represented by the Δ_2 value increased when the lipid mixture contained cholesterol (from 0.379 to 0.887) or when the temperature was lowered (from 0.379 to 1.02); under acidic conditions the entirely same trend was noted. These findings mean that the order of dibucaine binding with lipid membranes was lowered by cholesterol and by lowering the temperature. On the other hand, in dibucaine-d_9, under both neutral and acidic conditions, the Δ_2 value decreased when the lipid mixture contained cholesterol, but again increased when the temperature was lowered. This former result means that in contrast to the case in dibucaine-d_1, the cholesterol increases the order of the butoxy group of dibucaine in the lipid bilayer. Because the butoxy group is attached to the carbon adjacent to the 3 position in the quinoline ring, this finding can be a good clue to the location of dibucaine.

^{2}H-NMR spectra of palmitic acid probes in the lipid mixture with cholesterol

To investigate the effects of dibucaine on the orientational order of methylene groups of multilamellar dispersions of phospholipids, we have observed ^{2}H-NMR spectra for deuterated palmitic acids incorporated into the lipid mixture with cholesterol. The usefulness of deuterated fatty acid probes for determining the order of phospholipid membranes is well demonstrated (Stockton et al., 1974, 1976; Pauls et al., 1983; Vogt et al., 1994). Fig. 8 shows ^{2}H-NMR spectra observed for palmitic-d_{31} acid (25 mol%), which is intercalated into multilamellar dispersions of the lipid mixture with cholesterol at pH 7.2; spectrum a was obtained in the presence of no dibucaine, whereas spectra b and c were obtained in the presence of 1 mM and 3 mM dibucaine, respectively. Each of these spectra had only six peaks, because the ^{2}H-NMR spectrum of palmitic-d_{31} acid is com-

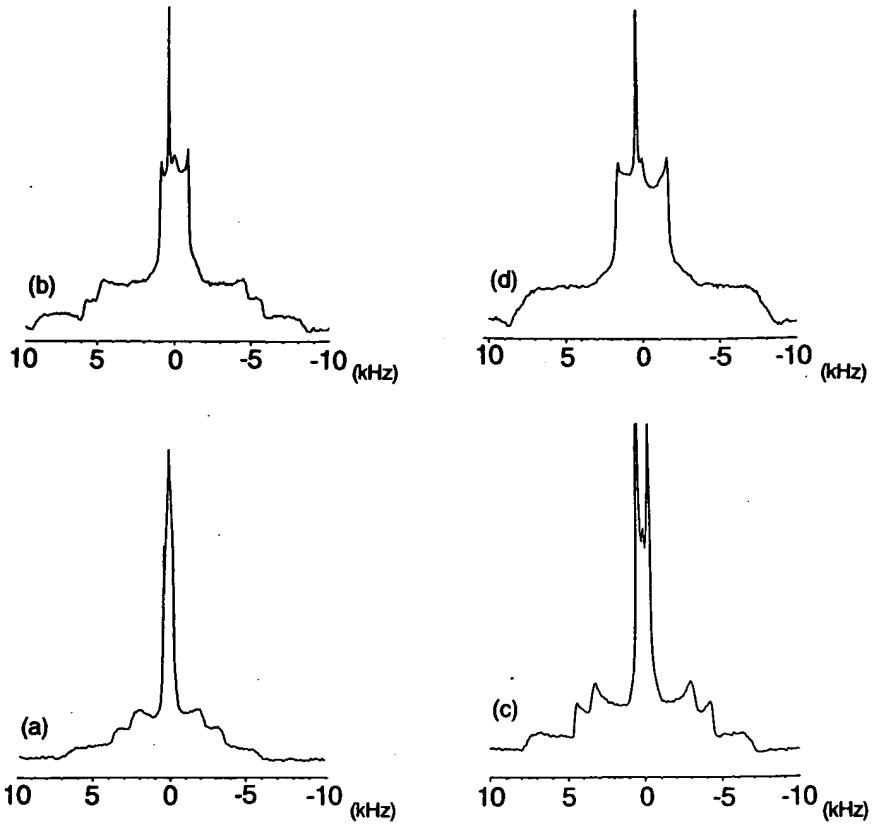

FIGURE 7 (*a*) ^{2}H-NMR spectrum of dibucaine-d_9 (3 mM) mixed lipid (PC:PS:PE = 1:1:2.5 molar ratio, 70 mM) solution at pH 4.8 and at 300 K. (*b*) As in *a*, but contains cholesterol at pH 4.6. (*c*) As in *a*, but at 279 K. (*d*) As in *b*, but at 279 K.

posed of many overlapping resonances; in an acidic condition (pH 5.2) the situation was the same as in the neutral condition. The sharp peak at around 0 kHz should be attributed to the residual HO^2H resonance of the solvent. The quadrupole splittings ($\Delta\nu q$) in spectrum a were decreased by adding dibucaine to the multilamellar dispersions. However, we found that the peaks showing the quadrupole splitting of 32.1 kHz (labeled by an asterisk in spectrum c) did not change on the addition of dibucaine; the peaks were later found to be assignable to the C2 methylene deuterons by comparison with the ^{2}H-NMR spectrum for palmitic 2,2-d_2 acid. For all methylene and methyl group deuterons, the spectrum observed at pH 7.2 was broader than that at pH 5.2. Thus it is conceivable that the order of the acyl chains of lipids under the acidic condition is lower than that under the neutral condition. The quadrupole splittings of 5.91, 20.5, and 26.6 kHz can be assigned to the terminal methyl (C16), methylene groups at 15- (C15), and 14- (C14) positions, respectively; the corresponding splittings under the acidic condition were 4.95, 17.9, and 23.8 kHz, respectively.

To obtain an order parameter for a specific carbon segment in the acyl chain, some palmitic acids that were deuterated at the specific methylene groups were incorporated into the lipid mixture. Fig. 9, *a* and *b*, shows ^{2}H-NMR spectra of palmitic-2,2-d_2 acid in the lipid mixture with and without dibucaine, respectively. A quadrupole splitting of 32.1 kHz was observed when the lipid mixture contained no dibucaine. However, notably, this quadrupole splitting scarcely changed, even when the lipid mixture contained dibucaine. A similar observation was noted for the probe under acidic conditions; a quadrupole splitting of 31.0 kHz was decreased very slightly (30.6 kHz) by the addition of dibucaine. In contrast, for example, as shown in Fig. 10, *a*

TABLE 1 Moment data for the dibucaine-d_1-mixed lipids (PC:PS:PE = 1:1:2.5 molar ratio) and dibucaine-d_1-mixed lipids-cholesterol (total lipids:cholesterol = 7:3 molar ratio) systems

Membrane	pH	Temperature	$M_1 \times 10^{-4}$(rad/s)	$M_2 \times 10^{-8}$(rad^2/s^2)	$S_{CD} \times 10^2$	Δ_2
Mixed lipids	7.4	300	1.16	2.51	3.56	0.379
		279	0.715	1.40	2.19	1.02
	5.8	300	1.03	1.64	3.16	0.141
		279	0.904	1.51	2.77	0.364
Mixed lipids + cholesterol	7.4	300	0.333	0.282	1.02	0.887
		279	0.707	1.14	2.17	0.689
	5.8	300	0.366	0.542	1.12	2.00
		279	0.955	1.69	2.93	0.375

TABLE 2 Moment data for the dibucaine-d_9-mixed lipids (PC:PS:PE = 1:1:2.5 molar ratio) and dibucaine-d_9-mixed lipids-cholesterol (total lipids:cholesterol = 7:3 molar ratio) systems

Membrane	pH	Temperature	$M_1 \times 10^{-4}$(rad/s)	$M_2 \times 10^{-8}$(rad^2/s^2)	$S_{CD} \times 10^2$	Δ_2
Mixed lipids	7.4	300	1.02	2.08	3.37	0.477
		279	1.20	3.02	3.96	0.558
	4.8	300	1.13	2.73	3.74	0.579
		279	1.22	2.71	4.02	0.360
Mixed lipids + cholesterol	7.4	300	1.55	4.18	5.11	0.293
		279	1.98	6.57	6.53	0.242
	4.6	300	1.44	3.70	4.76	0.322
		279	1.96	6.55	6.47	0.264

and *b*, dibucaine decreased the quadrupole splitting (39.2 kHz) in the palmitic-9,9-d_2 acid probe appreciably (37.1 kHz). Thus it seems that under both neutral and acidic conditions, dibucaine is situated in a position that does not so much affect the order parameter of the methylene groups near the polar region, but affects appreciably that of the methylene groups at an intermediate region of the acyl chain. Interestingly, Boulanger et al. (1981) have reported the same sort of finding in a tetracaine-deuterated PC dispersions system; they found that tetracaine affects only slightly the quarupole splittings of the deuterons at position 2 in the deuterated PC dispersions. They ascribed this finding to the location of the benzenoid group around the acyl chain position 2. To further understand the effect of dibucaine on the quadrupole splittings throughout the acyl chain methylene groups, we have observed ^{2}H-NMR spectra for the probes deuterated at C3, C4, C6, and C10. All of the observed quadrupole splittings at pH 7.2 and pH 5.2, with and without dibucaine, are summarized in Table 3.

Order parameter profiles for palmitic acids intercalated into the lipid mixture containing cholesterol

To discuss differences in the order among chain segments, we have calculated an order parameter (S_{CD}) for each carbon number of the palmitic acid probe, according to Eq. 4 (Stockton et al., 1976). The S_{CD} values for the neutral and acidic solutions, calculated by assuming the static e^2qQ/h value of 170 kHz (Stockton et al., 1976), are summarized in Table 3. To focus our attention on the changes in S_{CD} caused by 3 mM dibucaine (ΔS_{CD}) (Fig. 11), we plotted the ratios $\Delta S_{CD}/S_{CD}$ against carbon numbers. ΔS_{CD} represents the amount of decrease in the S_{CD} value caused by dibucaine. It appears that under both neutral and acidic condi-

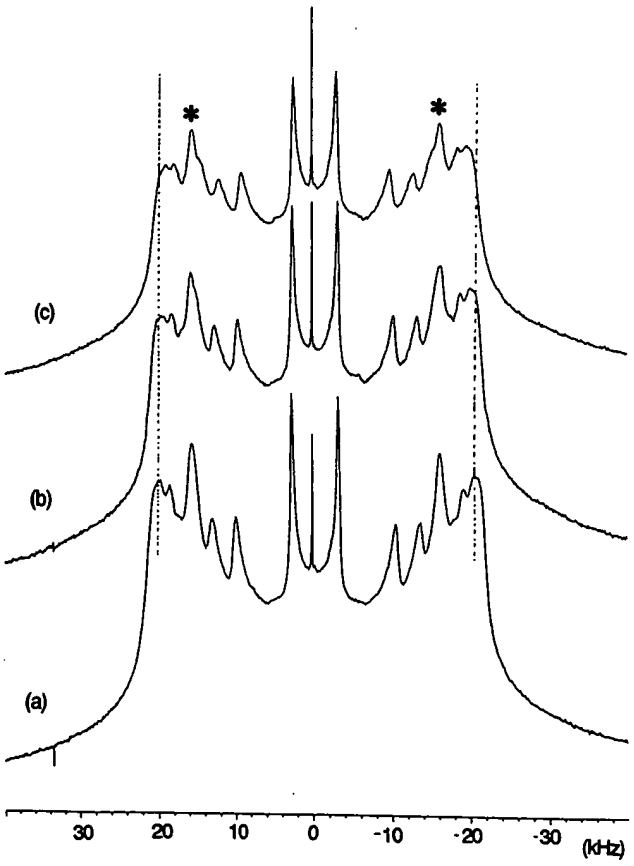

FIGURE 8 ^{2}H-NMR spectra of palmitic-d_{31} acid (20 mM) in mixed lipid (PC:PS:PE = 1:1:2.5 molar ratio, 60 mM) solution with cholesterol (total lipids:cholesterol = 7:3 molar ratio) at pH 7.2 and at 300 K. (*a*) Without dibucaine. (*b*) With dibucaine (1 mM). (*c*) With dibucaine (3 mM).

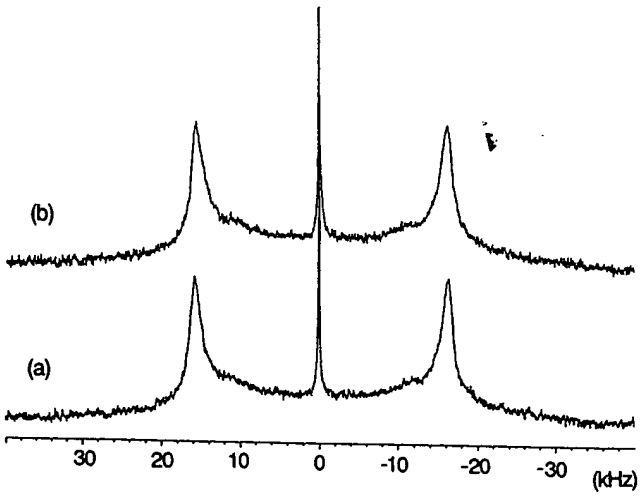

FIGURE 9 ^{2}H-NMR spectra of palmitic-2,2-d_2 acid (20 mM) in mixed lipid (PC:PS:PE = 1:1:2.5 molar ratio, 60 mM) solution with cholesterol (total lipids:cholesterol = 7:3 molar ratio) at pH 7.2 and at 300 K. (*a*) Without dibucaine. (*b*) With dibucaine (3 mM).

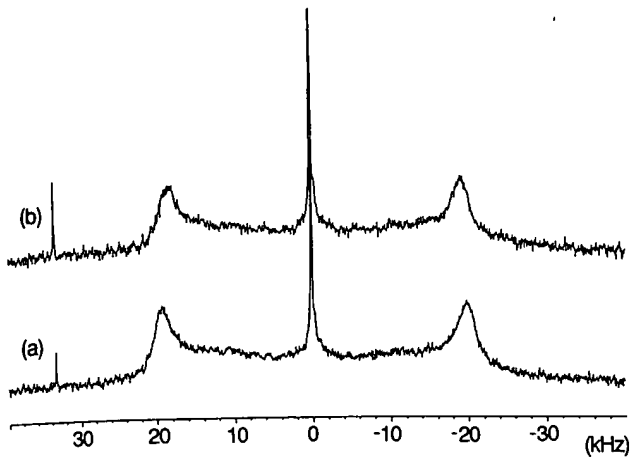

FIGURE 10 ^{2}H-NMR spectra of palmitic-9,9-d_2 acid (20 mM) in mixed lipids (PC:PS:PE = 1:1:2.5 molar ratio, 60 mM) with cholesterol (total lipids:cholesterol = 7:3 molar ratio) at pH 7.2 and at 300 K. (*a*) Without dibucaine. (*b*) With dibucaine (3 mM).

tions, the ratios monotonously increase from C2 to C10, and then gradually increase or remain approximately constant from C10 to the terminal methyl group, C16. Moreover, we notice that the ratio for the acidic solution is larger than that at the corresponding carbon number for the neutral solution. To confirm whether this finding is due to a larger amount of dibucaine partitioning into the lipid mixture under acidic than under neutral conditions, we have measured the partition coefficient K_p of dibucaine for the lipid mixture, which involves cholesterol and palmitic acid. The results are summarized in Table 4; the K_p value of 1108 at pH 7.2 compares favorably with that reported by Papahadjopoulos et al. (1975) for the lipid composition of PS/cholesterol (K_p = 1150). Evidently, the partition coefficient at pH 7.2 was greater than that at pH 5.2. Thus we should invoke another reason for the differences in the ratio. Interestingly, Boulanger et al. (1981) have reported a similar finding for tetracaine interacting with multilamellar dispersions of specifically deuterated phosphatidylcholine, namely that the charged tetracaine has a greater disordering effect on the phospholipid chain region and perturbs to a greater extent the dimensions of this region than does the uncharged one. The pK_a value of dibucaine reported is 8.0 (Kuroda et al., 1994) or 8.5 (Ritchie and Greengard, 1961). Furthermore, it is considered that the pK_a value of the tertiary amino group of the membrane bound drug would decrease by approximately 1 pK_a unit from the corresponding value in the aqueous phase (Lee, 1978). Accordingly, at pH 7.2, about half of the dibucaine molecules can be considered to be in an uncharged molecular form, whereas at pH 5.2 all of the dibucaine molecules are expected to exist as a cationic form. Consequently, the differences in the ratio $\Delta S_{CD}/S_{CD}$ between pH 7.2 and pH 5.2 should also be ascribed to the changes in the relative amount of uncharged versus charged species. Changes in the location due to protonation and/or electrostatic interactions between cationic drugs and lipid headgroups may be reasons for the finding in Fig. 11; in the Discussion, however, we favor only the latter view.

^{1}H-NMR spectra of dibucaine and Na^+ channel inactivation gate peptide (MP-1) in a phosphate buffer

To investigate a plausible interaction between dibucaine and MP-1, especially the expected π-stacking interaction (Hunter, 1993; Hunter and Sanders, 1990; Jorgensen and Severance, 1990) between the quinoline ring of dibucaine and the phenyl group of Phe, we have measured ^{1}H-NMR spectra of dibucaine in the absence and in the presence of MP-1. As a control experiment, we also measured ^{1}H-NMR spectra of dibucaine in the presence of MP-2, in which the Phe has been substituted by Gln. Fig. 12, *a*, *b*, and *c*, shows, respectively, ^{1}H-NMR spectra of MP-1 (3 mM), dibucaine (3 mM), and dibucaine (3 mM)-MP-1 (3 mM) solutions in a phosphate buffer at pH 7.4. In spectrum a the peaks in a range of 7.2–7.4 ppm are due to aromatic ring protons of Phe, and the other peaks are due to amide protons of the peptide. In spectrum b the quinoline ring proton resonances are assignable from high to low frequency, respectively, to the 5, 8, 7, 6, and 3 positions. As can be seen in spectrum c, it is evident that the quinoline ring protons at the 3 and 8 positions shifted appreciably to a lower frequency. Fig. 13, *a* and *b*, shows ^{1}H-NMR spectra of dibucaine (3 mM) and dibucaine (3 mM)-MP-2 (3 mM) solutions in a phosphate buffer at pH 7.4. Interestingly, in contrast to the observations in Fig. 12, no appreciable chemical shift changes were noted for the proton resonances at the 3 and 8 positions. In Fig. 14, we have schematically summarized observed changes in chemical shifts (in units of hertz at 600 MHz) of dibucaine protons as a result of interaction with MP-1 and MP-2. As can be seen in Fig. 14, both MP-1 and MP-2 shifted the resonances due to polar side-chain moiety (protons a–d) of dibucaine to a higher frequency. These high-frequency shifts can be ascribed to the electrostatic interaction between the positively charged quaternary ammonium group of dibucaine and the negatively charged carboxyl group of Asp, Glu, or the C-terminus. On the other hand, MP-1 shifted the resonances due to the butoxy group (protons f, g, and h) and all of the quinoline ring protons (protons 3, 5, 6, 7, and 8) to a lower frequency. These low-frequency shifts can be considered to be due to the ring-current effect (Pople et al., 1959) originating from the π-stacking interactions between the quinoline ring of dibucaine and the phenyl group of Phe in MP-1, because no such chemical shift changes were caused by the presence of MP-2 in the solution.

^{1}H-NMR spectra of dibucaine and a Na^+ channel inactivation gate peptide in phosphatidylserine liposomes

To determine whether the dibucaine molecules that are binding with lipids can interact with the Na^+ channel inac-

TABLE 3 Observed quadrupole splittings ($\Delta\nu_q$) and order parameters (S_{CD})* for deuterated palmitic acid probes intercalated in mixed lipids with cholesterol at pH 7.2 and 5.2

	pH 7.2				pH 5.2			
	Dibucaine 0 mM		Dibucaine 3 mM		Dibucaine 0 mM		Dibucaine 3 mM	
Chain segment	$\Delta\nu_q$(kHz)	S_{CD}	$\Delta\nu_q$(kHz)	S_{CD}	$\Delta\nu_q$(kHz)	S_{CD}	$\Delta\nu_q$(kHz)	S_{CD}
2	32.1	0.252	32.0	0.251	31.0	0.243	30.6	0.240
3	32.5	0.255	31.9	0.250	33.6	0.264	33.3	0.261
4	36.3	0.285	35.5	0.278	36.3	0.285	35.3	0.277
6	39.2	0.307	37.5	0.294	39.4	0.309	37.0	0.290
9	39.2	0.307	37.1	0.291	38.6	0.303	35.8	0.281
10	37.6	0.295	35.4	0.278	36.1	0.283	31.8	0.249
14#	26.6	0.209	24.9	0.195	23.8	0.187	20.9	0.164
15#	20.5	0.161	18.9	0.148	17.9	0.140	15.8	0.124
16#	5.91	0.046	5.49	0.043	4.95	0.039	4.38	0.034

*Calculated from the observed quadrupole splittings by using Eq. 4.
#Taken from the palmitic-d_{31} acid probe.

tivation gate peptide, we have observed ^{1}H-NMR spectra of dibucaine and the peptide in sonicated PS liposomes prepared in deuterated phosphate buffer at pH 7.4. Fig. 15, *a*, *b*, and *c*, shows, respectively, ^{1}H-NMR spectra of dibucaine (3 mM), dibucaine (3 mM)-MP-2 (3 mM), and dibucaine (3 mM)-MP-1 (3 mM) in the PS liposomes. As expected, the quinoline ring proton resonances of dibucaine appeared as broad resonances, reflecting interactions with the PS liposomes; the resonance at the 5 position shifted to a higher frequency, whereas all of the remaining resonances shifted to a lower frequency as compared to the corresponding chemical shift positions in the phosphate buffer solution. It is worth noting that all of the quinoline proton resonances shifted to a lower frequency, even on the addition of MP-2 (spectrum b). However, more remarkable is the fact that MP-1 caused a larger low-frequency shift to those resonances than did MP-2 (spectrum c). In Fig. 16 we show the changes in chemical shifts of quinoline ring proton resonances schematically. The reason for the changes in chemical shift on the addition of MP-2 is not clear at present; this should be explained together with the changes in chemical shift of those resonances as a result of interaction with PS liposomes. However, undoubtedly the larger low-frequency shift caused by MP-1 compared to that caused by MP-2 should be ascribed to the π-stacking interaction with the phenyl group of Phe. Moreover, we notice that the chemical shift differences between resonances in spectrum c and spectrum b are two to six times larger than observed changes in chemical shifts on the addition of MP-1 in the phosphate buffer (Fig. 14). This finding indicates that π-stacking interaction is enhanced when dibucaine molecules simultaneously interact with both lipids and MP-1.

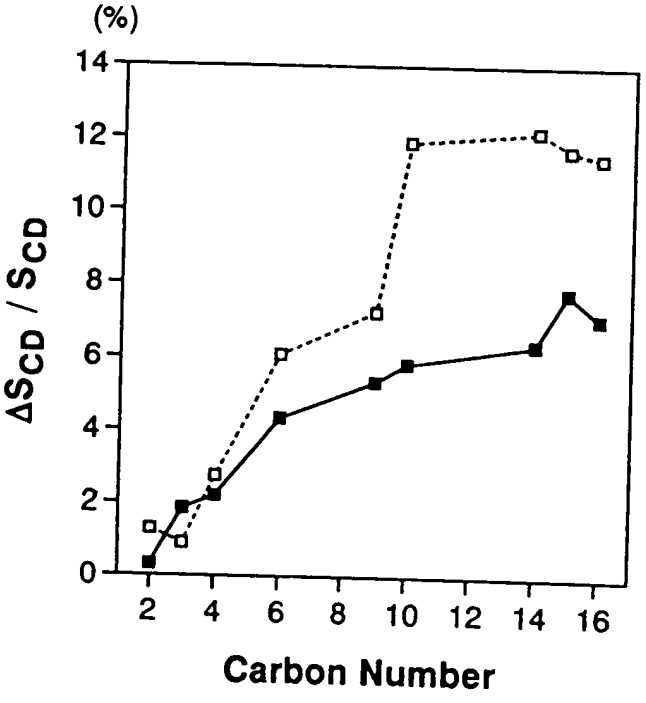

FIGURE 11 Plot of $\Delta S_{CD}/S_{CD}$ against positions of deuteration for specifically deuterated palmitic acid probes intercalated in mixed lipids with cholesterol at pH 7.2 (■) and pH 5.2 (□). ΔS_{CD} represents the amount of decrease in the S_{CD} value caused by 3 mM dibucaine.

^{1}H-NMR spectra of the phenyl group protons of phenylalanine in MP-1

Fig. 17, *a* and *b*, shows ^{1}H-NMR spectra of the phenyl group protons of Phe, in the absence and in the presence of dibucaine in the phosphate buffer, respectively. The spin-coupled peaks at around 7.36, 7.32, and 7.27 ppm are due to

TABLE 4 Partition coefficients of dibucaine in the bilayer of lipid mixture* with cholesterol# and palmitic acid§ at pH 7.2 and 5.2

	K_p	
Lipid	pH 7.2	pH 5.2
PC:PS:PE	1108	557.1

*PC:PS:PE = 1:1:2.5 molar ratio.
#Total lipids:cholesterol = 7:3 molar ratio.
§Total lipids:palmitic acid = 3:1 molar ratio.

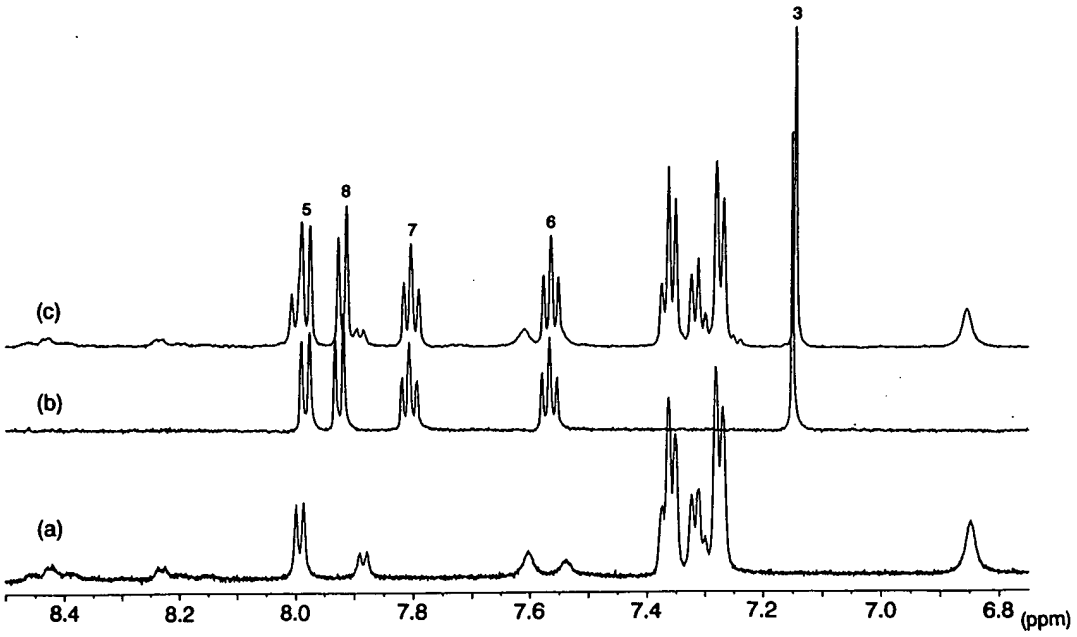

FIGURE 12 (*a*) ^{1}H-NMR spectrum of MP-1 (3 mM) in a phosphate buffer at pH 7.4. (*b*) ^{1}H-NMR spectrum of dibucaine (3 m) in a phosphate buffer at pH 7.4. (*c*) ^{1}H-NMR spectrum of dibucaine (3 mM)-MP-1 (3 mM) solution in a phosphate bufffer at pH 7.4. Assignments for the quinoline ring proton resonances are given on top of the spectrum (*c*).

meta, *para*, and *ortho* protons, respectively. It was found that dibucane shifted the phenyl group resonances very slightly to a lower frequency (0.4 Hz in *meta*, 0.0 Hz in *para*, and 1.3 Hz in *ortho* protons). Fig. 17, *c* and *d*, shows ^{1}H-NMR spectra of the phenyl group protons of Phe of MP-1 in PS liposomes. In Fig. 17 *c*, the chemical shifts of the phenyl group protons were nearly identical to those of the corresponding resonances in the phosphate buffer (Fig. 17 *a*), suggesting that the phenyl group of Phe locates at a region that does not receive any shielding or deshielding effect from the PS liposomes. However, in the presence of dibucaine, we noticed that in contrast to the large low-frequency shift of the quinoline ring proton resonances of dibucaine, the phenyl group resonances of MP-1 shifted slightly to a higher frequency (4.6 Hz in *meta* and *para* protons, and 5.0 Hz in *ortho* protons). This result indicates that the phenyl group protons are situated in positions with respect to the quinoline ring that receive deshielding field due to the ring current effect from the quinoline ring. According to the theory for the aromatic ring-current effect (Pople, 1959), this relative arrangement of the two aromatic rings can be considered to be such that the ring protons of Phe locate at the side of the quinoline ring of dibucaine and that the quinoline ring protons locate on the plane of the phenyl group of Phe. Although we cannot imagine the interaction model that satisfies these situations for all of the

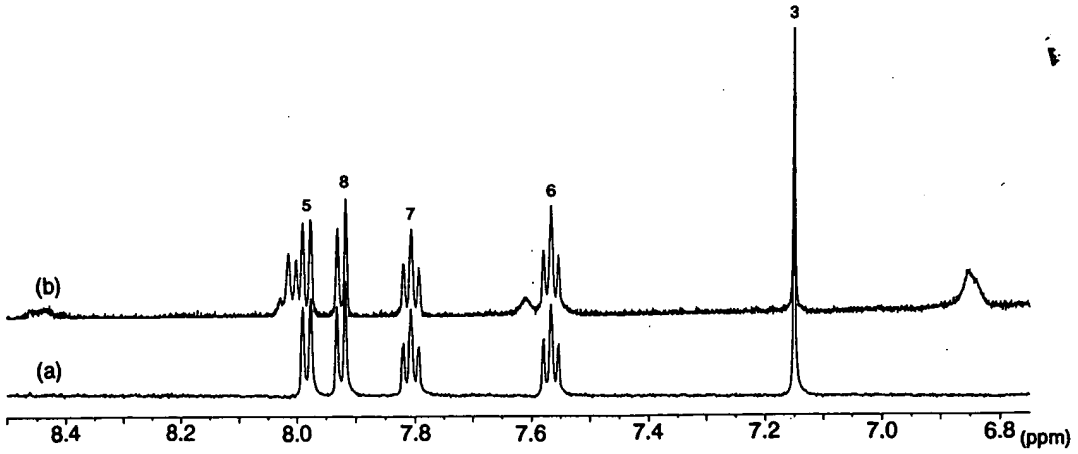

FIGURE 13 (*a*) ^{1}H-NMR spectrum of dibucaine (3 mM) in a phosphate buffer at pH 7.4. (*b*) ^{1}H-NMR spectrum of dibucaine (3 mM)-MP-2 (3 mM) solution in a phosphate buffer at pH 7.4. Assignments for the quinoline ring proton resonances are given on top of the spectrum (*b*).

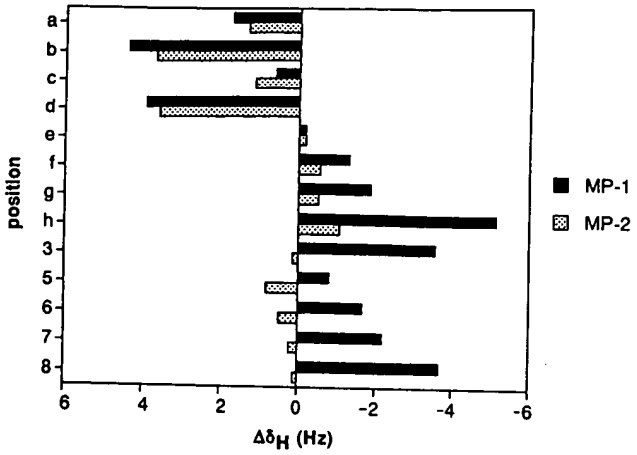

FIGURE 14 Changes in chemical shifts (in units of hertz at 600 MHz) of dibucaine as a result of interaction with MP-1 and MP-2 in a phosphate buffer at pH 7.4.

ring protons within one relative arrangement of the two aromatic rings, an edge-on or T-shaped geometry for the two π-stacking aromatic rings seems to be a reasonable one (Hunter and Sanders, 1990; Jorgensen and Severance, 1990). Taking rule 6 of Hunter et al. into account (Hunter and Sanders, 1990), the quinoline ring can be considered to be a "π-deficient atom" and the phenyl group to be a "π-rich atom"; this finding agrees well with the a priori expected result when we consider the differences in the substituents on the aromatic rings.

DISCUSSION

Locations of dibucaine in model membranes

In the present study the location of dibucaine in model membranes can be deduced by noting the following points: 1) changes in the quadrupole splittings of dibucaine-d_1 and dibucaine-d_9 by cholesterol, by temperature, and by pH; 2) changes in the quadrupole splittings of deuterated palmitic acids by dibucaine. In conclusion, the quinoline ring of dibucaine locates at a polar headgroup region, penetrating the butoxy group between the acyl chains of the lipids. In Fig. 18 we show this situation with computer graphics. The lipid demonstrated here is dipalmitoylphosphatidylserine, and its molecular structure is drawn tentatively, fully extending the acyl chains. The structure of cholesterol in egg phosphatidylcholine bilayers is well investigated by x-ray (Franks, 1976) and neutron diffraction (Worcester and Franks, 1976) studies. Thus, in Fig. 18, the cholesterol was so positioned as to locate its 3β-hydroxyl group in the vicinity of the acyl ester linkage or glycerol backbone, spanning the polycyclic ring up to the first 8 to 10 methylene segments of the acyl chains, and extending the side chain up to about the same depth in the bilayer (Stockton and Smith, 1976). The dibucaine is presented as taking a face-to-face π-stacked dimer, because it has been shown that dibucaine can exist as an aggregate in the lipid bilayer (Wakita et al., 1992; Kuroda et al., 1994). One of the most important results for deducing the location of dibucaine is that the quadrupole splitting of dibucaine-d_1 dramatically decreased when the multilamellar dispersions included cholesterol, whereas those of dibucaine-d_9 increased by including cholesterol. At first sight, the former observation appears to be explicable by changes in the membrane-aqueous partitioning of the anesthetic by cholesterol. In fact, it is reported that the partition coefficient of tetracaine between dimyristoylphosphatidylcholine and a buffer at pH 9.5 decreases from 200 to 110 by including a 7:3 molar ratio of cholesterol; at pH 5.5 it decreases from 21 to 8 (Auger et al., 1988). However, the same reasoning cannot be applied to the finding for the latter dibucaine-d_9 data, because the quadrupole splittings of methylene and methyl groups were increased by cholesterol. Because it is known that cholesterol induces a high degree of order for the acyl chains of phospholipids, it might be expected that if both the deuteron at the 3 position of the quinoline ring and the deuterons of the butoxy group that is attached to the 2 position locate inside the glycerol backbone, the magnitude of their quadrupole splittings in both dibucaine-d_1 and dibucaine-d_9 spectra would increase, reflecting the increased degree of order caused by cholesterol molecules. However, this was not the case; only the butoxy group deuterons showed increased quadrupole splittings by cholesterol. To settle this problem, it is inevitable that the carbon atom of the 3 position of the quinoline ring will be located near the acyl ester linkage or glycerol backbone, causing the butoxy chain to be approximately parallel to the acyl chains, as shown in Fig. 18. For this binding situation, we can ascribe the observed dramatic reduction in the quadrupole splitting of dibucaine-d_1 caused by cholesterol to the decreased order of the C-D vector at the 3 position; in fact, this was clearly reflected in the increased Δ_2 value shown in Table 1. The decrease in order of the C-D vector at the 3 position seems to arise from variations in the orientation of the quinoline ring plane relative to the bilayer normal. Order parameter profiles for palmitic acid probes shown in Fig. 11 give support to the deduced location of dibucaine. We might expect that if such a bulky group as a quinoline ring were located in the middle of the acyl chain, the relevant part would become rigid and result in an increased degree of order. However, this was not the case, because the S_{CD} values of all of the monitored chain segments were decreased by the addition of dibucaine. This implies that the bulky quinoline ring is located at the polar headgroup region and not between the hydrophobic acyl chains. This applies to both neutral and acidic conditions employed in this study. Under neutral conditions, about half of the dibucaine molecules can be considered to exist in an uncharged molecular form, whereas in the acidic condition, all of the dibucaine molecules exist in a cationic form. Boulanger et al. (1981) have shown that the positively charged tetracaine at low pH mostly locates at the PC headgroup level, whereas the uncharged form at high pH is intercalated partly in the

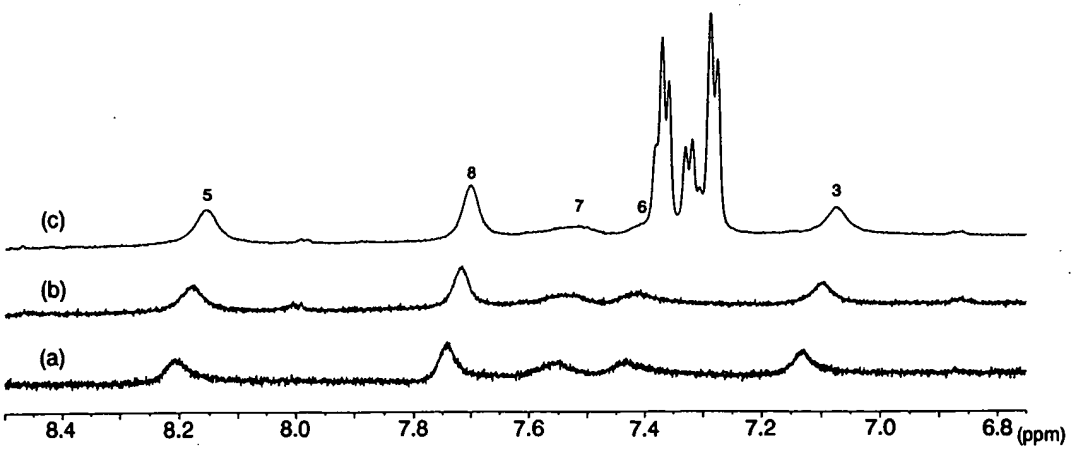

FIGURE 15 (*a*) ^{1}H-NMR spectrum of dibucaine (3 mM) in sonicated PS liposomes prepared in deuterated phosphate buffer at pH 7.4. (*b*) ^{1}H-NMR spectrum of dibucaine (3 mM)-MP-2 (3 mM) in the sonicated PS liposomes. (*c*) ^{1}H-NMR spectrum of dibucaine (3 mM)-MP-1 (3 mM) in the PS liposomes. Assignments for the quinoline proton resonances are given on top of the spectrum (*c*).

headgroup region and partly in the fatty acyl chains of the PC bilayers. The somewhat deeper binding of the neutral tetracaine is also pointed out by the fluorescence quenching experiment (Sikaris and Sawyer, 1982); the drug is oriented in the bilayer so that its aromatic amine is near carbon 9 of the fatty acyl chain of PC bilayers. For the PS bilayers, it is also concluded that the charged and uncharged tetracaine occupy different sites in the PS bilayer (Kelusky et al., 1986). In the present data, however, we find no definite reason to assume that the molecular form of dibucaine and its protonated form locate at different depths in the bilayer, at least to the precision of setting the carbon atom at the 3 position, based on the reasoning above. The differences in the ratio $\Delta S_{CD}/S_{CD}$ noted between pH 7.2 and pH 5.2 can be explained by the electrostatic interaction between the charged dibucaine and the polar headgroup; hence we need not invoke the changes in location of dibucaine upon protonation. The quadrupole splittings of both dibucaine-d_1 and dibucaine-d_9 are always smaller at the acidic condition than at the neutral condition. This can be explained by the increased freedom of movement of dibucaine at the polar headgroup region caused by the electrostatic interaction, which separates lipid molecules from each other and results in loose packing.

From the conclusions drawn about the location of dibucaine in model membranes, we may be allowed to conclude that all local anesthetic molecules reside at the polar headgroup region of the membranes, which is capable of interacting simultaneously with the hydrophobic amino acid

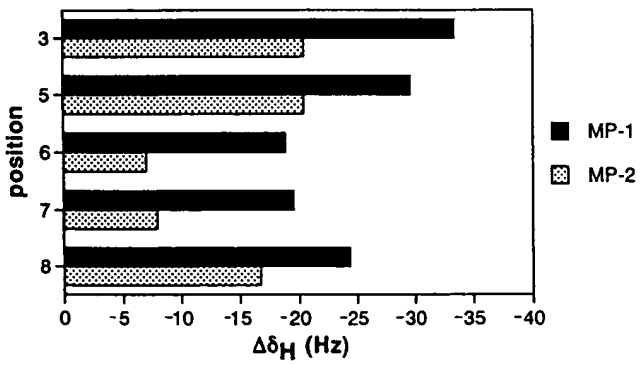

FIGURE 16 Changes in chemical shifts (in units of Hz at 600 MHz) of the quinoline proton resonances of dibucaine as a result of the interaction with MP-1 and MP-2 in the PS liposomes.

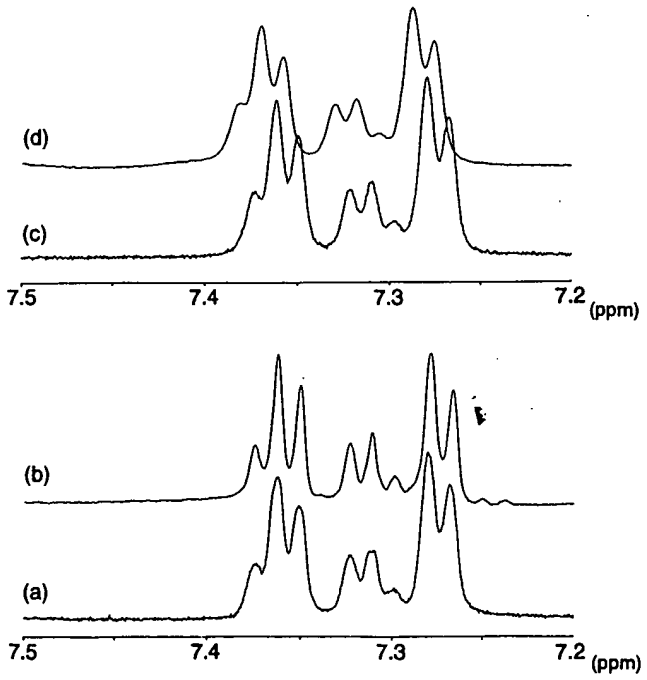

FIGURE 17 (*a*) ^{1}H-NMR spectrum of the phenyl group protons of MP-1 (3 mM) in a phosphate buffer at pH 7.4. (*b*) ^{1}H-NMR spectrum of the phenyl group protons of dibucaine (3 mM)-MP-1 (3 mM) solution in a phosphate buffer at pH 7.4. (*c*) ^{1}H-NMR spectrum of the phenyl group protons of MP-1 in the PS liposomes at pH 7.4. (*d*) ^{1}H-NMR spectrum of the phenyl group protons of dibucaine (3 mM)-MP-1 (3 mM) solution in the PS liposomes at pH 7.4.

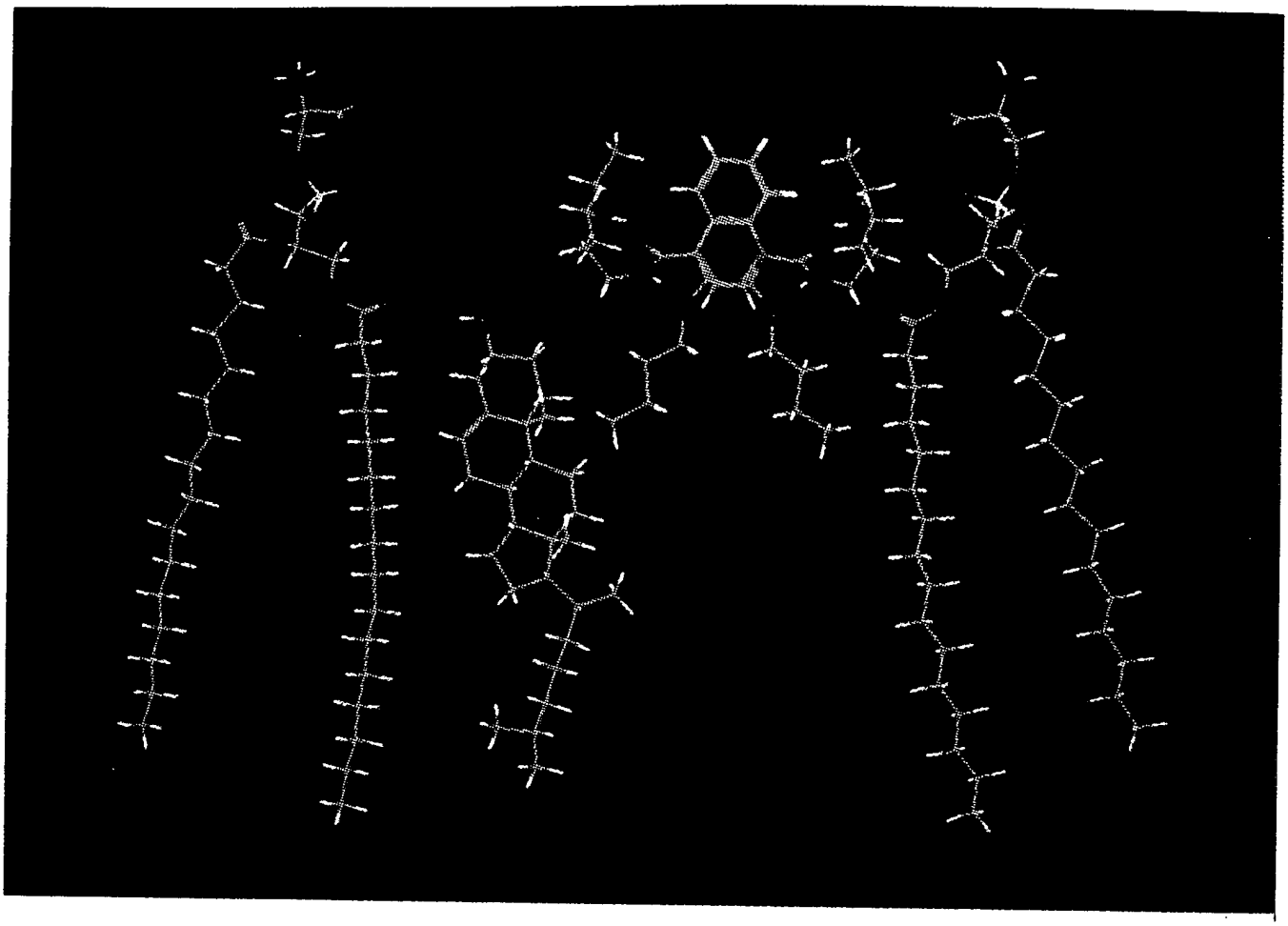

FIGURE 18 Computer graphics view of relative arrangements among local anesthetic dibucaine, cholesterol, and dipalmitoylphosphatidylserine. The dibucaine is presented as a face-to-face π-stacked dimer.

residues at the intracellular linker part (Fig. 2). Interestingly, Wang et al. have shown that there is a large hydrophobic region within the Na^+ channel pore in its cytoplasmic side, which accepts up to 18 methylene groups of the quaternary ammonium compounds; the hydrophobic domain also interacts with local anesthetics such as cocaine and mepivacaine (Wang et al., 1991). It seems very reasonable to assume that the hydrophobic domain is formed by the lipids surrounding the channel protein. Moreover, the lipids are not always required to be organized as a bilayer, but they can exist as a hexagonal phase (Dibble and Feigenson, 1994; Tournois et al., 1987), implying that the drug, especially its aromatic ring, can assume any convenient orientation to accommodate the three hydrophobic amino acids of the intracellular linker.

Molecular mechanisms of local anesthesia

Local anesthetics are chemicals that reversibly block action potentials in excitable membranes (Strichartz and Ritchie, 1987). They are usually composed of an aromatic ring, an intermediate chain including an amide or an ester linkage, and a tertiary amine nitrogen. They are amphiphilic in nature and can exist as either cationic or uncharged molecular forms, depending on the pK_a of the drugs and pH of the medium. As for the molecular mechanisms of anesthesia, it is generally established that tertiary amine-type local anesthetics penetrate into the nerve sheath and nerve membrane with their uncharged forms and bind to the Na^+ channel at the axoplasmic side of nerve membranes with their cationic forms (Narahashi et al., 1970). However, benzocaine, which lacks the ionizable tertiary amine at physiological pH, is also known to be a local anesthetic drug. Thus there still remain many controversial questions about the molecuar mechanisms of local anesthesia: What is the site of anesthetic action? Is the site within lipids or within the Na^+ channel protein? How many sites are there? Do both cationic and molecular forms of the drug bind at the same site? etc. In attempting to solve these problems, we noticed the publications on Na^+ channel inactivation gate (Patton et al., 1992; West et al., 1992), because it has already been shown that local anesthetics promote the channel to close its inactivation gate, stabilizing the inactivated state (Hille, 1977; Postma and Catterall, 1984). Accordingly, we supposed that

local anesthetics directly interact with the inactivation gate, especially with its phenylalanine residue in the three clustered hydrophobic amino acids of Ile-Phe-Met (Fig. 2), because the phenylalanine residue is playing an essential role in Na^+ channel inactivation (West et al., 1992). This assumption was also suggested to us by the fact that all local anesthetics essentially bear an aromatic ring in their structures. We believe that the aromatic ring might be a prerequisite group, not only for conferring lipophilicity on a drug that allows it to pass through membranes, but also for π-stacked binding with the phenyl group of the phenylalanine residue. Thus we studied the interaction of local anesthetic dibucaine and the Na^+ channel inactivation gate peptides MP-1 and MP-2. One of the most serious concerns, however, was whether dibucaine in a solution and in a lipid bilayer membrane really interacts with the peptide at its hydrophobic moieties. The present data shown in Figs. 14 and 16 clearly removed this concern. In addition, it was found that the presence of lipids enhances the interaction. This finding suggests firm evidence regarding the molecular mechanisms of local anesthesia that the drug residing at the polar headgroup region of the so-called boundary lipids in the vicinity of the Na^+ channel pore binds with the clustered hydrophobic amino acids, especially with the phenylalanine residue and results in stabilization of the inactivated state. The drug binding with the phenylalanine residue may also be facilitated by electrostatic interactions of its protonated nitrogen with the negatively charged amino acids on both sides of the IFM domain. Interestingly, Sheldon et al. have shown in their structure-activity relationship study on the lidocaine derivatives that there is an optimal distance between the aromatic ring and the tertiary amine nitrogen for binding with the Na^+ channel (Sheldon et al., 1991). Now we can assign the optimal length to a range of distances between the phenyl group of the phenylalanine residue and the negative charge on the carboxyl group of the aspartic acid, or between two glutamic acid residues that are situated in positions before and after the IFM domain, respectively (Fig. 2). Postma and Catterall (1984) and Wang et al. (1994) have shown from their Hill coefficient data that one local anesthetic drug binds with one inactivated channel. This finding lends further support to our view that a local anesthetic drug binds to the IFM domain in the manner described above. In Fig. 19 we show schematically the inter-

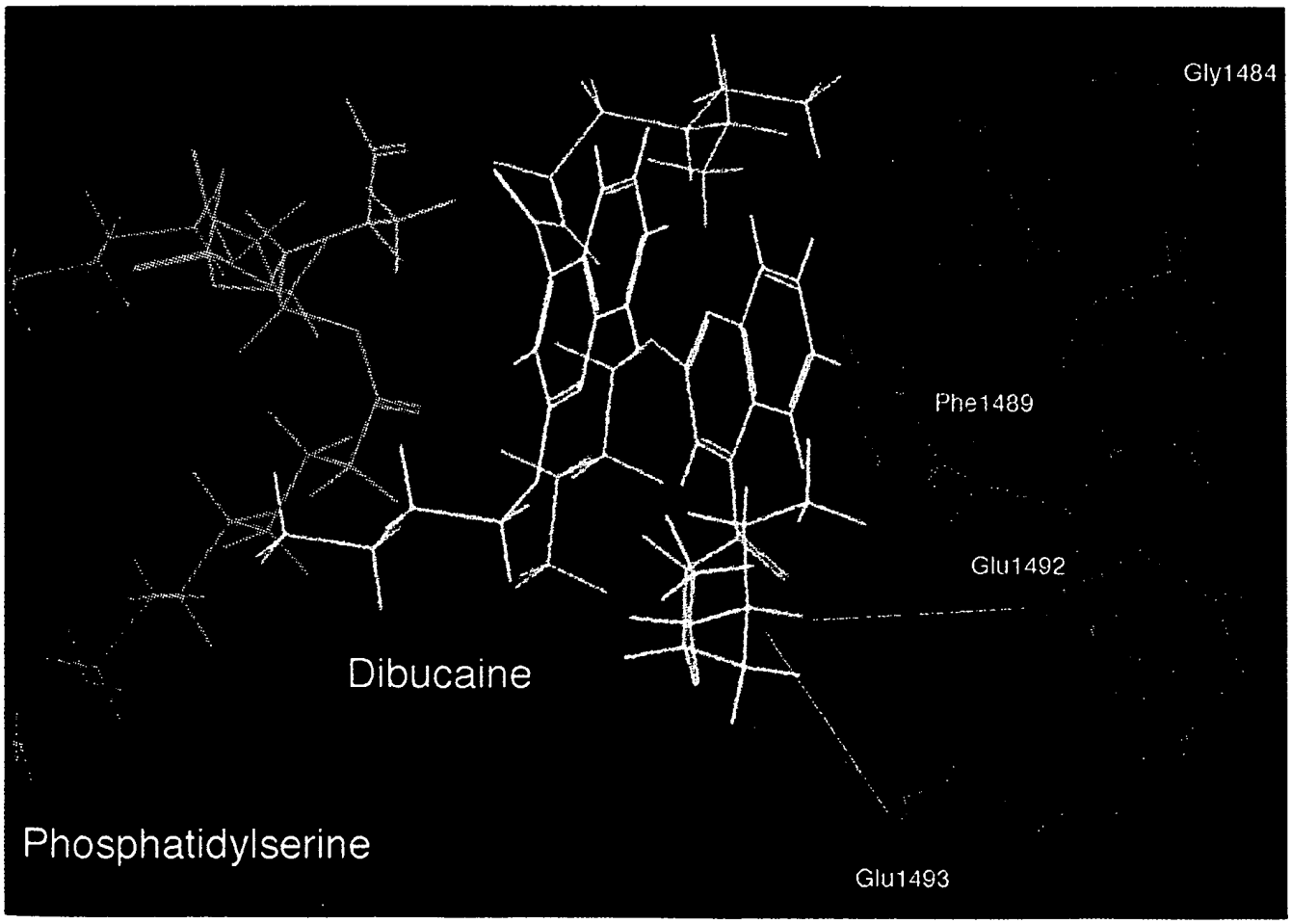

FIGURE 19 Computer graphics view for showing schematically the interaction between dibucaine, which resides at the polar headgroup region of phosphatidylserine, and the inactivation gate peptide. The dibucaine is shown as a face-to-face π-stacked dimer.

action between dibucaine and the inactivation gate peptide; one dibucaine dimer located at the polar headgroup region of phosphatidylserine, π-stacking face-to-face with the other, also interacts with the phenyl group of Phe-1489 by π-stacking interaction with a T-shaped geometry, allowing its protonated quaternary nitrogen to interact electrostatically with the negatively charged carboxyl groups of two adjacent glutamic acid residues of Glu-1492 and Glu-1493.

Finally, it should be added that Ragsdale et al. (1994) have recently assigned the Phe-1764 residue in the sixth segment of domain IV (Fig. 1) of rat brain type IIA Na^+ channel to a plausible site of action of the local anesthetic etidocaine. The Phe-1764 locates in the intermediate region of the transmembrane helix and plays an important role in fast inactivation of the Na^+ channel (McPhee et al., 1995). Interestingly, such a binding situation is reminiscent of the binding of local anesthetic agents acting as noncompetitive channel blockers for the nicotinic acetylcholine receptor (Giraudat et al., 1987; Charnet et al., 1990), in the sense that local anesthetic molecules can interact directly with transmembrane helices that form the lumen of the channel pore. More recently, on the other hand, Bennett et al. (1995) have indicated the importance of the IFM domain in the III-IV linker for the lidocaine block of the human cardiac Na^+ channel. This result strongly supports our conclusion. Evidently more work is required to enlighten us about the molecular mechanisms of local anesthesia.

REFERENCES

Auger, M., H. C. Jarrell, and I. C. P. Smith. 1988. Interactions of the local anesthetic tetracaine with membranes containing phosphatidylcholine and cholesterol: a ^{2}H-NMR study. *Biochemistry.* 27:4660–4667.

Bennett, P. B., C. Valenzuela, L.-Q. Chen, and R. G. Kallen. 1995. On the molecular nature of the lidocaine receptor of cardiac Na^+ channels. Modification of block by alterations in the α-subunit III-IV interdomain. *Circ. Res.* 77:584–592.

Bloom, M., J. H. Davis, and F. W. Dahlquist. 1978. Determination of orientational order in bilayer systems using moments of deuterium magnetic resonance spectra. *In* XXth Ampere Congress Proceedings, Tallinn, Estonia. E. Kundla, E. Lippmann, and T. Saluvere, editors. Springer-Verlag, New York. 551.

Bloom, M., and O. G. Mouritsen. 1988. The evolution of membranes. *Can. J. Chem.* 66:706–712.

Boulanger, Y., S. Schreier, and I. C. P. Smith. 1981. Molecular details of anesthetic-lipid interaction as seen by deuterium and phosphorus-31 nuclear magnetic resonance. *Biochemistry.* 20:6824–6830.

Burnett, L. J., and B. H. Muller. 1971. Deuteron quadrupole coupling constants in three solid deuterated paraffin hydrocarbons: C_2D_6, C_4D_{10}, C_6D_{14}. *J. Chem. Phys.* 55:5829–5831.

Chacko, G. K., G. M. Villegas, F. V. Barnola, R. Villegas, and D. E. Goldman. 1976. The polypeptide and the phospholipid components of axon plasma membranes. *Biochim. Biophys. Acta.* 443:19–32.

Charnet, P., C. Labarca, R. J. Leonard, N. J. Vogelaar, L. Czyzyk, A. Gouin, N. Davidson, and H. A. Lester. 1990. An open-channel blocker interacts with adjacent turns of α-helices in the nicotinic acetylcholine receptor. *Neuron.* 2:87–95.

Courtney, K. R., and G. R. Strichartz. 1987. Structural elements which determine local anesthetic activity. *In* Local Anesthetics. G. R. Strichartz, editor. Springer-Verlag, New York. 53–94.

Covino, B. G. 1987. Local anesthetic agents. *In* Practical Anesthetic Pharmacology. R. R. Attia, A. W. Grogono, and F. R. Domer, editors. Appleton-Century-Crofts, East Norwalk, CT. 55–77.

Davis, J. H., and K. R. Jeffrey. 1977. The temperature dependence of chain disorder in potassium palmitate-water. A deuterium NMR study. *Chem. Phys. Lipids.* 20:87–104.

Davis, J. H., K. R. Jeffrey, M. Bloom, M. I. Valic, and T. P. Higgs. 1976. Quadrupolar echo deuteron magnetic resonance spectroscopy in ordered hydrocarbon chains. *Chem. Phys. Lett.* 42:390–394.

Davis, J. H., B. Maraviglia, G. Weeks, and D. V. Godin. 1979. Bilayer rigidity of the erythrocyte membrane. ^{2}H-NMR of a perdeuterated palmitic acid probe. *Biochim. Biophys. Acta.* 550:362–366.

Dibble, A. R. G., and G. W. Feigenson. 1994. Detection of coexisting fluid phospholipid phases by equilibrium Ca^{2+} binding: peptide-poor L_α and peptide-rich H_{II} phase coexistence in gramicidin A′/phospholipid dispersions. *Biochemistry.* 33:12945–12953.

Franks, N. P. 1976. Structural analysis of hydrated egg lecithin and cholesterol bilayers. I. X-ray diffraction. *J. Mol. Biol.* 100:345–358.

Giraudat, J., M. Dennis, T. Heidmann, P.-Y. Haumont, F. Lederer, and J.-P. Changeux. 1987. Structure of the high-affinity binding site for noncompetitive blockers of the acetylcholine receptor: [^{3}H]chlorpromazine labels homologous residues in the β and δ chains. *Biochemistry.* 26:2410–2418.

Greaves, W. S., R. P. Linstead, B. R. Shephard, S. L. S. Thomas, and B. C. L. Weedon. 1950. Anodic syntheses. Part I. New syntheses of stearic, myristic, and other acids. *J. Chem. Soc.* 3326–3330.

Hille, B. 1977. Local anesthetics: hydrophilic and hydrophobic pathways for the drug-receptor reaction. *J. Gen. Physiol.* 69:497–515.

Hunter, C. A. 1993. Arene-arene interactions: electrostatic or charge transfer? *Angew. Chem. Int. Ed. Engl.* 32:1584–1586.

Hunter, C. A., and J. K. M. Sanders. 1990. The nature of π-π interactions. *J. Am. Chem. Soc.* 112:5525–5534.

Jorgensen, W. L., and D. L. Severance. 1990. Aromatic-aromatic interactions: free energy profiles for the benzene dimer in water, chloroform, and liquid benzene. *J. Am. Chem. Soc.* 112:4768–4774.

Kelusky, E. C., Y. Boulanger, S. Schreier, and I. C. P. Smith. 1986. A ^{2}H-NMR study on the interactions of the local anesthetic tetracaine with membranes containing phosphatidylserine. *Biochim. Biophys. Acta.* 856: 85–90.

Kuroda, Y., M. Wakita, and T. Nakagawa. 1994. Interaction between dibucaine and pig erythrocyte membranes as studied by NOESY experiments in ^{1}H-NMR spectroscopy. Which form of dibucaine interacts more strongly, cationic or uncharged? *Chem. Pharm. Bull.* 42: 2418–2425.

Lee, A. G. 1978. Effects of charged drugs on the phase transition temperatures of phospholipid bilayers. *Biochim. Biophys. Acta.* 514:95–104.

Maraviglia, B., J. H. Davis, M. Bloom, J. Westerman, and K. W. A. Wirtz. 1982. Human erythrocyte membranes are fluid down to −5°C. *Biochim. Biophys. Acta.* 686:137–140.

McDonald, R. S., and P. A. Wilks, Jr. 1988. JCAMP-DX: a standard form for exchange of infrared spectra in computer readable form. *Appl. Spectrosc.* 42:151–162.

McPhee, J. C., D. S. Ragsdale, T. Scheuer, and W. A. Catterall. 1995. A critical role for transmembrane segment IVS6 of the sodium channel α subunit in fast inactivation. *J. Biol. Chem.* 270:12025–12034.

Miescher, K. 1932. Studien über Lokalanasthetica. *Helv. Chim. Acta.* 15:163–190.

Narahashi, T., D. Frazier, and M. Yamada. 1970. The site of action and active form of local anesthetics. I. Theory and pH experiments with tertiary compounds. *J. Pharmacol. Exp. Ther.* 171:32–51.

Nichol, C. P., J. H. Davis, G. Weeks, and M. Bloom. 1980. Quantitative study of the fluidity of *Escherichia coli* membranes using deuterium magnetic resonance. *Biochemistry.* 19:451–457.

Noda, M., T. Ikeda, T. Kayano, H. Suzuki, H. Takeshima, M. Kurasaki, H. Takahashi, and S. Numa. 1986. Existence of distinct sodium channel messenger RNAs in rat brain. *Nature.* 320:188–192.

Oldfield, E., M. Meadows, D. Rice, and R. Jacobs. 1978. Spectroscopic studies of specifically deuterium labeled membrane systems. Nuclear magnetic resonance investigation of the effects of cholesterol in model systems. *Biochemistry.* 14:2727–2740.

Op den Kamp, J. A. F. 1979. Lipid asymmetry in membranes. *Annu. Rev. Biochem.* 48:47–71.

Papahadjopoulos, D., K. Jacobson, G. Poste, and G. Shepherd. 1975. Effects of local anesthetics on membrane properties. I. Changes in the fluidity of phospholipid bilayers. *Biochim. Biophys. Acta.* 394:504–519.

Patton, D. E., J. W. West, W. A. Catterall, and A. L. Goldin. 1992. Amino acid residues required for fast Na^+-channel inactivation: charge neutralizations and deletions in the III-IV linker. *Proc. Natl. Acad. Sci. USA.* 89:10905–10909.

Pauls, K. P., A. L. MacKay, and M. Bloom. 1983. Deuterium nuclear magnetic resonance study of the effects of palmitic acid on dipalmitoylphosphatidylcholine bilayers. *Biochemistry.* 22:6101–6109.

Pople, J. A., W. G. Schneider, and H. J. Bernstein. 1959. High-Resolution Nuclear Magnetic Resonance. McGraw-Hill, New York. 180–183.

Postma, S. W., and W. A. Catterall. 1984. Inhibition of binding of [^{3}H]batrachotoxinin A 20-α-benzoate to sodium channels by local anesthetics. *Mol. Pharmacol.* 25:219–227.

Ragsdale, D. S., J. C. McPhee, T. Scheuer, and W. A. Catterall. 1994. Molecular determinants of state-dependent block of Na^+ channels by local anesthetics. *Science.* 265:1724–1728.

Ritchie, J. M., and N. M. Greene. 1985. Local anesthetics. *In* The Pharmacological Basis of Therapeutics. A. G. Gilman, L. S. Goodman, T. W. Rall, and F. Murad, editors. Macmillan, New York. 302–321.

Ritchie, J. M., and P. Greengard. 1961. On the active structure of local anesthetics. *J. Pharmacol. Exp. Ther.* 133:241–245.

Seelig, J. 1977. Deuterium magnetic resonance: theory and application to lipid membranes. *Q. Rev. Biophys.* 10:353–418.

Sheldon, R. S., R. J. Hill, M. Taouis, and L. M. Wilson. 1991. Aminoalkyl structural requirements for interaction of lidocaine with the class I antiarrhythmic drug receptor on rat cardiac myocytes. *Mol. Pharmacol.* 39:609–614.

Sikaris, K. A., and W. H. Sawyer. 1982. The interaction of local anaesthetics with synthetic phospholipid bilayers. *Biochem. Pharmacol.* 16: 2625–2631.

Stockton, G. W., C. F. Polnaszek, L. C. Leitch, A. P. Tulloch, and I. C. P. Smith. 1974. A study of mobility and order in model membranes using ^{2}H-NMR relaxation rates and quadrupole splittings of specifically deuterated lipids. *Biochem. Biophys. Res. Commun.* 60:844–850.

Stockton, G. W., C. F. Polnaszek, A. P. Tulloch, F. Hasan, and I. C. P. Smith. 1976. Molecular motion and order in single-bilayer vesicles and multilamellar dispersions of egg lecithin and lecithin-cholesterol mixtures. A deuterium nuclear magnetic resonance study of specifically labeled lipids. *Biochemistry.* 15:954–966.

Stockton, G. W., and I. C. P. Smith. 1976. A deuterium nuclear magnetic resonance study of the condensing effect of cholesterol on egg phosphatidylcholine bilayer membranes. I. Perdeuterated fatty acid probes. *Chem. Phys. Lipids.* 17:251–263.

Strichartz, G. R., and J. M. Ritchie. 1987. The action of local anesthetics on ion channels of excitable tissues. *In* Local Anesthetics. G. R. Strichartz, editor. Springer-Verlag, New York. 21–52.

Tournois, H., J. Leunissen-Bijvelt, C. W. M. Haest, J. de Gier, and B. de Kruijff. 1987. Gramicidin-induced hexagonal H_{II} phase formation in erythrocyte membranes. *Biochemistry.* 26:6613–6621.

Trudell, J. R. 1977. A unitary theory of anesthesia based on lateral phase separations in nerve membranes. *Anesthesiology.* 46:5–10.

Trudell, J. R. 1980. Biophysical concepts in molecular mechanisms of anesthesia. *Prog. Anesthesiol.* 2:261–270.

Vogt, T. C. B., J. A. Killian, and B. de Kruijff. 1994. Structure and dynamics of the acyl chain of a transmembrane polypeptide. *Biochemistry.* 33:2063–2070.

Wakita, M., Y. Kuroda, Y. Fujiwara, and T. Nakagawa. 1992. Conformations of dibucaine and tetracaine in small unilamellar phosphatidylcholine vesicles as studied by nuclear Overhauser effects in ^{1}H nuclear magnetic resonance spectroscopy. *Chem. Phys. Lipids.* 62:45–54.

Wang, G. K., W. M. Mok, and S.-Y. Wang. 1994. Charged tetracaine as an inactivation enhancer in batrachotoxin-modified Na^+ channels. *Biophys. J.* 67:1851–1860.

Wang, G. K., R. Simon, and S.-Y. Wang. 1991. Quaternary ammonium compounds as structural probes of single batrachotoxin-activated Na^+ channels. *J. Gen. Physiol.* 98:1005–1024.

West, J. W., D. E. Patton, T. Scheuer, Y. Wang, A. L. Goldin, and W. A. Catterall. 1992. A cluster of hydrophobic amino acid residues required for fast Na^+-channel inactivation. *Proc. Natl. Acad. Sci. USA.* 89: 10910–10914.

Westman, J., Y. Boulanger, A. Ehrenberg, and I. C. P. Smith. 1982. Charge and pH dependent drug binding to model membranes. A. ^{2}H-NMR and light absorption study. *Biochim. Biophys. Acta.* 685:315–328.

Worcester, D. L., and N. P. Franks. 1976. Structural analysis of hydrated egg lecithin and cholesterol bilayers. II. Neutron diffraction. *J. Mol. Biol.* 100:359–378.

Zamponi, G. W., and R. J. French. 1994. Amine blockers of the cytoplasmic mouth of sodium channels: a small structural change can abolish voltage dependence. *Biophys. J.* 67:1015–1027.

STIC-ILL

From: Gabel, Gailene
Sent: Wednesday, February 12, 2003 4:14 PM
To: STIC-ILL
Subject: 09/905,439

Please provide a copy of the following references ASAP:

1) Gillies et al., NMR in Physiology and Biomedicine, Academic Press: San Diego (1994).

2) Yamazaki et al., J. Am. Chem. Soc. 120: 5591-5592 (1998).

3) Severinov et al., J. Biol. Chem. 273: 16205-16209 (1998).

4) Muir et al. (Proc. Natl. Acad. Sci USA, 95: 6705-6710 (1998).

5) Xu et al. Proc. Natl. Acad. Sci., 96: 388-393 (1999).

6) Lippens et al., In NMR in Supramolecular Chemistry, Pons M. Ed., Kluwer Academic Publishers, 191-226 (1999).

Thanks a bunch,
Gail R. Gabel
7B15
CM1
305-0807

STRUCTURAL DIVERSITY OF THE OSMOREGULATED PERIPLASMIC GLUCANS OF GRAM-NEGATIVE BACTERIA BY A COMBINED GENETICS AND NUCLEAR MAGNETIC RESONANCE APPROACH

GUY LIPPENS[a]* AND JEAN-PIERRE BOHIN[b]*

[a]*CNRS URA 1309, Pasteur Institute of Lille, 1 rue du Professeur Calmette, 59019 Lille, France*

[b]*CNRS UMR 111 , Université des Sciences et Technologies de Lille, 59655 Villeneuve d'Ascq Cedex, France,*

**Laboratoire Européen Associé "Analyse structure-fonction des biomolécules" (CNRS, France and FNRS, Belgium).*

1. Abstract

The periplasmic space is a cellular compartment lying between the inner and the outer membranes of gram-negative bacteria. Located in this region are the peptidoglycan layer, the osmoregulated periplasmic glucans (OPGs), and a number of proteins implicated in the detection, the processing and the transport into the cell of nutrients, the detoxification of deleterious substances, and the biogenesis of the envelope. OPGs exhibit structural features that are characteristic of a bacterial genus. However, they share several major traits: glucose is the only monosaccharide; they are oligosaccharides made of a limited number of units (c.a. 10-20); they are accumulated in the periplasmic space in a higher amount in response to a lower osmolarity of the medium.

NMR has been extensively used in our laboratories to establish the primary sequences of different OPGs. Homonuclear COSY, and relayed COSY or TOCSY experiments are used to assign all protons in every individual glucose

M. Pons (ed.), NMR in Supramolecular Chemistry, 191–226.

ring, and are combined with HSQC and HSQC-TOCSY experiments for complete carbon assignments. NOESY and HMBC spectra, exploiting respectively the short distance between protons on both sides of the glycosidic linkage and the heteronuclear coupling over the linkage, are used to establish the sequential assignments, but suffer from poor separation in all but the anomeric proton signals. We exploited the wider spread in carbon chemical shifts by implementing the NOESY experiment in its HSQC-NOESY version. Alternatively, the assignment can be done solely on the basis of the anomeric proton region by the NOESY-TOCSY and/or TOCSY-NOESY pulse sequences.

Determination of the 3D structures of the OPGs has been addressed in our laboratories after the discovery of several cyclic OPGs that contain one single α–(1-6) linkage next to all β–(1-2) linkages. This single α–(1-6) linkage introduces conformational strains to such an extent that all anomeric protons can be observed separately. We have focused on the cyclic OPG of *Ralstonia solanacearum*, that because of its small size (DP13) makes an ideal model to address the problems of potential cavities or other structural features that might be relevant for the function of these intriguing molecules. In contrast to protein NMR, the number of experimental parameters that can be used to derive a structural model are very limited. They basically are the same as the parameters used for the sequential assignment, i.e. the NOE between the H1-H2' proton pair and the ^{3}J H1-C2' and C1-H2' long-range coupling constants. A last parameter that has been correlated to the glycosidic conformation is the direct ^{1}J (H1-C1) coupling constant. The limited number of experimental structures, however, leads to a probably imperfect parametrization of the Karplus relationships that relate coupling constants to structure in oligosaccharides.

Model building led to different structures, but none was compatible with all experimental observations. Further indication of dynamical equilibrium came from the line broadening as observed on the anomeric proton of the b unit. This was confirmed by a detailed relaxation study, and we concluded that the molecule undergoes slow dynamics on the microsecond time scale. The biological relevance of this dynamics is currently under investigation in our groups.

In order to address question of the molecular mobility of the OPGs in the periplasm, we have started *in vivo* experiments, with bacteria containing isotopically enriched OPGs. The obtaining of workable NMR spectra indicates that at least a majority of the molecules maintain a high degree of diffusional mobility.

2. Diversity of the OPGs

The periplasmic space lies between the inner and the outer membranes of gram-negative bacteria [1]. A number of processes that are vital to the growth and viability of the cell occur within this compartment. Proteins residing in the periplasm fulfill important functions in the detection and processing of essential nutrients and their transport into the cell. The contents of the periplasmic space provide a microenvironment of small and middle-sized molecules that buffer the cell from changes that occur in its local surroundings. In fulfilling these essential roles, the periplasm is not static but dynamic, capable of regulation to accommodate changes in the external and internal environments that surround it. While an overall understanding of the structure and contents of the periplasmic space has been obtained, the periplasm still remains the most controversial and poorly defined compartment in the gram-negative bacterial cell. The exact size and internal architecture of the periplasm remain area of dispute, and the fine structure that leads to low mobility of periplasmic proteins needs further clarification [1]. Osmoregulated periplasmic glucans (OPG) are general components of the periplasm of gram-negative bacteria [2] and share the following features: glucose as the sole sugar, glucose units linked, at least partially, by β–glycosidic bonds, and synthesis under osmotic control and that is inversely correlated to the osmolarity of the growth medium of the cells [3]. Recent investigations have revealed that beyond these common features OPGs from various bacterial species show an unexpected structural diversity. Four families can be distinguished (Figure 1).

Family 1. OPGs of *E. coli*, also known as MDOs (Membrane-Derived Oligosaccharides), appear to range from 5 to 12 glucose residues, with the principal species containing 8 or 9 glucose residues (4-5)]. The structure is highly branched, the backbone consisting of β–(1-2)-linked glucose units to which the branches are attached by β–(1-6) linkages. Similar structures were found for the OPGs of the closely related species *Erwinia chrysanthemi* [6] and also for the OPGs of the more distantly related species *Pseudomonas syringae* [7].

Family 2. Among members of the family *Rhizobiaceae*, periplasmic glucans are cyclic [8]. Studies have demonstrated that *Agrobacterium* and *Rhizobium* species synthesize periplasmic glucans with similar structure [9, 10, 11]. In both genera, periplasmic glucans are composed of a cyclic β–(1-2)-glucan backbone containing 17 to 24 glucose residues. Bundle et al. [12] reported that *Brucella*

spp. synthesize cyclic β–(1-2)-glucans essentially identical to those synthesized by members of the *Rhizobiaceae*.

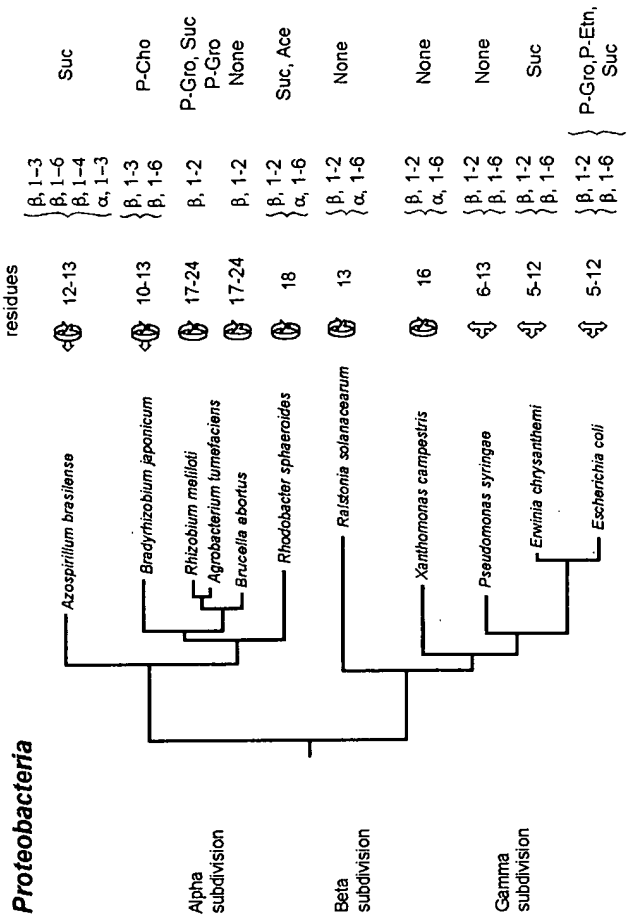

Figure 1. OPG structures in relation to the phylogenetic tree of representative species from three subdivisions of the purple bacteria (Proteobacteria); see the text for details. (Ace= acetate, Suc= succinate, P-Cho= phosphocholine, P-Gro= phosphoglycerol, P-Etn= phosphoethanolamine).

Family 3. Extracts of *Bradyrhizobium* spp. revealed the presence of β–(1-6)- and β–(1-3) cyclic glucans containing 10 to 13 glucose units per ring [13, 14] Three distinct glucans (I, II, and III) are synthesized by cells of *Azospirillum brasilense* [15]. The three glucans consist of a cyclic structure. Glucan I is made of 12 glucose units linked by 3 β–(1-3), 8 β–(1-6) and one β–(1-4) linkages. Glucan II is derived from the glucan I by the addition of a glucose linked by an α–(1-3) linkage, and glucan III is derived from glucan II by the addition of a 2-O-methyl group onto the α linked glucose unit.

Family 4. *Ralstonia solanacearum* [16], *Xanthomonas campestris* [16, 17, 18] and *Rhodobacter sphaeroides* [19] synthesize OPGs of very similar structural features. OPGs have a unique degree of polymerization [13, 16, and 18, respectively]. All the glucose residues are linked by β–(1-2) linkage with the exception of one α–(1-6) linkage.

OPG substitutions. In *E. coli*, the OPGs are highly substituted with *sn*-1-phosphoglycerol, phosphoethanolamine, and succinyl ester residues [5]. In *E. chrysanthemi*, succinyl residues are the sole substituent [6] while OPGs of *P. syringae* are not substituted [7].

In *A. tumefaciens*, one or more phosphoglycerol moieties are substituted for approximately 50% of the total periplasmic glucans [20]. In *R. meliloti*, anionic moieties may be substituted for as much as 90% of the periplasmic cyclic β–(1-2) glucans and the predominant anionic substituent present is phosphoglycerol [21].

Periplasmic glucans of *Bradyrhizobium* spp. are predominantly neutral [13] but Rolin and co-workers [14] have purified a phosphocholine substituted β–(1-6)- and β–(1-3) glucan from *B. japonicum* USDA 110. The OPGs of *A. brasilense* can be substituted by one succinyl residue [15].

The OPGs of *R. solanacearum* and *X. campestris* are neutral [16] while the OPGs of R. sphaeroides are highly substituted succinyl and acetyl residues [19].

3. Primary sequences of OPGs by NMR

3.1 INTRA-RESIDUE ASSIGNMENTS (COSY, RELAYED COSY, TOCSY, HSQC)

Intra-residue proton assignments are obtained through the conventional use of COSY, relayed COSY and TOCSY experiments. Heteronuclear assignments are obtained from the correlation of proton and carbon resonances in a HMQC or

HSQC experiment, and can be completed by a HSQC-TOCSY experiment. The following Figure 2 shows the fully assigned ^{1}H-^{13}C spectrum of the DP13 of *R. solanacearum*.

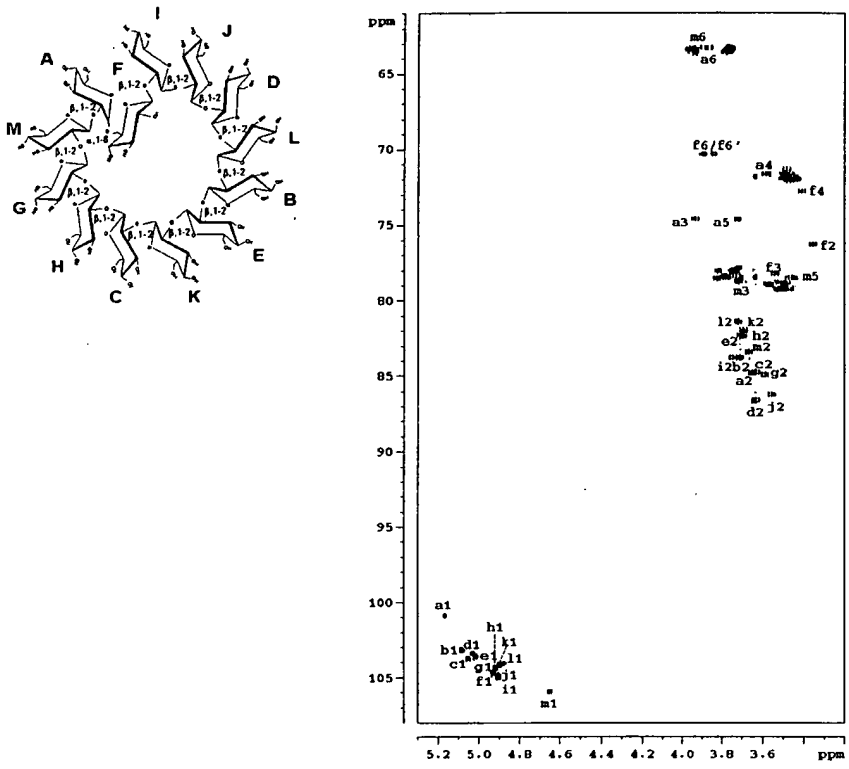

Figure 2. Heteronuclear Single Quantum Experiment correlating the 1H and 13C resonances of the non-enriched DP13 molecule of *R. solanacearum* at 301K. The numbering of the units goes from a for the unit in α–(1-6) to m, as depicted on the macrocycle on the left.

3.2 **INTER-RESIDUE ASSIGNMENTS**

The NOE between the two protons flanking the linkage forms a self-evident and easily accessible probe to establish the linkage between the different units. Unfortunately, the limited chemical shift dispersion for all but the anomeric

protons makes this method less obvious in the case of the cyclic OPGs. However, homonuclear techniques can still be used to establish the connectivities between the units, through the linking of the anomeric resonances in a NOESY-TOCSY and/or TOCSY-NOESY experiment.

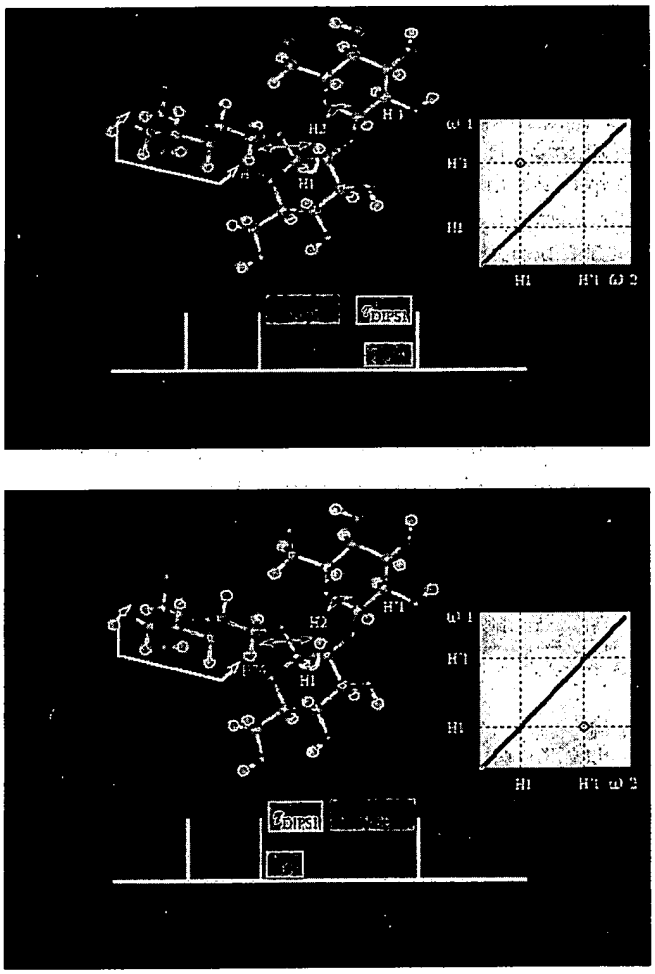

Figure 3. Homonuclear NOESY-TOCSY (Top) and TOCSY-NOESY (Bottom) pulse sequences and the resulting anomeric proton spectral zones, showing the asymmetry of the cross peaks. The magnetization transfer is shown on a trisaccharide where two units are linked in β-(1-2), and two in α-(1-6). Only the cross-peak corresponding to the β-(1-2) linkage is shown

The sequences are shown in the Figure 3. They can easily be understood as a merging of the regular NOESY mixing period, during which the dipolar cross-relaxation will establish a transfer of magnetization between the protons flanking the glycosidic linkage, combined with a z-TOCSY period, where the magnetization is again transferred to the anomeric proton.

Schematically, the magnetization transfer for a typical disaccharide linked in β–(1-2) can be seen in the same Figure 3: during the t_1 period, magnetization at the anomeric frequency of unit i evolves and gives rise to a peak at $\omega_{ano}(i)$. In a NOESY-TOCSY experiment, it is first transferred during the NOESY period to the H2 proton of unit i+1, and then by scalar coupling to the anomeric proton of this same unit i+1. We therefore will observe a cross peak between the anomeric protons of units i (in ω_1) and (i+1) (in ω_2). Its symmetric counterpart is missing in this experiment, because of the order of the NOESY and TOCSY transfer. In the equivalent TOCSY-NOESY experiment, however, the other peak will appear, because magnetization labeled in ω_1 by the frequency of the anomeric proton of residue i will first be transferred to the H2 proton of the same residue, and then transfer through cross-relaxation to the anomeric proton of the preceding unit. We therefore will observe a cross peak between the anomeric protons of units i (in ω_1) and (i-1) (in ω_2). Both experiments allow a sequential walk through the sequence of the cyclic OPGs, as is demonstrated in Figure 4.

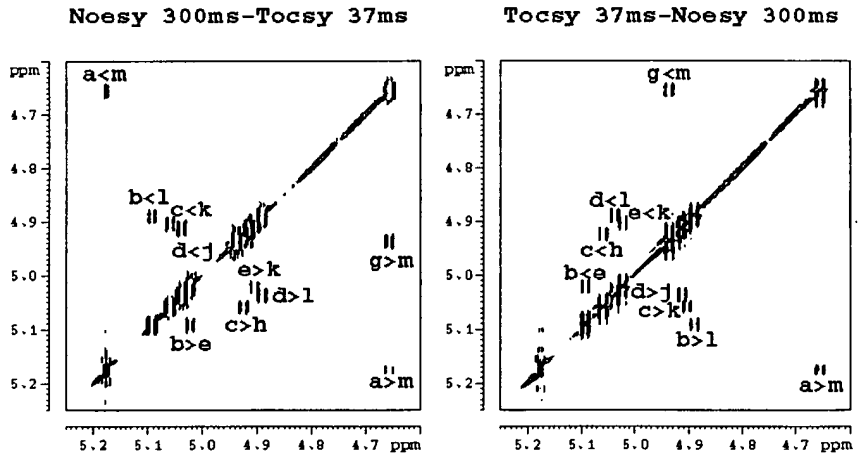

Figure 4. Homonuclear NOESY-TOCSY (Left) and TOCSY-NOESY (Right) experiments on the DP13 molecule of *R. solanacearum* at 301K.

In the case of a β–(1-2) linkage as in the above cited example, short mixing periods for both NOE and scalar coupling transfer will be sufficient, because of the short distance between the protons flanking the linkage and the large ^3J coupling constant between H1 and H2 protons. Special care should be exerted when one expects a (1-6) linkage, where especially the z-TOCSY delay should be considerably increased. An example is shown in Figure 5 , where the sequential peak between the c and (k or l) units linked by an β–(1-6) linkage is not present when using a 80 ms TOCSY period, but becomes visible upon applying a 160 ms TOCSY mixing period.

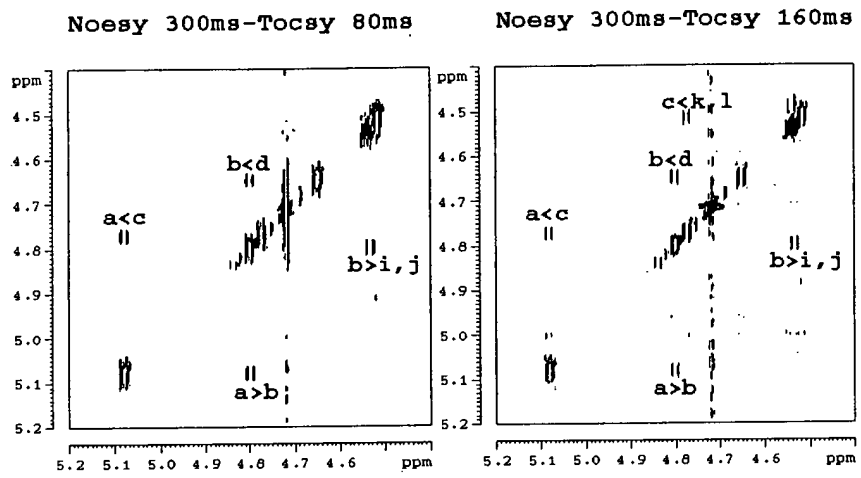

Figure 5. NOESY-TOCSY experiments on the cyclic OPG of *Azospirillum brasilense* using a shorter (Left) and longer (Right) TOCSY mixing time. The contact between the anomeric proton of k or l (same resonance position) linked in β–(1-6) to the c unit is only visible when using the longer TOCSY transfer time.

The heteronuclear sequences rely on the homonuclear NOE or the long-range heteronuclear coupling constant over the glycosidic linkage to establish sequential contacts. The NOE between flanking protons H1 and H2', where the latter is encoded by its corresponding carbon frequency to improve chemical shift dispersion, is at the basis of the HSQC-NOESY experiment. The ^3J (H1-C2') and ^3J(C1-H2') coupling constants are used in the HMBC experiment. The delay during which the long-range coupling creates antiphase was optimized for a ^3J coupling constant of 5 Hz in our HMBC experiment on the DP13 molecule.

4. Beyond the primary sequence – towards a tertiary structure

4.1 INTRODUCTION

The structure of cyclic osmoregulated periplasmic glucans (OPG) synthesized by different Gram-negative bacteria might shed light on the role that these molecules play in the adaptation to osmotic stress and in the phytopathogenicity of these bacteria [11]. The cyclic nature of these molecules could be essential for these two aspects, but a precise structural model is needed to assess this point. The glucans produced by members of the *Rhizobiaceae* family are cyclic molecules composed of 17 to 40 glucose units, all linked in β–(1-2) ; their structure determination presents an enormous challenge, as the NMR spectrum of a purified subspecies is completely degenerate and equivalent to that of a single D-glucopyranosyl unit [22, 23, 24, 25]. Whereas this might be the indication of a completely symmetric molecule, with magnetic equivalence for every glucose unit, recent work has shown that no rigid cyclic structure can be formed with identical (Φ,Ψ) angles for all linkages [26]. The proposed origin for the equivalence of all NMR signals is the high flexibility of the molecule, where each glucose unit rapidly samples a number of conformations. The NMR parameters are therefore averaged twice, over all equivalent units and over time.
Beyond this problem of time-averaging, the scarceness of experimental constraints in oligosaccharides makes an accurate structure determination extremely challenging. In proteins, sequential assignment can be obtained from NOE contacts between neighbouring residues or on the basis of J-coupling in the so-called triple-resonance experiments, but the 3D structure is calculated on the basis of a large number of long-range NOE constraints. For the cyclic glucan under study, the experimental parameters used for the sequential assignment are the only ones available for the complete structure determination.

4.2 ONE A-(1-6) LINKAGE CHANGES IT ALL.

Recently, the structures of three fundamentally different cyclic glucans extracted from cells of *R. solanacearum* [16, 27], *X. campestris* [18, 16, 27] and *R. sphaeroides* (19) were described. Although they share the cyclic nature with the OPG of members of the *Rhizobiaceae* family, they can be distinguished by the unique degree of polymerization (DP ; 13, 16 or 18 units) and one α–(1-6) linkage, whereas all other glucose residues are linked by β–(1-2) linkages. The

presence of this α–(1-6) linkage induces structural constraints in this molecule to such extent that all individual anomeric proton resonances can be distinguished (Figure 6).

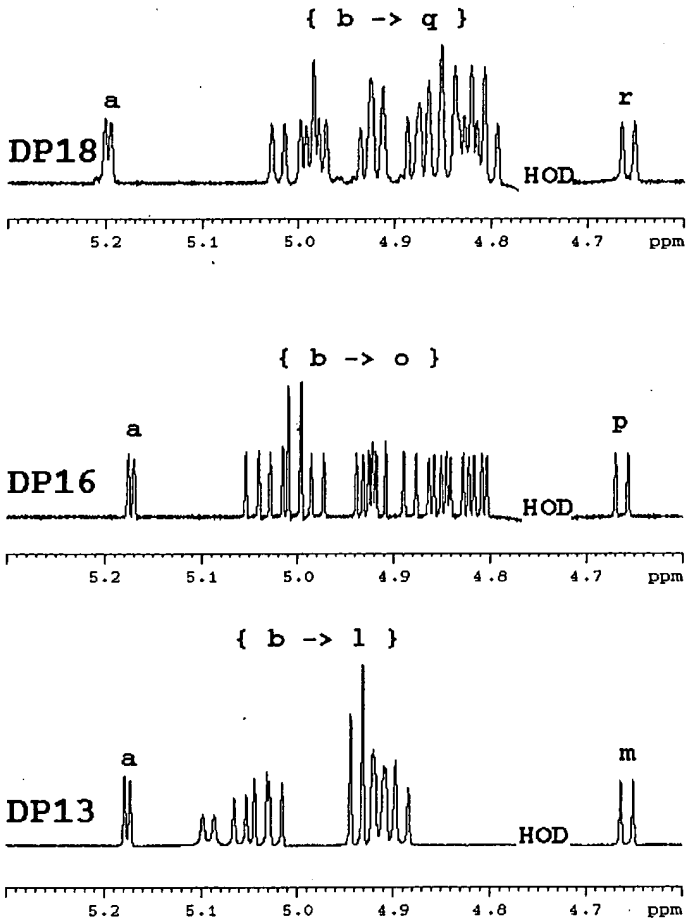

Figure 6. Anomeric proton regions of the DP18 (top), DP16 (middle) and DP13 (bottom) molecules. The two groups of chemical shifts discussed in the text for the DP13 molecule are present as well in the two other molecules, confirming their belonging to the same structural family.

Its minimal size and the complete resonance assignment of the cyclic OPG from *R. solanacearum* make this molecule an ideal candidate for a detailed structural study, and we will focus on the results we have recently obtained on this molecule.

4.3 CHEMICAL SHIFT PATTERN ON THE DP13 AND DP16

While the chemical shift remains one of the most easily measured parameter, it simultaneously is one of the most difficult to calculate from a structure. Still, it is a parameter which is extremely sensitive to the precise three-dimensional environment of the nucleus. The observation by both our group and Dr. W. York (CCRC, Athens, USA) that the chemical shifts of the H_1 and C_2 atoms flanking the glycosidic β–(1-2) linkage show an alternating pattern (Figure 7), suggests therefore a non-uniform location of the interglycosidic linkages in the (Φ, Ψ) map. This is in general agreement with the observed alternating pattern for the ^1J coupling constants, that have been related in different theoretical studies [28] to the conformation of the linkage.

Residue	H_1	C_1	H_2	C_2	$^1J_{H_1C_1}$
a	5.18	99.48	3.66	83.43	175.0
f	4.94	103.3	3.36	74.86	165.0
i	4.91	103.4	3.56	84.80	167.0
j	4.94	103.5	3.75	82.39	164.6
d	5.04	102.0	3.64	85.17	167.0
l	4.89	102.6	3.72	79.96	165.6
b	5.09	101.8	3.72	82.36	167.0
e	5.02	102.2	3.72	80.91	167.6
k	4.90	102.7	3.70	80.50	164.6
c	5.06	102.3	3.63	83.36	167.0
h	4.93	102.9	3.70	80.90	165.6
g	4.94	103.3	3.60	83.50	165.0
m	4.66	104.5	3.67	81.97	162.7

Figure 7. Alternating chemical shift values and $^1J(^1H\text{-}^{13}C)$ coupling constant values for the different glucose units of the DP13 molecule.

4.4 LABELING THE MOLECULE

Chemical shift dispersion in the carbon dimension being far superior to the one in the proton dimension, especially for the C2 carbons, both distance and coupling constant measurements could greatly benefit of a heteronuclear detection scheme. For this purpose, we decided to produce a ^{13}C enriched sample. *R. solanacearum* T11 was grown at 24°C with agitation in a low osmolarity medium which contained K_2HPO_4 (1 mM), $(NH_4)_2SO_4$ (1.5 mM), $MgCl_2$ (0.08 mM), $FeSO_4$ (0.5 mg l^{-1}), thiamin (2 mg l^{-1}), and casein hydrolysate (4 g l^{-1} ; casamino acids, vitamin free, Difco Laboratories). This medium was adjusted to pH 7.0 with Tris-free base. ^{13}C enrichment was obtained by replacing one fourth of the casein hydrolysate by an equal amount of a mixture of uniformly enriched amino acids and glucose ("sugar mix ", EMBL, Heidelberg, Germany). The cyclic glucan was purified from cell extract (16). Mass spectrometry spectra on both the native and ^{13}C enriched DP13 samples indicated an average mass increase of 37.5 Da due to the ^{13}C labeling. Taking into account that the DP13 molecule contains 78 carbon atoms, this gives a mean enrichment of 48%. A similar result close to 50% was found on the basis of integrations made on the non-decoupled ^{1}H spectrum.

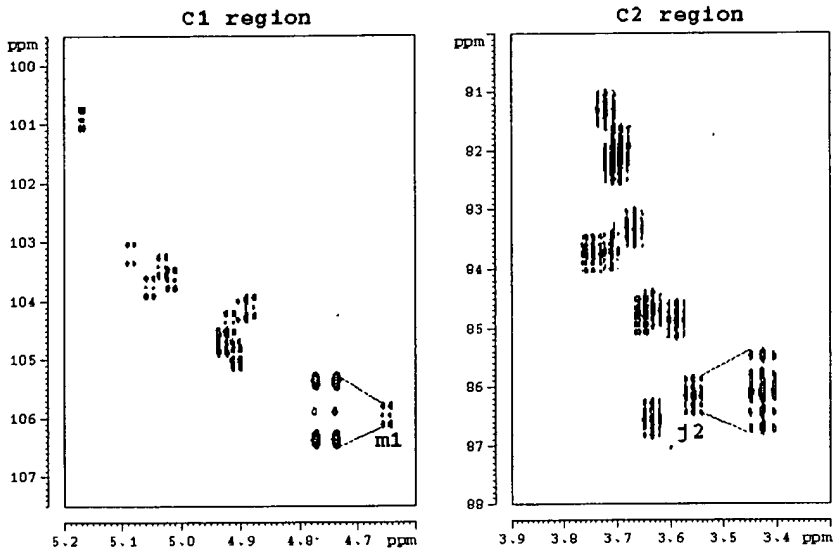

Figure 8. Heteronuclear Single Quantum Experiment correlating the ^{1}H and ^{13}C resonances of the ^{13}C enriched DP13 molecule of *R. solanacearum* at 301K. The doublet and quintuplet ^{13}C line shapes of units m and j, respectively, are magnified.

The regular HSQC spectrum, where the ^{13}C-^{13}C coupling constants are not refocused in a constant-time period [29] indicates that the labeling is not random. Indeed, we observed a doublet for the C_1 resonances (Figure 8, left panel), but a quintuplet for the C_2 correlation peaks (Figure 8, right panel). ^{13}C enrichment of the C_1 position implying ^{13}C enrichment of the C_2 position leads to the doublet structure for C_1, and the quintuplet structure for the C_2 resonances can be explained by the simultaneous presence of $^{13}C_1$ - $^{13}C_2$ - $^{12}C_3$ triplets, leading to a doublet for C_2, and $^{13}C_1$ - $^{13}C_2$ - $^{13}C_3$ triplets on other molecules leading to a triplet structure. Considering the usual bacterial glucose synthesis pathway [30], this implies that the ^{13}C enriched amino acids have been broken down to the level of a two-carbon containing molecule (probably acetyl CoA or acetate), and ^{13}C has been incorporated in a pair-wise fashion.

4.5 A GEOMETRIC INTERPRETATION OF THIS ALTERNATING CHARACTER

A limited number of studies [31, 32] have attempted to examine the conformational behavior of glycosidic linkages on the basis of precise NOE curves. However, whereas the small number of distance restraints between the two pyranosyl units requires a precise determination of the latter, the flexibility of the glycosidic linkage may lead to wrong distances due to a difference in dynamics with the proton pair considered as the internal distance reference. To take into account the possible variations of internal flexibility, at least two independent measures should be obtained for each pair of protons. The off-resonance ROESY technique [33] allows the measurement of the dipolar cross-relaxation rates along an effective field axis in the rotating frame tilted by an angle θ with respect to the static magnetic field. By varying this angle from zero to higher values, the longitudinal (σ) and transverse (μ) dipolar cross-relaxation rates can be determined with a high accuracy since they result from an over-determined fitting procedure. Finally these two values can be exploited simultaneously to obtain distances without the requirement of any internal reference [34].

Build-up rates for the normalized cross-peaks in HSQC-NOESY spectra were determined on the basis of four mixing times between 100 and 400 ms with a good linear behavior up to at least 300 ms. The off-resonance ROESY spectra were recorded as a series of 2D spectra with a constant spin-lock field strength γB_1=7 kHz but with varying offset Δ of the spin-lock field. Eleven values of θ= arc tangent($\gamma B_1/\Delta$) were sampled between 5° and 55°, with two

mixing times of 150 ms and 300 ms for every angle. Build-up curves were determined independently for every angle, using the cross-peak volumes normalized to the diagonal peak ones in order to extend the validity of the initial slope approximation. A least square fit of the resulting slopes as a function of the angle θ to the theoretical expression $\sigma'=\sigma\cos^2(\theta) + \mu\sin^2(\theta)$ yields both relaxation rates.

We observe excellent agreement between the σ rates determined by the classical NOE build up rates and those obtained by the off-resonance ROESY fit (Table I). The independent determination of σ and μ allows extraction of pairwise structural (r) and dynamic (τ_{cp}) parameters (Table I, columns 5 and 6).

	HSQC-NOE	HSQC-(off-resonance ROESY)			
	$\sigma(s^{-1})$	$\sigma(s^{-1})$	μ (s^{-1})	r(Å)	τ_{cp} (ns)
f1-i2	ND	ND	ND	ND	ND
i1-j2	ND	ND	ND	ND	ND
j1-d2	-0.35	-0.37	1.0	2.19	0.9
d1-l2	-0.20	-0.20	0.52	2.47	0.9
l1-b2	-0.40	-0.40	1.43	2.06	0.7
b1-e2	-0.38	-0.38	0.93	2.25	1.0
e1-k2	-0.19	-0.18	0.49	2.46	0.8
k1-c2	-0.33	-0.32	1.10	2.14	0.7
c1-h2	-0.21	-0.20	0.58	2.43	0.8
h1-g2	-0.42	-0.37	1.15	2.09	0.7
g1-m2	-0.39	-0.46	1.22	2.14	0.9
m1-a2	-0.48	-0.59	1.70	2.00	0.8

Table I : Longitudinal cross-relaxation rates as determined from the HSQC-NOE build-up curves (column 2) and the HSQC-(off resonance ROESY) fitting procedure (column 3), transverse cross-relaxation rates by the same procedure (column 4), and resulting pairwise distances r and dipolar correlation times τ_{cp} (columns 5 and 6). ND = not determined due to overlap.

Two classes of interglycosidic distances can be distinguished, those linking a H1 proton from group 1 [b-e] to the H2 proton from group 2 [f-l], with values

around 2.45 Å, and those where a unit from group 2 substitutes a unit from group 1, with significantly shorter distances (around 2.15 Å). An averaged distance between these both extremes is found for the pair b1-e2. However, the anomeric proton of residue b is appreciably broadened (around 0.5 Hz at 301 K) compared to the other anomeric resonances. At lower temperatures (288K), the splitting due to the homonuclear coupling constant disappeared completely due to the line broadening, proving that the glycosidic linkage exhibits some low frequency jumps between two (or more) positions. The longer correlation time observed for this NOE contact indicates that, in the nanosecond range, this glycosidic bond is more rigidly fixed than are the other glucose units. The b–e glycosidic bond is diametrically opposed to the α–(1-6) linkage between units a and f, and it links two units within group 1 ; these two observations might be the basis of its particular behavior.

Relaxed energy maps for β–sophorose [35] show the main low-energy region at $20° < \Phi < 80°$ and $-60° < \Psi < 60°$. A comparison of the calculated energy map with a map showing the H1-H2' inter-proton distance of β–sophorose as a function of the interglycosidic angles together with the observed strong NOEs indicates that all β–(1-2) bonds of the cyclic OPG of *B. solanacearum* are situated in this main low-energy zone. However, the calculated precision of the interglycosidic distances (Table I) allows us to discern a pattern of alternating shorter and longer H1'-H2 distances along the primary sequence, following closely the alternating pattern of chemical shift values. The deviating distance found for the b1-e2 contact is accompanied by a similar perturbation for the H1 and C2 chemical shift values of this particular linkage.

4.6 MEASUREMENTS OF LONG-DISTANCE ^{3}J COUPLING CONSTANTS.

The delay in the HMBC during which the long-range H-C correlations were established for the sequential assignment was optimized for a hypothetical coupling constant of 5 Hz. The resulting spectrum showed uniformly intense cross-peaks in the region connecting C1 and H2' resonances, whereas the C2'-H1 region showed important differences in intensity for the various cross peaks [36]. This observation suggests uniform $^3J(C_1\text{-}H_2')$ coupling constants with values close to 5 Hz, but a less uniform distribution for the $^3J(H_1\text{-}C_2')$ coupling constants. However, differential relaxation rates as well as any other long range carbon coupling might in part contribute to the latter intensity difference, and the absolute value character of the cross peaks makes a quantitative evaluation of the coupling constants far from straightforward. Numerous other techniques for measuring the ^{3}J coupling constants have been described in the literature [37,

38]. Poppe *et al.* (23) described a ^{13}C filtered (^{1}H, ^{1}H) ROESY experiment based on the general ^{1}J-resolved E.cosy approach (39). This experiment resulted in accurate ^{3}J values on the homogeneous cyclic β–(1-2)-glucan icosamer isolated from *Rhizobium trifolii*. The experiment was performed on a 5mM natural abundance sample, but the high flexibility of this molecule leads to a completely degenerate ^{1}H and ^{13}C spectrum , equivalent to that of one single unit [22, 23, 24, 25]. This reduces the information content of the measured coupling constants, as they represent time-averaged values, but enhances simultaneously the feasibility of the experiment, as the 5 mM sample results in an effective glucose concentration of 100 mM. Despite this high concentration, the resulting experiment took 54 hours. A similar experiment on a natural-abundance DP13 sample, where no degeneracy exists, would not be feasible, making ^{13}C labeling essential.

The original experiment as proposed by Poppe et al. [23] exploits the presence of $^{13}C_1$-$^{12}C'_2$ and $^{12}C_1$-$^{13}C'_2$ carbon pairs at natural abundance. The 50% incorporation of ^{13}C in the present DP13 molecule optimized the number of such carbon pairs, but forced us to introduce an additional step of ^{12}C filtering. The complete sequence is depicted in Figure 9, and can easily be broken down into three modules : first, a ^{13}C filter is applied in order to select for the t_1 evolution only those protons that are ^{13}C bound. We used a gradient-enhanced scheme (Figure 9A) that is quite similar to the solvent suppression scheme used in the ^{1}H-^{15}N HSQC experiment [40]. When the first gradient is applied, ^{13}C bound proton magnetization is in the IzSz state, whereas all other magnetization components are in the *xy* plane and will be effectively scrambled by G_1. After refocusing of the proton magnetization, it is stored temporarily along the z-axis, and the second gradient removes effectively all residual terms.

In contrast to the ^{13}C half-filter of Poppe et al. [23], our sequence selects no anti-phase proton magnetization with respect to the $^{1}J_{CH}$ coupling but pure in-phase proton magnetization (term Ix). This magnetization will evolve during t_1 under the influence of both the chemical shift and the $^{1}J_{CH}$ scalar coupling term, and terms of the form $Iz \cos(\omega_1 t_1) \cos(\pi J\ t_1)$ will enter the NOESY mixing time (Figure 9B). The length of the mixing time should be a compromise between two requirements : it should be long enough to allow an efficient transfer of proton magnetization between the H_1 and H_2' positions, but it should not be too long such that ^{13}C T_1 relaxation will destroy the E.cosy type pattern that was constructed during t_1. Intuitively, the second requirement can be understood as follows: during t_1, two populations of proton spins can be distinguished, depending on the state of the attached ^{13}C spin.

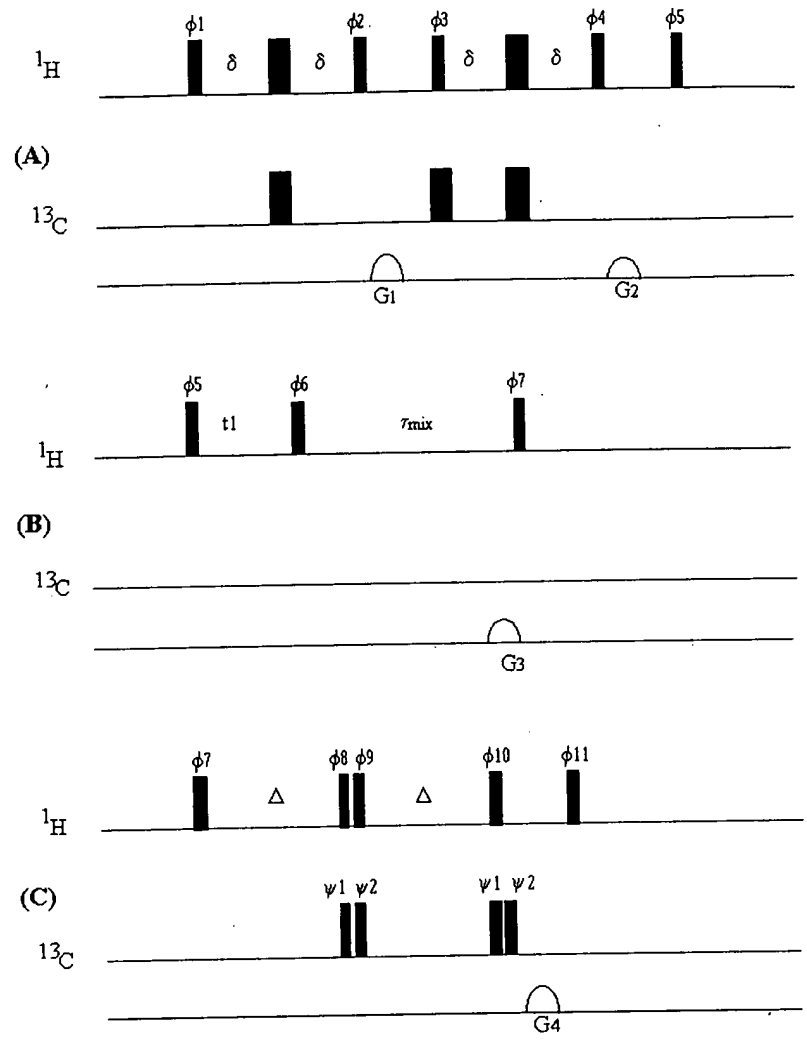

Figure 9. Pulse sequence for the double half-filtered NOESY spectrum. The sequence has been divided in three parts, the ^{13}C filter (A), the t_1 evolution and subsequent NOE mixing time (B), and the final ^{12}C filter (C). Phases used are: Φ_1=y, Φ_2=(x, -x), Φ_3=(8*x,8*(-x)), Φ_4=(x, x, -x, -x, y, y, -y, -y), Φ_5=(4*x, 4*y), Φ_6=(-x, -x, x, x, -y, -y, y, y), Ψ_1=x, Ψ_2=x or -x (according to the choice of the subspectra), acquisition phase = (x, -x, -x, x, y, -y, -y, y, -x, x, x, -x, -y, y, y, -y).

During the NOE mixing time, we want this relationship to be conserved, but it will tend to disappear due to T_1 relaxation. If the mixing time is so long that the correlation between initial and final ^{13}C spin state has completely disappeared, no displacement in ω_2 representative for the ^3J value will be observed [41]. In the case of the cyclic glucan, both requirements can easily be fulfilled by a short mixing time of 100 ms, as the H_1-H_2' distances are all very short [42].

After the mixing time, we apply a ^{12}C filter that is similar to the one used for distinguishing NOEs in macromolecular complexes in which one of the components has been enriched with a stable isotope [43, 44, 45] or intra- from inter-subunit NOE cross peaks in symmetrical homodimers [46, 47]. The same two ^{13}C 90° pulses that are used for ^{12}C selection (once with the phases Ψ_1 and phases Ψ_2 equal and once opposite) have to be applied at the end of the filter, in order to maintain the ^{13}C spin state (Figure 9C). Failure of applying those pulses leads to E.cosy type cross peaks that for the two spectra are oppositely shifted in ω_2 with respect to the ^3J coupling value, making the addition of the two subspectra in order to produce a ^{12}C filtered spectrum impossible.

In the resulting 2D spectrum, suppression of the diagonal peaks at the level of the anomeric proton resonances was optimized by introducing a correction factor of 1.08 when adding both subspectra.

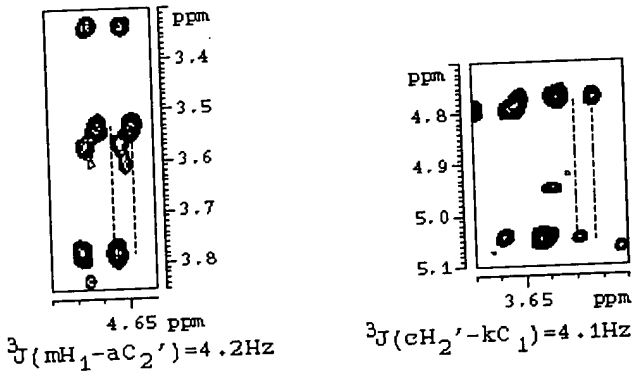

Figure 10. Final 2D spectrum obtained by adding the two subspectra obtained with the sequence of Figure 10. The zooms show the aH'2-mH1 cross peak and the extraction of the corresponding ^3J (mH1 - aC'2) coupling constant (Left), and similar for the kH1-cH2' cross peak and corresponding ^3J (kC1 - cH2') coupling constant (Right).

The left panel of Figure 10 shows an enlargement of the aH_2'-mH_1 cross peak: in ω_1, the central frequency of the doublet is that of the aH_2' proton, and we observe the doublet with respect to the $^1J_{HC}$ coupling constant of 145.8 Hz. In ω_2, both lines correspond to a ^{12}C bound mH_1 proton, but the upper line of the ω_1 doublet is displaced with respect to the lower one by 4.2 Hz, which is the value for the corresponding ^3J (mH_1 - aC_2') coupling constant. In the other quadrant of the spectrum, we will observe H_2 magnetization, and the right panel shows a zoom of the kH_1-cH_2' cross peak. The upper triplet (corresponding to cH_2' magnetization coupled through a long-range ^3J constant to a k $^{13}C_1$ nucleus in a well-defined state) is displaced by 4.1 Hz with respect to the lower one, corresponding to the c H_2' proton bound to a k $^{13}C_1$ is in the other state. In both cases the fine structure of the observed cross peak (a doublet for the anomeric protons, and a triplet for the H_2 protons) increases the level of confidence for the measurement of the coupling constant : indeed, we can measure the displacement of every component of the multiplet at $\omega_1+{}^1J/2$ with respect to the corresponding component in the multiplet at $\omega_1-{}^1J/2$. From this multiple measurement, we estimated error bars of ± 0.2 Hz on the reported ^3J values reported in Table II.

	$^3J(H_1\text{-}C'_2)$	Φ	$^3J(C_1\text{-}H'_2)$	Ψ
f1-i2	ND	ND	ND	ND
i1-j2	ND	ND	ND	ND
j1-d2	4.1	32	4.0	327
d1-l2	2.2	54	4.2	329
l1-b2	3.0	44	4.7	336
b1-e2	3.4	39	3.8	324
e1-k2	2.9	45	3.9	326
k1-c2	4.1	32	4.1	328
c1-h2	2.9	45	4.1	328
h1-g2	4.0	33	4.2	329
g1-m2	3.0	44	4.3	330
m1-a2	4.2	30	4.0	327

Table II : Long-range ^1H-^{13}C coupling constants obtained for the cyclic glucan *of Ralstonia solanacearum*. The angles were derived according to the Karplus relationship [48] and assuming that the linkages are in the main low-energy zone. The first two values were not determined due to overlap of the corresponding cross peaks.

The presence of intra-residue H5-H1 cross peaks despite the combined ^{13}C and ^{12}C filters stems from glucose residues that contain a $^{13}C_1$ but a $^{12}C_5$ nucleus , and is compatible with the pairwise incorporation of ^{13}C nuclei (*vide supra*). From these cross peaks, coupling constants for H_1-C_5 smaller than 0.5 Hz were measured, in agreement with the very weak cross peaks observed in the HMBC.

Using both quadrants, 10 values of both ^3J values could be extracted (Table II). The missing values could not be determined because of heavy overlap of the corresponding cross peaks. Finally, it should be noted that the single α–(1-6) linkage can equally be characterized by the same procedure, as we could measure the coupling constants between H_6-C_1 and H_6'-C_1 (the notation H_6-H_6' being at this moment arbitrary). The values found are $^3J(aC_1\text{-}fH_6) = 2.4$Hz, and $^3J(aC_1\text{--}f H_6') = 3.0$ Hz.

4.7 A UNIQUE STRUCTURE OF THE MOLECULE?

The techniques of Distance Geometry and/or Simulated Annealing are commonly used to generate families of protein structures compatible with the majority of the experimental data. However, it has been amply demonstrated that the reliability of both techniques depends to a large extent on the number of experimental constraints that can be imposed rather than on the accuracy of these constraints. In the case of our cyclic oligosaccharide molecule, however, this number of constraints is limited to the distance measurements between protons flanking the glycosidic linkages, and the long-range coupling constants. An additional problem with the latter is that the empirical Karplus relationship, well parametrized for protein structures due to the large number of crystal structures and coupling constants, is not as reliable for oligosaccharides. Indeed, the majority of experimental points that were used for the actual parametrization of the Karplus relationship concern a series of conformationally rigid carbohydrate derivatives with dihedral angles between 90° and 270° [48]. As the authors had not yet prepared rigid compounds containing fixed C-O-C-H segments with dihedral angles outside this region, they included three experimental values for compounds where the dihedral angles were not directly determined by X-ray crystallography. Therefore, we believe that for our compound characterized mainly by dihedral angles outside of the (90°, 270°) region, the current parametrization ($^3J_{C\text{-}H} = 5.7\ \cos^2(\Phi) - 0.6\ \cos(\Phi) + 0.5$) and thus the angles derived from the coupling constant values have to be used with caution.

For the reasons mentioned above, we developed a genetic algorithm approach to generate different structures [49] The solvent contribution, which plays an important role in oligosaccharide stability, is taken implicitly into account by the

boundary element method [50, 51], which averages over all possible water configurations. The distance results stemming from the off-resonance ROESY experiment were included as a harmonic energy term.

The algorithm yielded several interesting structures, characterized by an overall low energy. These structures consistently contain fragments that adopt the ribbon-like right-handed helix as was described for the DP16 molecule [18]. However, we found no single structure that was of low energy and compatible with all experimental data simultaneously. For this reason, we decided to first look at the dynamics of the molecule in solution. The result of this study is described in the paragraph below.

5. Complex dynamics of the DP13 molecule

5.1 IMPORTANCE OF DYNAMICS

The dynamics of biomolecules has been an intensive field of research over the last years [for a review, see 52]. In the field of protein dynamics, numerous studies have probed the rapid motions on the pico- to nanosecond time scales, with relatively small amplitudes. These motions are generally considered as librations or hindered motions in an energetic well, and contribute by influencing barriers for slower motions and by modulating entropic changes that might be associated with functional processes. Recent studies in the field of oligosaccharide NMR have also focused on this rapid dynamics. Slower domain motions, however, have proved to be more difficult to study, despite their enormous biological relevance, as they are close to the time scales on which docking, catalysis and ligand release take place. Examples are long-range loop-flip motions in proteins, or the "flipped-out" substrate base in the crystal structure of DNA cytosine-5-methyltransferase. However, to our knowledge, no such slow-time scale motions have been reported for isolated oligosaccharides. As we will show further, the DP13 molecule of *R. solanacearum* does exhibit fluctuations of probably large amplitude on the μs time-scale, adding to its intriguing function *in vivo* the question of the functional relevance of this complex dynamics.

5.2 RESULTS OF HOMONUCLEAR EXPERIMENTS

A side result of the off-resonance ROESY experiments as described above is the set of τ_c values describing the individual correlation functions describing the pair-

wise dipolar interaction between H1 and H2' protons. These values were found to be fairly homogeneous, with an average value of 0.9 ns. At first, we attributed them to the overall tumbling of the hypothetical rigid molecule, but fast internal dynamics could also contribute to the modulations of the dipolar terms. However, a separation of overall and fast internal dynamics, as is often done following heteronuclear relaxation studies, is not of much use here, as every individual dipolar interaction is described by its own τ_c.

Indication of slow dynamics came from the observation that the b anomeric proton resonance is appreciably broadened compared to all other anomeric resonances. We therefore decided to start a detailed heteronuclear relaxation study to better understand the complex dynamics of the DP13 molecule.

5.3 HETERONUCLEAR RELAXATION EXPERIMENTS INDICATE A SLOW CONFORMATIONAL EXCHANGE

A nowadays well-established approach to the investigation of dynamical properties in carbohydrates (and other biomolecules) is by means of heteronuclear relaxation measurements. A "model-free" analysis of the relaxation rates has been proposed, decoupling the overall tumbling motion and the local motion where the extent and dynamics of the latter are characterized by an order parameter S^2 and a local correlation time [53]. Moreover, in several studies, especially in proteins, it has been necessary to extend the parameter set to obtain consistency between the different relaxation data. An example is the *ad hoc* inclusion of an exchange term into the expression of the T_2 relaxation rate [54], or, recently, the anisotropy of the rotational diffusion as a supplementary parameter [55].

A complete heteronuclear relaxation study on the cyclic glucan of *R. solanacearum* has allowed an experimental verification of the agreement between the correlation times stemming from the off-resonance ROESY experiment (that describe the motion of the proton-proton vector) and the ones from the heteronuclear relaxation experiments, describing the motion of the ^1H-^{13}C vector. Secondly, the heteronuclear relaxation data yield very important information about the slow dynamics of the molecule, with exchange rates of the order of several microseconds.

The T_1 values of all carbon C1 resonances, when fitting the magnetization curves measured on a ^{13}C labeled sample to a mono-exponential are fairly homogeneous, with values centered around 276 ms (Table III). Error bars on the individual T_1 times were estimated to ±3 ms. When measuring the T_1 relaxation rates on a non-

enriched sample, we systematically found longer values. We checked for a possible influence of the sample concentration by comparing one-dimensional T_1 data on a native and ^{13}C enriched sample at the same concentration, but the difference consistently showed up. The average decrease of 14 ms for the C1 relaxation times upon ^{13}C enrichment was therefore attributed to the contribution of the carbon-carbon dipolar interaction to the relaxation pathway, and is in good agreement with the 4.6% variation in the Cα T_1 time when going from a singly towards a uniformly ^{13}C-labeled alanine residue dissolved in perdeuterated glycerol at 40°C where its correlation time τ_c is equal to 1ns [56]. The magnitude of the contribution of the $^{13}C2$-$^{13}C1$ homonuclear dipolar interaction being a monotonic function of correlation time, the observed difference is an independent estimate of a correlation time of the order of 1ns.

Residue	T_1 (C1) (ms)	T_1(C2) (ms)	NOE (C1) %	NOE (C2) %
a	269	257	35	33
f	283@	296	36@	42
i	274&	257	35&	34
j	274&	261	35&	33
d	281	262	34	26
l	280§	278	34§	29
b	268	284	34	36
e	274	281#	34	32°
k	280§	268	34§	31
c	274	280	32	32
h	269	281#	35	32°
g	283@	279	36@	34
m	281	273	35	38

Carbon	T_1 (C1) (ms)	NOE (%)
aC3	274	34
aC5	272	35
fC3	308	36
fC4	289	35
mC3	279	33
mC5	294	38

Table III. (a) T_1 and NOE values for the C1 and C2 carbons of the cyclic OPG of *B. solanacearum*, as measured on a ^{13}C enriched sample at 301K. Residues are labeled as in Figure 2. Overlapping resonances were grouped in pairs, indicated by special symbols. The average value is reported. (b) T_1 and NOE values for other selected carbon resonances.

The good chemical dispersion around the α–(1-6) linkage both at the ^{1}H and ^{13}C level allowed the determination of the T_1 times of some other carbon nuclei. Therefore, we could verify whether the ring carbons in each ring are dynamically equivalent. For both the a and m units, the values for all carbons in the hexacycle are very uniform (Table III), confirming that this unit moves as a rigid body. For the f unit, we see some more variation, which might point to an enhanced mobility for this residue implicated in the α–(1-6) linkage.

The NOE values are also in good agreement with the theoretical value calculated for a τ_c=0.9 ns correlation time. As we do not expect any influence of the carbon-carbon dipolar coupling, the measurements were only performed on the enriched sample. The theoretical expression for the NOE value contains spectral density terms in both the numerator and enumerator. Therefore, this parameter shows no explicit dependency on the order parameter S^2, leaving us with a pure estimation of τ_c. The average value of 34% is in excellent agreement with the previously determined value of 0.9 ns for τ_c.

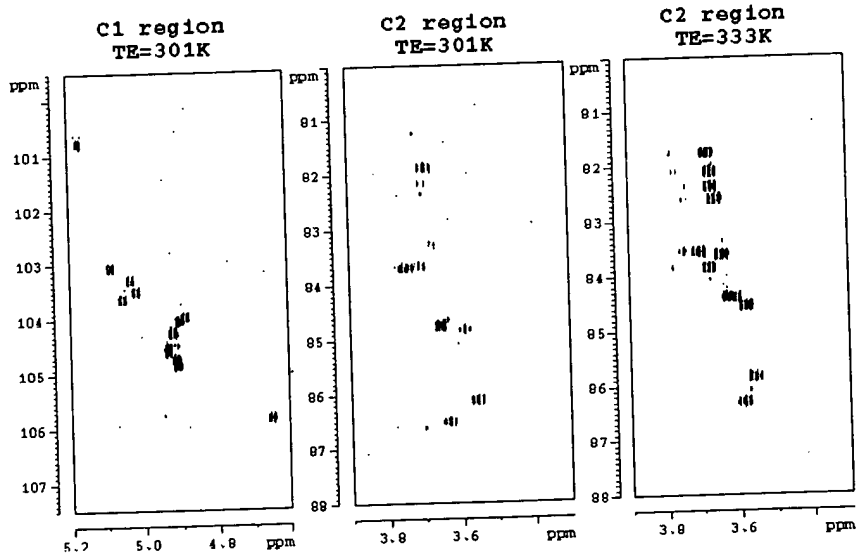

Figure 11. Selected regions of a constant-time HSQC spectrum of the ^{13}C enriched DP13. a) H1-C1 region at 301K; b) H2-C2 region at 301K; c) H2-C2 region at 333K. The intensities were normalized with respect to the f H2-C2 correlation peak.

Based on the same estimates of the correlation times τ_c=0.9 ns and order parameter S^2 = 0.85, we expect T_2 relaxation times of the order of 190 ms. A first indication of a discrepancy between these theoretical value and the experimental ones came from the observation of the constant-time HSQC on a ^{13}C enriched sample. The constant-time period for the evolution of the chemical shift was set to 44 ms, allowing a correct refocusing of the average ^{13}C-^{13}C one-bond J-coupling constant. In the spectrum of Figure 11 (left) recorded at 301K, all H1-C1 direct correlation peaks are visible, be it with a weaker intensity for the bC1 resonance. In the same spectrum, all H2-C2 correlation peaks are substantially weaker, and certain resonances such as the l unit almost disappear (Figure 12, middle).

A strong indication that the additional line broadening is due to chemical exchange comes from the temperature dependence of the line broadening. Already for the anomeric proton resonance of unit b, we had found an increased broadening at lower temperatures. At higher temperatures, the chemical exchange rate k_{ex} should increase, and hence contribute less to the exchange broadening. We tested this by recording constant-time HSQC spectra at different temperatures ranging from 20 °C to 60 °C. As can be seen in Figure 11 (right), the C2 resonances gain considerably in intensity at the higher temperature, in agreement with the hypothesis of exchange broadening. The fC2 resonance, that is not involved in a linkage, provides a reference as it hardly changes in intensity upon increasing temperatures.

More precise measurements of the T_2 values were obtained with the 2D extension of the Carr-Purcell-Meiboom-Gill (CPMG) sequence [57, 58]. The large distribution of expected T_2 times (inferior to 40 ms for certain C2 resonances, based on the results of the constant-time HSQC experiment, and of the order of 150 ms for the a and m C1 resonance, based on preliminary 1D relaxation experiments) led to the delicate problem of choosing the CPMG times that should be used in the series of 2D experiments. The CPMG times were selected according to the results of a recent theoretical study where the Cramér-Rhao theory was used to define an optimal sampling strategy [59] The results of the T_2 measurements are summarized in Table IV The series was repeated twice at a two-months interval, and the results proved reproducible to within ± 2ms

Residue	T_2 (C1) (ms)	T_2(C2) (ms)	Δ_{ex} C2 (Hz)
a	130	117	3
f	93@	151	-
i	81#	64	11
j	81#	53	14
d	107	33	25
l	92§	19	54
b	47	27	33
e	89	18#	50
k	92§	45	15
c	81	21	38
h	124	18#	50
g	93@	29	28
m	136	24	35

Table IV. ^{13}C T_2 values measured on the non-enriched OPG of *R. solanacearum* at 301K and 150 MHz. We used the CPMG sequence with a delay δ=500 µs between the π pulses, and 11 CPMG times ranging from 1ms to 240 ms (see text). Overlapping resonances were grouped in pairs, indicated by special symbols. The average value is reported. Exchange contributions were calculated from ($1/T_2^{obs} = 1/T_2^{dip} + \Delta_{ex}$) with a T_2^{dip}= 190 ms.

Whereas the values of all C1 resonances except for the b unit experience relatively little exchange broadening, the bC1 and even more all C2 resonances are dramatically broadened. With a purely dipolar T_2 value of 190 ms based on the estimates of 0.9 ns for the correlation time and 0.85 for the order parameter S^2, the exchange contribution to the bC1 linewidth can be estimated to 14 Hz, whereas for certain C2 resonances, it obtains values as large as 54 Hz (Table IV). Alternatively, we could consider the fC2 T_2 relaxation time as the basis for the non-exchange broadened T_2 value, but this leads to no major differences for the exchange term.

In the constant time HSQC experiment, only one 180° ^{13}C pulse is applied during the delay of 44 ms, therefore no refocusing of the chemical exchange can happen (*vide infra*), and the exchange contribution is given by (60)

$$[1]\quad \Delta_{ex} = \Omega_{ex}^2 / 8 / k_{ex}$$

The quadratic dependence on Ω_{ex}, the chemical shift separation (in radial units) of the different chemical species, emphasizes that physically an exchange process is similar to the molecular self-diffusion process, here in one dimension.

Furthermore, the analytical dependence of the exchange contribution on the quadratic difference in chemical shift for the co-existing conformations suggests a straightforward way of verifying the nature of the broadening mechanism. We recorded at 301K a series of T_2 experiments at the lower field of 7.1 T (or 75 MHz for ^{13}C). The disadvantage of the lower field strength was the decrease in sensitivity and the increased spectral overlap, leading to considerably higher uncertainties in the T_2 values. Still, the good separation of the H2-C2 correlation peaks allowed us to extract a certain number of them (Table V). If again we estimate the dipolar contribution to the T_2 relaxation time based on a correlation time τ_c = 0.9 ns and an average order parameter S^2 = 0.85, we obtain a value of 133 ms. Subtracting this dipolar

Residue	T_2 (C2) (ms)	Δ_{ex} C2 (Hz)	Δ_{ex} (14T)/ Δ_{ex} (7T)
a	ND	ND	ND
f	122±5	0	-
i	84±7	4.4	3.2
j	84±6	4.4	3.2
d	75±6	5.8	4.3
l	59±10	9.4	5.7
b	64±6	8.1	4.1
e	ND	ND	ND
k	ND	ND	ND
c	ND	ND	ND
h	ND	ND	ND
g	73±10	6.2	4.5
m	57±7	10.0	3.5

Table V. ^{13}C T_2 values measured on the non-enriched OPG of *R. solanacearum* at 301K and 75 MHz. Exchange contributions were calculated from ($1/T_2^{obs} = 1/T_2^{dip} + \Delta ex$) with T_2^{dip}= 133 ms.

contribution from the observed relaxation rates, we obtain the exchange contribution at 75 MHz (Table V), and can evaluate the ratio of the exchange contributions at 14.1T and 7.1T. Taking into account the large uncertainties on the T_2 values at the lower field of 7.1T, the obtained ratios are reasonably close to the theoretical value of 4 as expected from Eq. 1.

5.4 STRUCTURAL IMPLICATIONS OF THE RELAXATION DATA

The above described results indicate unambiguously that the oligosaccharide passes through different conformations that are in dynamic exchange on the microsecond time scale [61]. One major problem of any NMR study on a system that shows rapid chemical exchange is the average nature of all obtained structural parameters. A very illustrative example is formed by the cyclic decapeptide antanamide, for which the available NOE and J coupling data could not be satisfied by one single conformation [62]. The simplest model compatible with all NMR parameters required two different conformations. Another extreme example of the average nature of the NMR parameters is formed by the all β–(1-2) cyclic glucans of the *Rhizobiaceae*. Both the chemical shift values and the ^3J coupling constants measured over the glycosidic linkage reflect an average behaviour over both the individual monomers and over the different conformations adopted by the macrocycle over time.

Our initial hope when starting the structural studies on the OPG of *R. solanacearum* was that the single α–(1-6) linkage would induce structural constraints to such an extent that both mechanisms of averaging would be greatly reduced. Whereas the first averaging evidently has disappeared - we observe all anomeric protons resonances individually - the above described relaxation data show that our structural data still result from an average over two or more conformations.

It is illustrative to map the exchange contribution on the macrocycle (Figure 12). With the exception of the b unit, only the C2 carbon T_2 values are appreciably affected by the chemical exchange, implying the most important variation for the Ψ angle between the different conformations. We further observe that chemical exchange is not uniformly distributed over the macrocycle, as the residues around the α–(1-6) linkage are relatively little affected, whereas the main exchange phenomenon takes place around the b unit, diametrically opposed to the α–f linkage. For the latter b residue, both C1 carbon and C2 carbon are considerably broadened. In the case of the DP16 molecule of *Xanthomonas campestris*, York presented recently (18) a structural model, and proposed a topological reversal point between the two helical domains to occur at the level of the flexible α–(1-6) linkage and at the residue where a frameshift in the alternating chemical shift pattern was observed. Our current hypothesis is that this point of asymmetry in the DP13 molecule of *R. solanacearum* occurs at the level of the b residue, but not in a static fashion - i.e. that the point hops between both linkages preceding or following this b residue.

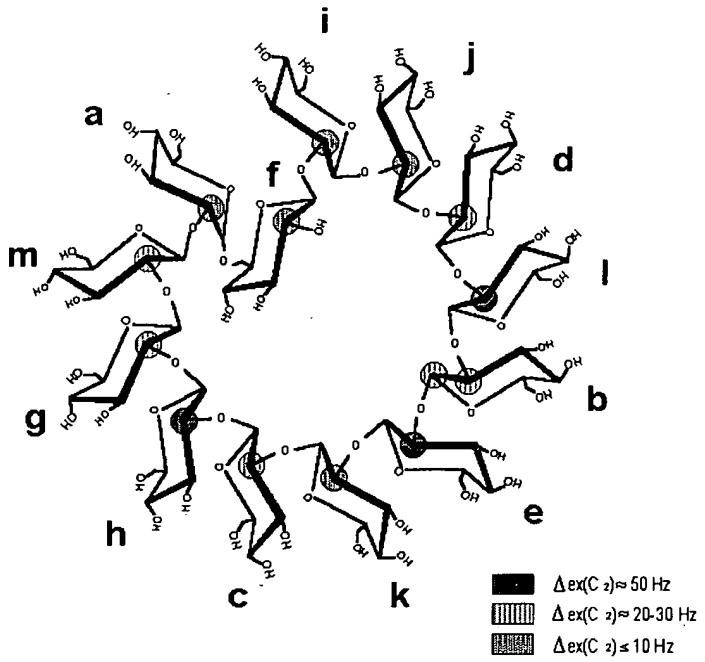

Figure 12. The macrocycle of the DP13 OPG of *R. solanacearum*. The circles on the C2 carbons graphically represent the exchange contribution to the T_2 relaxation of the C2 nucleus. All C1 carbons except for the bC1 have values of Δ_{ex} inferior to 10Hz.

In the ^{13}C NMR spectra of oligo- and poly-saccharides, the chemical shifts of the carbon atoms on either side of the glycosidic linkage have been found to vary over a range of up to 12 ppm, depending on the conformation of the linkage [63]. Excluding the fC2 carbon that is not implicated in a linkage, the variations for the C2 resonance positions have to be very large to lead to the observed line broadenings, indicating a large conformational variety. The combination of the explicit dependence of the chemical shift on the conformation of the glycosidic linkage, at least in a β–(1-2) linked disaccharide, with the previously determined short distances and ^3J coupling constants will probably allow to alleviate this ambiguity

6. *In vivo* observation of the OPGs.

The functional relevance of the complex internal dynamics of the OPG in vitro is not clear at this moment. However, NMR allows equally to probe the motional freedom of the OPG molecules in the bacterial periplasm, which might be more directly related to its function. In vivo NMR studies have mostly focused on small molecules, aiming to detect and quantify metabolites by ^{31}P NMR or ^{13}C NMR, but have not yet been used to investigate more complex biomolecules in the organism, and to address the question of conformation in vivo. The aim of our study was therefore twofold : can we observe the molecule, and hence deduce a certain degree of molecular mobility? and can we see whether the conformational slow exchange as observed in vitro is still present in the complex environment that forms the periplasm?

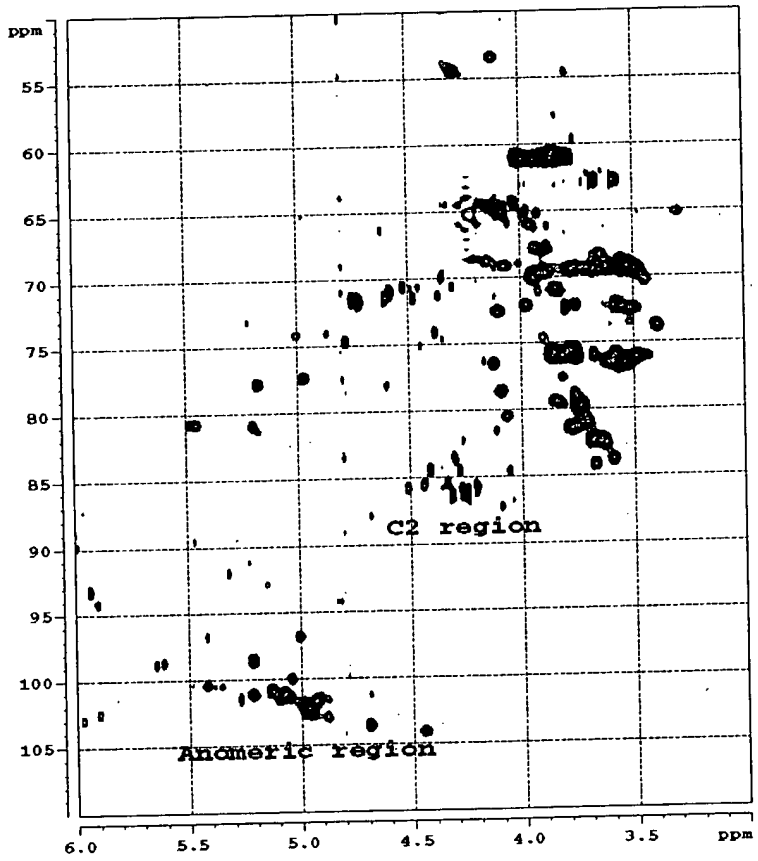

Figure 13 ^{1}H-^{13}C HSQC spectrum of a cellular suspension of *R solanacearum* in D_2O

One of the prerequisites of high-resolution NMR is that the external magnetic field is extremely homogeneous over the volume of the detection coil. Modern techniques of magnet and coil design have led to the impressive achievement of a homogeneity smaller than one Hz, on a total frequency that approaches the GHz. However, when bodies with a different magnetic susceptibility are introduced in the sample, this resolution is partly lost, due to the macroscopic dipolar fields that are generated at the interface of differential magnetic susceptibility. Recent efforts aimed at minimizing such effects have used the technique of Magic Angle Spinning [64, 65], borrowed from solid state NMR, to minimize macroscopic inhomogeneities, and obtain high-resolution spectra on heterogeneous samples such as polystyrene resin-bound organic molecules or peptides [66, 67].

We performed a first experiment with a 60ml solution of concentrated cells in a 4mm rotor, but the spinning at 4kHz altered the hydration of the cells, and no workable NMR spectra could be obtained. In a second attempt, we recorded a spectrum of the same solution in a regular non-spinning 5mm tube, and here, we were able to obtain a good spectrum, where both the anomeric and C2 region could be clearly distinguished (Figure 13). We ascribe the success of this experiment to the small difference in magnetic susceptibility between the cells and the aqueous solvent, as had been observed earlier for entire embryos [68]. Future work of our groups will therefore be directed to selective labeling of the OPG by using C1 or C2 labeled glucose as sole carbon source, and further investigate the structure and dynamics of the OPG in the bacterial periplasm.

7. Acknowledgments

Dr. J.-M. Wieruszeski has contributed greatly to all NMR results presented in this lecture. Dr. P. Talaga was responsible for all biochemistry work, and Dr. D. Horvath performed all modeling studies. Without these three persons, we would not have been able to present this lecture, and we want to express our warmest thanks. We thank Dr. H. Desvaux (CEA, France) for fruitful collaboration in the off-resonance ROESY experiment, Prof. P. Albersheim (Complex Carbohydrate Research Center, University of Georgia) for access to the mass spectrometer and Dr. W. S. York for performing the MALD-TOF MS analysis. The 600 MHz facility used in this study was funded by the European funds of the FEDER attributed to the Région Nord - Pas de Calais (France), by the CNRS and by the Institut Pasteur de Lille.

8. References

1 – Oliver, D. B. (1996) in *Escherichia coli* and *Salmonella*. Cellular and Molecular Biology, Neidhardt, F.C. (ed.), American Society for Microbiology, Washington, D.C., pp. 88-103.

2 – Schulman, H., and Kennedy, E. P.(1979) *J. Bacteriol.* **137**, 686-688.

3 – Miller, K. J., Kennedy, E. P., and Reinhold, V. N. (1986) *Science* **231**, 48-51.

4 – Van Golde, L. M. G., Schulman, H., and Kennedy, E. P. (1973) *Proc. Natl. Acad. Sci. USA* **70**, 1368-1372.

5 – Kennedy, E. P. (1996) in *Escherichia coli* and *Salmonella*. Cellular and Molecular Biology, Neidhardt, F.C. (ed.), American Society for Microbiology, Washington, D.C., pp. 1064-1071;

6 – Talaga, P., and Bohin, J.-P. (unpublished).

7 – Talaga, P., Fournet, B., and Bohin, J.-P.(1994) *J. Bacteriol.* **176**, 6538-6544.

8 – Dell, A., York, W. S., McNeil, M., Darvill, A. G., and Albersheim, P. (1983) *Carbohydr. Res.* **117**,185-200.

9 – Koizumi, K., Okada,Y., Horiyama, S., and Utamura, T.(1983) *J. Chromat.* **265**, 89-96.

10 – Hisamatsu, M. (1992) *Carbohydr. Res.* **231**, 137-146.

11 – Breedveld, M. W., and Miller, K. J. (1994) *Microbiol. Rev.* **58**, 145-161

12 – Bundle, D. R., Cherwonogrodzky, J. W., and Perry, M. B. (1988) *Infect. Immun.* **56**, 1101-1106.

13 – Miller, K. J., Gore, R. S., Johnson, R., Benesi, A. J., and Reinhold, V. N. (1990) *J. Bacteriol.* **172**, 136-142.

14 – Rolin, D. B., Pfeffer, P. E., Osman, S. F.,Szwergold, B. S., Kappler, F., and Benesi, A. J. (1992) *Biochim. Biophys. Acta* **1116**, 215-225.

15 – Altabe, S. G., Talaga, P., Wieruszeski, J.-M., Lippens, G., Ugalde, R., and Bohin, J.-P. (1998) in Biological Nitrogen Fixation for the 21st Century, C. Emelrich et al. (eds), p 390.

16 – Talaga, P., Stahl, B., Wieruszeski, J.-M., Hillenkamp, F., Tsuyumu, S., Lippens, G., and Bohin, J.-P. (1996) *J. Bacteriol.* **178**, 2263-2271.

17 – Amerura, A., and Cabrera-Crespo, J. (1986) *J. Gen. Microbiol.* **132**, 2443-2452.

18 – York, W. S. (1995) *Carbohydr. Res.* **278**, 205-225

19 – Talaga, P, Wieruszeski, J.-M., Cogez, V., Bohin, A., Lippens, G., and Bohin, J.-P. (in preparation)

20 – Miller, K. J., Reinhold, V. N., Weissborn, A. C., and Kennedy, E. P. (1987) *Biochim. Biophys. Acta* **901**, 112-118.

21 – Miller, K. J., Gore, R. S., and Benesi, A. J. (1988) *J. Bacteriol.* **170**, 4569-4575.

22 – Serrano, G., Franco-Rodriguez, G., Gonzalez-Jimenez, I., Tejero-Mateo, P., Molina Molina, J., Dobado, J. A. , Mégias, M. and Romero, M. J. (1993) *J. Mol. Struct.* **301**, 211

23 – Poppe, L., York, W. S. and van Halbeek, H. (1993) *J. Biomol. NMR* **3**, 81- 89

24 – André, I., Mazeau, K., Taravel, F. R., and Tvaroska, I. (1995a) *Int. J. Biol. Macromol.* **17**, 189.

25 – André, I., Mazeau, K., Taravel, F. R., and Tvaroska, I. (1995b) *New J. Chem.* **19**, 331.

26 – York, W. S., Thomsen, J. U., and Meyer, B. (1993) *Carbohydr. Res.* **248**, 55-80

27 – Lippens, G., Talaga, P., Wieruszeski, J.-M., and Bohin, J.-P. (1995), in *Spectroscopy of Biological Molecules*, Merlin, J. C., Turrell, S., and Huvenne, J.-P. (ed.), Kluwer Academic Publishers, Dordrecht, the Netherlands.

28 – Tvaroska, I., and Taravel, F. R. (1992) *J. Biomol. NMR* **2**, 421-430

29 – Vuister, G. and Bax, A. (1992) *J. Magn. Res.* **98**, 428-435

30 – Gottschalk, G. (1986) *Bacterial Metabolism*, Springer, New York, NY

31 – Widmalm, G., Byrd, R. A. , and Egan, W. (1992) *Carbohydr. Res.* **229,** 195.

32 – Peters, T., and Weimar, T.(1994) *J. Biomol. NMR*, **4**, 97

33 – Desvaux, H., Berthault, P., Birlirakis, N. Goldman, M. (1994) *J. Magn. Res. A* , **108**, 219.

34 – Desvaux, H., Berthault, P., and Birlirakis, N. (1995) *Chem. Phys. Letters* **233**, 545.

35 – Dowd, M. K., French, A. D. and Reilly, P. J. (1992) *Carbohydr. Res.* **233**, 15.

36 – Lippens, G, Wieruszeski, J.-M., Talaga, P., and Bohin, J.-P. (1996) *J. Biomol. NMR* **8**, 311-318.

37 – Poppe, L., and van Halbeek, H. (1991) *J. Magn. Res.* **93**, 214-217

38 – Uhrin, D., Mele, A., Boyd, J., Wormald, M. R. and Dwek, R. A. (1992) *J. Magn. Res.* **97**, 411-418

39 – Montelione, G. T., Winkleer, M. E., Rauenbuehler, P., and Wagner, G. (1989) *J. Magn. Res.* **82**, 198-204

40 – Wider, G., and Wüthrich, K.(1993) *J. Magn. Res. Series B* **102**, 239-241

41 – Harbison, G. S. (1993) *J. Am. Chem. Soc.* **115**, 3026-3027

42 – Lippens, G., Wieruszeski, J.-M., Talaga, P., Bohin, J.-P., and Desvaux H. (1998) *J. Am. Chem. Soc.* **118**, 7227-7228.

43 – Otting, G. and Wüthrich, K. (1990) *Q. Rev. Biophys.* **23**, 39-96

44 – Fesik, S. W., Gampe, R. T., Eaton, H. L., Gemmecker, G., Olejniczak, E. T., Neri, P., Holzman, T. F., Egan, D. A., Edalji, R., Simmer, R., Helfrich, R., Hochlowski, J. and Jackson, M. (1991) *Biochemistry* **30**, 6574-6583

45 – Weber, C., Wider, G., Von Freyberg, B., Traber, R., Braun, W., Widmer, H., and Wüthrich, K. (1991) *Biochemistry* **30**, 6563-6574

46 – Lee, W., Harvey, T.S., Yin, Y., Yau, P. Litchfield, D., and Arrowsmith (1994) *Nat. Struct. Biol* **1**, 877-890.

47 – Zhang, H., Zhao, D., Revington, M., Lee, W., Jia, X., Arrowsmith, C., and Jardetzky, O. (1994) *J. Mol. Biol.* **238**,592-614.

48 – Tvaroska, I., Hricovini, M., and Petrakova, E. (1989) *Carbohydr. Res.* **189**, 359-362

49 – Horvath, D., and Lippens, G. (unpublished).

50 – Horvath, D., Lippens, G., and Van Belle, D. (1996) *J. Chem. Phys.* **105**, 4197-4210.

51 – Horvath, D.,Van Belle, D., Lippens, G., and. Wodak, S. J. (1996) *J. Chem. Phys.* **104**, 17.

52 – Palmer III, A. G., Williams, J., McDermott, A. (1996) *J. Phys. Rev.* **100**, 13293-13310,

53 – Lipari, G., Szabo, A. (1982) *J. Am. Chem. Soc.* **104**, 4546-4559.

54 – Clore, G. M., Driscoll, P. C., Wingfield, P. T., Gronenborn, A. M. (1990) *Biochemistry* **29**, 7387-7401.

55 – Brüschweiler, R., Liao, X., Wright, P. (1995) *Science* **268**, 886-889.

56 – Yamazaki, T., Muhandiram, R., Kay, L. E. (1994) *J. Am. Chem. Soc.* **116**, 8266-8278.

57 – Carr, H. Y., Purcell, E. M. (1954) *Phys. Rev.* **94**, 630-638.

58 – Meiboom, S., and Gill, D. (1958) *Rev. Sci. Instrum.* **29**, 688-691.

59 – Jones, J. A., Hodgkinson, P., Barker, A. L. , Hore, P. J. (1996) *J. Magn. Res. B* **113**, 25-34

60 – Kaplan, J I (1995) in " Encyclopedia in Nuclear Magnetic Resonance" , Ed Grant and Harris, vol 2, pp 1252

61 – Lippens, G., Wieruszeski, J.-M., Horvath,, D., Talaga, P., and Bohin, J.-P. (1998) *J. Am. Chem. Soc.* **120**, 170-177.

62 – Kessler, H., Griesinger, C., Lautz, J., Müller, A., van Gunsteren, W. F., Berendsen, H. J. C. (1988) *J. Am. Chem. Soc.* **110**, 3393-3396.

63 – Jarvis, M. C. (1994) *Carbohydr. Res.* **259**, 311.

64 – Lowe, I.J. (1959) Phys. Rev. Lett. **2**, 285.

65 – Andrew, E. R., Bradbury, A., and Eades, R. G. (1958) Nature **182**, 1659

66 – Anderson, R. C., Jarema, M. A, Shapiro, M. J., Stokes, J. P., and Ziliox, M. (1995) J. Org. Chem. **60**, 2650.

67 – Pop, I., Dhalluin, C., Depréz, B., Melnyk, P., Lippens, G., and Tartar, A. (1996) Tetrahedron **52**, 12209 - 12222.

68 – Valles, J. M., Lin, K., Denegre, J. M., and Mowry, K. L. (1997) Biophys. J. **73**, 1130-1133.

STIC-ILL

RSI. J5
NPL

From: Gabel, Gailene
Sent: Wednesday, February 12, 2003 5:14 PM
To: STIC-ILL
Subject: 09/905,439

Please provide a copy of the following literature ASAP:

1) Killick, Real-time NMR studies on a transient folding intermediate of barstar. PROTEIN SCIENCE, (1999 Jun) 8 (6) 1286-91.

2) Guo et al., Identification of the binding surface on Cdc42Hs for p21-activated kinase. BIOCHEMISTRY, (1998 Oct 6) 37 (40) 14030-7.

3) Pfuhl et al., Secondary structure determination by NMR spectroscopy of an immunoglobulin-like domain from the giant muscle protein titin. JOURNAL OF BIOMOLECULAR NMR, (1995 Jul) 6 (1) 48-58.

4) Kennedy et al., Chemosensitization of a multidrug-resistant Leishmania tropica line by new sesquiterpenes from Maytenus magellanica and Maytenus chubutensis, Journal of Medicinal Chemistry, (December 20, 2001) Vol. 44, No. 26, pp. 4668-4676.

5) Carvalho et al., TCA cycle kinetics in the rat heart by analysis of C-13 isotopomers using indirect H-1[C-13] detection, AMERICAN JOURNAL OF PHYSIOLOGY-HEART AND CIRCULATORY PHYSIOLOGY, (SEP 2001) Vol. 281, No. 3, pp. H1413-H1421.

6) Sokolowski et al., Conformational analysis of a Chlamydia-specific disaccharide alpha-Kdo-(2-->8)-alpha-Kdo-(2-->O)-allyl in aqueous solution and bound to a monoclonal antibody: observation of intermolecular transfer NOEs. JOURNAL OF BIOMOLECULAR NMR, (1998 Jul) 12 (1) 123-33.

7) Kuroda et al., Locations of local anesthetic dibucaine in model membranes and the interaction between dibucaine and a Na+ channel inactivation gate peptide as studied by 2H- and 1H-NMR spectroscopies. BIOPHYSICAL JOURNAL, (1996 Sep) 71 (3) 1191-207.

8) Marceau et al., Contribution of a conserved arginine near the active site of Escherichia coli D-serine dehydratase to cofactor affinity and catalytic activity. JOURNAL OF BIOLOGICAL CHEMISTRY, (1989 Feb 15) 264 (5) 2753-7.

Thanks a bunch,
Gail R. Gabe
7B15
CM1
305-0807

Chemosensitization of a Multidrug-Resistant *Leishmania tropica* Line by New Sesquiterpenes from *Maytenus magellanica* and *Maytenus chubutensis*

María L. Kennedy,[†,‡] Fernando Cortés-Selva,[§,‡] José M. Pérez-Victoria,[§] Ignacio A. Jiménez,[†] Antonio G. González,[†] Orlando M. Muñoz,[∥] Francisco Gamarro,[§] Santiago Castanys,*[,§] and Angel G. Ravelo*[,†]

Instituto Universitario de Bio-Orgánica "Antonio González", Universidad de La Laguna, Avenida Astrofísico Francisco Sánchez, 2, 38206 La Laguna, Tenerife, Spain, Instituto de Parasitología y Biomedicina "López-Neyra", Consejo Superior de Investigaciones Científicas, Granada, Spain, and Facultad de Ciencias, Universidad de Chile, Casilla 653, Santiago de Chile, Chile

Received June 27, 2001

Parasite resistance to drugs has emerged as a major problem in current medicine, and therefore, there is great clinical interest in developing compounds that overcome these resistances. In an intensive study of South American medicinal plants, herein we report the isolation, structure elucidation, and biological activity of dihydro-β-agarofuran sesquiterpenes from the roots of *Maytenus magellanica* (**1**−**14**) and *M. chubutensis* (**14**−**17**). This type of natural products may be considered as *privileged structures*. The structures of 10 new compounds, **1**, **3**, **6**−**9**, and **12**−**15**, were determined by means of ^{1}H and ^{13}C NMR spectroscopic studies, including homonuclear (COSY and ROESY) and heteronuclear correlation experiments (HMQC and HMBC). The absolute configurations of eight hetero- and homochromophoric compounds, **1**, **3**, **6**−**9**, **12**, and **13**, were determined by means of CD studies. Fourteen compounds, **1**−**3** and **6**−**16**, have been tested on a multidrug-resistant *Leishmania tropica* line overexpressing a P-glycoprotein-like transporter to determine their ability to revert the resistance phenotype and to modulate intracellular drug accumulation. From this series, **1**, **2**, **3**, **14**, and **15** showed potent activity, **1** being the most active compound. The structure−activity relationships of the different compounds are discussed.

Introduction

The species of the Celastraceae family have a long history in traditional medicine.[1,2] The leaves and roots of different species of *Maytenus* are used in folk medicine around the world.[1] The stem bark of *M. senegalensis*[3] is used in Sudan for the treatment of tumors, dysentery, and snake bites, whereas *M. ilicifolia* has been used for anticancer and contraception in South America[4] and for the treatment of gastric ulcers, dyspepsia, and other intestinal disorders.[5,6] As part of an intensive investigation into biologically active metabolites from species of this family, we had previously reported quinone-methide[7,8] and dimeric triterpenes[9] showing antimicrobial and cytotoxic activities. On the other hand, sesquiterpene esters, based on the dihydro-β-agarofuran [5,11-epoxy-5β,10α-eudesman-4-(14)-ene] skeleton, are chemotaxonomic indicators of the family,[10] and they have attracted a great deal of interest because of their immunosuppressive,[11] cytotoxic,[12] insect-antifeedant, and insecticidal activities.[13] Recently, they have shown anti-HIV,[14] reversal multidrug resistance (MDR) phenotype,[15,16] and antitumor-promoting activities.[17] These data along with their structural characteristics make dihydro-β-agarofuran sesquiterpenes to be considered as *privileged structures*.[18]

Protozoan parasites are responsible for some of the most important and prevalent diseases of human and domestic animals, threatening the lives of nearly one-quarter of the human population. World Health Organization statistics show that with a 42-fold increase in the past 15 years leishmaniasis has become the second worldwide cause of death among parasitic diseases,[19] mainly because of the appearance of drug-resistance mechanisms. The MDR phenotype due to the increased expression of P-glycoprotein (Pgp)-like transporters has been characterized in tumor cells[20,21] and protozoan parasites,[22] including *Plasmodium*[23] and *Leishmania* spp.[24−26] Pgp belongs to the ABC (ATP−binding−cassette) superfamily of transporters and exports a wide range of drugs from the cell, decreasing their intracellular concentration and preventing their cytotoxic activity. Structural analysis of Pgp shows two homologous halves, each composed of a cytosolic nucleotide-binding domain whose ATPase activity provides the energy needed for the active export of cytotoxic compounds and a transmembrane domain, involved in drug efflux. Mammalian Pgp can be inhibited in vitro by reversal agents, also called chemosensitizers or modulators, such as verapamil and cyclosporin A, which compete with drug binding to the transmembrane domains.[27] However, most of these modulators are also pumped substrates and therefore require high concentrations for effective inhibition. These concentrations produce undesirable side effects that hamper their clinical use. In addition, these classical modulators of drug efflux in mammalian cancer cells only poorly sensitize the MDR phenotype in *Leishmania* parasites.[24,26,28] Thus, new

* To whom correspondence should be addressed. For S.C.: phone, 34-958-805185; fax, 34-958-203323; e-mail, castanys@ipb.csic.es. For A.G.R.: phone, 34-922-318576; fax, 34-922-318571; e-mail, agravelo@ull.es.
† Universidad de La Laguna.
‡ Both authors contribute equally to this paper.
§ Consejo Superior de Investigaciones Científicas.
∥ Universidad de Chile.

10.1021/jm010970c CCC: $20.00
Published on Web 11/22/2001

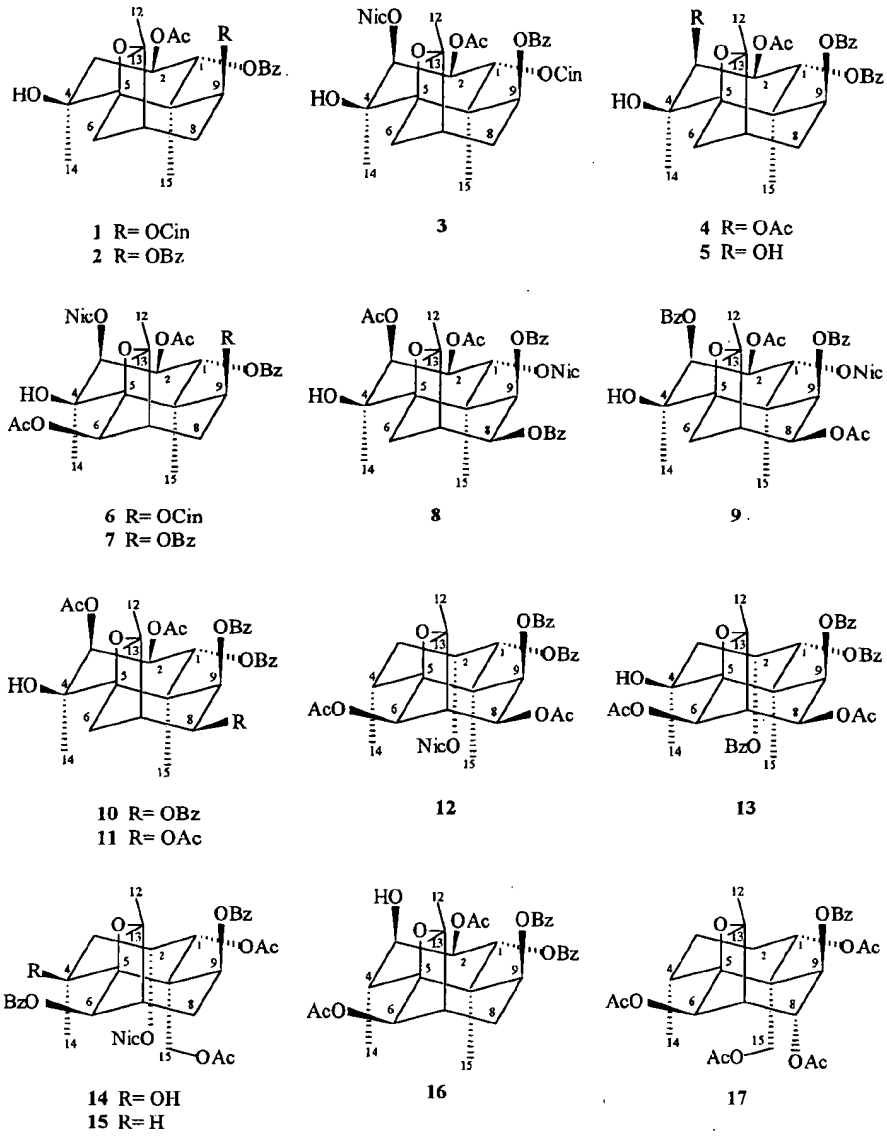

Figure 1. Sesquiterpenes from *Maytenus magellanica* and *M. chubutensis*.

classes of more specific, nontransported inhibitors of Pgp-like transporters with lower host toxicity need to be developed.

Dihydro-β-agarofuran sesquiterpenes are particularly promising modulators of the MDR phenotype in eukaryotic organisms. Interestingly, we have recently reported that a number of dihydro-β-agarofuran sesquiterpene derivatives from *Crossopetalum tonduzii* constituted efficient modulators of *Leishmania* MDR reverting significantly the Pgp-like transporter mediated daunomycin (DNM) resistance.[15] Besides, dihydro-β-agarofuran sesquiterpene derivatives isolated from the roots of *Celastrus orbiculatus* partially or completely reversed the MDR phenotype in cancer cells.[16]

This paper reports on the phytochemical analysis of the root bark extracts of the Chilean genus *Maytenus* (Celastraceae) (*M. chubutensis* and *M. magellanica*) and describes the isolation of 10 new sesquiterpenes (**1**, **3**, **6**–**9**, and **12**–**15**) with a dihydro-β-agarofuran skeleton. Their structures were elucidated by means of ^{1}H and ^{13}C NMR spectroscopic studies, including homonuclear (correlation spectroscopy (COSY) and rotating-frame Overhauser enhancement spectroscopy (ROESY)) and heteronuclear correlation experiments (heteronuclear multiple-quantum coherence (HMQC) and heteronuclear multiple-bond correlation (HMBC)). The absolute configurations of the eight compounds **1**, **3**, **6**–**9**, **12**, and **3** were determined by application of the circular dichroism (CD) exciton chirality method. The known compounds **2**,[29] **4**,[30] **5**,[30] **10**,[29] **11**,[31] **16**,[31] and **17**[32] were identified by spectroscopic methods and comparison with authentic samples or reported data. Fourteen compounds **1**–**3** and **6**–**16** have been tested on a MDR *Leishmania tropica* line overexpressing a Pgp-like transporter to determine their ability to revert the resistance phenotype and to modulate intracellular drug accumulation.

Results and Discussion

Repeated chromatography of the *n*-hexane/Et_2O (1:1) extract of the root bark of *M. magellanica* on Sephadex LH-20 and silica gel afforded, in addition to the known compounds **2**, **4**, **5**, **10**, and **11**, the new compounds **1**, **3**, **6**–**9**, and **12**–**14** (Figure 1), and

Table 1. ^{1}H NMR ($CDCl_3$) Chemical Shift δ and J (Hz) Values (in Parentheses) of Compounds **1**, **3**, **6**–**9**, and **12**–**15**

compd	H-1	H-2	H-3	H-6	H-7	H-8	H-9	H-15
1	5.94 d (10.5)	5.14 dt (4.8, 10.5)	2.07 m[b]	2.07 m[b] 1.80 d (12.4)	2.07 m[b]	2.07 m[b] 2.42 m	4.79 d (5.3)	1.45 s[b]
3	6.43 d (11.2)	5.41 dd (2.9, 11.2)	5.52 d (2.9)	2.16 m[b] 1.96 d (12.4)	2.12 m	2.16 m[b] 2.46 m	4.89 d (5.0)	1.55 s
6	6.41 d (10.9)	5.39 dd (2.8, 10.9)	5.40 d (2.8)	5.59 s	2.21 m[b]	2.21 m[b] 2.46 m	4.84 d (5.6)	1.60 s
7	6.42 d (11.2)	5.38 dd (2.8, 11.2)	5.41 d (2.8)	5.65 s	2.25 m[b]	2.47 m 2.25 m[b]	5.06 d (5.6)	1.59 s
8	6.35 d (10.8)	5.33 dd (2.9, 10.8)	5.31 d (2.9)	2.15 d (12.9) 2.67 dd (12.9,4.1)	2.46 t (4.1)	5.77 dd (4.1, 5.8)	5.51 d (5.8)	1.64 s
9[a]	6.78 d (11.2)	5.52 dd (2.7, 11.2)	5.86 d (2.7)	1.27 d (13.0) 2.08 dd (13.0,4.9)	1.76 m[b]	5.41 dd (4.4, 5.9)	5.60 d (5.9)	1.23 s
12	5.94 d (3.6)	6.04 m	2.43 m[b] 2.62 m[b]	5.52 s	2.55 d (2.7)	5.71 dd (2.7, 6.3)	5.36 d (6.3)	1.80 s
13	5.82 d (2.8)	5.93 m	2.30 dd_{AB} (3.6, 15.4)	5.73 s[b]	2.48 d (3.0)	5.73 dd[b] (3.0, 4.7)	5.38 d (4.7)	1.85 s
14	5.76 d (3.5)	5.86 m	2.22 m[b]	6.35 s	2.36 t (2.9)	2.69 m 2.22 m[b]	5.56 d (7.1)	4.51, 5.25 d_{AB} (12.8)
15	5.89 d (3.5)	5.93 m	2.15 m 2.65 m[b]	6.28 s	2.43 t (2.7)	2.65 m[b] 2.31 m[b]	5.53 d (7.2)	4.44, 5.34 d_{AB} (12.5)

[a] C_6D_6. [b] Overlapping signals.

Table 2. ^{13}C NMR ($CDCl_3$) Chemical Shift δ Values[a] of Compounds **1**, **3**, **6**–**9**, and **12**–**15**

carbon	**1**	**3**	**6**	**7**	**8**	**9**[b]	**12**	**13**	**14**	**15**
C-1	73.0 d	67.9 d	67.6 d	67.7 d	67.5 d	67.9 d	71.7 d	70.7 d	69.7 d[c]	71.4 d
C-2	69.4 d	69.0 d	67.7 d	68.6 d	68.8 d	72.2 d	71.6 d	69.9 d	68.9 d	71.0 d
C-3	42.7 t	77.0 d	77.5 d	77.6 d	75.6 d	77.0 d	31.1 t	42.3 t	42.4 t	31.0 t
C-4	70.6 s	70.4 s	70.8 s	70.6 s	69.9 s	70.3 s	33.6 d	69.6 s	69.7 s[c]	33.3 d
C-5	90.0 s	90.1 s	91.5 s	91.5 s	89.4 s	89.8 s	89.4 s	91.3 s	91.1 s	89.4 s
C-6	31.5 t	32.6 t	79.8 d	79.7 d	32.7 t	32.2 t	77.2 d	77.2 d	78.6 d	78.3 d
C-7	43.4 d	42.6 d	48.4 d	48.4 d	48.6 d	47.7 d	53.8 d	54.0 d	49.1 d	48.9 d
C-8	31.0 t	30.9 t	31.9 t	30.9 t	71.1 d	69.3 d	68.6 d	68.3 d	34.7 t	35.0 t
C-9	73.4 d	73.1 d	72.4 d	72.4 d	71.9 d	69.5 d	72.4 d	72.1 d	70.4 d	69.3 d
C-10	48.3 s	47.7 s	51.2 s	51.2 s	47.7 s	48.4 s	48.7 s	50.3 s	54.9 s	53.2 s
C-11	83.9 s	84.2 s	85.4 s	85.5 s	84.2 s	84.3 s	83.3 s	85.1 s	84.9 s	82.9 s
C-12	29.7 q	29.6 q	29.9 q	29.8 q	30.9 q	30.5 q	31.2 q	30.2 q	29.5 q	30.6 q
C-13	24.9 q	24.4 q	26.0 q	26.2 q	25.5 q	25.3 q	25.7 q	26.4 q	25.7 q	26.0 q
C-14	24.3 q	23.7 q	23.6 q	23.4 q	23.9 q	23.1 q	25.5 q	25.5 q	25.2 q	18.3 q
C-15	19.9 q	19.9 q	20.6 q	20.4 q	20.5 q	19.3 q	20.6 q	22.0 q	65.9 t	65.9 t

[a] Data are based on DEPT, HMQC, and HMBC experiments. [b] C_6D_6. [c] Overlapping signals.

repeated chromatography of the *n*-hexane/Et_2O (1:1) extract of the root bark of *M. chubutensis* on silica gel and Sephadex LH-20 afforded the new compounds **14** and **15** and two known compounds **16** and **17** (Figure 1).

Compound **1** has the molecular formula $C_{33}H_{38}O_8$, as determined by HRMS. The IR spectrum showed absorption bands for a hydroxyl group at 3541 cm^{-1} and esther groups at 1735 and 1708 cm^{-1}. The MS and HRMS exhibited peaks consistent with losses of acetic acid (*m/z* 502 $[M - HOAc]^+$), benzoic acid (*m/z* 440 $[M - PhCO_2H]^+$), and cinnamic acid (*m/z* 414 $[M - PhCH{=}CHCO_2H]^+$) units. This was confirmed by the ^{1}H NMR spectrum, which also indicated the presence of signals for one acetyl group at δ 1.83 (3H, s), 12 protons in the aromatic region for one benzoyl and one cinnamoyl group at δ 6.46 (1H, d, J = 16.0 Hz), 7.29 (2H, m), 7.40 (3H, m), 7.46 (2H, m), 7.56 (2H, m), and 7.78 (2H, m), which were confirmed by ^{13}C NMR. When **1** was treated with acetic anhydride in pyridine, compound **1** was unaltered, a fact that together with the presence of a singlet at δ 2.86 in the ^{1}H NMR spectrum, interchangeable with D_2O, confirmed the presence of a tertiary hydroxyl group. The ring protons could be unequivocally assigned from its homonuclear COSY and chemical shift correlated spectral data. In its ^{1}H NMR spectrum (Table 1) were also observed an ABX_2 system of two methine and one methylene protons with signals at δ 5.94 (1H, d, J_{AB} = 10.5 Hz), 5.14 (1H, dt, J_{AB} = 10.5 Hz, J_{BX} = 4.8), and 2.07 (2H, m), assignable to protons H-1, H-2, and H-3, respectively. These data are only compatible with substitution at C-1 and C-2 in this type of sesquiterpene with a H-1ax, H-2ax stereochemistry and another methine proton at δ 4.79 (1H, d, J = 5.3 Hz) assigned to H-9. A tertiary methyl at δ 1.39 binding to a quaternary carbon at δ 70.6 in the ^{13}C NMR spectrum (Table 2) and two angular methyls were also observed. All these data indicate that compound **1** is a tetrasubstituted dihydro-β-agarofuran sesquiterpene. The relative stereochemistry of **1** was established on the basis of the coupling constants and confirmed by a ROESY experiment (Figure 2), showing nuclear Overhauser effects among H-14, H-2, and H-15 and between H-15 and H-9. The chemicals shifts for the carbons attached to protons were assigned according to a 2D heteronuclear COSY and the already known proton shift. Because the quaternary carbons could not be assigned by this method, the locations of the hydroxy and ester functions were determined by an HMBC experiment (Table 3), showing a three-bond correlation between the carboxyl signal of the acetate group at δ 170.4 with the ^{1}H signal at 5.14 (H-2); the carboxyl signal of the cinnamate group at δ 166.1 was correlated with the ^{1}H signal at δ 4.79 (H-9), and finally the carboxyl signal of

Table 3. Three-Bond $^1H-^{13}C$ Coupling (HMBC) in Compounds **1**, **3**, **6–9**, and **12–15**

compd	H-1	H-2	H-3	H-6	H-8	H-9	H-15
1	C-2,[a] C-9, C-10,[a] OBz	C-1[a] OAc				C-5, C-7, C-8,[a] C-10,[a] OCin	
3	C-9, C-10,[a] C-15, OCin	OAc	C-1, C-4,[a] C-5, ONic			C-5, C-10[a] C-15,[a] OBz	
6	C-2,[a] C-10,[a] C-15, OBz	C-4 OAc	C-4,[a] C-5, C-14, ONic	C-5,[a] C-8, C-10, C-11, OAc		C-5, C-7, C-10,[a] OCin	
7	C-2,[a] C-10,[a] C-15, OBz	C-1[a]	C-1, C-4,[a] C-5, ONic	C-10, C-11, OAc		C-5, C-10,[a] C-15, OCin	
8	C-2,[a] C-10,[a] C-15, ONic	C-1[a] OAc	C-1, C-4,[a] C-5, OAc		C-11, OBz	C-5, C-7, C-15, C-10,[a] OBz	
9	C-2,[a] C-10,[a] ONic	C-1[a] OAc	C-2, C-4,[a] C-5, OBz		C-11	C-5, C-10,[a] C-15, OBz	
12	C-10,[a] C-15, OBz			C-5,[a] C-10, C-11, OAc	C-11, OAc	C-5, C-7, C-15, C-10,[a] OBz	
13	C-2,[a] C-10,[a] C-15, OBz	C-4		C-5,[a] C-8, C-10, C-11, OAc	C-10, C-11, OAc	C-7, C-10,[a] C-15, OBz	
14	C-9, C-10,[a] C-15, OAc	C-10		C-5,[a] C-8, C-10, C-11, OBz		C-5, C-7, C-15, C-10,[a] OBz	C-5, C-9 OAc
15	C-10,[a] C-15	C-10		C-5,[a] C-7, C-8, C-10, C-11, OBz		C-5, C-10,[a] C-15, OBz	C-5, C-9 OAc

[a] Two bond coupling enhancement observed.

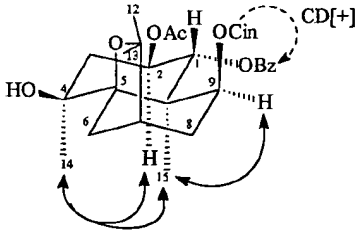

Figure 2. NOE (solid line) and CD exciton couplings (dashed line) for compound **1**.

Table 4. Circular Dichroism Data of Compounds **1**, **3**, **6–9**, **12**, and **13** (MeCN)

compd	λ_{ext}, nm ($\Delta\epsilon$)	λ_{ext}, nm ($\Delta\epsilon$)	$\Delta\epsilon = 0$
1	227.8 (−18.1)	270.7 (+20.3)	242.6
3	225.9 (−14.1)	262.6 (+4.3)	243.3
6	226.2 (−9.6)	277.5 (+1.6)	248.7
7	225.2 (−6.5)	238.9 (+3.9)	233.4
8		236.2 (+12.1)	
9	225.2 (−12.1)	237.5 (+8.2)	232.0
12	221.1 (−0.6)	238.7 (+7.1)	224.8
13	221.5 (−6.3)	236.9 (+25.7)	226.0

the benzoate group at δ 165.3 was correlated with the ^1H signal at δ 5.94 (H-1). The absolute configuration of compound **1** was determined from its CD spectrum.

Compound **3** was isolated as a colorless lacquer with the molecular formula $C_{41}H_{43}NO_{12}$ (HRMS). The ^1H and ^{13}C NMR data of **3** (Tables 1 and 2) indicate it to be 1,2,3,4,9-pentasubstituted-β-dihydroagarofuran sesquiterpene with one tertiary hydroxyl, one acetate, one benzoate, one cinnamate, and one nicotinate group. In its ^1H NMR spectrum an ABX system was also observed with signals at δ 6.43 (1H, d, J_{AB} = 11.2 Hz), 5.52 (1H, d, J_{BX} = 2.9 Hz), and 5.41 (1H, dd, J_{AB} = 11.2 Hz, J_{BX} = 2.9 Hz), assignable to protons H-1, H-3, and H-2 respectively, and a signal at δ 4.89 (1H, d, J = 5.0 Hz), assigned to the proton H-9. The relative stereochemistry was determined on the basis of the coupling constants and the nuclear Overhauser effects (NOE) from the ROESY spectrum. The regiosubstitution was established by HMBC experiment (Table 3) in a way similar to that for **1**, which allowed placement of the cinnamate, acetate, nicotinate, and benzoate groups at C-1, C-2, C-3, and C-9, respectively. The absolute stereochemistry was assigned by means of CD studies.

The structure and absolute configuration of compounds **6–9** were elucidated by spectral methods in a study of their IR, UV, and ^1H and ^{13}C NMR data (Tables 1 and 2), and 2D experiments showed that the compounds were pentasubstituted 4β-hydroxy-dihydro-β-agarofuran sesquiterpenes, which were located at positions 1, 2, 3, 6, and 9 for **6** and **7** and at positions 1, 2, 3, 8, and 9 for **8** and **9**. An HMBC experiment (Table 3) established the regiosubstitution partners; the relative stereochemistry was resolved by analysis of coupling constants and confirmed by ROESY experiments, and finally the absolute configuration was established by analysis of their CD data.

The structures of compounds **12–14** were elucidated by spectral methods, including HREIMS, IR, UV, and ^1H and ^{13}C NMR spectroscopy, and by 2D $^1H-^1H$ and $^1H-^{13}C$ experiments (Tables 1–3). On the other hand, the spectroscopic data of compound **15** and a comparison with those of **14** allowed us to determine its structure, while CD studies allowed the absolute stereochemistry of compounds **12** and **13** to be established.

The absolute configurations were resolved by the dibenzoate chirality method, an extension of the circular dichroism exciton chirality method.[30,33] The dihedral angle between the different chromophores (benzoate, and/or cinnamate, and/or nicotinate) were calculated from J values and molecular mechanics calculations using the PC model.[34] Heterochromophoric **1**, **3**, **6–9**, and **12** and homochromophoric **13** compounds were therefore considered suitable for a CD study, showing a Davydof-type split curve (Table 4), while compounds **14** and **15**, which had three chromophores located at C-2 (ONic), C-6 (OBz), and C-9 (OBz), were not suitable for CD because the opposite 2,6 and 2,9 pairwise interactions canceled each other and the 6,9 pairwise interaction was almost coplanar.[35]

The dihedral angle between the two chromophores (benzoate and cinnamate) was approximately 150° for **1**; its CD spectrum showed a strong split curve (Figure 1 and Table 4) with extremes at the right-hand-band wavelength, i.e., the first Cotton effect at 270.7 nm ($\Delta\epsilon$ = +20.3) and the second at 227.8 nm ($\Delta\epsilon$ = −18.1),

Table 5. Effect of Sesquiterpenes on Cytotoxicity of DNM in a MDR *L. Tropica* Line

	growth inhibition[a] (%)					
	30 μM		15 μM		7.5 μM	
compd	wild-type	DNM-R150	wild-type	DNM-R150	wild-type	DNM-R150
1	7.5 ± 7.5	94.3 ± 3.5	7.3 ± 8.9	92.8 ± 3.6	0.0 ± 0.0	88.2 ± 6.7
2	13.3 ± 14.6	94.0 ± 2.6	4.1 ± 5.8	89.7 ± 7.5	5.3 ± 7.4	82.0 ± 9.2
3	7.5 ± 7.3	94.7 ± 2.2	3.7 ± 4.7	90.3 ± 7.2	2.5 ± 3.5	82.0 ± 1.7
6	1.9 ± 2.0	45.0 ± 10.0	1.5 ± 2.1	13.5 ± 3.5	1.5 ± 2.1	7.3 ± 4.4
7	3.7 ± 2.9	69.5 ± 0.7	0.7 ± 0.9	30.7 ± 1.1	2.2 ± 3.1	10.0 ± 4.3
8	11.0 ± 7.6	89.0 ± 0.0	6.0 ± 2.8	54.0 ± 6.5	0.5 ± 0.7	23.9 ± 5.7
9	19.7 ± 4.1	69.7 ± 10.1	12.9 ± 5.4	44.0 ± 15.6	0.0 ± 0.0	21.4 ± 9.4
10	20.5 ± 7.2	93.0 ± 1.4	15.8 ± 6.8	79.0 ± 8.5	0.5 ± 0.7	48.7 ± 9.0
11	23.0 ± 2.0	90.0 ± 4.2	14.4 ± 20.4	65.0 ± 6.4	1.7 ± 2.3	39.0 ± 8.4
12	13.3 ± 13.0	94.5 ± 2.1	13.0 ± 2.8	79.3 ± 10.7	1.7 ± 1.0	42.2 ± 9.8
13	16.2 ± 1.9	92.0 ± 2.8	19.7 ± 6.6	82.2 ± 12.1	9.7 ± 2.3	60.3 ± 10.2
14	45.0 ± 10.0	94.8 ± 3.6	25.8 ± 1.7	91.3 ± 7.0	8.2 ± 8.2	80.7 ± 9.0
15	35.0 ± 10.0	93.7 ± 3.5	27.5 ± 7.7	87.9 ± 9.9	11.5 ± 0.7	83.7 ± 6.1
16	11.7 ± 3.7	77.5 ± 11.3	3.5 ± 4.9	54.0 ± 14.5	0.0 ± 0.0	32.0 ± 11.6

[a] Wild-type and MDR (DNM-R150) parasites were exposed to 30, 15, and 7.5 μM different sesquiterpenes in the absence and presence of 150 μM DNM, respectively. The results are expressed as a percentage of growth inhibition relative to control growth in the absence of sesquiterpene. The data shown are the average of three independent experiments ± SD.

defining the absolute configuration of **1** as (1*R*,2*R*,4*S*,5*R*,7*S*,9*S*,10*R*)-2-acetoxy-1-benzoyloxy-9-cinnamoyloxy-4-hydroxydihydro-β-agarofuran.

Compounds **3**, **6**, **7**, and **9** had three chromophore groups located at C-1, C-3, and C-9. An analysis of the dihedral angle showed that the opposite 1,3 and 1,9 pairwise interactions added to each other but did not cancel because of the different intensities of the different chromophores. On the other hand, the 3,9 pairwise interaction was almost coplanar.[30] Furthermore, compounds **3** and **6** showed a split curve very similar to that of **1** (Table 4), with a first positive and second negative Cotton effect around 270 and 226 nm, respectively, the weak value of $\Delta\epsilon$ for **3** and **6** with respect to **1** being due to the presence of an additional chromophore on C-3. These data allowed us to determine their absolute configurations of compounds **3** and **6**. On the other hand, an analysis of the CD spectra of compounds **7** and **9**, showing a Davydof-type split curve (Table 4), led to the assignment of their absolute configurations.

Compounds **8** and **9** have the same molecular formula, the main differences being the regiosubstitution patterns. Compound **8** had a nicotinate unit at C-1 and two benzoate units at C-8 and C-9; its CD spectra (Table 4) showed a first Cotton effect at 236.3 nm ($\Delta\epsilon = +12.1$), but we could not observe the second Cotton effect because of the opposite pairwise interactions between the three chromophores together with the strong positive absorption overlaying background ellipticity,[33] which destroyed the second component of the split curve. The absolute configuration of **8** was established as (1*R*,2*S*,3*S*,4*S*,5*R*,7*S*,8*S*,9*R*,10*R*)-2,3-diacetoxy-8,9-dibenzoyloxy-1-nicotinoiloxy-4-hydroxydihydro-β-agarofuran.

The CD spectra of **12** and **13** (Table 4) showed split curves with a first positive and a second negative Cotton effect due to the couplings of the C-9β with C-1α and C-1α with C-2α, supporting the absolute configuration as that ascribed to both compounds.

The new compounds have the basic polyhydroxy skeletons of 3,6-dideoxymagellanol (**1**),[30] 6-deoxymagellanol (**3**),[30] magellanol (**6** and **7**),[30] isomagellanol (**8** and **9**),[29] 2α-hydroxy-8-*epi*-celapanol (**12**),[29] 2α,4β-dihydroxy-8-*epi*-celapanol (**13**),[29] 3-deoxymaytol (**14**),[36] and 3,4-dideoxymaytol (**15**).[36]

Agarofuran sesquiterpenes are new promising MDR modulators in eukaryotic organisms.[15,16] The reversal effects of 15 dihydro-β-agarofuran sesquiterpenes in a MDR *L. tropica* (*L. tropica)* line grown in the presence of daunomycin (DNM) were studied by using an MTT-based assay. Their intrinsic parasite cytotoxicity was determined by using the same concentration of modulators in the parental wild-type parasites. Table 5 shows that after 72 h of incubation of MDR parasites in the presence of 150 μM DNM with increasing amounts of sesquiterpenes, a concentration-dependent growth inhibition (GI) was observed compared with control cells, grown with the same DNM concentration but in the absence of modulator. The chemosensitization to 150 μM DNM was very efficient for most of the sesquiterpenes tested, but the effective concentration varied between each one. In this form, 7.5 μM of **1**−**3**, **14**, and **15** produce more than 80% GI, requiring a double concentration (15 μM) of **10**, **12**, and **13** and around a 4-fold concentration (30 μM) of **8**, **11**, and **16** to obtain similar reversal effects. This effect is not due to an intrinsic cytotoxicity of sesquiterpenes, as deduced for the low growth inhibition produced by these compounds in the parental wild-type line (Table 5), except for compounds **14** and **15** that at 30 μM produce 45% and 35% GI in the wild-type line, respectively.

DNM resistance in the MDR *L. tropica* line is related to a decreased intracellular drug accumulation mainly due to the Pgp-like transporter overexpression.[24] To analyze if the reversal effect observed by some sesquiterpenes correlated with an increased drug accumulation, as a consequence of the Pgp inhibition, we studied by laser flow cytometry their effect on calcein (CAL) accumulation. Calcein acetoxymethyl ester (Cal-AM) is a highly lipophilic, nonfluorescent, mammalian Pgp substrate that rapidly penetrates the plasma membrane of cells. By cleavage of the ester bonds, intracellular esterases transform the dye into a hydrophilic and intensively fluorescent free acid form (Cal) that cannot be transported by Pgp. This property makes Cal-AM an excellent compound for studying the modulation of mammalian Pgp function,[37] and it has also been recently used to study ABC-like transporter activities in different *Leishmania* lines.[38] Flow cytometry analysis of intra-

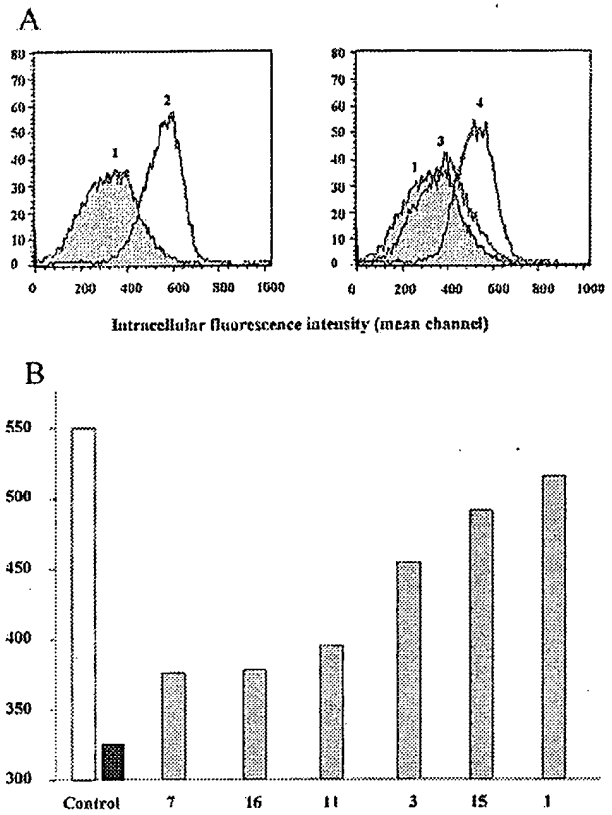

Figure 3. Differential modulation by sesquiterpenes of CAL accumulation in a resistant *L. tropica* line. Fluorescence intensity histograms were obtained by flow cytometry after incubation for 1 h at 28 °C with 2 μM CAL-AM in the presence or absence of 5 μM sesquiterpenes. A total of 10 000 cells were counted for each histogram. Experiments were repeated three times and gave essentially the same profiles as the ones shown here. (A) Profiles 1 and 2 correspond to fluorescence histograms of resistant and wild-type parasites, respectively, incubated in the absence of sesquiterpenes. Profiles 3 and 4 correspond to fluorescence histograms of resistant parasites incubated in the presence of 5 μM sesquiterpenes **7** and **1**, respectively. (B) Wild-type (white bar) and resistant (black bar) parasites incubated with 2 μM CAL-AM are used as control of CAL accumulation. Resistant parasites (gray bars) are incubated with 2 μM CAL-AM in the presence of 5 μM of different sesquiterpenes (**7**, **16**, **11**, **3**, **15**, and **1**).

cellular Cal accumulation (Figure 3A) demonstrated that, as expected, the resistant line accumulated a significantly lower amount of dye (Profile 1), expressed as the mean fluorescence channel ($m = 324$), than the wild-type line ($m = 550$) (profile 2). Co-incubation of the resistant parasites with 5 μM of the most active sesquiterpene **1** resulted in a significant shift of the peak of fluorescence distribution to the right, almost to the control level ($m = 514$) (profile 4). This reversal effect was a consequence of an increased CAL accumulation probably due to Pgp-like transporter inhibition. The same concentration of a sesquiterpene that gave a moderate reversal effect, **7**, only produced a slight increase in the intracellular dye ($m = 376$) (profile 3). Indeed, Figure 3B shows that different sesquiterpenes with distinct reversal efficiencies restored the dye accumulation in the MDR *Leishmania* line with an order of efficiency similar to that obtained with the DNM chemosensitization experiments: **1** > **15** ≥ **3** > **11** > **16** ≥ **7**, with no significant effects in the wild-type line (not shown). These results indicate that the measurement of CAL accumulation may be used to test the reversal effects of possible modulators of the Pgp-mediated MDR phenotype in *Leishmania*.

Preliminary structure–activity relationships from these natural sesquiterpenes revealed the following trends. The substituent at the C-6 position proved to be essential for the reversal activity because the presence of protons at C-6 produces a 10-fold higher chemosensitization with respect to the presence in the same position of an ester group (**3** versus **6**). On the other hand, the substituent at C-8 proved to be significant for the potency of the activity, **3** being 2- and 4-fold more active than **11** and **8**, respectively. In addition, the substituent at C-3 exhibited a slight decrease in the activity (**1** versus **3**), and the substituent at C-1 also modified the activity, being that **10** is 2-fold more active than **8**. Finally, the often tertiary hydroxy group at C-4β does not seem to be important for optimal reversal activity because its presence or absence does not produce significant modification of the activity (**14** versus **15**). These and previous results[15] suggest that the size of the substituent could strongly affect the reversal activity of the compound; the presence of additional ester groups on the basic polyhydroxy skeletons has probably made the compounds too bulky to bind at the active site, being detrimental to the reversal activity associated with these sesquiterpenes.

Dihydro-β-agarofuran sesquiterpenes have proven to be a very interesting class of natural products with a high reversal effect of the MDR phenotype mediated by Pgp-like transporters. Further efforts to elucidate the specific target of these compounds in the Pgp-like transporter, as well as to determine if they are transported, are underway for a better knowledge of their mechanism of action.

Experimental Section

General Experimental Procedures. Optical rotations were measured on a Perkin-Elmer 241 automatic polarimeter, and the $[\alpha_D]$ are given in 10^{-1} deg cm^2 g^{-1}. IR (film) spectra were recorded on a Bruker IFS 55 spectrophotometer, and UV spectra were collected in absolute EtOH on a JASCO V-560. ^{1}H and ^{13}C NMR spectra were recorded on a Bruker AMX-500, a Bruker Avance 400, or a Bruker Avance 300 spectrometer. EIMS and HREIMS were recorded on a Micromass Autospec spectrometer. Purification was performed using silica gel (particle size 40–63 μM, Merck and HPTLC-Platten-Sil 20 UV_{254}, Panreac), and Sephadex LH-20 (Pharmacia) and was monitored by TLC 1500/LS 25 Schleicher and Schüell foils. Compounds used for CD were purified by HPLC using a semipreparative μ-porasil column column (Waters, 10 μM, 19 mm × 25 cm) and were eluted with a mixture of *n*-hexane/EtOAc (1:1).

Plant Material, Extraction, and Isolation. *M. magellanica* was collected in December 1993 in the Novena Región in the Temuca province on the slopes of the Osorno volcano in Chile and was identified by Prof. Sebastián Teyller, and a voucher specimen is on file at the Facultad de Ciencias (93-5342-A), Universidad de Chile, Santiago. The root bark of the plant (390 g) was extracted with *n*-hexane/Et_2O (1:1) in a Soxhlet apparatus. The extract (7.8 g) was chromatographed on Sephadex LH-20 (*n*-hexane/$CHCl_3$/MeOH, 2:1:1) to afford 55 fractions. Fractions 28–40 after chromatography over silica gel (*n*-hexane/AcOEt of increasing polarity), Sephadex LH-20 (*n*-hexane-$CHCl_3$-MeOH, 2:1:1), and preparative HPTLC (HPTLC-Platten-Sil 20 UV_{254}) gave rise to the new compounds **1** (9.3 mg), **3** (10.7 mg), **6** (3.1 mg), **7** (1.9 mg), **8** (12.3 mg), **9**

(20.6 mg), **12** (1.9 mg), **13** (6 mg), and **14** (2.2 mg) and the known compounds **2**, **4**, **5**, **10**, and **11**.

M. chubutensis was collected in December 1994 in the Séptima Región in the Talca province, Chile, and was identified by Prof. José San Martín, and a voucher specimen is lodged with the Facultad de Ciencias (93-5200), Universidad de Chile, Santiago. Air-dried, chopped root bark of the plant (390 g) was extracted with *n*-hexane/Et_2O (1:1) in a Soxhlet apparatus. The extract (7.8 g) was chromatographed on silica gel using gradients of *n*-hexane/AcOEt as eluent to afford 180 fractions. Fractions 144−160 (900 mg) after chromatography over Sephadex LH-20 (*n*-hexane/$CHCl_3$/MeOH, 2:1:1) and preparative HPTLC (HPTLC-Platten-Sil 20 UV_{254}) gave rise to the new compounds **14** (12 mg) and **15** (6 mg) and the known compounds **16** and **17**.

(1*R*,2*R*,4*S*,5*R*,7*S*,9*S*,10*R*)-2-Acetoxy-1-benzoyloxy-9-cinnamoyloxy-4-hydroxydihydro-β-agarofuran (1). Colorless lacquer; $[\alpha]^{25}_D$ +14.8° (*c* 0.93, $CHCl_3$); UV λ_{max} (EtOH) 275, 223, 218 nm; IR γ_{max} (film) 3541, 2956, 2922, 1735, 1708, 1638, 1450, 1271, 1166, 756, 712 cm^{-1}; ^1H NMR ($CDCl_3$) δ 1.33 (3H, s), 1.39 (3H, s), 1.45 (3H, s), 1.83 (3H, s), 2.86 (1H, s), 6.46 (1H, d, *J* = 16.0 Hz), 7.29 (2H, m), 7.40 (3H, m), 7.46 (2H, m), 7.56 (2H, m), 7.78 (2H, m), for other signals, see Table 1; ^{13}C NMR ($CDCl_3$) δ 20.9 (q), 118.7 (d), 128.2 (4 × d), 128.7 (2 × d), 129.3 (2 × d), 130.1 (s, d), 132.8 (d), 134.7 (s), 144.6 (d), 165.3 (s), 166.1 (s), 170.4 (s), for other signals, see Table 2; MS (EI) *m/z* (%) 562 (M^+, 10), 547 (2), 502 (1), 440 (1), 414 (3), 399 (15), 372 (4), 339 (3), 249 (6), 232 (5), 217 (4), 203 (3), 188 (7), 147 (6), 131 (88), 105 (100), 77 (25), 57 (2). HRMS (EI) *m/z* Calcd for $C_{33}H_{38}O_8$: 562.256 67. Found: 562.259 03.

(1*R*,2*S*,3*S*,4*S*,5*R*,7*R*,9*S*,10*R*)-2-Acetoxy-9-benzoyloxy-1-cinnamoyloxy-3-nicotinoyloxy-4-hydroxydihydro-β-agarofuran (3). Colorless lacquer; $[\alpha]^{25}_D$ +33.2° (*c* 1.07, $CHCl_3$); UV λ_{max} (EtOH) 272, 223 nm; IR γ_{max} (film) 3532, 2966, 2932, 1732, 1282, 1263, 1026, 755, 710 cm^{-1}; ^1H NMR ($CDCl_3$) δ 1.34 (3H,s), 1.53 (3H, s), 1.61 (3H, s), 1.77 (3H, s), 3.41 (1H, s), 6.40 (1H, d, *J* = 16.0 Hz), 7.28 (4H, m), 7.38 (2H, m), 7.49 (4H, m), 7.98 (2H, m), 8.56 (1H, d, *J* = 8.0 Hz), 8.90 (1H, d, *J* = 3.3 Hz), 8.60 (1H, s), for other signals, see Table 1; ^{13}C NMR ($CDCl_3$) δ 20.6 (q), 118.0 (d), 123.4 (d), 126.2 (s), 128.7 (4 × d), 129.1 (2 × d), 129.2 (s), 129.5 (2 × d), 130.3 (d), 132.9 (d), 134.5 (s), 137.5 (d), 145.1 (d), 151.5 (d), 153.5 (d), 164.4 (s), 164.8 (s), 166.0 (s), 170.4 (s), for other signals, see Table 2; MS (EI) *m/z* (%) 683 (M^+, 4), 668 (11), 642 (4), 573 (3), 538 (11), 520 (5), 202 (2), 149 (21), 131 (40), 105 (100), 97 (13), 77 (17). HRMS (EI) *m/z* Calcd for $C_{39}H_{41}NO_{10}$: 683.273 05. Found: 683.273 24.

(1*R*,2*S*,3*S*,4*S*,5*S*,6*R*,7*R*,9*S*,10*R*)-2,6-Diacetoxy-1-benzoyloxy-9-cinnamoyloxy-3-nicotinoyloxy-4-hydroxydihydro-β-agarofuran (6). Colorless lacquer; $[\alpha]^{25}_D$ +9.7° (*c* 0.31, $CHCl_3$); UV λ_{max} (EtOH) 271, 223 nm; IR γ_{max} (film) 3531, 2924, 2854, 1735, 1459, 1236, 1107, 1026, 711 cm^{-1}; ^1H NMR ($CDCl_3$) δ 1.52 (3H, s), 1.57 (3H, s), 1.62 (3H, s), 1.75 (3H, s), 2.11 (3H, s), 3.56 (1H, s), 6.35 (1H, d, *J* = 16.0 Hz), 7.25 (2H, m), 7.46 (5H, m), 7.50 (3H, m), 7.69 (2H, m), 8.53 (1H, d, *J* = 7.9 Hz), 8.88 (1H, d, *J* = 3.9 Hz), 9.58 (1H, s), for other signals, see Table 1; ^{13}C NMR ($CDCl_3$) δ 21.5 (q), 22.7 (q), 117.9 (d), 123.5 (d), 126.2 (s), 128.3 (4 × d), 128.8 (2 × d), 129.3 (2 × d), 129.6 (s), 130.3 (d), 133.1 (d), 134.4 (s), 137.6 (d), 145.6 (d), 151.6 (d), 153.7 (d), 164.5 (s), 164.9 (s), 165.8 (s), 170.3 (s), 170.4 (s), for other signals, see Table 2; MS (EI) *m/z* (%) 741 (M^+, 12), 700 (15), 610 (4), 596 (24), 578 (7), 326 (6), 131 (100), 124 (16), 105 (29), 97 (26), 71 (28), 57 (36). HRMS (EI) *m/z* Calcd for $C_{41}H_{43}NO_{12}$: 741.285 23. Found: 741.282 47.

(1*R*,2*S*,3*S*,4*S*,5*S*,6*R*,7*R*,9*S*,10*R*)-2,6-Diacetoxy-1,9-dibenzoyloxy-3-nicotinoyloxy-4-hydroxydihydro-β-agarofuran (7). Colorless lacquer; $[\alpha]^{25}_D$ −5.3° (*c* 0.19, $CHCl_3$); UV λ_{max} (EtOH) 264, 225 nm; IR γ_{max} (film) 3350, 2955, 2856, 1736, 1451, 1368, 1284, 1236, 1111, 709 cm^{-1}; ^1H NMR ($CDCl_3$) δ 1.53 (3H, s), 1.62 (3H, s), 1.65 (3H, s), 1.71 (3H, s), 2.12 (3H, s), 3.66 (1H, s), 7.28 (3H, m), 7.44 (3H, m), 7.52 (3H, m), 7.99 (2H, m), 8.58 (1H, d, *J* = 7.8 Hz), 8.92 (1H, d, *J* = 3.9 Hz), 9.66 (1H, s), for other signals, see Table 1; ^{13}C NMR ($CDCl_3$) δ 21.4 (q), 22.6 (q), 123.4 (d), 126.1 (s), 128.0 (2 × d), 128.2 (2 × d), 129.1 (2 × d), 129.3 (s), 129.4 (s), 130.1 (2 × d), 132.9 (d), 133.1 (d), 137.4 (d), 151.5 (d), 153.7 (d), 163.5 (s), 164.4 (s), 164.5 (s), 169.5 (s), 170.2 (s), for other signals, see Table 2; MS (EI) *m/z* (%) 715 (M^+, 8), 700 (16), 594 (3), 578 (7), 536 (4), 139 (6), 124 (13), 105 (100), 91 (20), 71 (24), 57 (39). HRMS (EI) *m/z* Calcd for $C_{39}H_{41}NO_{12}$: 715.262 88. Found: 715.264 65.

(1*R*,2*S*,3*S*,4*S*,5*R*,7*S*,8*S*,9*R*,10*R*)-2,3-Diacetoxy-8,9-dibenzoyloxy-1-nicotinoiloxy-4-hydroxydihydro-β-agarofuran (8). Colorless lacquer; $[\alpha]^{25}_D$ +27.6° (*c* 1.23, $CHCl_3$); UV λ_{max} (EtOH) 264, 226 nm; IR γ_{max} (film) 3528, 2969, 1733, 1591, 1451, 1277, 1116, 1067, 1026, 755, 709 cm^{-1}; ^1H NMR ($CDCl_3$) δ 1.39 (3H, s), 1.52 (3H, s), 1.73 (3H, s), 1.75 (3H, s), 2.32 (3H, s), 3.42 (1H, s), 7.28 (3H, m), 7.45 (3H, m), 7.58 (3H, m), 7.96 (3H, m), 8.67 (1H, d, *J* = 4.4 Hz), 8.89 (1H, s), for other signals, see Table 1; ^{13}C NMR ($CDCl_3$) δ 20.1 (q), 21.0 (q), 123.1 (d), 125.4 (s), 128.0 (2 × d), 128.2 (2 × d), 129.2 (2 × d), 129.5 (s), 129.7 (s), 130.3 (2 × d), 132.9 (d), 133.2 (d), 137.0 (d), 150.8 (d), 153.5 (s), 164.0 (s), 164.7 (s), 165.7 (s), 170.3 (2 × s), for other signals, see Table 2; MS (EI) *m/z* (%) 715 (M^+, 2), 700 (30), 578 (24), 536 (3), 476 (2), 372 (1), 294 (2), 228 (3), 131 (4), 124 (15), 105 (100), 77 (11). HRMS (EI) *m/z* Calcd for $C_{39}H_{41}NO_{12}$: 715.284 01. Found: 715.2832.

(1*R*,2*S*,3*S*,4*S*,5*R*,7*S*,8*S*,9*R*,10*R*)-2,8-Diacetoxy-3,9-dibenzoyloxy-1-nicotinoyloxy-4-hydroxydihydro-β-agarofuran (9). Colorless lacquer; $[\alpha]^{25}_D$ +12.8° (*c* 0.21, $CHCl_3$); UV λ_{max} (EtOH) 271, 226 nm; IR γ_{max} (film) 3535, 2960, 2928, 1734, 1591, 1367, 1282, 1117, 1026, 754, 708 cm^{-1}; ^1H NMR (C_6D_6) δ 1.04 (3H, s), 1.12 (3H, s), 1.45 (3H, s), 1.58 (3H, s), 1.75 (3H, s), 3.43 (1H, s), 6.99 (3H, m), 6.78 (2H, m), 7.33 (1H, m), 7.52 (2H, m), 7.81 (2H, m), 8.40 (3H, m), 10.1 (1H, s), for other signals, see Table 1; ^{13}C NMR ($CDCl_3$) δ 20.0 (q), 20.8 (q), 123.5 (d), 126.1 (s), 128.2 (2 × d), 128.3 (2 × d), 129.2 (2 × d), 129.4 (s), 129.8 (s), 130.8 (2 × d), 133.0 (d), 133.1 (d), 135.7 (d), 151.5 (d), 153.9 (d), 164.3 (s), 164.5 (s), 165.6 (s), 169.7 (s), 170.4 (s), for other signals, see Table 2; MS (EI) *m/z* (%) 715 (M^+, 1), 700 (23), 578 (11), 536 (2), 354 (1), 294 (1), 231 (1), 189 (2), 131 (4), 124 (9), 105 (100), 77 (12). HRMS (EI) *m/z* Calcd for $C_{39}H_{41}NO_{12}$: 715.262 88. Found: 715.264 08.

(1*R*,2*S*,4*R*,5*S*,6*R*,7*R*,8*S*,9*R*,10*S*)-6,8-Diacetoxy-1,9-dibenzoyloxy-2-nicotinoyloxydihydro-β-agarofuran (12). Colorless lacquer; $[\alpha]^{25}_D$ +31.0° (*c* 0.19, $CHCl_3$); UV λ_{max} (EtOH) 264, 229 nm; IR γ_{max} (film) 2924, 2860, 1728, 1272, 1220, 1125, 1107, 711 cm^{-1}; ^1H NMR ($CDCl_3$) δ 1.30 (3H, d, *J* = 7.7 Hz), 1.52 (3H, s), 1.64 (3H, s), 1.84 (3H, s), 2.16 (3H, s), 2.62 (1H, m), 7.25 (2H, m), 7.26 (2H, m), 7.37 (3H, m), 7.43 (2H, m), 7.46 (2H, m), 7.82 (2H, m), 8.14 (1H, d, *J* = 8.1 Hz), 8.76 (1H, d, *J* = 3.9 Hz), 9.11 (1H, d; *J* = 0.7 Hz), for other signals, see Table 1; ^{13}C NMR ($CDCl_3$) δ 20.9 (q), 21.2 (q), 123.4 (d), 126.0 (s), 127.9 (2 × d), 128.0 (2 × d), 128.4 (s), 128.9 (s), 129.2 (2 × d), 130.0 (2 × d), 132.7 (d), 133.1 (d), 137.0 (d), 150.0 (d), 153.5 (d), 164.9 (s), 165.1 (s), 165.3 (s), 169.2 (s), 169.6 (s), for other signals, see Table 2; MS (EI) *m/z* (%) 699 (M^+, 3), 684 (12), 657 (19), 536 (2), 520 (3), 124 (12), 105 (100), 77 (10). HRMS (EI) *m/z* Calcd for $C_{39}H_{41}NO_{11}$: 699.267 96. Found: 699.270 32.

(1*R*,2*S*,4*S*,5*S*,6*R*,7*R*,8*S*,9*R*,10*S*)-6,8-Diacetoxy-1,2,9-tribenzolyoxy-4-hydroxydihydro-β-agarofuran (13). Colorless lacquer; $[\alpha]^{25}_D$ +9.7° (*c* 0.31, $CHCl_3$); UV λ_{max} (EtOH) 274, 231 nm; IR γ_{max} (film) 3545, 2959, 2924, 1727, 1451, 1265, 1110, 1027, 801, 756, 709 cm^{-1}; ^1H NMR ($CDCl_3$) δ 1.60 (3H, s), 1.61 (3H, s), 1.70 (3H, s), 1.84 (3H, s), 2.17 (3H, s), 2.98 (1H, s), 7.19 (2H, m), 7.45 (7H, m), 7.54 (2H, m), 7.83 (2H, m), 7.89 (2H, m), for other signals, see Table 1; ^{13}C NMR ($CDCl_3$) δ 20.6 (q), 21.5 (q), 127.9 (2 × d), 128.1 (2 × d), 128.6 (2 × d), 129.0 (s), 129.3 (2 × d, s), 129.4 (2 × d), 129.8 (s), 130.1 (2 × d), 132.7 (d), 133.1 (d), 133.2 (d), 165.0 (s), 165.2 (s), 165.6 (s), 169.1 (s), 169.9 (s), for other signals, see Table 2; MS (EI) *m/z* (%) 592 (M^+ − 122, 1), 532 (15), 472 (1), 419 (1), 335 (2), 246 (2), 202 (22), 151 (1), 105 (100), 77 (9). HRMS (EI) *m/z* Calcd for $C_{33}H_{36}O_{10}$: 592.230 85. Found: 592.228 79.

1α,15-Diacetoxy-6β,9β-dibenzoyloxy-2α-nicotinoyloxy-4β-hydroxydihydro-β-agarofuran (14). Colorless lacquer; $[\alpha]^{25}_D$ +15.4° (*c* 0.22, $CHCl_3$); UV λ_{max} (EtOH) 273, 229 nm; IR γ_{max} (film) 3555, 2955, 2925, 2854, 1747, 1718, 1591, 1452, 1274, 1106, 1024, 758, 713 cm^{-1}; ^1H NMR ($CDCl_3$) δ 1.57 (6H, s), 1.59 (3H, s), 1.62 (3H, s), 2.26 (4H, m), 2.71 (1H, m), 3.13

(1H, s), 7.47 (5H, m), 7.59 (2H, m), 8.07 (2H, m), 8.18 (2H, m), 8.40 (1H, d, $J = 7.9$ Hz), 8.80 (1H, s), 9.30 (1H, s), for other signals, see Table 1; ^{13}C NMR ($CDCl_3$) δ 20.3 (q), 21.2 (q), 123.6 (d), 125.3 (s), 128.4 (2 × d), 128.6 (2 × d), 128.9 (s), 129.7 (s), 130.1 (4 × d), 133.4 (d), 133.6 (d), 137.2 (d), 151.1 (d), 153.8 (d), 164.4 (s), 165.2 (s), 166.2 (s), 169.2 (s), 170.8 (s), for other signals, see Table 2; MS (EI) *m/z* (%) 715 (M^+, 4), 700 (4), 595 (2), 470 (19), 275 (5), 228 (9), 124 (14), 105 (100), 77 (10). HRMS (EI) *m/z* Calcd for $C_{39}H_{41}NO_{12}$: 715.262 88. Found: 715.255 19.

1α,15-Diacetoxy-6β,9β-dibenzoyloxy-2α-nicotinoyloxydihydro-β-agarofuran (15). Colorless lacquer; $[\alpha]^{25}_D$ +70.0° (*c* 0.39, $CHCl_3$); UV λ_{max} (EtOH) 264, 229 nm; IR γ_{max} (film) 2954, 2924, 2850, 1747, 1720, 1590, 1451, 1272, 1106, 1025, 757, 712 cm^{-1}; ^1H NMR ($CDCl_3$) δ 0.87 (3H, d, $J = 6.8$ Hz), 1.52 (6H, s), 1.53 (3H, s), 2.10 (3H, m), 2.34 (3H, s), 7.49 (5H, m), 7.60 (2H, m), 8.06 (4H, m), 8.41 (1H, d, $J = 8.0$ Hz), 8.79 (1H, s), 9.29 (1H, s), for other signals, see Table 1; ^{13}C NMR ($CDCl_3$) δ 20.3 (q), 21.2 (q), 123.5 (d), 125.4 (s), 128.3 (2 × d), 128.7 (2 × d), 129.0 (s), 129.5 (2 × d), 129.8 (s), 130.1 (2 × d), 133.5 (d), 133.6 (d), 137.4 (d), 151.3 (d), 153.3 (d), 164.6 (s), 165.3 (s), 165.6 (s), 169.3 (s), 170.9 (s), for other signals, see Table 2; MS (EI) *m/z* (%) 699 (M^+, 22), 684 (14), 228 (5), 174 (4), 124 (13), 105 (100), 77 (8). HRMS (EI) *m/z* Calcd for $C_{39}H_{41}NO_{11}$: 699.267 96. Found: 699.267 85.

Biological Assays. 1. Parasite Culture. The wild-type *L. tropica* LRC strain was a clone obtained by agar plating.[39] An *L. tropica* line highly resistant to DNM (DNM-R150) was maintained in the presence of 150 μM DNM and used as previously described.[24] This resistant line had an MDR phenotype similar to that of tumor cells, with a cross-resistance profile to several drugs and an overexpressed drug–efflux Pgp-like transporter.[24] Promastigote forms were grown at 28 °C in RPMI 1640-modified medium (Gibco)[40] and supplemented with 20% heat-inactivated fetal bovine serum (Gibco).

2. DNM Chemosensitization Experiments. The viability of parasites in the presence of the different sesquiterpenes was analyzed by an MTT-based assay.[41,42] The screening was performed in flat-bottomed 96-well plastic plates maintained at 28 °C. Promastigote forms from a logarithmic phase culture were suspended in fresh medium to yield 6×10^6 cells/mL. Each well was filled with 50 μL of the parasite suspension (3×10^5 cells). Stock solutions of sesquiterpenes dissolved in DMSO were diluted directly in the culture medium at suitable concentrations, and 50 μL was added to each well. The final DMSO content did not exceed 0.3%, which had no effect on parasite growth. To assess the chemosensitizing activity of sesquiterpenes, promastigotes of *L. tropica* MDR line were exposed to both DNM (150 μM) and sesquiterpenes. To determine the intrinsic toxicity of the sesquiterpenes, the wild-type *L. tropica* lines were exposed to the sesquiterpenes in the absence of DNM. After 72 h of incubation at 28 °C, the viability of promastigotes was determined by the colorimetric MTT assay. A total of 10 μL of 3-(4,5-dimethylthiazol-2-yl)-2,5-diphenyltetrazolium bromide (MTT) (5 mg/mL in PBS) was added to each well, and plates were incubated for an additional period of 4 h. Water-insoluble formazan crystals were dissolved by adding 100 μL of 20% SDS, and absorbance was read at 540 nm using a microplate reader (Beckman Biomek 2000). Cell survival was determined by dividing the absorbance at a given sesquiterpene concentration by the absorbance of control cells. The results are expressed as percent growth inhibition (GI).

3. Reversion of Calcein Accumulation in a MDR *L. tropica* Line Overexpressing a Pgp-like Transporter. The accumulation of CAL-AM fluorescent dye in wild-type and resistant *Leishmania* lines was estimated by flow cytometry using a Becton Dickinson FacScan, as described for mammalian cells[37] and for *Leishmania* spp.,[38] with some modifications. Briefly, parasites were incubated with 2 μM CAL-AM (Molecular Probes Europe BV, The Netherlands) for 1 h at 28 °C in HPMI/glucose buffer (10 mM HEPES, 120 mM NaCl, 5 mM Na_2HPO_4, 0.4 mM $MgCl_2$, 0.04 mM $CaCl_2$, 10 mM $NaHCO_3$, 10 mM glucose, 5 mM KCl, pH 7.4) in the presence or in the absence of different concentrations of sesquiterpenes. Parasites were then extensively washed, resuspended in cold phosphate-buffered saline (PBS: 1.2 mM KH_2PO_4, 8.1 mM Na_2HPO_4, 130 mM NaCl, 2.6 mM KCl adjusted to pH 7.4), and immediately analyzed. Cells were gated on the basis of size and complexity to eliminate dead cells and debris from the analysis. Quantification of intracellular fluorescence was carried out by scanning the emission between 515 and 545 nm (FL-1) using the Cell Quest software application.

Acknowledgment. This study was supported by the Spanish Grants CICYT-FEDER IFD97-0747-C04-03 (A.G. and S.C.), PPQ2000-1655-C02-02 (F.G.), PB98-0115 (S.C.) PB96-1033 and PB97-1039 (F.G.), BQU2000-0870-CO2-01 (I.A.J.), Gobierno Autónomo de Canarias, and ITC. We thank Pilar Navarro for her help in parasite culture and Prof. J. T. Vázquez for carrying out the CD experiments. We also acknowledge Pharmacia & Upjohn (Barcelona, Spain) for providing the daunomycin used in this study. M.L.K. thanks the A.E.C.I. for a fellowship (Becas MUTIS). F.C.S. was the recipient of a fellowship (B.E.F.I. exp 00/9068) from the Fondo de Investigación Sanitaria, Instituto de Salud Carlos III, Ministerio de Sanidad y Consumo, Spain.

Supporting Information Available: IR, UV, MS, HRMS, and NMR spectra for the new compounds described, and the CD spectra of compounds **1**, **3**, **6–9**, **12**, and **13**. This material is available free of charge via the Internet at http://pubs.acs.org.

References

(1) González, A. G.; Bazzocchi, I. L.; Moujir, L. M.; Jiménez, I. A. Ethnobotanical Uses of Celastraceae. Bioactive Metabolites. In *Studies in Natural Products Chemistry, Bioactive Natural Products (Part D)*; Elsevier Science Publisher: Amsterdam, 2000; Vol. 23, pp 649–738.

(2) Muñoz, O.; Peñaloza, A.; González, A. G.; Ravelo, A. G.; Crespo, A.; Bazzocchi, I. L.; Alvarenga, N. L. Celastraceae, Bioactive Metabolites. In *Studies in Natural Products*; Elsevier Science Publisher: Amsterdam, 1996; Vol. 18, pp 739–785.

(3) Hussein, G.; Nakamura, N.; Meselhy, R. M.; Hattori, M. Phenolics from *Maytenus senegalensis*. *Phytochemistry* **1999**, *50*, 689–694.

(4) Simoés, C. M. O.; Mentz, A. L.; Schenkel, P. E.; Irgang, E. B.; Stehmann, R. J. Plantas da Medicina Popular do Rio Grande do Sul. In *Universidade Federal do Rio Grande do Sul*: do Rio Grande do Sul: Brazil, 1986.

(5) Souza-Formigoni, M. L. O.; Oliveira, M. G. M.; Monteiro, M. G.; Gomes da Silveira-Filho, N.; Braz, S.; Carlini, E. A. Antiulcerogenic effects of two *Maytenus* species in laboratory animals. *J. Ethnopharmacol.* **1991**, *34*, 21–27.

(6) Oliveira, M. G. M.; Monteiro, M. G.; Macaúbas, C.; Barbosa, V. P.; Carlini, E. A. Pharmacologic and toxicologic effects of two *Maytenus* species in laboratory animals. *J. Ethnopharmacol.* **1991**, *34*, 29–41.

(7) Moujir, L. M.; Navarro-Gutiérrez, A. M.; González, A. G.; Ravelo, A. G.; Luis, J. G. Netzahualcoyone mode of actino. *Antimicrob. Agents Chemother.* **1991**, *35*, 211–213.

(8) González, A. G.; Alvarenga, N. L.; Ravelo, A. G.; Bazzocchi, I. L.; Ferro, E. A.; Navarro, A. G.; Moujir, L. M. Scutione, a new bioactive norquinonemethide triterpene from *Maytenus scutiodes* (Celastraceae). *Bioorg. Med. Chem.* **1996**, *4*, 815–820.

(9) González, A. G.; Alvarenga, N. L.; Estévez-Braun, A.; Ravelo, A. G.; Bazzocchi, I. L.; Moujir, L. M. Structure and absolute configuration of triterpene dimers from *Maytenus scutioides*. *Tetrahedron* **1996**, *52*, 9597–9608.

(10) Brüning, R.; Wagner, H. Übersicht über die celastraceen–inholtsstoffe: chemie, chemotaxonomie, biosynthese, pharmakologie. *Phytochemistry* **1978**, *17*, 1821–1858.

(11) Zheng, Y. L.; Xu, Y.; Lin, J. F. Immunosuppresive effects of wilfortrine and euonine. *Acta Pharm. Sin.* **1989**, *24*, 568–572.

(12) Kuo, Y.; King, M.; Chen, G.; Chen, H.; Chen, C.; Chen, L.; Lee, K. Two new macrolide sesquiterpene pyridine alkaloids from *Maytenus emarginata*: emarginatine G and the cytotoxic emarginate F. *J. Nat. Prod.* **1994**, *57*, 263–269.

(13) González, A. G.; Jiménez, I. A.; Ravelo, A. G.; Coll, J.; González, J. A.; Lloria, J. Antifeedant activity of sesquiterpenes from Celastraceae. *Biochem. Syst.. Ecol.* **1997**, *25*, 513−519.
(14) Duan, H.; Takaishi, Y.; Bando, M.; Kido, M.; Imakura, Y.; Lee, K. Novel sesquiterpene esters with alkaloid and monoterpene and related compounds from *Tripterygium hypoglaucum*: a new class of potent anti-HIV agents. *Tetrahedron Lett.* **1999**, *40*, 2969−2972.
(15) Pérez-Victoria, J. M.; Tincusi, B. M.; Jiménez, I. A.; Bazzocchi, I. L.; Gupta, M. P.; Castanys, S.; Gamarro, F.; Ravelo, A. G. New natural sesquiterpenes as modulators of daunomycin resistance in a multidrug-resistant *Leishmania tropica* line. *J. Med. Chem.* **1999**, *42*, 4388−4393.
(16) Kim, S. E.; Ho Kim, Y.; Lee, J. J. New sesquiterpene ester from *Celastrus orbiculatus* reversing multidrug resistance in cancer cells. *J. Nat. Prod.* **1998**, *61*, 108−111.
(17) González, A. G.; Tincusi, B. M.; Bazzocchi, I. L.; Tokuda, H.; Nishino, H.; Konoshima, T.; Jiménez, I. A.; Ravelo, A. G. Antitumor promoting effects of sesquiterpenes from *Maytenus cuzcoina* (Celastraceae). *Bioorg. Med. Chem.* **2000**, *8*, 1773−1778.
(18) Nicolaou, K. C.; Pfefferkorn, J. A.; Roecker, A. J.; Cao, G. Q.; Barluenga, S.; Mitchell, H. J. Natural product-like combinatorial libraries based on privileged structures. 1. General principles and solid-phase synthesis of benzopyrans. *J. Am. Chem. Soc.* **2000**, *122*, 9939−9953 and references therein.
(19) Hirst, S. I.; Stapley, L. A. Parasitology: the dawn of a new millennium. *Parasitol. Today* **2000**, *16*, 1−3.
(20) Ambudkar, S. V.; Dey, S.; Hrycyna, C. A.; Ramachandra, M.; Pastan, I.; Gottesman, M. Biochemical, cellular and pharmacological aspects of the multidrug transporter. *Annu. Rev. Pharmacol. Toxicol.* **1999**, *39*, 361−398.
(21) Endicott, J. A.; Ling, V. The biochemistry of P-glycoprotein-mediated multidrug resistance. *Annu. Rev. Biochem.* **1989**, *58*, 137−171.
(22) Ullman, B. Multidrug Resistance and P-glycoproteines in Parasitic Protozoa. *J. Bioenerg. Biomembr.* **1995**, *27*, 77−84.
(23) Wilson, C. M.; Serrano, A. E.; Wasley, A.; Bogenschutz, M. P.; Shankar, A. H.; Wirth, D. F. Amplification of a gene related to the mammalian mdr genes in drug resistance *Plasmodium falciparum*. *Science* **1989**, *244*, 1184−1186.
(24) Chiquero, M. J.; Pérez-Victoria, J. M.; O'Valle, F.; Gonzalez-Ros, J. M.; del Moral, R.; Ferragut, J. A.; Castanys, S.; Gamarro, F. Altered drug membrane permeability in a multidrug-resistant *Leishmania tropica* line. *Biochem. Pharmacol.* **1998**, *55*, 131−139.
(25) Chow, L. M. C.; Wong, A. K. C.; Ullman, B.; Wirth, D. F. Cloning and functional analysis of an extrachromosomally amplified multidrug resistance-like gene in *Leishmania enriettl*. *Mol. Biochem. Pharmacol.* **1993**, *60*, 195−208.
(26) Henderson, D. M.; Sifri, C. D.; Rodgers, M.; Wirth, D. F.; Hendrickson, N.; Ullman, B. Multidrug resistance in *Leishmania donovani* is conferred by amplification of a gene homologous to the mammalian mdr1 gene. *Mol. Cell. Biol.* **1992**, *12*, 2855−2865.
(27) Ford, J. M.; Hait, W. N. Pharmacology of drugs that alter multidrug resistance in cancer. *Pharmacol. Rev.* **1990**, *42*, 155−199.
(28) Pérez-Victoria, J. M.; Chiquero, M. J.; Conseil, G.; Dayan, G.; Di Pietro, A.; Barron, D.; Castanys, S.; Gamarro, F. Correlation between the affinity of flavonoids binding to cytosolic site of *Leishmania tropica* multidrug transporter and their efficiency to revert parasite resistance to daunomycin. *Biochemistry* **1999**, *38*, 1736−1743.
(29) González, A. G.; Núñez, M. P.; Jiménez, I. A.; Ravelo, A. G.; Bazzocchi, I. L. Minor sesquiterpenes from *Maytenus magellanica*. *J. Nat. Prod.* **1993**, *56*, 2114−2119.
(30) González, A. G.; Núñez, M. P.; Ravelo, A. G.; Sazatornil, J. A.; Vázquez, J. T.; Bazzocchi, I. L.; Morales, E. Q.; Muñoz, O. M. Structural elucidation and absolute configuration of novel β-agarofuran (epoxyeudesmene) sesquiterpenes from *Maytenus magellanica* (Celastraceae). *J. Chem. Soc., Perkin Trans. 1* **1992**, 1437−1441.
(31) González, A. G.; Núñez, M. P.; Bazzocchi, I. L.; Ravelo, A. G.; Jiménez, I. A. Sesquiterpenes from *Maytenus magellanica* (Celastraceae). *Nat. Prod. Lett.* **1993**, *2*, 163−170.
(32) Muñoz, O. M.; González, A. G.; Ravelo, A. G.; Luis, J. G.; Vázquez, J. T.; Núñez, M. P.; Jiménez, I. A. Sesquiterpenes esters from *Maytenus distica* (Celastraceae). *Phytochemistry* **1990**, *29*, 3225−3228.
(33) Harada, N.; Nakanishi, K. *Circular Dichroism Spectroscopy Exciton Coupling in Organic Stereochemistry*; University Science Books: Mill Valley, CA, 1983.
(34) PC Model from Serena Software, P.O. Box 3076, Bloomington, IN 47402-3076.
(35) Tincusi, B. M.; Jiménez, I. A.; Ravelo, A. G.; Missico, R. New sesquiterpenes from *Crossopetalum tonduzii*. *J. Nat. Prod.* **1998**, *61*, 1520−1523.
(36) Kupchan, S. M.; Smith, R. M. Maytoline, maytine, and maytolidine, novel nicotinoyl sesquiterpene alkaloids from *Maytenus serrata*. *J. Org. Chem.* **1977**, *42*, 115−118.
(37) Hollo, Z.; Homolya, L.; Davis, C. W.; Sarkadi, B. Calcein accumulation as a fluorometric functional assay of the multidrug transporter. *Biochim. Biophys. Acta* **1994**, *1191*, 384−388.
(38) Essodaigui M.; Frezard, F.; Moreira, E. S.; Dagger, F.; Garnier-Suillerot, A. Energy-dependent efflux from Leishmania promastigotes of substrates of the mammalian multidrug resistance pumps. *Mol. Biochem. Parasitol.* **1999**, *100*, 73−84.
(39) Iovannisci, D. M.; Ullman, B. High efficiency plating method for Leishmania promastigotes in semi-defined or completely-defined medium. *J. Parasitol.* **1983**, *69*, 633−636.
(40) Jackson, P. R.; Lawrie, J. M.; Stiteler, J. M.; Hawkins, D. W.; Wohlhieter, J. A.; Rowtin, E. D. Detection and characterization of Leishmania species and strains from mammals and vectors by hybridization and restriction endonuclease digestion of kinetoplast DNA. *Vet. Parasitol.* **1986**, *20*, 195−215.
(41) Mosmann, T. Rapid colorimetric assay for cellular growth and survival: application to proliferation and cytotoxicity assays. *J. Immunol. Methods* **1983**, *65*, 55−63.
(42) Alfieri, S. C.; Zilberfarb, V.; Rabinovitch, M. Destruction of Leishmania mexicana amazonensis amastigotes by leucine methyl ester: protection by other amino acid esters. *Parasitology* **1987**, *95*, 31−41.

JM010970C

PTO main QC762. J68

STIC-ILL

From: Gabel, Gailene
Sent: Wednesday, February 12, 2003 4:31 PM
To: STIC-ILL
Subject: 09/905,439

Please provide a copy of the following literature ASAP:

1) Kay et al., J. Magn. Reson., 89: 496-514 (1990).

2) Grzesiek et al., J. Magn. Reson. 96: 432-440 (1992).

Thanks a bunch,
Gail R. Gabel
7B15
305-0807
CM1

JOURNAL OF MAGNETIC RESONANCE 96, 432–440 (1992)

Improved 3D Triple-Resonance NMR Techniques Applied to a 31 kDa Protein

STEPHAN GRZESIEK* AND AD BAX

Laboratory of Chemical Physics, National Institute of Diabetes and Digestive and Kidney Diseases, National Institutes of Health, Bethesda, Maryland 20892

Received September 6, 1991

Recently proposed 3D triple-resonance techniques (*1–5*) make it possible to obtain sequential assignment of the backbone ^{1}H, ^{15}N, and ^{13}C resonances in proteins that can be isotopically labeled with ^{13}C and ^{15}N. This approach has been used successfully for a number of systems, including calmodulin (16.7 kDa) (*1*), calmodulin complexed with a 26-residue peptide (~20 kDa) (*6*), and the phospho-carrier protein III^{Glc} (*7*) (18 kDa). All of these triple-resonance experiments rely on transfer of magnetization via heteronuclear one-bond J couplings and the sensitivity of the experiments depends strongly on the ratio of the size of the J coupling and the linewidths of the nuclei involved in the magnetization transfer process. Our original experiments were designed to minimize the number of RF pulses required for a particular pulse sequence, and thus to minimize the effect of pulse imperfections. Subsequent experience with these experiments has indicated that the effect of pulse imperfections is not as severe as originally expected, provided that pulses are properly calibrated. Hence, in order to optimize the experiments it is more important to minimize the relaxation of transverse magnetization by keeping the dephasing and rephasing delays as short as possible, especially for larger proteins. Here we demonstrate the applicability of three improved triple-resonance experiments to the study of interferon-γ, a dimer with 134 residues per monomer and a total molecular weight of 31.4 kDa.

Correlation of the amide proton and ^{15}N resonance with the intraresidue $^{13}C\alpha$ can be obtained with an experiment known as HNCA (*1, 2*). Note that this experiment also provides connectivity to the Cα of the preceding residue, transferring coherence via the $^{2}J_{N\text{-}C\alpha}$ coupling. Because $^{1}J_{N\text{-}C\alpha}$ and $^{2}J_{N\text{-}C\alpha}$ can be of comparable magnitude (*8*) it may not always be possible to distinguish intra- from interresidue connectivities with this experiment. In contrast, the HN(CO)CA experiment (*4*) provides correlations exclusively to the Cα resonance of the preceding residue by relaying magnetization via the intervening carbonyl ^{13}C spin. The HN(CO)CA experiment is closely related to the HNCO experiment, which correlates the amide ^{1}H and ^{15}N with the ^{13}C of the preceding residue. In the present study of interferon-γ, we employ modified versions of these experiments, using INEPT (*9*) instead of HMQC (*10–12*) type coherence transfers, and overlay the ^{13}C–^{15}N dephasing period with a ^{15}N evolution period

* On leave from F. Hoffmann–LaRoche Ltd., Basel, Switzerland.

0022-2364/92 $3.00

of the "constant-time" variety (*5, 13–15*). Advantages of these modifications are discussed below.

The pulse schemes for the modified experiments are shown in Fig. 1. The third experiment, CT-HN(CO)CA (Fig. 1c), differs from the original version (*4*) only by the use of a constant-time t_1 evolution period in the present experiment. This eliminates decay of magnetization that normally occurs during the t_1 evolution period and it permits the use of linear prediction with "mirror image constraint" (*16*) since the signal in the t_1 dimension is a sum of undamped cosinusoidal oscillations of known phase (0°). A detailed description of the magnetization-transfer steps of the HN(CO)CA experiment was presented previously (*4*) and will not be repeated here. The new pulse schemes for the CT-HNCA and CT-HNCO experiments are more similar to those of the CT-HN(CO)CA experiment than to the original HNCA and HNCO sequences (*2*). The CT-HNCO and CT-HNCA schemes differ from one another only by the interchanged ^{13}CO and $^{13}C\alpha$ channels and a different choice of delay durations. Therefore, in the following discussion of the magnetization transfer during the pulse sequences we restrict ourselves to the CT-HNCA experiment.

For the CT-HNCA experiment, the relevant magnetization-transfer steps are outlined using the product-operator formalism. For clarity, relaxation terms are not included and constant multiplicative factors are omitted. Only terms that result in observable magnetization during the detection period, t_3, are retained. The spin operators used are I for the amide proton, N for the amide ^{15}N, S for the carbonyl ^{13}C, and A_1 and A_2 for the intraresidue $C\alpha$ and for the $C\alpha$ of the preceding residue, respectively. J_{XY} denotes the J coupling between spins X and Y and RF phases correspond to the first step of the phase cycle given in the legend to Fig. 1.

Longitudinal amide proton magnetization (I_z), present at the start of the experiment, is converted into antiphase ^{15}N magnetization by an INEPT type transfer. Thus, at time a in Fig. 1a the spin system is described by $\sigma_a = N_y I_z \sin(2\pi J_{NH}\tau)$. Evolution due to J coupling during the subsequent constant-time evolution period (of total duration $2T$) is independent of the duration of t_1, but ^{15}N chemical-shift evolution depends on t_1 in the regular manner. The constant time is set to an integral multiple of $1/J_{NH}$ (22 ms in the present case), such that at time b the ^{15}N magnetization has remained antiphase with respect to its attached proton spin. Ignoring the $\sin(2\pi J_{NH}\tau)$ term present at time a, the magnetization at time b is described by

$$\sigma_b = N_x I_z A_{1z} \sin(2\pi J_{A_1N}T)\cos(2\pi J_{A_2N}T)\cos(\Omega_N t_1) + N_x I_z A_{2z} \sin(2\pi J_{A_2N}T)\cos(2\pi J_{A_1N}T)\cos(\Omega_N t_1), \quad [1]$$

where Ω_N denotes the angular offset frequency of the ^{15}N spin. This magnetization is transferred into antiphase $C\alpha$ magnetization by the $90^\circ_{\phi 6}$ and $90^\circ_{\phi 7}$ pulses, yielding at time c

$$\sigma_c = A_{1y} N_z I_z + A_{2y} N_z I_z, \quad [2]$$

where the trigonometric terms of expression [1] again have been omitted temporarily. At the end of the t_2 evolution period, the terms that will be transferred back into observable magnetization are represented by

$$\sigma_d = A_{1y} N_z I_z \cos(\Omega_{A_1} t_2) + A_{2y} N_z I_z \cos(\Omega_{A_2} t_2). \quad [3]$$

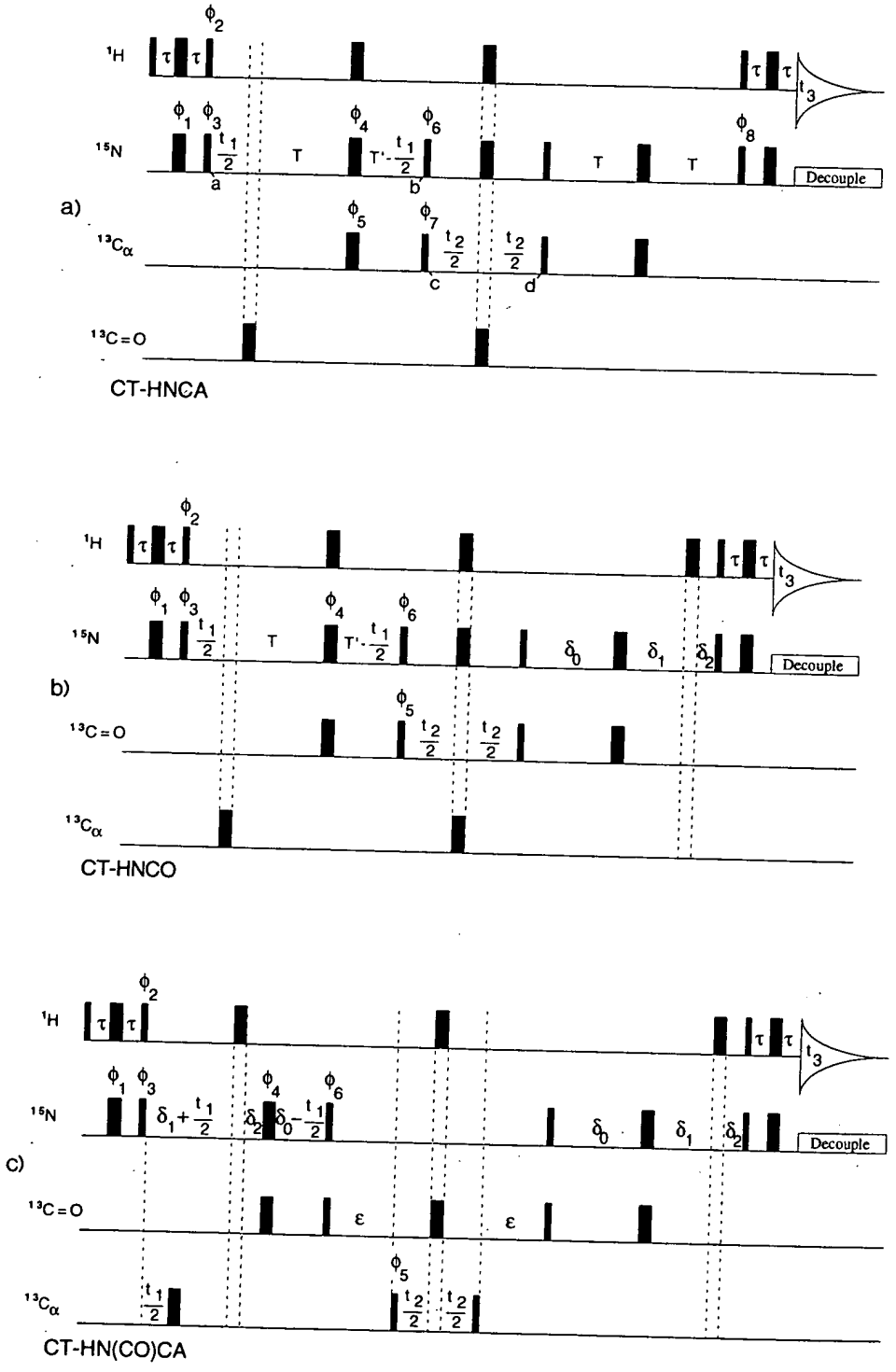

FIG. 1. Puls
Narrow pulses
marked are ap
a null in their
schemes are τ
(162 μs) for s
ms; $\delta_0 = \delta_1 +$
$\phi_2 = y, -y; \phi$
$x, -x, -x; \phi_8$
(b) and (c), ϕ
$x, -x$; Acq. =
by altering the
and ϕ_5 must b

Transfer of t
lows the rev
period, the o

$\sigma_e = \sin^2(2\pi$

where all re
identical to t
difference be
laxation ter
Because in t
gain in sensi

where AT_1 i
the ^{1}H-coup
24 ms, and
in sensitivity
pulse ^{1}H dec
(*17*) the ^{15}N
since the ^{15}
^{1}H. This inc
relaxation d
interferon-γ
and compar
1. However,
kDa) are co
the scheme
diffusion, th

In the pr
the ^{13}Cα tra

Transfer of this magnetization back into observable amide proton magnetization follows the reverse pathway of that described above. At the beginning of the detection period, the observable magnetization is described by

$$\sigma_e = \sin^2(2\pi J_{NH}\tau)\cos(\Omega_N t_1) I_x[\sin^2(2\pi J_{A_2N}T)\cos^2(2\pi J_{A_1N}T)\cos(\Omega_{A_2}t_2) + \sin^2(2\pi J_{A_1N}T)\cos^2(2\pi J_{A_2N}T)\cos(\Omega_{A_1}t_2)], \quad [4]$$

where all relevant trigonometric terms have been reintroduced. This expression is identical to that derived for the original HNCA experiment (eq. [4] in Ref. (*2*)). The difference between the constant-time and the original experiment is found in the relaxation terms which have been neglected in the discussions of both experiments. Because in the present experiment signal does not decay as t_1 increases, a substantial gain in sensitivity can be obtained. This again, G, is given approximately by

$$G = AT_1 \Big/ \int_0^{AT_1} \exp(-t_1/T_{2N})dt_1, \quad [5]$$

where AT_1 is the duration of the t_1 acquisition time and T_{2N} is the ^{15}N T_2 value in the ^1H-coupled mode. For the present study of interferon-γ, T_{2N} equals approximately 24 ms, and AT_1 = 22 ms, yielding a gain, G, in signal-to-noise of 1.5. A further gain in sensitivity can be obtained if the pulse schemes are modified to utilize composite-pulse ^1H decoupling instead of 180° pulses, as indicated in Fig. 2. As shown previously (*17*) the ^{15}N transverse relaxation rate becomes approximately 30% slower in this case since the ^{15}N transverse magnetization remains in-phase with respect to its attached ^1H. This increase in the apparent T_{2N} reduces the signal loss caused by ^{15}N transverse relaxation during the delays of total duration $4T$. Because of the limited stability of interferon-γ and the small amount of available sample, we have been unable to test and compare the schemes of Fig. 2 with the results obtained with the schemes of Fig. 1. However, when the experimental results obtained for the protein calmodulin (16.7 kDa) are compared, a gain of a factor 1.2 is observed with the schemes of Fig. 2 over the schemes of Fig. 1. For interferon-γ, which has a much faster rate of ^1H spin diffusion, this gain is expected to be ~1.5.

In the present experiment, the signal decay in the t_2 dimension is determined by the $^{13}C\alpha$ transverse relaxation time, whereas in the original HNCA experiment it was

FIG. 1. Pulse sequences of the (a) CT-HNCA, (b) CT-HNCO, and (C) CT-HN(CO)CA experiments. Narrow pulses correspond to a 90° flip angle and wide pulses to 180°. Pulses for which the RF phase is not marked are applied along the x axis. The power and duration of Cα pulses are adjusted such that they have a null in their excitation profile at the ^{13}CO frequency, and vice versa. Delay duration for the three pulse schemes are τ = 2.25 ms; T = 13.5 ms; $T' = T + \tau_{180°}(^{13}C)$, where $\tau_{180°}(^{13}C)$ is the 180° (CO) pulse width (162 μs) for scheme (a) and the 180° (Cα) pulse width (108 μs) for scheme (b); δ_1 = 7.25 ms; δ_2 = 2.75 ms; $\delta_0 = \delta_1 + \delta_2 + \tau_{180°}(^1H)$; ϵ = 6 ms. The phase cycling used is as follows. For scheme (a), $\phi_1 = x, -x$; $\phi_2 = y, -y$; $\phi_3 = x$; $\phi_4 = 4(x), 4(y), 4(-x), 4(-y)$; $\phi_5 = 16(x), 16(-x)$; $\phi_6 = 16(y), 16(-y)$; $\phi_7 = x, x, -x, -x$; $\phi_8 = y$; Acq. = $2(x, -x, -x, x, -x, x, x, -x), 2(-x, x, x, -x, x, -x, -x, x)$. For schemes (b) and (c), $\phi_1 = x, -x$; $\phi_2 = y, -y$; $\phi_3 = x$; $\phi_4 = 4(x), 4(y), 4(-x), 4(-y)$; $\phi_5 = x, x, -x, -x$; $\phi_6 = x, -x$; Acq. = $2(x), 4(-x), 2(x)$. For scheme (a), quadrature in the t_1 and t_2 dimensions is accomplished by altering the phases ϕ_3 and ϕ_7 in a States–TPPI manner (*20*). For schemes (b) and (c), the phases of ϕ_3 and ϕ_5 must be altered in a States–TPPI manner to obtain quadrature in these two dimensions.

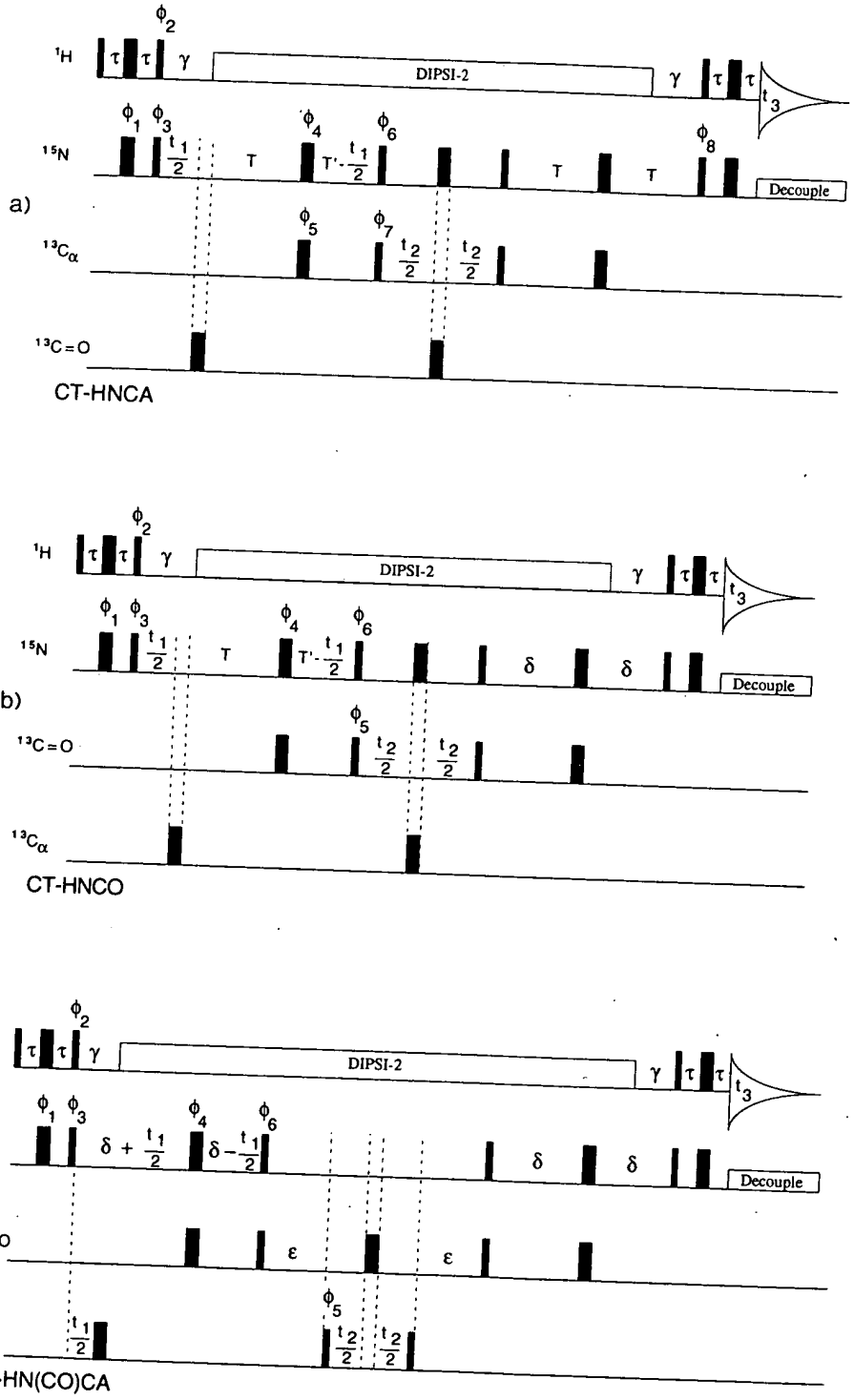
a)
CT-HNCA
b)
CT-HNCO
c)
CT-HN(CO)CA
DIPSI-2
Decouple

determined by the decay rate of three-spin (I, N, and A) coherence. In both cases, however, the resolution is limited by the fact that the Cα resonance is coupled to ^{13}Cβ and it is generally undesirable to resolve this J splitting. Therefore, the acquisition time in the t_2 dimension is kept shorter than $1/(2J_{C\alpha C\beta})$, about 10 ms in practice, and the difference in intrinsic relaxation rates of transverse ^{13}Cα magnetization and three-spin coherence is of no practical consequence.

The constant-time version of the HNCO experiment, shown in Fig. 1b, is essentially the same as the CT-HNCA scheme of Fig. 1a. Note, however, that a slightly longer constant-time acquisition period can be used in this experiment because, in contrast to the HNCA case, ^{15}N dephases only under the influence of coupling to a single ^{13}C spin. The time $2T$ is now set to an odd multiple of $1/(2J_{NH})$ (27 ms in our case), such that the magnetization is in-phase with respect to the amide proton spin (N_yS_z) when it is transferred to the ^{13}C spin. This is important because for t_2 acquisition times shorter than ~50 ms (i.e., before significant antiphase magnetization develops) this lengthens the apparent relaxation time of the ^{13}CO spin (which only has small long-range J couplings to other protons). If the ^{13}CO magnetization were antiphase with respect to the amide proton spin its decay rate would increase by the rate of ^{1}H–^{1}H spin flips. The comparable scheme of Fig. 2b provides the same initial decay rate in the t_2 dimension as the scheme of Fig. 1b, but is expected to yield superior ^{13}CO resolution if acquisition times much longer than 50 ms are used in the t_2 dimension. In addition, magnetization loss caused by ^{15}N relaxation during the intervals $2T$ and δ_0 and δ_1 is reduced in the scheme of Fig. 2b for reasons mentioned above. Note that in the original HNCO experiment (*2*), the ^{13}CO frequency was obtained from an HMQC type correlation with ^{15}N, and in that case, dephasing in the t_2 dimension caused by $^1J_{C\alpha N}$ and $^2J_{C\alpha N}$ limits the obtainable resolution.

The pulse schemes shown in Fig. 1 are demonstrated for the protein interferon-γ, a homodimer with 134 residues per monomer and a total molecular weight of 31.4 kDa. The protein was labeled uniformly with ^{13}C (>95%) and ^{15}N (~50%) and purified according to the procedure described by Doebeli *et al.* (*18*). Experiments were conducted on a sample containing 0.7 m*M* dimer in 95%/5% H_2O/D_2O, pH 6.3, 27°C, using an unmodified Bruker AMX-600 spectrometer.

Figure 3 shows three cross sections of the three different types of 3D spectra. All are taken perpendicular to the ^{15}N axis at a ^{15}N frequency of 119 ppm. The position of these slices in the ^{1}H–^{15}N shift correlation spectrum is indicated by a dotted line

FIG. 2. Alternative versions of the pulse schemes shown in Fig. 1, using composite-pulse decoupling to remove J coupling between protons and ^{15}N/^{13}C. The delay γ is set to $1/(2J_{NH})$: the phase cycling and all other durations are identical to those given in the legend to Fig. 1, except for ϕ_6 of schemes (b) and (c) which is given by $\phi_6 = y, -y$ and $\delta = 10$ ms. To minimize the effect of ^{15}N transverse magnetization decay caused by homonuclear J coupling, a decoupling scheme of the DIPSI type (*21*) is preferred. Note that the 90° and 180° pulses applied to the heteronucleus to which the proton is coupled interfere destructively with composite pulse decoupling and a higher power level is needed for the ^{1}H decoupling compared to the normal case in which decoupling is used while observing the second nucleus. For a ^{1}H RF field strength stronger than ~4 kHz this effect is not noticeable. For reproducible water suppression it is necessary to perform the DIPSI decoupling in a synchronous mode, i.e., to start the decoupling at the same position during the decoupling cycle each time it is used.

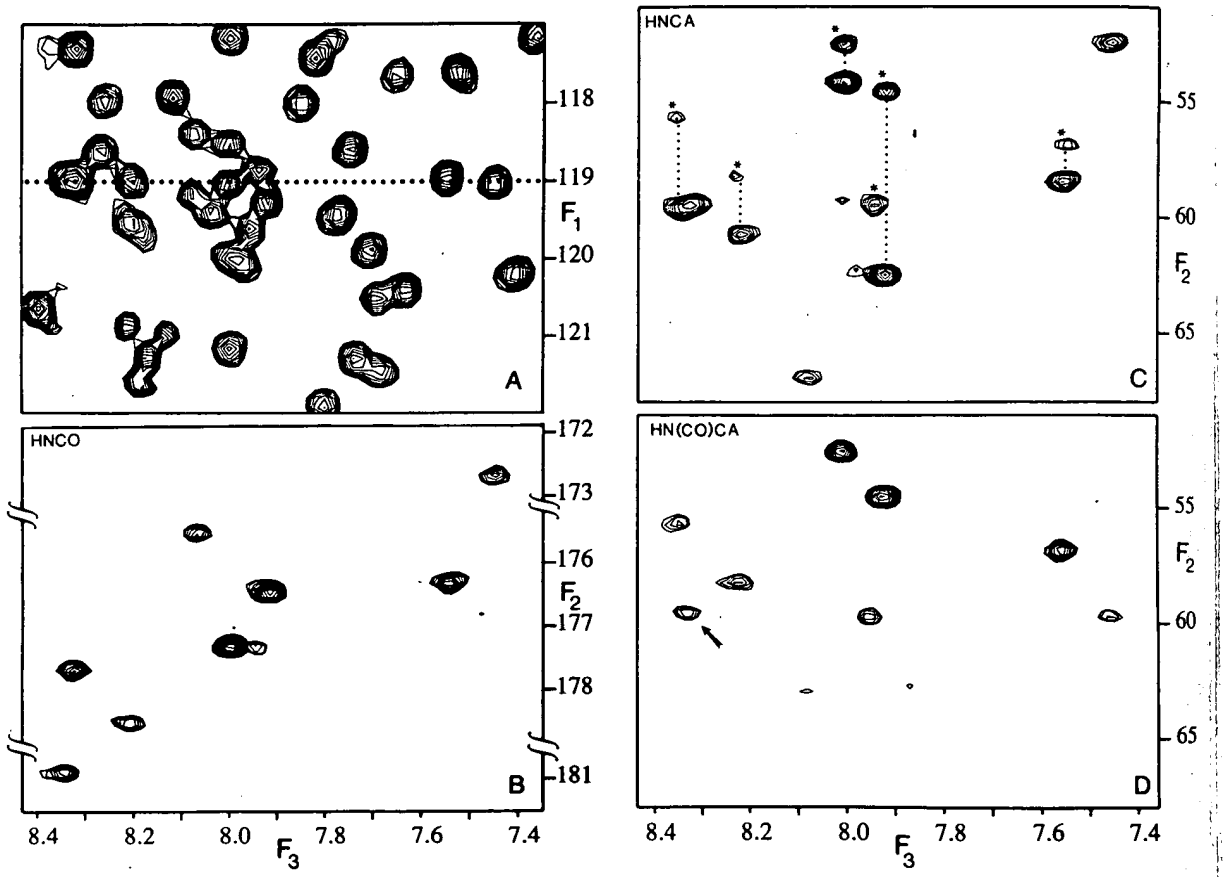

FIG. 3. Spectra obtained for a sample of interferon-γ (8.8 mg in 0.4 ml H_2O/D_2O), labeled uniformly with ^{13}C (>95%) and ^{15}N (50%). (A) Small region of the resolution-enhanced 2D Overbodenhausen (HSQC) spectrum. The dotted line marks the position where the slices through the 3D spectra are taken. (B) F_1 = 119 ppm slice of the CT-HNCO spectrum, recorded with the pulse sequence of Fig. 1b. (C) F_1 = 119 ppm slice of the CT-HNCA spectrum, recorded with the pulse sequence of Fig. 1a. (D) F_1 = 119 ppm slice of the CT-HN(CO)CA spectrum, recorded with the pulse sequence of Fig. 1c. All 3D spectra have been processed using linear prediction with mirror image constraint in the F_1 dimension. The CT-HNCA spectrum results from a (32 complex) × (48 complex) × (512 complex) data matrix with 256 scans per hypercomplex (t_1, t_2) increment, and acquisition times of 22.4, 10.0, and 55.3 ms in the t_1, t_2, and t_3 dimension, respectively. The CT-HNCO spectrum results from a (32 complex) × (64 complex) × (512 complex) data matrix with 64 scans per hypercomplex (t_1, t_2) increment, and acquisition times of 24.0, 34.5, and 55.3 ms in the t_1, t_2, and t_3 dimension, respectively. The CT-HN(CO)CA spectrum results from a (32 complex) × (46 complex) × (512 complex) data matrix with 128 scans per hypercomplex (t_1, t_2) increment, and acquisition times of 19.8, 9.6, and 55.3 ms in the t_1, t_2, and t_3 dimension, respectively.

in the 2D $^1H-^{15}N$ correlation spectrum of Fig. 3A. Because the linewidth in the F_1 (^{15}N) dimension of the 3D spectrum is approximately double the ^{15}N linewidth in the 2D spectrum, resonances in Fig. 3A that are close to the dotted line, with their ^{15}N chemical shift differing by less than 0.2 ppm from 119.0 ppm, also give rise to resonances in the (F_1 = 119 ppm) slice shown for each of the 3D spectra.

The HNCO spectrum of which the F_1 = 119 ppm slice is shown in Fig. 3B clearly has the highest signal-to-noise ratio of the three 3D spectra. This was expected since the ^{15}N–^{13}CO coupling is larger than the ^{15}N–$^{13}C\alpha$ J coupling, making transfer more efficient than in the HNCA experiment. Note that resonance intensity in the HNCA spectrum (Fig. 3C) is also lowered because the ^{15}N–$^{13}C\alpha$ transfer is attenuated by the presence of the additional passive ^{15}N–$^{13}C\alpha$ J coupling (cf. Eq. [4]). Nevertheless, in the HNCA spectrum of Fig. 3C both intra- and interresidue HN–N–Cα correlations are observed for the majority of the amides. The interresidue connectivities in Fig. 3C are distinguished from the intraresidue ones by comparison with the HN(CO)CA spectrum of Fig. 3D. A recent low-resolution X-ray study (*19*) indicates that interferon-γ is largely α-helical and contains no β-sheet. Two-bond ^{15}N–$^{13}C\alpha$ J couplings in α-helices (6.4 ± 0.4 Hz) are significantly smaller than those in β-sheets (8.4 ± 0.5 Hz) (*8*), and it is therefore remarkable that these connectivities are observable despite the fact that the ^{15}N linewidths are approximately twice the size of this coupling, and despite the fact that the protein accidentally was labeled at a level of only 50% with ^{15}N. Figure 3D has been acquired with the HN(CO)CA technique, which contains an extra relay step compared to the HNCA and HNCO methods. However, because the relay of magnetization via the ^{13}CO nucleus is quite efficient, sensitivity of the 3D spectrum is high. A number of additional interresidue connectivities are observed relative to the spectrum of Fig. 3C, and an interresidue correlation that was obscured by overlap with the intraresidue correlation in the HNCA spectrum is clearly observed in Fig. 3D and marked with an arrow.

Before the backbone assignment of interferon-γ can be completed, it is necessary to get residue type assignments for at least a significant fraction (>10%) of the amides. To this extent, preparation of more uniformly labeled sample, needed because of its limited stability, is currently in progress. The present report clearly indicates, however, that the triple-resonance assignment procedure outlined previously (*1*) is applicable to proteins of a molecular weight larger than anticipated. It is noteworthy that the present study was carried out at a relatively low temperature (27°C), and that after correcting for the low level of ^{15}N labeling, the effective protein monomer concentration was only 0.7 m*M*. Of course, the spectral complexity for a symmetric dimer such as interferon-γ is much lower than that for a regular protein of the same molecular mass. However, in the present 3D spectra, resonance overlap is rather minimal and a doubling of the total number of correlations is not expected to cause unsurmountable problems.

ACKNOWLEDGMENTS

We thank Drs. R. Gentz and H. Doebeli for the expression and purification of the labeled interferon-γ, Dr. W. Vetter and W. Meister for analytical mass spectroscopy, Dr. M. Zulauf for quasi-electric light scattering analysis, Dr. W. Klaus for the initial NMR characterization, and Dr. A. M. Labhardt for his enthusiastic support. S.G. acknowledges funding by the ROCHE Research Foundation. This work was supported by the Intramural AIDS targeted Anti-Viral Program of the Office of the Director of the National Institutes of Health.

REFERENCES

1. M. IKURA, L. E. KAY, AND A. BAX, *Biochemistry* **29**, 4659 (1990).
2. L. E. KAY, M. IKURA, R. TSCHUDIN, AND A. BAX, *J. Magn. Reson.* **89**, 496 (1990).
3. L. E. KAY, M. IKURA, AND A. BAX, *J. Magn. Reson.* **91**, 84 (1991).

4. A. BAX AND M. IKURA, *J. Biomol. NMR* **1**, 99 (1991).
5. R. POWERS, A. M. GRONENBORN, G. M. CLORE, AND A. BAX, *J. Magn. Reson.* **94**, 209 (1991).
6. M. IKURA, L. E. KAY, M. KRINKS, AND A. BAX, *Biochemistry* **30**, 5498 (1991).
7. J. G. PELTON, D. A. TORCHIA, N. D. MEADOW, C.-Y. WONG, AND S. ROSEMAN, *Biochemistry* **30**, 10,043 (1991).
8. F. DELAGLIO, D. A. TORCHIA, AND A. BAX, *J. Biomol. NMR*, in press.
9. G. A. MORRIS AND R. FREEMAN, *J. Am. Chem. Soc.* **101**, 760 (1979).
10. L. MUELLER, *J. Am. Chem. Soc.* **101**, 4481 (1979).
11. M. R. BENDALL, D. T. PEGG, AND D. M. DODDRELL, *J. Magn. Reson.* **52**, 81 (1983).
12. A. BAX, R. H. GRIFFEY, AND B. L. HAWKINS, *J. Magn. Reson.* **55**, 301 (1983).
13. A. BAX, A. F. MEHLKOPF, AND J. SMIDT, *J. Magn. Reson.* **35**, 373 (1979).
14. A. BAX AND R. FREEMAN, *J. Magn. Reson.* **44**, 542 (1981).
15. O. W. SØRENSEN, *J. Magn. Reson.* **90**, 433 (1990).
16. G. ZHU AND A. BAX, *J. Magn. Reson.* **90**, 405 (1990).
17. A. BAX, M. IKURA, L. E. KAY, D. A. TORCHIA, AND R. TSCHUDIN, *J. Magn. Reson.* **86**, 304 (1990).
18. H. DOEBELI, R. GENTZ, W. JUCKER, G. GAROTTA, D. W. HARTMANN, AND E. HOCHULI, *J. Biotechnol.* **7**, 199 (1988).
19. S. E. EALICK, W. J. COOK, S. VIJAY-KUMAR, M. CARSON, T. L. NAGABHUSHAN, P. P. TROTTA, AND C. E. BUGG, *Science* **252**, 698 (1991).
20. D. MARION, M. IKURA, R. TSCHUDIN, AND A. BAX, *J. Magn. Reson.* **85**, 393 (1989).
21. A. J. SHAKA, C. J. LEE, AND A. PINES, *J. Magn. Reson.* **77**, 274 (1988).

NMR, Basic
Robert, Editor.
3-540-52946-2

This book b
recounts key de
in simulated spe
at 100, 500, and
spectra with inc
by a quote fro
that high resol
it *seemed* to do
further explosi

In the secon
entation at hig
to average anis
interactions m
spectra. From
formation, as

The effect o
matical relatio
to 800 MHz f
properties is d
with field, wit
long correlatic
statement des

The very si
points out tha
that of confor
is devoted to
interactions a
more than m
the benefits t
more sophisti

The last, a
"Solid State
problems to b
troscopy of s
range from p
to spinning r

STIC-ILL

Q8521.852

From: Gabel, Gailene
Sent: Wednesday, February 12, 2003 5:14 PM
To: STIC-ILL
Subject: 09/905,439

Please provide a copy of the following literature ASAP:

1) Killick, Real-time NMR studies on a transient folding intermediate of barstar. PROTEIN SCIENCE, (1999 Jun) 8 (6) 1286-91.

2) Guo et al., Identification of the binding surface on Cdc42Hs for p21-activated kinase. BIOCHEMISTRY, (1998 Oct 6) 37 (40) 14030-7.

3) Pfuhl et al., Secondary structure determination by NMR spectroscopy of an immunoglobulin-like domain from the giant muscle protein titin. JOURNAL OF BIOMOLECULAR NMR, (1995 Jul) 6 (1) 48-58.

4) Kennedy et al., Chemosensitization of a multidrug-resistant Leishmania tropica line by new sesquiterpenes from Maytenus magellanica and Maytenus chubutensis, Journal of Medicinal Chemistry, (December 20, 2001) Vol. 44, No. 26, pp. 4668-4676.

5) Carvalho et al., TCA cycle kinetics in the rat heart by analysis of C-13 isotopomers using indirect H-1[C-13] detection, AMERICAN JOURNAL OF PHYSIOLOGY-HEART AND CIRCULATORY PHYSIOLOGY, (SEP 2001) Vol. 281, No. 3, pp. H1413-H1421.

6) Sokolowski et al., Conformational analysis of a Chlamydia-specific disaccharide alpha-Kdo-(2-->8)-alpha-Kdo-(2-->O)-allyl in aqueous solution and bound to a monoclonal antibody: observation of intermolecular transfer NOEs. JOURNAL OF BIOMOLECULAR NMR, (1998 Jul) 12 (1) 123-33.

7) Kuroda et al., Locations of local anesthetic dibucaine in model membranes and the interaction between dibucaine and a Na+ channel inactivation gate peptide as studied by 2H- and 1H-NMR spectroscopies. BIOPHYSICAL JOURNAL, (1996 Sep) 71 (3) 1191-207.

8) Marceau et al., Contribution of a conserved arginine near the active site of Escherichia coli D-serine dehydratase to cofactor affinity and catalytic activity. JOURNAL OF BIOLOGICAL CHEMISTRY, (1989 Feb 15) 264 (5) 2753-7.

Thanks a bunch,
Gail R. Gabe
7B15
CM1
305-0807

Identification of the Binding Surface on Cdc42Hs for p21-Activated Kinase†

Wei Guo,‡ Michael J. Sutcliffe,§ Richard A. Cerione,‡ and Robert E. Oswald*,‡

Department of Molecular Medicine, Cornell University, Ithaca, New York 14853, and Department of Chemistry, Leicester University, Leicester, LE1 7RK, U.K.

Received June 8, 1998; Revised Manuscript Received August 7, 1998

ABSTRACT: The Ras superfamily of GTP-binding proteins is involved in a number of cellular signaling events including, but not limited to, tumorigenesis, intracellular trafficking, and cytoskeletal organization. The Rho subfamily, of which Cdc42Hs is a member, is involved in cell morphogenesis through a GTPase cascade which regulates cytoskeletal changes. Cdc42Hs has been shown to stimulate DNA synthesis as well as to initiate a protein kinase cascade that begins with the activation of the p21-activated serine/threonine kinases (PAKs). We have determined previously the solution structure of Cdc42Hs [Feltham et al. (1997) *Biochemistry* 36, 8755−8766] using NMR spectroscopy. A minimal-binding domain of 46 amino acids of PAK was identified (PBD46), which binds Cdc42Hs with a K_D of approximately 20 nM and inhibits GTP hydrolysis. The binding interface was mapped by producing a fully deuterated sample of ^{15}N-Cdc42Hs bound to PBD46. A ^{1}H,^{15}N-NOESY-HSQC spectrum demonstrated that the binding surface on Cdc42Hs consists of the second β-strand (β2) and a portion of the loop between the first α-helix (α1) and β2 (switch I). A complex of PBD46 bound to ^{15}N-Cdc42Hs·GMPPCP exhibited extensive chemical shift changes in the ^{1}H,^{15}N-HSQC spectrum. Thus, PBD46 likely produces structural changes in Cdc42Hs which are not limited to the binding interface, consistent with its effects on GTP hydrolysis. These results suggest that the kinase-binding domain on Cdc42Hs is similar to, but more extensive than, the c-Raf-binding domain on the Ras antagonist, Rap1 [Nassar et al. (1995) *Nature 375*, 554−560)].

A superfamily of low molecular weight G-proteins, for which the Ras proteins serve as prototypes, is involved in many biological pathways including cell cycle progression, cytoskeletal organization, protein trafficking, and secretion (*1*). The most intensively studied members of this superfamily are the Ras subfamily proteins which play a major role in cell growth, differentiation, and possibly, apoptosis. The Rho subfamily, however, has been shown to control various cellular signaling pathways leading to changes in cell morphology and polarity, as well as increased DNA synthesis and cell cycle progression (*2*−*4*). Recent experiments suggest that Cdc42Hs, a member of Rho subfamily, may work closely with Ras to provide a full complement of cell growth regulatory events (*5*). The evidence includes the regulation of Cdc42Hs by the oncogenic protein Dbl (*6, 7*) and the fact that activated mutants of Cdc42Hs can transform cells (*5, 8*).

During the past several years, a variety of Cdc42Hs target proteins have been identified including the p85 subunit of the PI3 kinase (*9*), the Wiscott−Aldrich syndrome protein [WASP (*10*)], the IQ-GAP molecules (*11, 12*), the ACK tyrosine kinase (*13, 14*), and members of the PAK[1] family of serine/threonine kinases (*15, 16*). Although these potential Cdc42Hs signaling responses are assumed to be coordinated, how these molecules interact with each other and how these interactions are regulated remains unknown. Recent studies of the interaction between Cdc42Hs and Rac with PAKs (*17*−*21*) support the idea that activation of PAK by Cdc42Hs/Rac initiates a protein kinase cascade that leads to the nucleus and culminates in the activation of two nuclear MAP kinases, JNK1 and p38. This kinase cascade pathway is similar to a pathway in *Saccharomyces cerevisiae*, where STE20 (the PAK homolog) initiates a kinase cascade that results in the activation of the MAP kinase Fus3/Kss1 (*22*) and resembles the Ras-signaling pathway that begins with the Raf serine/threonine kinase and culminates in the activation of the nuclear MAP kinase Erk (*23*). However, while the main role of Ras appears to be to recruit Raf to the membrane where it then becomes activated, Cdc42Hs or Rac is absolutely essential for the stimulation of PAK activity. Without one or more activated Rho proteins, the PAKs cannot be autophosphorylated and show no kinase activity. Structural studies of the Ras-binding domain on the Ras antagonist, Rap1A, (*24*) reveals that the interaction between the two proteins is mediated by an antiparallel

† Supported by grants from the American Cancer Society and the NIH (R01 GM56233) to R.E.O. W.G. was supported by an NIH predoctoral training grant (T32GM08210). M.J.S. is a Royal Society University Research Fellow.

* To whom correspondence should be addressed. Phone: 1-607-253-3877. Fax: 1-607-253-3659. E-mail: reo1@cornell.edu.

‡ Cornell University.

§ Leicester University.

[1] Abbreviations: DTT, dithiothreitol; EDTA, ethylenediaminetetraacetic acid; GAP, GTPase-activating protein; GDP, guanosine 5′-diphosphate; GMPPCP, β,γ-methylene derivative of GTP; GSH, glutathione (reduced form); GST, glutathione *S*-transferase; GTP, guanosine 5′-triphosphate; HSQC, heteronuclear single quantum correlation; IPTG, isopropyl β-D-thiogalactopyranoside; NMR, nuclear magnetic resonance; NOESY, nuclear Overhauser effect spectroscopy; PAK, p21 activated kinase; PBD, Cdc42Hs binding domain on PAK; PBS, phosphate-buffered saline; PMSF, phenylmethanesulfonyl fluoride; RBD, Ras-binding domain; sNBD, succinimidyl-6-[(7-nitrobenz-2-oxa-1,3-diazol-4-yl)amino]hexanoate; Tris-HCl, tris[hydroxymethyl]-aminomethane hydrochloride.

S0006-2960(98)01352-X CCC: $15.00
Published on Web 09/15/1998

β-sheet formed by strand β2 from RBD (Ras-binding domain) and strand β2 from Rap1A. In contrast to the interaction between Ras and Raf, PAK can decrease the rate of GTP hydrolysis by Cdc42Hs, suggesting that the interaction may be different or more extensive than the Ras-Raf interaction.

Presented here is the delineation of the binding interface on Cdc42Hs for PAK and the backbone chemical shift changes of Cdc42Hs upon binding of a peptide derived from PAK. This peptide encompasses the CRIB (Cdc42/Rac interactive binding) domain, which is also present in WASP and the ACKs and has been identified on the basis of sequence alignment as an important determinant in the binding of Cdc42Hs and Rac (*25*). The binding interface is more extensive than that described for Rap1A-RBD (*24*), and the chemical shift changes encompass a large surface of Cdc42Hs, suggesting that PAK binding has significant effects on the tertiary structure of this GTP-binding protein.

EXPERIMENTAL PROCEDURES

Protein Expression. Cdc42Hs used in these experiments was expressed as a hexa-histidine-tagged protein in *Escherichia coli* strain BL21(DE3) from pET-15b-Cdc42Hs. This expression plasmid was subcloned to contain the N-terminal 181 amino acids (including a glycine, serine, and histidine before the starting methionine) from the original pGEX-Cdc42Hs expression plasmid (*26*) to improve the yield and to remove the unstructured C-terminal tail (*27*). For samples labeled homogeneously with ^{15}N or $^{15}N/^{13}C$, $^{15}NH_4Cl$ and ^{13}C-glucose were substituted for their unlabeled counterparts in the M9 media (*28*). Specifically, a single colony containing plasmid pET-15b-Cdc42Hs was grown for 8 h in 5 mL of LB containing 50 μg/mL ampicillin (this concentration of ampicillin was maintained in all media). This 5 mL culture was washed twice with 5 mL of fresh 2×M9 unlabeled media and transferred to 200 mL of 2×M9 unlabeled media to grow 12 h at 37 °C in a shaker flask. The 200 mL culture was then washed twice with 200 mL of 2×M9 unlabeled media, resuspended in 2 L of 2×M9 ^{15}N- or $^{15}N/^{13}C$-labeled media, and grown in a Hi-Density Fermentor (Lab-Line Instrument, Melrose Park, IL) to OD_{560} = 0.7. Cells were harvested 6 h after induction with 0.5 mM IPTG by centrifugation at 10000*g* for 15 min (4 °C) and stored at −70 °C.

Several modifications of this procedure were required to produce $^{15}N,^{2}H$-Cdc42Hs. $^{15}NH_4Cl$ and ^{2}H-sodium acetate were used in the 2×M9 as the sole nitrogen and carbon sources, and 50 μg/mL carbenicillin was used throughout the procedure. A single bacterial colony containing expression plasmid pET-15b-Cdc42Hs was grown in 3 mL of 33% D_2O LB for 12 h at 37 °C in a 15 mL culture tube. An aliquot (100 μL) was then transferred to 3 mL of 67% D_2O LB for an additional 12 h. Finally, 100 μL was transferred to 3 mL of >98% D_2O LB for 12 h. An aliquot (50 μL) of this culture was transferred to 50 mL of >98% D_2O 2×M9 and was grown for 3 days at 37 °C in a shaker flask. This 50 mL culture was then transferred to 2 L of >98% D_2O 2×M9 and grown for 2 days at 37 °C. When OD_{560} = 0.5 was reached, induction began with 0.5 mM IPTG. Cells were harvested after 36 h of induction as described above.

PBD46 was expressed as a GST fusion protein (pGEX-2T-PBD46) in *Escherichia coli* strain BL21(DE3). This expression plasmid was subcloned from the original pET-15b-PBD (*29*) and contained 46 amino acids, including glycine and serine introduced as an N-terminal linker before the PBD sequence. Expression was achieved in the same manner as for Cdc42Hs, except that 4 L of LB medium was used and induction by IPTG began when the medium reached OD_{560} = 1.0 in the fermentor.

Protein Purification. All procedures were performed at 4 °C unless otherwise specified. Frozen cells containing Cdc42Hs were thawed in 100 mL lysis buffer (5 mM imidazole, 500 mM NaCl, 20 mM Tris-HCl, pH 8.0) with 0.1 mM GDP and a cocktail of protease inhibitors (2 μg/mL aprotinin, leupeptin and pepstatin, and 10 μg/mL benzamidine and PMSF). Cells were homogenized using a Teflon-glass homogenizer, and lysozyme and deoxycholic acid were added to 1 mg/mL and 0.8 mg/mL respectively. Cell lysates were incubated for 30 min, followed by the addition of DNase I and $MgCl_2$ to final concentration of 20 μg/mL and 20 mM, respectively. The lysates were then disrupted using a Polytron. The insoluble fraction was removed by centrifugation at 20000*g* for 20 min. The supernatant was applied to an iminodiacetic acid column (15 mL) previously charged with Ni^{2+} and equilibrated with binding buffer (5 mM imidazole, 500 mM NaCl, and 20 mM Tris-HCl, pH 8.0). The column was washed with binding buffer and washing buffer (25 mM imidazole, 500 mM NaCl, and 20 mM Tris-HCl, pH 8.0) and eluted with a 25 to 300 mM imidazole gradient containing 500 mM NaCl and 20 mM Tris-HCl, pH 8.0. Thrombin was added to the pooled Cdc42Hs-GDP (identified by 10% SDS−PAGE) and dialyzed against 4 L of 20 mM Tris-HCl (pH 8.0) for at least 5 h before the addition of 10 μg/mL PMSF to stop the reaction. The mixture (containing Cdc42Hs·GDP, hexa-histidine tag, and thrombin) was loaded on a 15 mL Q-Sepharose column (equilibrated with 20 mM Tris-HCl, pH 8.0), washed with 20 mM Tris-HCl (pH 8.0), and eluted with a 0 to 300 mM NaCl gradient. Cdc42Hs·GDP was the only protein in the mixture that bound to this column. Following elution, Cdc42Hs·GDP was identified by 10% SDS−PAGE, concentrated to 20 mg/mL [Bradford assay (*30*) after correction based on an amino acid analysis (*27*)], and dialyzed against NMR buffer (25 mM NaCl, 5 mM NaH_2PO_4, 5 mM $MgCl_2$, and 1 mM NaN_3, pH 5.5). Exchange of GDP for GMPPCP was performed as described by John et al. (*31*). Cdc42Hs·GMPPCP was further dialyzed extensively in NMR buffer and concentrated to 20 mg/mL.

A supernatant containing GST-PBD46 was extracted from bacteria in the same manner as described for His-Cdc42Hs except that PBS was used as the lysis buffer. The supernatant was mixed with 50 mL of GST Sepharose-4B beads which were equilibrated with PBS. The mixture was poured onto a column, washed with 300 mL of PBS and 100 mL of 20 mM Tris-HCl, pH 8.0. The GST fusion protein was eluted with 10 mM GSH in 20 mM Tris-HCl (pH 8.0), and fractions containing GST-PBD46 (identified by 10% SDS−PAGE) were pooled (~100 mL) and incubated with thrombin for 5 h. The solution was lyophilized, resuspended in 3 mL of H_2O, centrifuged, and loaded on to a Sephacryl S-100 gel filtration column prior equilibrated with 20 mM Tris-HCl and 150 mM NaCl, pH 8.0. Purified PBD46 was eluted, identified by SDS−PAGE, lyophilized, resuspended in 2 mL of H_2O, dialyzed in the NMR buffer described above, and

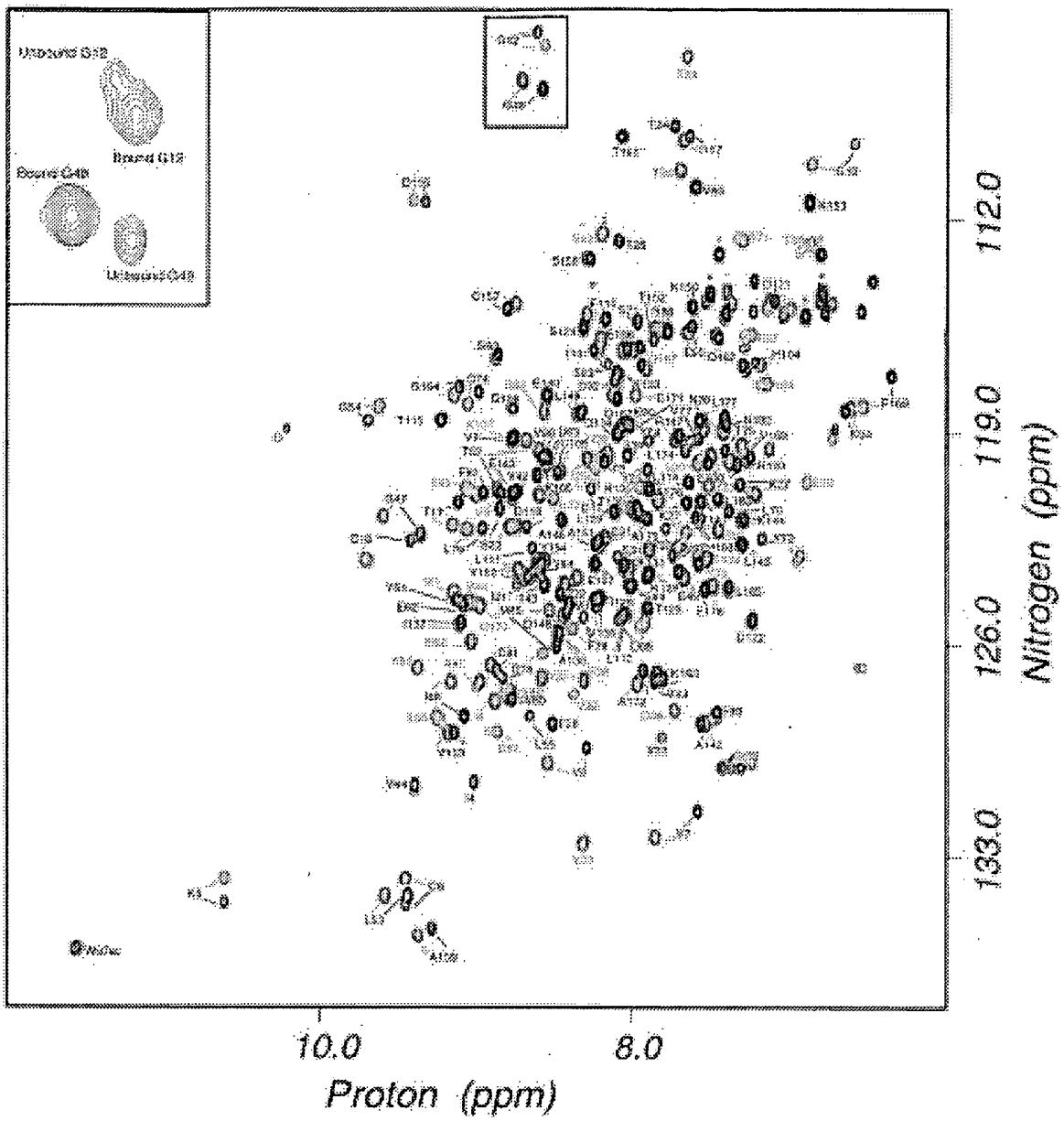

FIGURE 1: The ^{1}H,^{15}N-HSQC spectra of ^{15}N-Cdc42Hs·GMPPCP (black) and ^{15}N-Cdc42Hs·GMPPCP-PBD46 (red) are shown with peaks labeled with assignments. Side-chain glutamine and asparagine correlations are not labeled. Since only Cdc42Hs is uniformly labeled with ^{15}N, only correlations between nitrogen and amide protons on Cdc42Hs are observable. Note: the extensive chemical shift changes between the PBD-bound and PBD-free forms of ^{15}N-Cdc42Hs·GMPPCP. The insert is an enlargement at lower contour levels of a partially bound ^{15}N-Cdc42Hs·GMPPCP preparation showing both bound and unbound peaks, indicating that the complex is in slow exchange.

concentrated to 5 mg/mL. PBD46 and Cdc42Hs·GMPPCP were then mixed (1 mL each of the protein stocks) and incubated at 4 °C overnight. The complex was purified on a Sephacryl S-100 column equilibrated with NMR buffer.

Protein samples used for NMR experiments were supplemented with 10% D_2O. The concentration of ^{15}N-Cdc42Hs·GMPPCP was 1.0 mM, ^{15}N-Cdc42Hs·GMPPCP-PBD46 was 1.0 mM, and ^{15}N,^{2}H-Cdc42Hs·GMPPCP-PBD46 was 0.8 mM. All samples were in NMR buffer at pH 5.5 without pH correction to counter isotope effects.

Binding of PBD46 to Cdc42Hs. A fluorescence reporter group, sNBD, was covalently attached to Lys150 on Cdc42Hs (*32*). sNBD-labeled Cdc42Hs undergoes a characteristic fluorescence decrease when bound to PBD [excitation at 488 nm and emission at 545 nm (*32*)], providing an environment-sensitive probe for monitoring the binding of Cdc42Hs to PBD. Accordingly, 55 nM of sNBD-Cdc42Hs·GTP in NMR buffer was excited at 488 nm, aliquots of concentrated PBD constructs were added, and the fluorescence quenching was monitored. The K_D was determined by nonlinear least-squares fit to the following equation:

$$F = F_i + F_f\left[\frac{(K_D + L_t + R_t) - \sqrt{(K_D + L_t + R_t)^2 - 4R_tL_t}}{2R_t}\right]$$

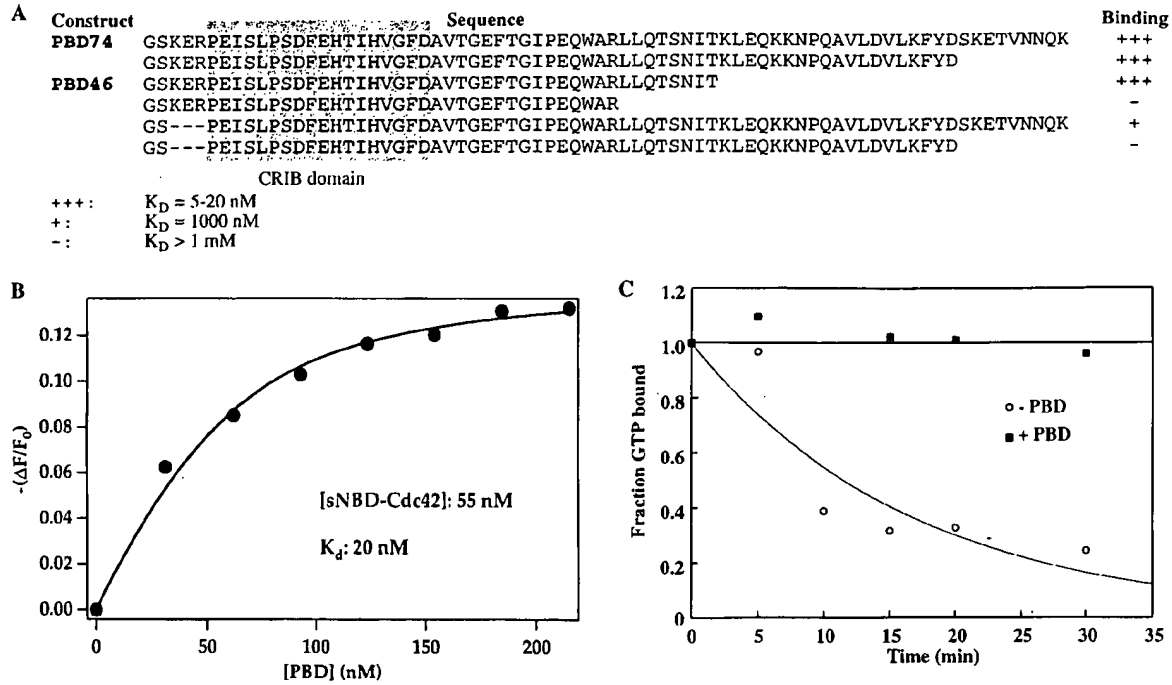

FIGURE 2: Sequence and characterization of PBD46. (A) The amino acid sequences of the PBD constructs tested are shown along with an indication of the affinity of each sequence for Cdc42Hs·GMPPCP based on the sNBD-binding assay. PBD46 was the shortest construct which bound with high affinity. (B) Binding of PBD46 to sNBD-Cdc42Hs·GMPPCP results in a fluorescence decrease upon binding (the *y*-axis represents a decrease in fluorescence intensity). A K_D of 20 nM was calculated as described in the Experimental Procedures. (C) Inhibition of Cdc42Hs-catalyzed GTP hydrolysis by PBD46. In the absence of PBD46, Cdc42Hs hydrolyzed GTP with $t_{1/2}$ of approximately 14 min. In the presence of 10 μM of PBD46, a significant decrease in the rate of ^{32}P release from the GTPase was observed. The curve shown for the GTPase activity in the absence of PBD is a single-exponential fit to the data.

where F is the change in fluorescence over the initial fluorescence ($\Delta F/F_o$), F_i is the initial value of $\Delta F/F_o$, F_f is the final value of $\Delta F/F_o$, L_t is the total concentration of PBD, and R_t is the total concentration of Cdc42Hs.

Measurement of GTPase Activity of Cdc42Hs. The hydrolysis of GTP by Cdc42Hs was measured by monitoring the release of ^{32}P from [γ-^{32}P]GTP bound to Cdc42Hs (*29*). Purified Cdc42Hs (10 μM) was complexed with 7 μM [γ-^{32}P]-GTP (360 000 cpm/pmol) in TEDA buffer (20 mM Tris-HCl, pH 7.5, 10 mM EDTA, 1 mM DTT, and 50 mM NaCl) and 80 μg/mL bovine serum albumin for 20 min at room temperature. To initiate hydrolysis of the bound GTP, aliquots of the Cdc42Hs were then diluted into a reaction mixture containing 25 mM Tris-HCl, pH 7.5, 1.3 mM DTT, 40 mM NaCl, 5 mM $MgCl_2$, 200 μg/mL bovine serum albumin, 100 μM nonradioactive GTP, and either purified PBD46 or control buffer (TEDA buffer, 40% glycerol). Aliquots were filtered on BA-85 nitrocellulose filters (Schleicher and Schuell) and washed under negative pressure. The amount of ^{32}P remaining associated with Cdc42Hs was determined by liquid scintillation counting of the filters.

NMR Spectroscopy. NMR experiments were performed at 25 °C on a Varian Inova 600 spectrometer with a triple resonance pulsed-field gradient probe. Data were collected in the States-TPPI mode (*33, 34*) for quadrature detection. Chemical shifts were referenced as described previously (*27*).

2D Heteronuclear Experiments. 2D ^1H,^{15}N heteronuclear single quantum coherence [HSQC (*35*)] spectra were acquired on Cdc42Hs, and Cdc42Hs-PBD46 samples in which Cdc42Hs was homogeneously labeled with ^{15}N.

3D Experiments for Sequential Backbone Assignments. For both ^{15}N,^{13}C-Cdc42Hs·GMPPCP and ^{15}N,^{13}C-Cdc42Hs·GMPPCP-PBD46, an HNCA was collected (HNCA with decoupling of C_β nuclei) as in Yamazaki et al. (*36*) except for the removal of sensitivity enhancement pulses. During t_1, WALTZ-16 decoupling was applied to protons, allowing the removal of T_c (C_α constant time period), and WURST decoupling (*37, 38*) is applied to both the carbonyls and C_β nuclei (*39*). An HN(CO)CA experiment used a nonsensitivity-enhanced version of the pulse sequence in Yamazaki et al. (*40*), except for the addition of SEDUCE decoupling of C_α nuclei during τ_c (in which coupling develops between nitrogen and the carbonyl) and WURST decoupling of C_β nuclei in t_1, as well as WALTZ-16 decoupling of protons in t_1, allowing the removal of T_c (C_α constant time period). An additional series of experiments were used to correlate backbone amides and amide protons to C_β nuclei: HBCB-CACONNH and HNCACB (*41*−*43*).

3D NOESY Experiments. ^1H,^{15}N-NOESY-HSQC (*34, 44*) experiments were acquired on ^{15}N-Cdc42Hs·GMPPCP, ^{15}N-Cdc42Hs·GMPPCP-PBD46, ^{15}N,^2H-Cdc42Hs·GMPPCP, and ^{15}N,^2H-Cdc42Hs·GMPPCP-PBD46 using a pulse sequence which features water suppression by a selective pulse on the water resonance followed by dephasing with a gradient during the mixing period, as well as by a gradient applied while the magnetization of interest is spin-ordered during the final INEPT transfer step.

Processing of NMR Experiments. Data were processed with version 2.3 of Felix software (Molecular Simulations, Inc.) on an SGI Indy workstation, with preprocessing for sensitivity-enhanced experiments (*45*). Data were, in most

cases, zero-filled to double the original number of data points and apodized by convolution with a squared sinebell window function shifted by 60−90°, depending on the relative amount of signal in the data. Linear prediction was sometimes applied during the transformation of this final dimension to increase resolution. Data visualization and spectral assignment utilized the XEASY (*46*) program.

RESULTS AND DISCUSSION

Optimization of Cdc42Hs and PBD Constructs. A complex of full-length ^{15}N-Cdc42Hs (*27*) with a 74 amino acid PBD construct described previously (*16*) gave rise to ^{1}H,^{15}N-HSQC spectra with unacceptably broad lines (data not shown). By removing the flexible C- and N-terminal portions of the original Cdc42Hs construct [note that the original construct contained 9 amino acids that were not native to Cdc42Hs, but remained from the cloning of the cDNA (*27*)], the resulting 178 amino acid protein produced excellent spectra (Figure 1).

The original 74 amino acid PBD construct was found to be unstable due to proteolysis during purification. Therefore, to determine the core binding sequence of PBD, a series of truncation mutants of both the N- and C-termini surrounding the CRIB sequence [Figure 2A (*25*)] was expressed and purified as GST fusion proteins. Following removal of GST by thrombin and purification, binding assays of each peptide to sNBD-labeled Cdc42Hs were performed according to Nomanbhoy et al. (*32*) as described in the Experimental Procedures. Among the constructs tested, PBD46 was the smallest peptide which maintained an affinity for the GTP-bound form of Cdc42Hs close to that of native mPAK-3 (Figure 2B, K_D = 20 nM vs 5 nM for the wild-type protein). In addition, like mPAK-3, PBD46 inhibited the hydrolysis of GTP by Cdc42Hs (Figure 2C). As shown in Figure 2C, Cdc42Hs hydrolyzed GTP rapidly ($t_{1/2}$ of approximately 14 min) in the absence of PBD46. However, in the presence of 10 μM of PBD46, no GTP hydrolysis was observed within the time of the experiment. Thus, both the binding affinity and function of the p21-binding domain found in mPAK-3 (*15, 16*) is preserved in PBD46. As shown in Figure 1, the complex of PBD46 with ^{15}N-Cdc42Hs·GMPPCP produced excellent ^{1}H,^{15}N-HSQC spectra.

Backbone Assignments of Cdc42Hs·GMPPCP and Its Complex with PBD46. The assignments for a full-length construct of Cdc42Hs·GMPPCP have been reported previously (*27*). The truncated form used in the current experiments showed minor chemical shift changes, and the assignments (^{13}C,^{15}N-Cdc42Hs·GMPPCP) were verified using four triple resonance experiments (HNCO, HNCA, HBCBCACONNH, and HNCACB) which provided assignments for all backbone resonances as well as C_β resonances with the exception of several resonances broadened by conformational dynamics on an intermediate time scale [resonances in the P-loop (residues 14−15), switch I (residues 36−41) and switch II (residues 59−61) (*27*)].

As described above, the binding of PBD46 to Cdc42Hs·GMPPCP exhibits high affinity, and HSQC spectra of ^{15}N-Cdc42Hs·GMPPCP partially complexed with PBD46 exhibits peaks arising from both bound and unbound ^{15}N-Cdc42Hs·GMPPCP, indicating that the complex is in slow exchange (Figure 1, inset). As shown in Figure 1, a large

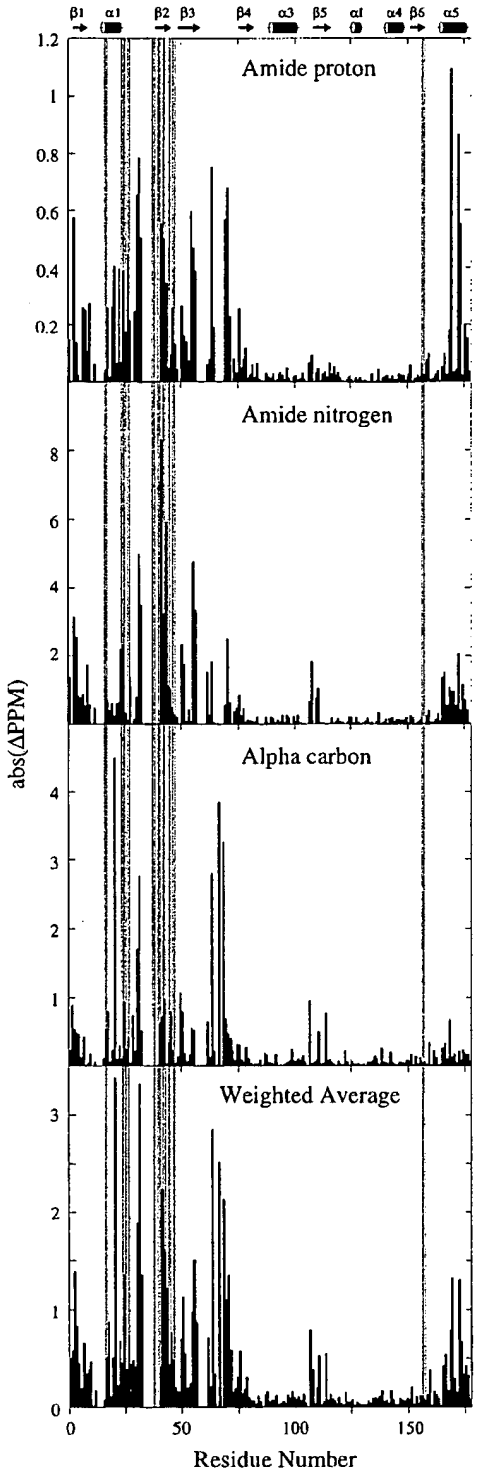

FIGURE 3: Changes in chemical shift as a function of residue number upon Cdc42Hs·GMPPCP binding to PBD46. The changes for the amide proton and amide nitrogen are derived from the ^{1}H,^{15}N-HSQC spectra and the changes in the C_α nuclei are derived from an HNCA spectrum. The weighted average was generated by scaling to the range of chemical shifts in the sample for ^{1}H and ^{15}N nuclei (4.3 and 29.6 ppm, respectively) and to the average chemical shift range for $^{13}C_\alpha$ nuclei [6.6 ppm, calculated from the data in Wishart et al. (*52*)]. The gray bars indicate the residues for which intermolecular contacts have been observed from the NOE experiment shown in Figure 5. Ambiguity due to missing assignments in either the bound or unbound spectra is present for positions 13−15, 35−40, 58−61, and 66−68.

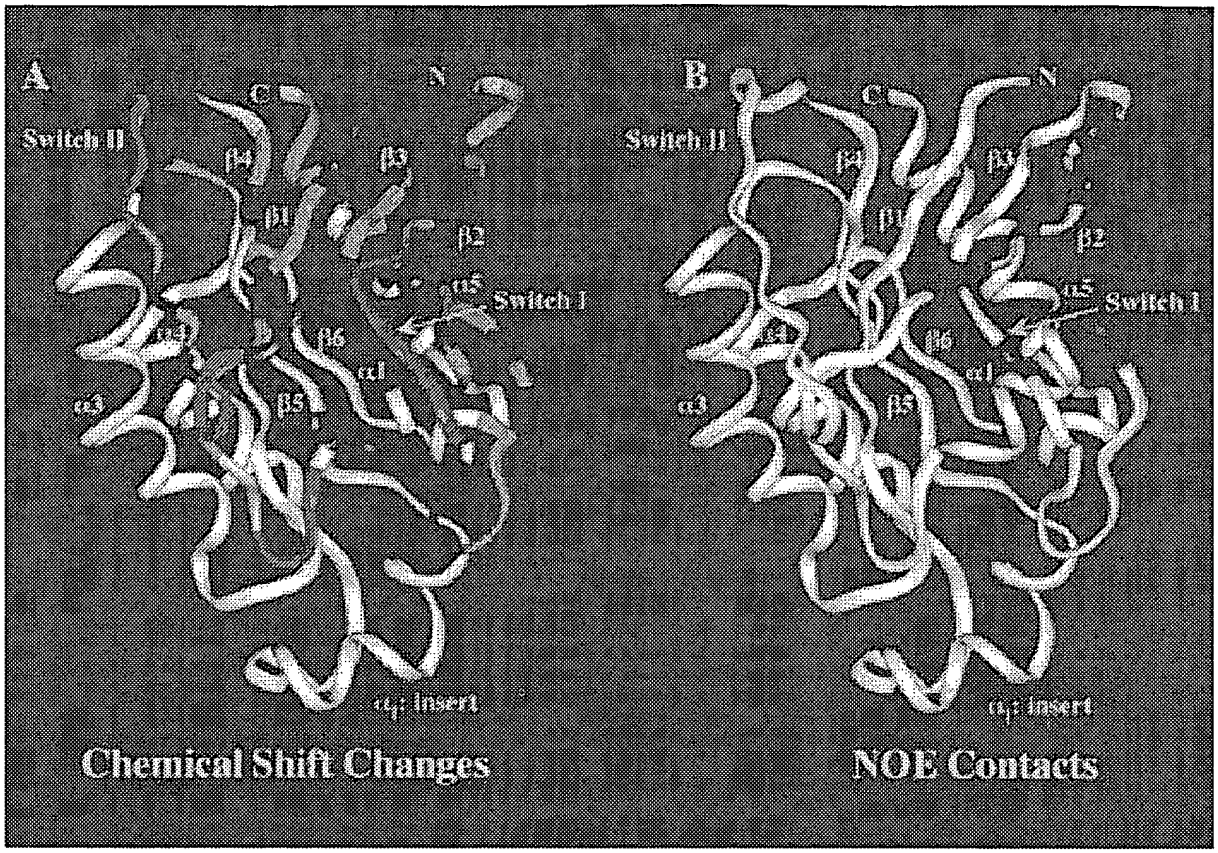

FIGURE 4: (A) The structure of Cdc42Hs·GDP (*27*) colored to indicate the chemical shift changes upon binding of PBD46. Large chemical shift changes (absolute value of the weighted average of the chemical shift change from Figure 3 is greater than 0.5) are shown in red and smaller changes (absolute value of the weighted average of the chemical shift change from Figure 3 is greater than 0.2) are shown in cyan. Residues for which there is an uncertainty are shown in green. The greatest uncertainty arises because a number of peaks in switch I are not observable in the absence of PBD46 but can be observed and assigned in the complex, thus changes in chemical shift cannot be determined. (B) The same structure colored red to indicate positions of the residues which have intermolecular NOEs to PBD46.

number of resonances exhibit significant chemical shift changes to the extent that the assignments could not be made solely upon inspection of the HSQC spectrum. The same four triple resonance experiments used for the uncomplexed form of Cdc42Hs·GMPPCP (HNCO, HNCA, HBCBCA-CONNH, and HNCACB) were used to assign the $^{13}C,^{15}N$-Cdc42Hs·GMPPCP-PBD46 complex. Unlike uncomplexed Cdc42Hs·GMPPCP, all resonances in switch I (residues 25−38) could be assigned in the complex. One likely explanation, consistent with the data presented below, is that interaction with PBD46 modifies the dynamics of switch I, presumably by stabilizing the structure of this region of the protein. The observed chemical shift changes (Figures 1 and 3) are extensive and map to the N-terminal half of Cdc42Hs and the α5 helix. Figure 4A indicates where on the structure of Cdc42Hs the chemical shift changes are observed.

The chemical shift changes map to the face of the protein that encompasses switch I (residues 25−38), switch II (residues 58−67), and a portion of the P-loop (residues 10−15). Thus, the binding of PBD46 might be expected to affect the binding and hydrolysis of nucleotide as well as interaction with GAP proteins [which bind to the switch I and switch II region of Cdc42Hs (*47*)]. As shown above, PBD46 inhibits GTP hydrolysis (Figure 2), and other studies have shown that it decreases the dissociation of nonhydrolyzable GTP analogues (*29*). Likewise, the original 74 amino acid construct of PBD inhibits the binding of Cdc42Hs-GAP to Cdc42Hs (*29*). Thus, the chemical shift changes are entirely consistent with the functional effects of PBD46. In contrast, the binding of RBD to H-Ras does not modify the GTPase activity of H-Ras (*48*). Likewise, the structure of Rap1, a Ras antagonist, bound to RBD (*24*) is identical to the structure of H-Ras, suggesting that RBD does not produce a structural change in H-Ras upon binding. Thus, the interaction of PBD46 with Cdc42Hs is qualitatively different than the interaction of RBD with H-Ras.

Identification of the Binding Surface on Cdc42Hs. Chemical shift changes indicate where the chemical environment is modified upon binding PBD46. Although the changes often map to the binding interface, other regions of the protein experiencing conformational changes upon binding may also exhibit changes in chemical shift. For this reason, a more precise method of mapping the interface is to measure intermolecular NOE interactions (*49*). A fully deuterated ^{15}N-Cdc42Hs·GMPPCP sample was purified in H_2O-containing buffers and complexed with natural abundance PBD46. During the purification procedure, protons were exchanged back onto the amides, providing a Cdc42Hs sample with deuterons on the carbons and protons on the amides. A three-dimensional $^{1}H,^{15}N$-NOESY-HSQC can then be used to detect NOE interactions between amide protons within Cdc42Hs and, more importantly, intermolecular NOE interactions between Cdc42Hs and PBD46. In a $^{1}H,^{15}N$-NOESY-HSQC spectrum of uncomplexed $^{2}H,^{15}N$-

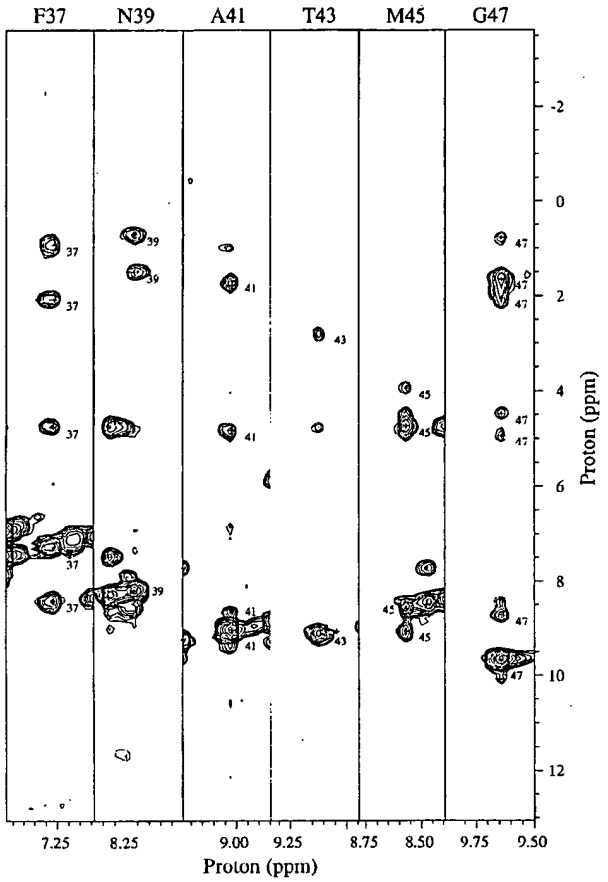

FIGURE 5: Slices from a 3D $^{1}H,^{15}N$-NOESY-HSQC spectrum of $^{15}N,^{2}H$-Cdc42Hs·GMPPCP complexed with natural abundance PBD46. Since all protons attached to carbon were replaced by deuterons, all upfield NOE peaks (>6 ppm, with the exception of NOEs to water at 4.75 ppm) are intermolecular NOEs from amide protons on Cdc42Hs to protons attached to carbon on PBD46.

Cdc42Hs·GMPPCP, the only NOE peaks observed were those between amide protons. Thus, in the complex, NOEs from nonamide protons to amide protons on Cdc42Hs arise from the dipolar interactions across the binding interface, and thus, can be used to map the binding surface. Several slices from a three-dimensional $^{1}H,^{15}N$-NOESY-HSQC spectrum are shown in Figure 5. One of the most striking features is that every other backbone amide proton from residue 37 to residue 47 of Cdc42Hs exhibits an intermolecular NOE, suggesting that a portion of the binding surface arises from an intermolecular β-sheet formed along $\beta 2$ of Cdc42Hs. In addition, the interactions continue into switch I and are present in several neighboring residues in the $\alpha 5$-helix (Figure 4B).

These data are entirely consistent with the mutagenesis work on the binding interface between Cdc42Hs and PAK. Lamarche et al. (*50*) demonstrated that a Y40C mutation of the constitutively active Q61L mutant of Cdc42Hs abolished binding of $p65^{PAK}$ but that the F37A mutant of the same protein had no affect on the interaction. Likewise, Leonard et al. (*51*) showed that a D38E mutant of Cdc42Hs significantly weakened the binding of PAK. On the basis of the pattern of intermolecular NOEs and assuming an intermolecular β-sheet, the side chains of residues 38 and 40 face (and possibly interact with) PBD, whereas, the side chain of residue 37 points away from the interface with PBD. Thus, mutations of critical residues facing PBD at the interface would be expected to interfere significantly with the binding interaction.

This binding surface is much more extensive than that observed for the Rap1−RBD interaction (*24*). In that case, the interaction was an intermolecular antiparallel β-sheet extending from E37 to R41 of Rap1. The pattern of NOEs defining the interface suggest that an antiparallel β-sheet is also present at the Cdc42Hs−PBD46 interface, but that the β-sheet, in this case, extends for an additional six residues. These results suggest that the $\beta 2$ and switch I region of Ras-like proteins may be an effector interface; however, the extent of the interface likely varies and this variation could explain the specificity of interaction and variety of functional effects observed in different members of the Ras superfamily. The indication that a number of other regions on the Cdc42Hs molecule are affected by PBD (compare panels A and B of Figures 4) raises the attractive possibility that the binding of one effector (e.g., PAK) influences the contact sites for other effectors or regulatory proteins. There is increasing evidence that the signaling activities mediated by small GTP-binding proteins require multiple effector interactions and probably occur within multicomponent complexes (*7*). Thus, the ability of one effector (PAK) to influence the binding of other effectors could provide a mechanism for coordinating multiple signaling pathways emanating from a single G-protein. Future work will be directed toward extending these observations to establish whether PAK influences specific effector interactions and what the biological consequences might be for such types of interplay.

ACKNOWLEDGMENT

The authors would like to thank Volker Dötsch, Gerhard Wagner (Harvard Medical School), Joanna Feltham (University of Massachusetts), Shubha Bagrodia, Tyzoon Nomanbhoy, Rob McFeeters, Linda Nicholson, and Greg Weiland (Cornell University) for helpful advice and assistance.

REFERENCES

1. Hall, A. (1990) *Science 249*, 635−640.
2. Ridley, A. J. (1995) *Curr. Biol. 5*, 710−712.
3. Vojtek, A. B., and Cooper, J. A. (1995) *Cell 82*, 527−529.
4. Chant, J., and Stowers, L. (1995) *Cell 81*, 1−4.
5. Qiu, R.-G., Abo, A., McCormick, F., and Symons, M. (1997) *Mol. Cell Biol. 17*, 3449−3458.
6. Hart, M. J., Eva, A., Evans, T., Aaronson, S. A., and Cerione, R. A. (1991) *Nature 354*, 311−314.
7. Cerione, R. A., and Zheng, Y. (1996) *Curr. Opin. Cell Biol. 8*, 216−222.
8. Lin, R., Bagrodia, S., Cerione, R., and Manor, D. (1997) *Curr. Biol. 7*, 794−797.
9. Zheng, Y., Bagrodia, S., and Cerione, R. A. (1994) *J. Biol. Chem. 269*, 18727−18730.
10. Aspenstrom, P., Lindberg, U., and Hall, A. (1996) *Curr. Biol. 6*, 70−75.
11. Hart, M. J., Callow, M. G., Souza, B., and Polakis, P. (1996) *EMBO J. 15*, 2997−3005.
12. McCallum, S. J., Wu, W. J., and Cerione, R. A. (1996) *J. Biol. Chem. 271*, 21732−21737.
13. Yang, W., and Cerione, R. A. (1997) *J. Biol. Chem. 222*, 24819−24824.
14. Manser, E., Leung, T., Salihuddin, H., Tan, L., and Lim, L. (1993) *Nature 363*, 364−367.

15. Manser, E., Leung, T., Salihuddin, H., Zhao, Z., and Lim, L. (1994) *Nature 367*, 40−46.
16. Bagrodia, S., Taylor, S., Creasy, C., Chernoff, J., and Cerione, R. A. (1995) *J. Biol. Chem. 270*, 22731−22737.
17. Minden, A., Lin, A., Claret, F. X., Abo, A., and Karin, M. (1995) *Cell 81*, 1147−1157.
18. Martin, G. A., Bollag, G., McCormick, F., and Abo, A. (1995) *EMBO J. 14*, 1970−1978.
19. Zhang, S., Han, J., Sells, M. A., Chernoff, J., Knaus, U. G., Ulevitch, R. J., and Bokoch, G. M. (1995) *J. Biol. Chem. 270*, 23934−23936.
20. Coso, O. A., Chiariello, M., Yu, J. C., Teramoto, H., Crespo, P., Xu, N., Miki, T., and Gutkind, S. (1995) *Cell 81*, 1137−1146.
21. Bagrodia, S., Derigard, B., Davis, R. J., and Cerione, R. A. (1995) *J. Biol. Chem. 270*, 27995−27998.
22. Ottilie, S., Miller, P. J., Johnson, D. I., Creasy, C. L., Sells, M. A., Bagrodia, S., Forsburg, S. L., and Chernoff, J. (1995) *EMBO J. 14*, 5908−5919.
23. Buday, L., and Downward, J. (1993) *Cell 73*, 611−620.
24. Nassar, N., Horn, G., Herrmann, C., Scherer, A., McCormick, F., and Wittinghofer, A. (1995) *Nature 375*, 554−560.
25. Burbelo, P. D., Drechsel, D., and Hall, A. (1995) *J. Biol. Chem. 270*, 29071−29074.
26. Shinjo, K., Koland, J. G., Hart, M. J., Narasimhan, V., Johnson, D. I., Evans, T., and Cerione, R. A. (1990) *Proc. Natl. Acad. Sci. U.S.A. 87*, 9853−9857.
27. Feltham, J. L., Dötsch, V., Raza, S., Manor, D., Cerione, R. A., Sutcliffe, M. J., Wagner, G., and Oswald, R. E. (1997) *Biochemistry 36*, 8755−8766.
28. Muchmore, D. C., McIntosh, L. P., Russell, C. B., Anderson, D. E., and Dahlquist, F. W. (1989) in *Methods in Enzymology* (Oppenheimer, N. J., and James, T. L., Eds.) pp 44−73, Academic Press, Inc., San Diego.
29. Leonard, D. A., Satoskar, R. S., Wu, W. J., Bagrodia, S., Cerione, R. A., and Manor, D. (1997) *Biochemistry 36*, 1173−1180.
30. Bradford, M. M. (1976) *Anal. Biochem. 72*, 248−254.
31. John, J., Sohmen, R., Feurstein, J., Linke, R., Wittinghofer, A., and Goody, R. S. (1990) *Biochemistry 29*, 6058−6065.
32. Nomanbhoy, T. K., Leonard, D. A., Manor, D., and Cerione, R. A. (1996) *Biochemistry 35*, 4602−4608.
33. States, D. J., Haberkorn, R. A., and Ruben, D. J. (1982) *J. Magn. Reson. 48*, 286−292.
34. Marion, D., Driscoll, P. C., Kay, L. E., Wingfield, P. T., Bax, A., Gronenborn, A., and Clore, G. M. (1989) *Biochemistry 28*, 6150−6156.
35. Bodenhausen, G., and Ruben, D. J. (1980) *Chem. Phys. Lett. 69*, 185−189.
36. Yamazaki, T., Lee, W., Revington, M., Mattiello, D. L., Dahlquist, F. W., Arrowsmith, C. H., and Kay, L. E. (1994) *J. Am. Chem. Soc. 116*, 6464−6465.
37. Kupce, E., and Wagner, G. (1995) *J. Magn. Reson., Ser. B 109*, 329.
38. Kupce, E., and Freeman, R. (1996) *J. Magn. Reson., Ser. A 118*, 299.
39. Matsuo, H., Kupce, E., Li, H., and Wagner, G. (1996) *J. Magn. Reson., Ser. B 113*, 91.
40. Yamazaki, T., Lee, W., Arrowsmith, C. H., Muhandiram, D. R., and Kay, L. E. (1994) *J. Am. Chem. Soc. 116*, 11655−11666.
41. Grzesiek, S., and Bax, A. (1992) *J. Am. Chem. Soc. 114*, 6291−6293.
42. Grzesiek, S., and Bax, A. (1992) *J. Magn. Reson. 99*, 201−207.
43. Muhandiram, D. R., and Kay, L. E. (1994) *J. Magn. Reson. 103*, 203−216.
44. Fesik, S., and Zuiderweg, E. R. P. (1988) *J. Magn. Reson. 78*, 588−593.
45. Kay, L. E., Keifer, P., and Saarinen, T. (1992) *J. Am. Chem. Soc. 114*, 10663−10665.
46. Bartels, C., Xia, T.-H., Billeter, M., Guntert, P., and Wüthrich, K. (1995) *J. Biomol. NMR 6*, 1−10.
47. Rittinger, K., Walker, P. A., Eccleston, J. F., Smerdon, S. J., and Gamblin, S. J. (1997) *Nature 389*, 758−762.
48. Herrmann, C., Martin, G. A., and Wittinghofer, A. (1995) *J. Biol. Chem. 270*, 2901−2905.
49. Walters, J. K., Matsuo, H., and Wagner, G. (1997) *J. Am. Chem. Soc. 119*, 5958−5959.
50. Lamarche, N., Tapon, N., Stowers, L., Burbelo, P. D., Aspenström, P., Bridges, T., Chant, J., and Hall, A. (1996) *Cell 87*, 519−529.
51. Leonard, D., Hart, M. J., Platko, J. V., Eva, A., Henzel, W., Evans, T., and Cerione, R. A. (1992) *J. Biol. Chem. 267*, 22860−22868.
52. Wishart, D. S., Sykes, B. D., and Richards, R. M. (1991) *J. Mol. Biol. 222*, 311−333.

BI981352+

STIC-ILL

From: Gabel, Gailene
Sent: Wednesday, February 12, 2003 4:14 PM
To: STIC-ILL
Subject: 09/905,439

Please provide a copy of the following references ASAP:

1) Gillies et al., NMR in Physiology and Biomedicine, Academic Press: San Diego (1994).

2) Yamazaki et al., J. Am. Chem. Soc. 120: 5591-5592 (1998).

3) Severinov et al., J. Biol. Chem. 273: 16205-16209 (1998).

4) Muir et al. (Proc. Natl. Acad. Sci USA, 95: 6705-6710 (1998).

5) Xu et al. Proc. Natl. Acad. Sci., 96: 388-393 (1999).

6) Lippens et al., In NMR in Supramolecular Chemistry, Pons M. Ed., Kluwer Academic Publishers, 191-226 (1999).

Thanks a bunch,
Gail R. Gabel
7B15
CM1
305-0807

Proc. Natl. Acad. Sci. USA
Vol. 96, pp. 388–393, January 1999
Biochemistry

Chemical ligation of folded recombinant proteins: Segmental isotopic labeling of domains for NMR studies

(segmental labeling/expressed protein ligation/structural biology/Src homology domains)

RONG XU*†, BRENDA AYERS†‡, DAVID COWBURN*§, AND TOM W. MUIR‡§

Laboratories of *Physical Biochemistry and ‡Synthetic Protein Chemistry, The Rockefeller University, 1230 York Avenue, New York, NY 10021

Communicated by Bruce Merrifield, The Rockefeller University, New York, NY, November 9, 1998 (received for review August 17, 1998)

ABSTRACT **A convenient *in vitro* chemical ligation strategy has been developed that allows folded recombinant proteins to be joined together. This strategy permits segmental, selective isotopic labeling of the product. The src homology type 3 and 2 domains (SH3 and SH2) of Abelson protein tyrosine kinase, which constitute the regulatory apparatus of the protein, were individually prepared in reactive forms that can be ligated together under normal protein-folding conditions to form a normal peptide bond at the ligation junction. This strategy was used to prepare NMR sample quantities of the Abelson protein tyrosine kinase-SH(32) domain pair, in which only one of the domains was labeled with ^{15}N. Mass spectrometry and NMR analyses were used to confirm the structure of the ligated protein, which was also shown to have appropriate ligand-binding properties. The ability to prepare recombinant proteins with selectively labeled segments having a single-site mutation, by using a combination of expression of fusion proteins and chemical ligation *in vitro*, will increase the size limits for protein structural determination in solution with NMR methods. *In vitro* chemical ligation of expressed protein domains will also provide a combinatorial approach to the synthesis of linked protein domains.**

Many large cellular and extracellular proteins are composed of independently folded protein modules with distinct biochemical properties. Specific recombinations of these modules provide the overall functional character of the complete protein *in vivo* (1, 2). Consequently, there is some interest in understanding the structural and functional interplay that occurs between such domains in the context of the multidomain protein. Experimentally, this can be achieved by manipulating the spatial and/or functional organization of the domains by using standard recombinant DNA techniques. An alternative protein-engineering strategy would involve the *in vitro* assembly of multidomain proteins from individual "off-the-shelf" protein domains. Advantages of the latter strategy include the ability to prepare a large number of chimeric proteins from a small number of premade building blocks, the ability to prepare fused proteins that are cytotoxic from individually expressed domains that are not, the potential incorporation of nonnatural residues in an efficient combination of *in vivo* and chemosynthetic approaches, and the labeling of one segment of a protein for structural or biochemical investigation. In this paper we demonstrate that ligation of native expressed domains can be accomplished and that segmental labeling, especially valuable for NMR, can be achieved.

A practical size limit for protein structural determination by NMR spectroscopy arises because of the length of the protein, which is a function of the number of residues, n (3). This limit is attributable to the loss of resolution, proportional to n, occurring because signals with longer correlation times exhibit increased line widths and because of the increased number of signals that have similar chemical shifts.

Isotopic labeling can be used for the selection of coupled nuclei pairs, the perturbation of relaxation of complex or isochronous spin systems, and the observation of low sensitivity nuclei (specifically ^{13}C and ^{15}N). The application of this labeling to proteins is well exploited (for examples, see refs. 4 and 5). Although early examples of highly tailored isotopic syntheses of peptides by chemical means (for example, see ref. 6) were useful, that approach was subsumed by the more general ability to uniformly label proteins by overexpression in isotopically substituted media. However, labeling a segment of a protein remains an important goal generally and especially in connection with the study of multidomain or modular proteins (for examples, see refs. 7 and 8). Labeling a segment permits the direct assignment of chemical shifts in that segment, because of reduced spectral complexity. Moreover, in cases in which the subdomains are individually folded, segmental labeling permits the structural determination of the independent segment and possible comparison of the structure in isolated and multidomain forms. Segmental labeling also permits simplified observation of the individual subdomain for spin relaxation, residual dipolar coupling analysis (9), or study of ligand binding by chemical shift perturbation/structure-activity-relationship (SAR)-by-NMR (10).

In principle, selectively labeled proteins can be obtained by joining labeled and unlabeled recombinant proteins together *in vitro*. Along these lines, Yamazaki *et al.* (11) recently exploited trans-protein splicing (12–14) to generate a segmentally labeled protein for NMR analysis. By using a genetically dissected protein-splicing system, this group was able to join together labeled and unlabeled peptides derived from the α subunit of *Escherichia coli* RNA polymerase (11). Although elegant, this strategy resulted in the insertion of five unwanted amino acids at the splice junction and required a chemical denaturation step. These features, along with the moderate yields often associated with the trans-splicing process (12) may reduce the general applicability of this approach.

Previously, we described a protein-engineering approach, expressed protein ligation, that allows synthetic peptides to be chemically ligated to the C terminus of recombinant proteins (15, 16). Key to this process is the generation of a recombinant protein α-thioester derivative that can react with an N-terminal cysteine residue in the peptide to form a normal peptide bond. Reactive recombinant protein α-thioesters can be prepared by exploiting the natural process, protein splicing, a posttranslational event known to involve thioester intermediates (17). It is possible to chemically intercept the splicing process with a suitable thiol by appending the recombinant fragment in question to the N terminus of a genetically modified protein-splicing element (an

The publication costs of this article were defrayed in part by page charge payment. This article must therefore be hereby marked "*advertisement*" in accordance with 18 U.S.C. §1734 solely to indicate this fact.

PNAS is available online at www.pnas.org.

Abbreviations: ESMS, electrospray mass spectrometry; CBD, chitin-binding domain; SH2, src homology type 2 domain; Abl, human Abelson protein tyrosine kinase; SAR, structure-activity-relationship.
A Commentary on this article begins on page 332.
†These authors contributed equally to this work.
§To whom reprint requests should be addressed. e-mail: muirt@rockefeller.edu or cowburn@rockefeller.edu.

intein), thereby generating the corresponding recombinant protein α-thioester (15, 16). Suitable protein expression vectors are commercially available that allow recombinant proteins to be expressed as an N-terminal intein–CBD fusion, in which the CBD is a chitin-binding domain affinity handle (17). After affinity purification on chitin beads, the immobilized fusion protein is exposed to an aqueous solution containing the synthetic peptide and a catalytic amount of thiophenol at pH 7.0. Under these conditions, near quantitative ligation of the peptide to the protein is observed (15, 16). Expressed protein ligation has thus far been used only to generate semisynthetic proteins (15, 16, 18); however, the approach could, in principle, be adapted to allow two recombinant, folded proteins to be ligated together. Such an extension permits segmental isotopic labeling of multidomain proteins for use in multidimensional NMR analysis, as well as other uses of combinatorial chemistry with protein domains.

MATERIALS AND METHODS

Analytical. Electrospray mass spectrometry (ESMS) was performed on a Perkin–Elmer-Sciex (Thornhill, ON, Canada) API-100 mass spectrometer. Predicted masses were calculated by using MACBIOMASS (S. Verumi and T. Lee, City of Hope, Duarte, CA). Analytical HPLC was performed on a Hewlett–Packard 1100 series instrument. Preparative HPLC was performed on a Waters DeltaPrep 4000 system. Linear gradients of 0.1% aqueous trifluoroacetic acid (solvent A) versus 90% CH_3CN plus aqueous 0.1% trifluoroacetic acid (solvent B) were used for all runs.

Cloning and Expression of Abl-[C^{121}]SH2. Suitable SH2 constructs were generated from a pGEX2T vector containing the human Abl-SH(32)-coding sequence (19). Two restriction sites, *Nco*I and *Xma*I, were introduced on either side of the linker region between SH3 and the SH2 domains by using PCR mutagenesis. After the plasmid was treated with *Nco*I and *Xma*I and alkaline phosphatase, a double-stranded 5′-phosphorylated DNA cassette (comprising synthetic oligonucleotides 5′-CCG GTC ATC GAA GGT CGT TGC CTG GAG AAA CAT TCC TGG TAT-3′ and 5′-C ATG ATA CCA GGA ATG TTT CTC CAG GCA ACG ACC TTC GAT GA-3′) was inserted into the pGEX2T plasmid. This oligonucleotide creates an insertion of a factor Xa cleavage site (IEGR-C) and a $S^{121} \rightarrow C$ point mutation in the coding sequence. DNA sequencing was used to confirm the presence of the insertion and mutation. The glutathione *S*-transferase-Abl-SH3-IEGRC-SH2 fusion protein was expressed in *E. coli* DH5-α cells grown in M9 medium with ^{15}N-ammonium chloride. Mid-log phase cells were induced with 1 mM isopropyl-1-thio-β-D-galactopyranoside for 4 h at 37°C and harvested by centrifugation. Cells were resuspended in 4.3 mM sodium phosphate, 137 mM NaCl, 2.7 mM KCl, and 1.4 mM potassium phosphate, pH 7.2, which contained 100 mM EDTA, 1 mM DTT, 1 mM phenylmethylsulfonyl fluoride, 1% (vol/vol) Triton X-100, and 1% (wt/vol) aprotinin, and then lysed by using sonication. The soluble fraction was then passed over glutathione agarose beads, which were then washed with 137 mM NaCl, 8 mM sodium phosphate, 2.7 mM KCl, and 1.4 mM potassium phosphate, pH 7.2, which contained 100 mM EDTA. Abl-SH3-IEGRC-SH2 was cleaved from the glutathione beads with thrombin (20). After thrombin cleavage, Abl-SH3-IEGRC-SH2 was exchanged with factor Xa reaction buffer (1 mM $CaCl_2$/100 mM NaCl/50 mM Tris·HCl, pH 7.8, with 0.01% NaN_3). About 200 units of factor Xa (Pharmacia) were used to cleave 15 mg of Abl-SH3-IEGRC-SH2 in 4 ml of a reaction buffer at room temperature for 20 h. The resulting Abl-[C^{121}]SH2 was purified by fast protein liquid chromatography with a Superdex-75 gel filtration column (Pharmacia) and 137 mM NaCl, 4.3 mM sodium phosphate, 2.7 mM KCl, and 1.4 mM potassium phosphate, pH 7.2, with 2 mM EDTA and 0.1 mM sodium azide as the eluent. The purified protein was concentrated to 0.5 mM with a Centricon 3 concentrator (Amicon). Purity and characterization were confirmed by analytical HPLC and ESMS: observed = 11,997.8 ± 1.4 Da; expected (average isotope composition) = 11,998.2 Da.

Cloning and Expression of Abl-SH3-Intein-CBD. The DNA encoding the Abl-SH3 domain (residues L^{65}–V^{119}) was isolated by PCR from a cloned Abl-SH(32) gene (pGEX2T, ref. 19) with the oligonucleotide primers Abl 1 (5′-GGA TCC CCT GGT CAT ATG CTT TTT GTG GCA CTC TAT GAT TTT GTG-3′) and Abl 2 (5′-ATG TTT CTC CAG GCT GTT AAC GGG GGT GAT GTA GTT GCT TGG-3′). The PCR-amplified SH3 domain was purified and digested simultaneously with *Nde*I and *Hpa*I and then recloned into the *Nde*I–*Sma*I-treated plasmid pTYB2 (New England Biolabs). The resulting plasmid, $pTYB2_{Abl\text{-}SH3}$, expresses the Abl-SH3 domain fused via a single G residue to the intein-CBD from an isopropyl-1-thio-β-D-galactopyranoside-inducible T7 promoter. The $pTYB2_{Abl\text{-}SH3}$ plasmid was shown to be free of mutations in the Abl-SH3-coding region by DNA sequencing. *E. coli* BL21 cells transformed with $pTYB2_{Abl\text{-}SH3}$ were grown to mid-log phase in Luria–Bertani medium and induced with 1 mM isopropyl-1-thio-β-D-galactopyranoside at 37°C for 5 h. No protein was detected by SDS/PAGE in the soluble fraction of the cell lysate under these conditions. Expression conditions were modified by inducing mid-log phase cells with 0.1 mM isopropyl-1-thio-β-D-galactopyranoside at room temperature for 2 h to yield protein in the soluble fraction. After centrifugation, cells were resuspended in 60 ml of lysis buffer (25 mM Hepes, pH 8.0/0.1 mM EDTA/250 mM NaCl/5% glycerol/1.0 mM phenylmethylsulfonyl fluoride) and lysed with a French press. The lysate was clarified first by low speed centrifugation and further clarified by ultracentrifugation. The clarified lysate (≈45 ml) was loaded onto a 15-ml chitin column preequilibrated in column buffer (20 mM Hepes, pH 7.0/250 mM NaCl/1 mM EDTA/0.1% Triton X-100), and the column was extensively washed with the same buffer and then stored at 4°C until further use. The column loading was determined by treating 100 μl of beads overnight with a buffer containing 0.2 M phosphate, pH 7.2, 0.2 M NaCl, and 100 mM DTT. After the beads were washed extensively with 1:1 acetonitrile:water, the amount of cleaved Abl-[G^{120}]SH3 in solution was quantified by analytical HPLC through comparison to an Abl-SH3 standard of known concentration. This analysis indicated a loading of ≈0.35 mg/ml Abl-[G^{120}]SH3. Results of ESMS of the cleavage product were: observed = 6,259.4 ± 0.5 Da; expected (average isotope composition) = 6,260.0 Da.

Peptide Synthesis. A model peptide NH_2-CGRGRGRK[fluorescein]-$CONH_2$ was chemically synthesized on a methylbenzhydrylamine resin with *in situ* neutralization/2-[1H-benzotriazolyl]-1,1,3,3-tetramethyluronium hexafluorophosphate activation protocols for *t*-butyloxycarbonyl solid phase peptide synthesis (21). Orthogonal protection of the ε-amino group of the C-terminal K residue with fluorenylmethoxycarbonyl allowed solid phase attachment of fluorescein (activated as a succinimide ester) before the final cleavage step. The peptide was purified by reverse-phase HPLC and characterized by ESMS: observed mass = 1,245.9 ± 0.5 Da; expected (average isotope composition) = 1,246.5 Da.

Model Ligation Reactions. Typically, 100 μl of chitin beads were equilibrated with a buffer containing 0.2 M phosphate and 0.2 M NaCl at pH 7.2. To these beads was added a solution of synthetic peptide (1 mg/ml) in the above buffer (100 μl) along with 1.5% (vol/vol) thiophenol. The suspension was then gently agitated at room temperature overnight, the supernatant was removed, and the beads were washed with 1:1 acetonitrile:water. The combined supernatant and washes were then analyzed by analytical HPLC and ESMS, which indicated the presence of the ligation product in excellent (>90%) yield: observed mass = 7,488.0 ± 1.5 Da; expected (average isotope composition) = 7,488.5 Da.

Preparation of Abl-[G^{120}]SH3-Ethyl-α-thioester. The chitin column, loaded and washed as described above, was equilibrated and suspended in 0.2 M phosphate, pH 6.0, and 0.2 M NaCl buffer

to which 3% (vol/vol) ethanethiol was then added. This suspension was agitated overnight, the supernatant was removed, and the beads were washed several times with 1:1 acetonitrile:water. All washes were combined with the supernatant and purified by preparative reverse-phase HPLC by using a Vydac (Hesperia, CA) C_{18} column. The purity and composition of the resulting Abl-[G^{120}]SH3-ethyl-α-thioester were confirmed by analytical HPLC and ESMS: observed mass = 6,305.4 ± 1.5 Da; expected (average isotope composition) = 6,304.2 Da.

Preparation of Abl-[$G^{120}C^{121}$][SH2-^{15}N]SH(32). Purified Abl-[G^{120}]SH3-ethyl-α-thioester (2 mg) and purified ^{15}N-labeled Abl-[C^{121}]SH2 (8 mg) were reacted in 1.5 ml of 0.2 M phosphate, pH 7.2, and 0.2 M NaCl buffer containing both thiophenol and benzyl mercaptan each at final concentrations of 1.5% (vol/vol). After ≈90 h of reaction, the desired ligation product was purified by preparative HPLC and characterized by ESMS: observed mass = 18,240.1 ± 5.4 Da; expected (average isotope composition) = 18,240.2 Da. The lyophilized ligated product (≈2.5 mg) was then dissolved in 200 μl of 6 M Gdn·HCl (where Gdn is guanidine), 0.2 M phosphate, pH 7.2, and 0.2 M NaCl buffer and refolded by rapid dilution (10-fold) into 0.2 M phosphate, pH 7.2, and 0.2 M NaCl buffer. Note that the SH3 domain was also prepared with ^{15}N labeling: observed mass = 6,376.8 ± 0.5 Da; expected (average isotope composition) = 6,378.0 Da. This material could be ligated to [C^{121}]SH2, resulting in analytical quantities of [$G^{120}C^{121}$][SH3-^{15}N]SH(32): observed mass = 18,163.3 ± 6.0 Da; expected (average isotope composition) = 18,156.2 Da.

NMR Measurements on Abl-[SH2-^{15}N]SH(32). Protein samples were exchanged in 200 mM NaCl, 4.3 mM sodium phosphate, 2.7 mM KCl, and 1.4 mM potassium phosphate, pH 7.2, which contained 8% (vol/vol) D_2O, 2 mM [$^2H_{12}$]EDTA, 0.02% (wt/vol) NaN_3, and either 2 or 10 mM DTT-$^2H_{10}$ for wild-type [U-^{15}N]SH(32) and [SH2-^{15}N]SH(32), respectively. The final concentration of the ligated sample was 0.2 mM and that of the wild-type sample was 0.8 mM. ^{1}H-^{15}N heteronuclear single-quantum correlation spectroscopy was performed at 35°C on a DMX-500 NMR spectrometer (Bruker, Billerica, MA) with a 5-mm probe (Nalorac Cryogenics, Martinez, CA). The spectral widths were 14 ppm for the ^{1}H axis and 33 ppm for the ^{15}N axis. The spectra were processed by using XWINNMR (Bruker). The resulting resolution in the final spectra was 1.75 Hz in the proton dimension and 3.2 Hz in the ^{15}N dimension.

Fluorescence Binding Assay. The equilibrium dissociation constants of the protein constructs for the consolidated ligand were determined by using the previously described fluorescence-based titration assay (22). The binding constant for the segment labeled construct was 300 (±100) nM. Experiments were performed on a Fluorolog-3 (Spex Industries, Metuchen, NJ) spectrophotometer fitted with a Neslab Instruments (Portsmouth, NH) temperature control unit.

RESULTS AND DISCUSSION

In this report we describe the development of procedures that allow two folded recombinant protein domains to be efficiently linked together by *in vitro* chemical ligation. This strategy has been used to prepare NMR quantities of the Abl regulatory apparatus, Abl-SH(32), in which only one domain was uniformly labeled with ^{15}N.

The cellular signaling protein, c-Abl, is one of the few nonreceptor protein tyrosine kinases directly linked to human malignancies (23). The kinase activity of c-Abl is tightly controlled *in vivo* and is thought to be partly regulated by specific interactions of its SH3 and SH2 domains with other cytoplasmic and nuclear proteins (19, 24). The three-dimensional structures of the Abl-SH3 and Abl-SH2 domains have been studied in solution by NMR methods, both individually (20, 25) and together in the context of the domain pair (20). This level of structural characterization combined with the importance of these regulatory domains in c-Abl function suggested the Abl-SH(32) domain pair as an excellent target system for segmental labeling studies.

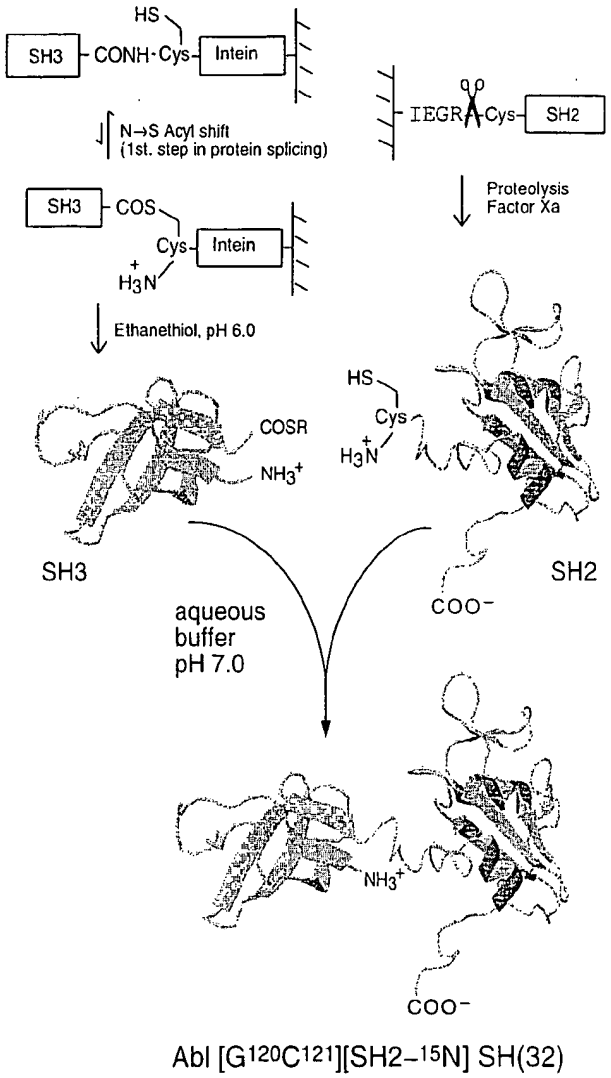

FIG. 1. *In vitro* chemical ligation of folded recombinant proteins is illustrated by the preparation of Abl-SH(32). The Abl-SH3 domain is generated as an ethyl α-thioester derivative from the corresponding intein fusion protein, and the Abl-SH2 domain is generated with a cysteine at the N terminus via a factor Xa proteolysis strategy. Note that the linkage between the SH3 domain and the fused intein protein-splicing domain is naturally in equilibrium between an amide and a thioester (15–17). Exposure of this fusion protein to ethanethiol at pH 6.0 results in the formation of an ethyl α-thioester derivative of the SH3 domain. Combining these SH3 and SH2 protein derivatives under conditions that maintain them as folded results in a chemoselective ligation reaction and the generation of a normal peptide bond at the ligation junction (26). The sequence of the final ligation product is m{65}LFVALYDFVASGDNTLSITKGEKLRVLGYNHNGEWAEAQTKNGQGWVPSNYITPVGCLEKHSWYHGPVSRNAAEYLLSSGINGSFLVRESESSPGQRSISLRYEGRVYHYRINTASDGKLYVSSESRFNTLAELVHHHSTVADGLITTLHYPAPKR{220}gihrd. Lowercase letters indicate nongene residues from the expression systems used. This construct uses a $C^{101} \rightarrow$ S mutation internal to the SH3, which had previously been inserted to improve stability for NMR experiments. This is also in the "wild-type" sequence. Note that native chemical ligation reactions can be performed in the presence of multiple internal cysteine residues in either of the reacting segments (27); only the N-terminal cysteine participates in the ligation reaction.

As illustrated in Fig. 1, our *in vitro* chemical ligation strategy called for the generation of a recombinant Abl-SH3 domain

activated at its C terminus as an α-thioester and a recombinant Abl-SH2 domain containing an N-terminal cysteine residue. These two, folded protein domains should, when combined under physiological conditions, chemoselectively react via the well established native chemical ligation reaction (26, 28) to form an amide linkage at the ligation junction. The location of the ligation site was chosen to be within the short linker region that connects the two domains and involved mutation of the wild-type residues N^{120} and S^{121} to G and C, respectively. The S → C mutation was required to facilitate the ligation reaction, whereas the N → G mutation was expected to improve the kinetics of ligation.[¶] Residue numbering is referenced to the complete Abl protein; the C^{121} mutation is then the N terminus of the Abl-SH2 domain. Previous studies had indicated this linker region to be relatively flexible (20), and it was anticipated that the mutations would lead to minimal significant structural perturbations.

The Abl-SH3 sequence (residues L^{65}–V^{119}) was subcloned into the commercially available pTYB2 expression vector, which allowed the generation of an Abl-SH3-intein-CBD fusion protein. After soluble expression in *E. coli*, the desired fusion protein was affinity purified on chitin beads. A small aliquot of the loaded beads was treated overnight with DTT, and the reaction supernatant was analyzed by reverse-phase HPLC and ESMS. This indicated that the expected Abl-SH3 construct was present in >90% homogeneity (data not shown) and that approximately 0.35 mg of the Abl-SH3 domain was immobilized per ml of chitin beads.

Initial attempts to generate the [C^{121}]SH2 construct involved cyanogen bromide cleavage of a glutathione *S*-transferase-Abl-SH(32) fusion containing a unique M-C unit at the appropriate position within the interdomain linker.[‖] This synthetic strategy was unsuccessful because of irreversible oxidation of the C residue to cysteic acid during the chemical cleavage step; the resulting Cys(O_3H)-Abl-SH2 analog could not participate in subsequent chemical ligation reactions. An alternative approach was therefore used that applied the factor Xa cleavage strategy previously described by Verdine and coworkers (29). With this approach a glutathione *S*-transferase-Abl-SH(32) fusion protein was generated that contained an -I-E-G-R-C- motif inserted within the linker region connecting the Abl-SH3 and Abl-SH2 domains, before L^{122}. Proteolysis of this fusion protein with factor Xa afforded the desired [C^{121}]SH2 construct in good yield. A similar strategy was also used to prepare uniformly ^{15}N-labeled [C^{121}]SH2 (see *Materials and Methods*).

In preliminary ligation studies, we investigated whether a short synthetic peptide, NH_2-CGRGRGRK[fluorescein]-$CONH_2$, could be reacted with the immobilized Abl-SH3-intein-CBD fusion protein. Consistent with previously published examples (15, 16), nearly quantitative ligation of the synthetic peptide to the recombinant Abl-SH3 domain was observed, as indicated by reverse-phase HPLC, ESMS, and fluorescence spectroscopy (data not shown). These studies thus established that expressed protein ligation reactions could be performed on the folded Abl-SH3 domain.

Initial attempts to ligate [C^{121}]SH2 to the immobilized SH3/thioester domain produced no detectable product formation.

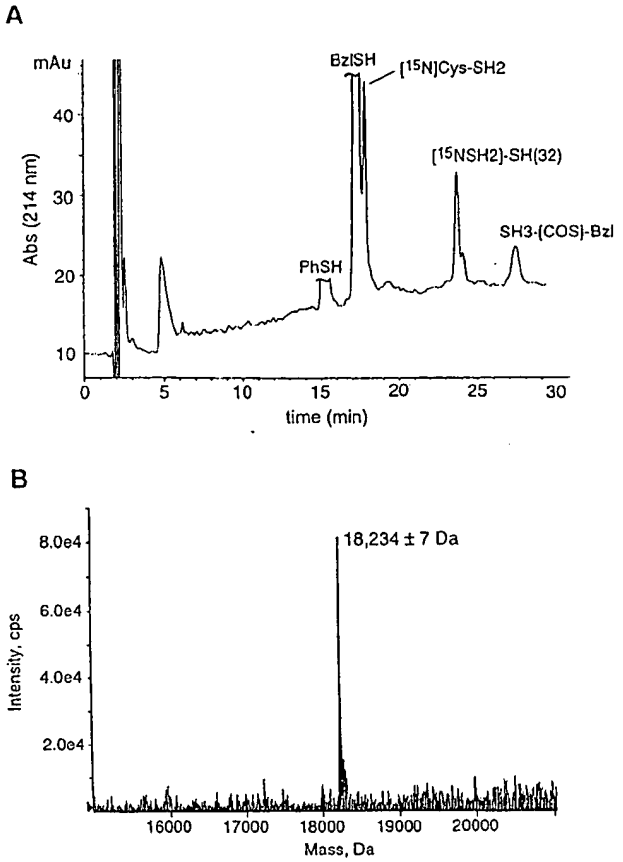

FIG. 2. Chemical ligation of Abl-[G^{120}]SH3 to Abl-[C^{121}][U-^{15}N]SH2. (*A*) Analytical reverse-phase HPLC profile of the crude ligation mixture after a 90-h reaction. A linear gradient of 32–46% of solvent B over 30 min was used. ESMS was used to identify the various components in the mixture, which are labeled accordingly. Note that the Abl-SH3 domain is converted to the more reactive benzyl- and phenyl-α-thioester derivatives *in situ*. (*B*) Electrospray mass spectrum (mass reconstruction) of the purified product, Abl-[$G^{120}C^{121}$][SH2-^{15}N]SH(32); expected mass (average isotope composition) = 18,240.2 Da.

These studies used approximately equimolar amounts of the two reactants, requiring ≈2 ml of beads (≈700 μg of SH3 α-thioester) for every mg of [C^{121}]SH2 used. The net effect of performing this reaction directly from the chitin beads was, therefore, to dilute greatly the [C^{121}]SH2 domain (<50 μM), leading to a kinetically unfavorable reaction.[**] Note that this kinetic problem was not encountered with the model ligation described above because the synthetic peptide was present in large molar excess and millimolar concentration. However, emulating these pseudo-first-order conditions for the [C^{121}]SH2 ligation was impractical because of the large amounts of the protein required (e.g., ≈100 mg of [C^{121}]SH2 would be required for a preparative scale 10-ml reaction).

An alternative and more efficient synthetic approach was developed that overcame the kinetic problems associated with the immobilized Abl-SH3-intein-CBD fusion protein. This approach generates a soluble, stable α-thioester derivative of Abl-SH3 that can be easily purified and stored but whose reactivity can be modulated through transthioesterification during the ligation reaction. Previous studies have shown that alkyl α-thioester derivatives of synthetic peptides are relatively unreactive as acyl

[¶]Recent studies indicate that the majority of naturally occurring amino acids (with the exception of I, V, E, D, N, Q, and P) can be tolerated at the N-terminal side of the ligation junction without dramatically altering ligation yield/kinetics (Hackeng, P. M., Griffin, J. H. & Dawson, P. E., presented at the Twelfth Symposium of the Protein Society, San Diego, July 25–29, 1998). Thus, in future applications only a single amino acid mutation (i.e., X → C) may be necessary for expressed protein ligation.

[‖]The M-C unit was introduced into the linker region connecting the Abl-SH3 and Abl-SH2 domains by cassette mutagenesis by using an *Nco*I and *Xma*I restriction strategy. This resulted in N^{120} → M and S^{121} → C mutations in the Abl-SH(32) construct. The Abl-SH(32) sequence does not contain any endogenous M residues.

[**]It is well established that efficient chemical ligation reactions require high concentrations (near mM) of both reactants (26–28, 30–33).

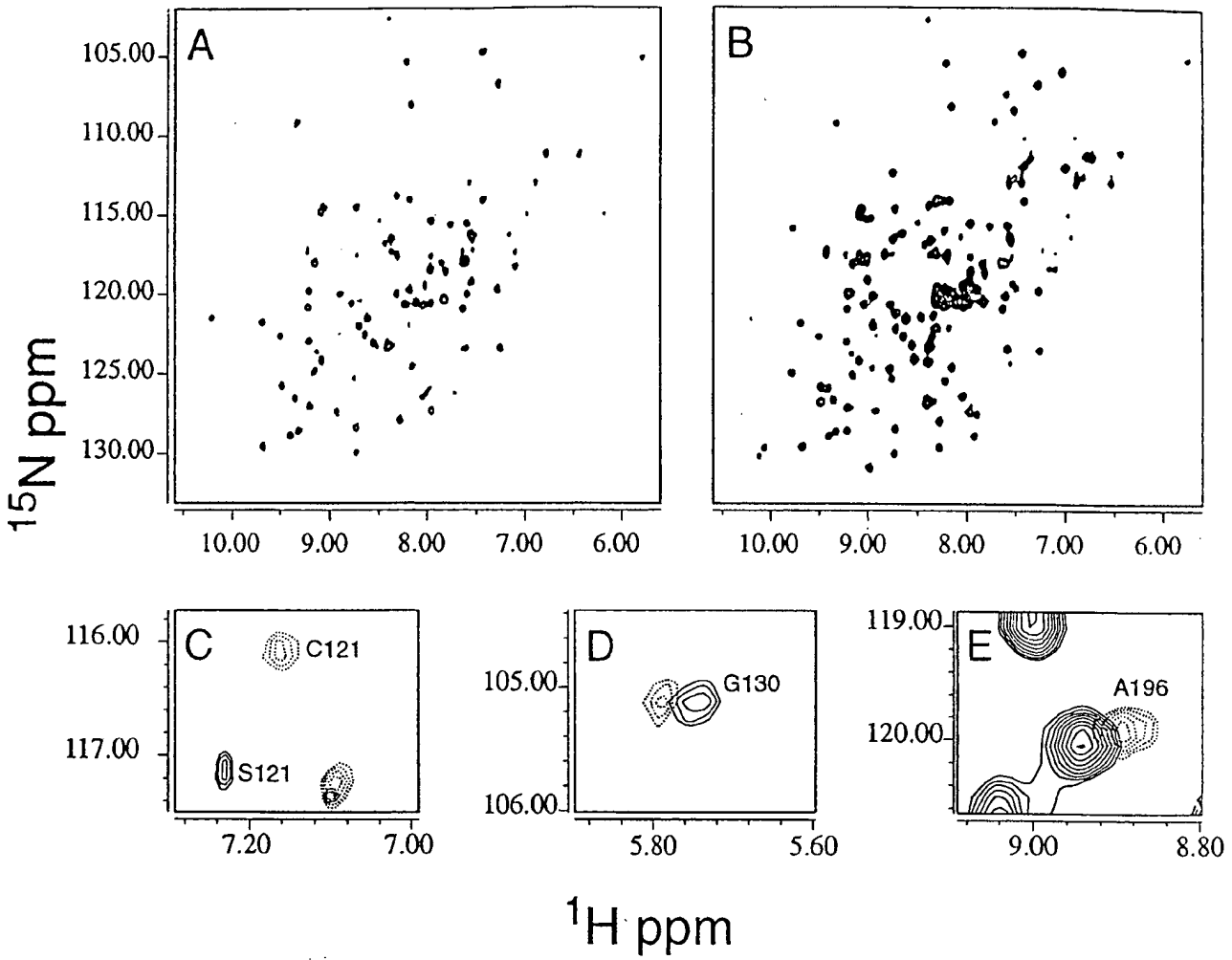

FIG. 3. $^{1}H\{^{15}N\}$ NMR spectra at 500 MHz of Abl-[$G^{120}C^{121}$][SH2-^{15}N]SH(32) (*A*) and wild-type Abl-SH(32) (*B*) with uniform ^{15}N labeling. The peaks in *A* are the SH2-associated subset of those in *B*. (*C–E*) The peaks showing detectable chemical shift changes away from their position in the wild type are illustrated. (*C*) S^{121} in the wild type is mutated to C^{121} in the segment-labeled material. (*C–E*) The wild type subspectrum is shown in solid lines, and the segment-labeled protein is shown in dashed lines. Residue G^{130} shows a small ^{1}H chemical shift (*D*), as does A^{196} (*E*). Both of these residues are spatially close to the junction between SH3 and SH2 and presumably are slightly structurally perturbed.

donors (33, 34). We found that overnight exposure of the chitin beads to ethanethiol at pH 6.0 led to the generation of an ethyl α-thioester derivative of the Abl-SH3 domain (Fig. 1). This transthioesterification/cleavage reaction was found to be remarkably clean as indicated by HPLC/ESMS analyses of the reaction supernatant and SDS/PAGE analysis of the residual immobilized protein on the chitin beads. The Abl-SH3 ethyl α-thioester derivative was easily purified by HPLC (gel filtration or dialysis could also be used provided the pH is kept at 6.0 or below) and could be stored as a lyophilized powder for several months.

The [G^{120}]SH3 ethyl α-thioester derivative and [C^{121}][U-^{15}N]SH2 domain were combined in phosphate buffer at pH 7.2, conditions under which the two protein domains are known to adopt stable tertiary folds (20, 25). To our knowledge this is the first time that the chemical ligation of two folded proteins has been attempted.†† Three steps were thus taken to ensure efficient reaction, namely: the two domains were kept at a moderately high concentration (≈0.5 mM); one of the reactants, [C^{121}]SH2, was added in molar excess; and the cofactors, thiophenol and benzyl mercaptan, were each included in the reaction medium. These cofactors are known to catalyze native chemical ligation reactions through *in situ* transthioesterification (30). The progress of the ligation reaction was monitored by using a combination of analytical HPLC and ESMS, which indicated that the reaction had gone to ≈70% completion after 4 days (Fig. 2*A*). At this point, the ligation product, Abl-[$G^{120}C^{121}$][SH2-^{15}N]SH(32), was purified by preparative HPLC, and its covalent structure was characterized by ESMS (Fig. 2*B*).

Preliminary studies had indicated that HPLC-purified recombinant Abl-SH(32) could be lyophilized and then refolded by rapid dilution from a 6 M Gdn·HCl-containing buffer into phosphate buffer at pH 7.2. Under these conditions, no protein precipitation was observed, and NMR analysis indicated that the sample had adopted a native fold (data not shown). A similar strategy was therefore used to prepare the complete [SH2-^{15}N]SH(32) construct for functional and structural analysis. The binding affinity of Abl-[$G^{120}C^{121}$][SH2-^{15}N]SH(32) for the consolidated ligand,‡‡ NH_2-PVpYENVG$_6$>(PPAYPPPPVPK-$CONH_2$), which binds both the SH3 and the SH2 domains simultaneously (22), was studied by a fluorescence-based titration assay. This revealed the equilibration dissociation constant for

††Although chemical denaturants were not present in the example here, such agents can be added if required and do not interfere with native ligation chemistry (26–28, 30–33, 35).

‡‡> denotes that the C-terminal glycyl residue is linked to the N^{α} of lysyl in the second peptide segment.

binding to the ligand, 300 nM, was essentially that previously reported for the Abl-SH(32) construct, 249 nM (22). This affinity is characteristic of the dual domain construct.

The purified ligation product was stable under NMR sample conditions. In Fig. 3*A*, the $^{1}H\{^{15}N\}$ heteronuclear single-quantum correlation spectroscopy map of the $[G^{120}C^{121}][SH2\text{-}^{15}N]SH(32)$ may be compared with the $[U\text{-}^{15}N]SH(32)$; these spectra are essentially fingerprints of the folded proteins. All peaks in the heteronuclear single-quantum correlation spectroscopy map of $[G^{120}C^{121}][SH2\text{-}^{15}N]SH(32)$ almost exactly coincide with those of $[U\text{-}^{15}N]SH(32)$ and are in agreement with the previous assignments by analogy (20) and from triple resonance data (R.X., unpublished results). There are no extraneous peaks. These NMR data are highly indicative that the structures are very similar and that the ligation reaction did not affect folding. At the ligation site, chemical shift changes are expected and observed for the NS → GC double mutation. The ^{15}N-labeled amide of C^{121}, assigned by analogy and difference, indicates the expected standard amide bond formation after the ligation reaction. The G^{120} is not labeled. The new spectra permit identification of the amide for E^{123}, previously only ambiguously identified because of low intensity, and overlap with an SH3 amide resonance. Some subtle, but experimentally significant, shifts are observed for G^{130} and A^{196} (Fig. 3 *D* and *E*). From the expected contacts (20, 25) and observed flexibility of the linker (20, 36), these two residues are believed to be spatially close to the ligation site, where minor effects of the N → G and S → C mutations might be expected for changes in the side chain environment. The small magnitude of these chemical shift perturbations (<0.06 ppm, ^{1}H; <0.1 ppm ^{15}N, excluding the S^{121} →C mutation) further support the conclusions that the $[G^{120}C^{121}][SH2\text{-}^{15}N]SH(32)$ is topologically very similar to the wild type.

CONCLUSIONS

Significantly larger protein systems can be studied with new methods for spectral observation and structure determination by NMR (9, 37). The approach of segment labeling makes possible assignment and high resolution structural determination of large proteins without requiring the natural spectral simplification that occurs because of molecular symmetry. For example, it would seem practical to obtain highly resolved fragment spectra for about 100 residues of an 800-residue protein (≈110 kDa), comparable to those reported for the highly symmetric 7,8-dihydroneoptrin aldolase, a homooctomer (5). The effects of "context" of the surrounding domains on a segmentally labeled domain can now be practically studied by appropriate mutation and chemical ligation. Fragment labeling also permits segmental determination of dynamic properties, residual dipolar couplings (9), and SAR-by-NMR (10). Unlike the previously described trans-splicing approach (11), the chemical ligation strategy presented here can be extended to allow three recombinant protein segments to be regioselectively linked together; the feasibility of such an approach was recently demonstrated in a model synthetic peptide system (33). In principle, this important extension would allow internal domains of a protein to be isotopically labeled for NMR analysis. Other applications of our approach include the incorporation of selenomethionyl-labeled domains into a larger protein, facilitating structure determination of proteins by using multi-wavelength anomalous dispersion x-ray experiments for phasing (38), the incorporation of ^{2}H-labeled segments for neutron scattering or diffraction, and the incorporation of highly magnetically anisotropic domains to provide additional orientation for NMR dipolar coupling measurements (39).

We gratefully acknowledge the cooperation of, and discussion with, the members of the Muir and Cowburn laboratories. We are indebted to Prof. B. J. Mayer for helpful suggestions concerning cloning and constructs. This work was supported by Grant R29-GM55843-01 (to T.W.M.), Grant R01-GM47021 (to D.C.), and Grant F32-AI-09537 (to R.X.) from the National Institutes of Health; a grant from the Pew Charitable Trusts (to T.W.M); and a grant from the National Leukemia Research Association (to T.W.M.).

1. Jaenicke, R. (1991) *Biochemistry* **30,** 3147–3161.
2. Bork, P., Schultz, J. & Ponting, C. P. (1997) *Trends Biochem. Sci.* **22,** 296–298.
3. Wuthrich, K. (1986) *NMR of Proteins and Nucleic Acids* (Wiley, New York).
4. Clore, G. M. & Gronenborn, A. M. (1997) *Nat. Struct. Biol.* **4,** Suppl., 849–853.
5. Wuthrich, K. (1998) *Nat. Struct. Biol.* **5,** Suppl., 492–495.
6. Cowburn, D., Live, D. H., Fischman, A. J. & Agosta, W. C. (1983) *J. Am. Chem. Soc.* **105,** 7435–7442.
7. Campbell, I. D. & Downing, A. K. (1998) *Nat. Struct. Biol.* **5,** Suppl., 496–499.
8. Kuriyan, J. & Cowburn, D. (1997) *Annu. Rev. Biophys. Biomol. Struct.* **26,** 259–288.
9. Tjandra, N. & Bax, A. (1997) *Science* **278,** 1111–1114.
10. Shuker, S. B., Hajduk, P. J., Meadows, R. P. & Fesik, S. W. (1996) *Science* **274,** 1531–1534.
11. Yamazaki, T., Otomo, T., Oda, N., Kyogoku, Y., Uegaki, K. & Ito, N. (1998) *J. Am. Chem. Soc.* **120,** 5591–5592.
12. Southworth, M. W., Adam, E., Panne, D., Bayer, R., Kautz, R. & Perler, F. (1998) *EMBO J.* **17,** 918–926.
13. Shingledecker, K., Jiang, S. Q. & Paulus, H. (1998) *Gene* **207,** 187–195.
14. Mills, K. V., Lew, B. M., Jiang, S. & Paulus, H. (1998) *Proc. Natl. Acad. Sci. USA* **95,** 3543–3548.
15. Severinov, K. & Muir, T. W. (1998) *J. Biol. Chem.* **273,** 16205–16209.
16. Muir, T. W., Sondhi, D. & Cole, P. A. (1998) *Proc. Natl. Acad. Sci. USA* **95,** 6705–6710.
17. Chong, S., Mersha, F. B., Comb, D. G., Scott, M. E., Landry, D., Vence, L. M., Perler, F. B., Benner, J., Kucera, R. B., Hirvonen, C. A., *et al.* (1997) *Gene* **192,** 271–281.
18. Evans, T. C., Jr., Benner, J. & Xu, M.-Q. (1998) *Protein Sci.* **7,** 2256–2264.
19. Mayer, B. J. & Baltimore, D. (1994) *Mol. Cell. Biol.* **14,** 2883–2894.
20. Gosser, Y. Q., Zheng, J., Overduin, M., Mayer, B. J. & Cowburn, D. (1995) *Structure* **3,** 1075–1086.
21. Alewood, P., Alewood, D., Miranda, L., Love, S., Meutermans, W. & Wilson, D. (1997) *Methods Enzymol.* **289,** 14–29.
22. Cowburn, D., Zheng, J., Xu, Q. & Barany, G. (1995) *J. Biol. Chem.* **270,** 26738–26741.
23. Rosenberg, N. & Witte, O. N. (1988) *Adv. Virus Res.* **35,** 39–81.
24. Muller, A. J., Pendergast, A. M., Havlik, M. H., Puil, L., Pawson, T. & Witte, O. N. (1992) *Mol. Cell. Biol.* **12,** 5087–5093.
25. Overduin, M., Rios, C., Mayer, B., Baltimore, D. & Cowburn, D. (1992) *Cell* **70,** 697–704.
26. Dawson, P. E., Muir, T. W., Clark-Lewis, I. & Kent, S. B. H. (1994) *Science* **266,** 776–779.
27. Hackeng, T. M., Mounier, C. M., Bon, C., Dawson, P. E., Griffin, J. H. & Kent, S. B. H. (1997) *Proc. Natl. Acad. Sci. USA* **94,** 7845–7850.
28. Muir, T. W., Dawson, P. E. & Kent, S. B. H. (1997) *Methods Enzymol.* **289,** 266–298.
29. Erlanson, D. A., Chytil, M. & Verdine, G. L. (1996) *Chem. Biol.* **3,** 981–991.
30. Dawson, P. E., Churchill, M. J., Ghadiri, M. R. & Kent, S. B. H. (1997) *J. Am. Chem. Soc.* **119,** 4325–4329.
31. Canne, L., Bark, S. & Kent, S. B. H. (1996) *J. Am. Chem. Soc.* **118,** 5891–5896.
32. Lu, W., Qasim, M. A., Laskowski, M. & Kent, S. B. H. (1997) *Biochemistry* **36,** 673–679.
33. Camarero, J. A., Cotton, G. J., Adeva, A. & Muir, T. W. (1998) *J. Pept. Res.* **51,** 303–316.
34. Hojo, H. & Aimoto, S. (1991) *Bull. Chem. Soc. Jpn.* **64,** 111–117.
35. Camarero, J. P., Pavel, J. & Muir, T. W. (1998) *Angew. Chem. Int. Ed. Engl.* **37,** 345–348.
36. Nam, H. J., Haser, W. G., Roberts, T. M. & Frederick, C. A. (1996) *Structure* **4,** 1105–1114.
37. Pervushin, K., Riek, R., Wider, G. & Wuthrich, K. (1997) *Proc. Natl. Acad. Sci. USA* **94,** 12366–12371.
38. Hendrickson, W. A. (1991) *Science* **254,** 51–58.
39. Prestegard, J. H. (1998) *Nat. Struct. Biol.* **5,** Suppl., 517–522.